

# **Unravelling the Mechanisms of Acquired Immunomodulatory Drug Resistance in Multiple Myeloma**

**Sarah Anne Bird**

The Institute of Cancer Research

University of London



This thesis is submitted for the degree of PhD

## Declaration

---

### Statement concerning joint work

This thesis is based on the results of my own investigations except where otherwise stated. Contributions from others include:

- Generation of MM1s resistant cell lines – Dr Charlotte Pawlyn and Dr Amy Barber, ICR.
- Generation of MM1s *CRBN* knockout cell lines – Dr Laura Chan and Dr Yakinthi Chrisochidou, ICR.
- Processing of RNA-Seq and WES data for MM1s and H929 resistant cell lines – WES and RNA-Seq of the resistant cell lines was carried out by BGI (China). Dr Harvey Che (ICR) performed initial analysis of the WES and RNA-Seq data and I identified top hits and performed pathway analysis. Dr Pradeep Ramagiri kindly provided the copy number plots shown in this thesis.
- Proteomics and phosphoproteomics of the resistant cell lines and patient samples – Samples I had prepared were analysed by the proteomics core facility (ICR). Initial data analysis was performed by the core, and I identified top hits and performed pathway analysis.
- SETD2 RNA-Seq and ChIP-Seq experiments – RNA-Seq was performed at BGI (China). ChIP-Seq was performed at the genomics core facility (ICR). I analysed the RNA-Seq and ChIP-Seq from the raw data stage and Dr Alan Mackay helped with data visualisation.
- Generation and validation of the Brunello CRISPR knockout library plasmid pool – Dr Paul Clarke and Dr Marco Licciardello (ICR) provided the validated plasmid pool and gave advice regarding optimisation of the CRISPR screen.
- GC-MS analysis of stable isotope labelling experiments using  $^{13}\text{C}_6$ -glucose as a tracer - collaboration with Professor Hector Keun and Mr Yitao Xu, Imperial College London. I performed the initial preparation of samples (including incubation with labelled glucose and methanol quenching and extraction). Further sample processing, GC-MS and initial data analysis were carried out by Mr Xu.

- Analysis of patient RNA-Seq data – collaboration with Dr Saleh Tamim and Dr Erin Flynt (Celgene/Bristol Myers Squibb, USA) who provided the mRNA expression plots shown in this thesis.
- Analysis of patient RNA-Seq data from the MMRF Compass dataset - collaboration with Professor Brian Walker and Dr Enze Liu (Indiana University, USA) who provided the Kaplan-Meier plots shown in this thesis.

I also received support in the laboratory from Mr Salomon Morales, a Scientific Officer within the team who acted under my direction to perform a small number of experimental replicates and patient sample preparation.

**Statement concerning work previously submitted for another award**

This work has not previously been submitted for a degree, or a similar award, at the Institute of Cancer Research or any other institution.

**Statement of impact**

During the first year my PhD I was re-deployed to the NHS to support clinical work during the winter 2020/21 wave of the Covid pandemic. The month spent away from the lab led to a month extension of my PhD fellowship.

## Publications

---

The following manuscript arose from work presented in this thesis:

**Bird S**, Pawlyn C. IMiD resistance in multiple myeloma: current understanding of the underpinning biology and clinical impact. *Blood*. 2023 Jul 13;142(2):131-140.

The following presentations at international/national meetings arose from work presented in this thesis:

Oral presentations:

**Bird S**, Barber A, Sialana F *et al.* Multiomics Analysis of IMiD/CELMoD Resistant Multiple Myeloma Models Uncovers Novel and Targetable Vulnerabilities in the SREBP Lipid Synthesis Pathway. American Society of Haematology (ASH) Annual Meeting, New Orleans, USA, 2022. For this work I received an ASH abstract achievement award and a UK Myeloma Society (UKMS) bursary.

**Bird S**, Barber A, Sialana F *et al.* Multiomics Analysis of IMiD/CELMoD Resistant Multiple Myeloma Models Uncovers Novel and Targetable Vulnerabilities in the SREBP Lipid Synthesis Pathway. UKMS Meeting, London, UK, 2022.

Poster presentations:

**Bird S**, Licciardello M, Chrisochidou Y *et al.* SETD2 is a novel and druggable dependency in IMiD/CELMoD resistant Multiple Myeloma models. American Association for Cancer Research (AACR) Annual Meeting, Florida, USA, 2023.

**Bird S**, Xu Y, Sialana F *et al.* Altered Lipid Metabolism in IMiD/CELMoD Resistant Multiple Myeloma Confers Novel and Targetable Vulnerabilities. International Myeloma Society (IMS) Annual Meeting, Athens, Greece, 2023. For this work I received the IMS Young Investigator Award.



## Acknowledgements

---

Working within the Myeloma Biology and Therapeutics team to complete this thesis has been a pleasure. I would like to thank all past and present members of the team for their support and guidance over the last three years, including Yakinthi Chrisochidou, Salomon Morales, Shannon Martin, Yigen Li, Amy Barber and Laura Chan. This project has also given me the fantastic opportunity to collaborate with several other teams within the Institute of Cancer Research, as well as external groups. I would particularly like to thank Fernando Sialana, Habib Bouguenina, Marco Licciardello, Paul Clarke, Alan Mackay, Yura Grabovska, Pradeep Ramagiri, Harvey Che, Mara Mandelia, James Smith, Jack Cheung, Ben Bellenie, John Caldwell, Mark Stubbs, Rosemary Burke, Martin Kaiser, Amy Holroyd, Ian Collins, Raj Chopra, Yitao Xu, Hector Keun, Saleh Tamim, Erin Flynt, Enze Liu and Brian Walker for spending the time to teach me new skills and their contribution to this work.

I would also like to thank all the members of the Myeloma team at the Royal Marsden Hospital, including Charlotte Pawlyn, Kevin Boyd, Martin Kaiser and Simon Stern, for teaching me to how to best care for patients and giving me the opportunity to get involved in clinical research. Also I'm so grateful to all the patients who have asked about my research and have always been so encouraging.

Most of all I would like to thank my supervisor and mentor Charlotte Pawlyn for her guidance since I started as an Academic Clinical Fellow at the Royal Marsden 5 years ago. I have loved discussing science with you and feel very fortunate to have had the opportunity to learn from you.

I would also like to thank my family, David Bird, Julia Bird, Elizabeth Haynes, and Sam Haynes, for all their support over the years. Finally, I would like to thank my husband David Barlow for his unwavering support and faith in my work.

## Abstract

---

Immunomodulatory drugs (IMiDs) are a cornerstone of multiple myeloma treatment and newer cereblon E3 ligase modulating drugs (CELMoDs) are in clinical trials. However, a major barrier to improving patient outcomes is the inevitable development of resistance to these agents.

IMiDs/CELMoDs bind to the cereblon (CRBN) component of the cullinA-RING E3 ubiquitin ligase and designate a new set of substrates for degradation via the proteasome. Generation of resistance is frequently associated with decreased CRBN expression, and this is associated with genetic alteration in ~1/3rd of patients. However, alternative drivers of the low CRBN state, and other mechanisms of resistance, need to be elucidated.

My aim was to better understand the mechanisms driving acquired IMiD/CELMoD resistance and develop strategies to treat the resistant disease state. To tackle this complex problem, I generated and characterised myeloma cell line models with acquired IMiD/CELMoD resistance and performed multiomics analyses. The key findings of these analyses were then validated and explored further.

Quantitative proteomics analysis identified common changes in lipid synthesis proteins across the resistant cell lines and glucose labelling experiments confirmed altered lipid flux. Proteomic analysis of paired patient samples, from diagnosis and relapse on IMiD, suggested similar changes in lipid pathways. A genome wide CRISPR screen performed in a cell line with acquired CELMoD resistance identified potential novel dependencies in the lipid pathway genes Stearoyl-CoA Desaturase (*SCD*) and Membrane Bound Transcription Factor Peptidase Site 1 (*MBTPS1*). This work has led to novel insights into lipid pathway changes in the IMiD/CELMoD-resistant state which may represent targetable vulnerabilities.

Another novel dependency identified in the resistant lines was SET Domain Containing 2, Histone Lysine Methyltransferase (*SETD2*). SETD2 inhibition led to a greater reduction in proliferation in the IMiD/CELMoD-resistant cell lines compared to their sensitive control lines, and this was associated with a greater reduction in Neural Cell Adhesion Molecule 1 (*NCAM1/CD56*), Epithelial

Membrane Protein 2 (*EMP2*), and Thymosin Beta 15A (*TMSB15A*) expression, suggesting these genes may be key mediators of the effect.

This work provides insights into the generation of IMiD/CELMoD resistance and identifies potential novel targeted treatment strategies for drug resistant myeloma.

## Contents

---

Declaration.....	1
Publications.....	3
Acknowledgements.....	4
Abstract.....	5
Contents .....	7
List of Figures and Tables.....	14
Chapter 1 Introduction .....	21
1.1 Myeloma pathogenesis and treatment.....	22
1.1.1 The pathogenesis of myeloma .....	22
1.1.2 Treatment approaches in myeloma .....	27
1.2 Concepts of drug resistance in cancer.....	31
1.3 An introduction to IMiDs/CELMoDs .....	33
1.3.1 The development of IMiDs .....	33
1.3.2 The molecular target of IMiDs .....	33
1.3.3 IMiD anti-myeloma activity .....	36
1.3.4 The development of CELMoDs .....	36
1.3.5 Response to sequential generations of IMiDs/CELMoDs.....	39
1.3.6 The use of IMiDs/CELMoDs in other malignancies .....	39
1.4 Mechanisms of IMiD/CELMoD resistance.....	40
1.4.1 Concepts of resistance .....	40
1.4.2 Myeloma cell intrinsic mechanisms of resistance .....	41
1.4.3 Myeloma cell extrinsic mechanisms of resistance .....	46
1.5 Targeting the IMiD/CELMoD resistant state.....	48
1.5.1 Further exploration of resistance mechanisms.....	48
1.5.2 Overcoming resistance in the clinical setting.....	49
1.6 Rationale and hypothesis.....	50

1.7	Aims and objectives .....	51
1.7.1	Objective 1: Generation and characterisation of cell line models of acquired IMiD/CELMoD-resistant disease .....	51
1.7.2	Objective 2: Compound screening in an IMiD/CELMoD-resistant cell line .....	51
1.7.3	Objective 3: Genome wide CRISPR screening in an IMiD/CELMoD-resistant cell line .....	51
1.7.4	Objective 4: Validation of pathways and targets identified in objectives 1-3 in cell line models and patient samples .....	52
Chapter 2	Methods .....	53
2.1	General methods .....	53
2.1.1	Cell lines and cell culture.....	53
2.1.2	Compounds.....	53
2.1.3	EC50 assays .....	54
2.1.4	RNA extraction .....	54
2.1.5	Reverse transcription .....	55
2.1.6	Quantitative PCR.....	55
2.1.7	Preparation of protein samples .....	55
2.1.8	Gel electrophoresis and western blotting .....	56
2.1.9	DNA gels .....	57
2.1.10	Plasmid preparation .....	57
2.1.11	Antibiotic selection .....	57
2.2	Characterisation of the resistant cell lines.....	58
2.2.1	Whole exome sequencing .....	58
2.2.2	RNA-Seq .....	59
2.2.3	Whole proteome analysis .....	59
2.2.4	Re-expression of CRBN in the IMiD-resistant cell lines.....	60
2.3	Compound screen .....	60

2.3.1	Preparation of compound list for screening, firing of compounds and cell plating.....	60
2.3.2	Viability assays using CellTiter-Blue.....	61
2.3.3	Data analysis.....	62
2.4	Genome wide knockout CRISPR screen .....	62
2.4.1	Lentivirus production .....	62
2.4.2	Lentiviral multiplicity of infection calculation .....	64
2.4.3	Introduction of Cas9 lentivirus .....	64
2.4.4	Assessment of Cas9 activity .....	64
2.4.5	Genome wide CRISPR screen with the Brunello library.....	65
2.4.6	Genomic DNA extraction and PCR of gRNAs for next generation sequencing .....	66
2.5	14-day SETD2 inhibitor assays.....	67
2.6	Paired RNA-Seq and CHIP-Seq for exploration of SETD2 sensitivity in the resistant cell lines .....	67
2.6.1	RNA-Seq .....	67
2.6.2	CHIP-Seq.....	67
2.7	Labelled glucose experiments .....	69
2.7.1	Labelling with <sup>13</sup> C <sub>6</sub> -glucose .....	69
2.7.2	Methanol quenching and extraction.....	69
2.7.3	Sample preparation, GC-MS and data analysis .....	69
2.8	Processing patient samples .....	70
Chapter 3	Generation and Characterisation of Models to Explore Acquired IMiD/CELMoD Resistance .....	71
3.1	Introduction .....	71
3.2	Results.....	73
3.2.1	Generation of IMiD/CELMoD-resistant cell lines .....	73
3.2.2	Whole exome sequencing of the resistant cell lines.....	86
3.2.3	RNA-Seq analysis in the resistant cell lines .....	92

3.2.4	Proteome and phosphoproteome analysis in the resistant cell lines .	97
3.2.5	Generation and characterisation of knockout CRBN cell lines ....	107
3.2.6	Re-expression of CRBN in the resistant cell lines .....	113
3.2.7	The effect of removing selection pressure on the resistant cell lines.	117
3.3	Discussion .....	124
Chapter 4	Identification of Pharmacological Sensitivities in IMiD/CELMoD Resistance .....	128
4.1	Introduction .....	128
4.2	Results.....	130
4.2.1	Drug screening with the Selleck and Epigenetics libraries .....	130
4.2.2	Secondary screen of hit compounds .....	133
4.3	Discussion .....	136
Chapter 5	Reversing IMiD/CELMoD Resistance and Identifying Genetic Vulnerabilities in the IMiD/CELMoD-Resistant State.....	137
5.1	Introduction .....	137
5.2	Results.....	140
5.2.1	Genome wide loss-of-function CRISPR screen in Iber-R-MM1s .	140
5.2.2	Identifying ways to reverse IMiD/CELMoD resistance.....	141
5.2.3	Identifying novel vulnerabilities in the IMiD/CELMoD-resistant setting .....	146
5.3	Discussion .....	157
Chapter 6	SETD2 Inhibition in IMiD/CELMoD Resistance .....	160
6.1	Introduction .....	160
6.2	Results.....	162
6.2.1	SETD2 expression in the IMiD/CELMoD resistant cell lines.....	162
6.2.2	The effect of SETD2 inhibitors in the IMiD/CELMoD-resistant cell lines .....	163

6.2.3	Paired CHIP-Seq and RNA-Seq analysis .....	169
6.3	Discussion .....	185
Chapter 7	Changes in Lipid Synthesis Pathways in the IMiD/CELMoD-Resistant State.....	188
7.1	Introduction .....	188
7.2	Results.....	189
7.2.1	Whole proteome analysis in the resistant cell lines .....	189
7.2.2	The effect of compounds targeting lipid synthesis pathways in the resistant cell lines .....	190
7.2.3	Clonal competition assays to assess the impact of <i>SCD</i> and <i>MBTPS1</i> knockout on cell fitness .....	194
7.2.4	Lipidomics analysis in the resistant cell lines .....	196
7.2.5	Exploration of changes in lipid pathways in Myeloma patient samples .....	200
7.2.6	Exploration of lipid targeting compounds in patient samples.....	209
7.3	Discussion .....	214
Chapter 8	Discussion.....	218
8.1	The importance of IMiD resistance in the treatment of myeloma patients .....	218
8.2	Mechanisms driving the development of IMiD/CELMoD resistance...220	
8.2.1	Reduction in CRBN expression as a key driver of resistance generation.....	220
8.2.2	The multifactorial nature of CRBN reduction .....	222
8.2.3	Implications for patients.....	222
8.3	Treating the IMiD/CELMoD resistant state.....	223
8.3.1	Reversing the IMiD/CELMoD resistant state .....	224
8.3.2	Targeting novel vulnerabilities that develop during the acquisition of IMiD/CELMoD resistance.....	224
8.4	Wider implications.....	228



8.4.1	Implications for other malignancies .....	228
8.4.2	The future of IMiD/CELMoD resistance research .....	229
Chapter 9	Supplementary Results .....	231
9.1	Generation and Characterisation of Models to Explore Acquired IMiD/CELMoD Resistance.....	231
9.1.1	Proliferation in the resistant and control cell line pairs.....	231
9.1.2	Mutations in the resistant cell lines.....	232
9.1.3	Common transcriptome changes in the resistant cell lines.....	233
9.1.4	Common proteome changes in the resistant cell lines .....	235
9.1.5	Common sites of altered phosphorylation in the resistant cell lines .. .....	237
9.1.6	Validation of the <i>CRBN</i> knockout MM1s cell lines.....	240
9.2	Identification of Pharmacological Sensitivities in IMiD/CELMoD Resistance.....	243
9.2.1	Hit compounds from the screen .....	243
9.3	Reversing IMiD/CELMoD Resistance and Identifying Genetic Vulnerabilities in the IMiD/CELMoD-Resistant State.....	247
9.3.1	Validation of the Brunello library.....	247
9.3.2	Optimisation of polybrene concentration .....	247
9.3.3	Assessment of Cas9 activity with the EGFP reporter assay.....	248
9.3.4	Calculation of multiplicity of infection.....	250
9.3.5	CRISPR screen flow.....	251
9.3.6	Processing CRISPR screen samples and quality control.....	252
9.3.7	Assessment of data quality .....	253
9.4	SETD2 Inhibition in IMiD/CELMoD Resistance.....	256
9.4.1	Transcripts altered with EPZ-719 treatment .....	256
9.4.2	NCAM1/CD56 expression in the resistant cell lines .....	259
9.5	Changes in Lipid Synthesis Pathways in the IMiD/CELMoD-resistant State .....	260

9.5.1	SCD inhibition with GSK1940029 in the resistant cell lines .....	260
9.5.2	The effect of opaganib on viability in the resistant cell lines .....	261
Chapter 10	Supplementary Methods .....	263
10.1	Whole proteome analysis .....	263
10.2	Genome wide knockout CRISPR screen .....	266
10.2.1	Genomic DNA extraction.....	266
10.2.2	PCR of Brunello gRNAs for NGS .....	266
10.3	ChIP-Seq.....	269
10.3.1	High-throughput ChIP-Seq.....	269
10.3.2	ChIP protocol for input controls.....	272
10.4	Labelled glucose experiments .....	274
10.4.1	Sample preparation.....	274
10.4.2	GC-MS and data analysis .....	275
References.....		276

## List of Figures and Tables

---

Table 1-1 Diagnostic criteria for plasma cell disorders.....	23
Table 1-2 Current myeloma treatment modalities. ....	29
Figure 1-1 Average response rates and remission times to sequential lines of therapy.....	30
Table 1-3 Primary mechanisms of drug resistance in cancer cells. ....	32
Figure 1-2 Components of the CRL4 <sup>CRBN</sup> E3 ubiquitin ligase complex, COP9 signalosome and Ikaros/Aiolos/IRF4 axis. ....	35
Table 1-4 IMiDs/CELMoDs currently used in clinical practice.....	38
Figure 1-3 Concepts of IMiD resistance.....	41
Table 2-1 Frequently used compounds.....	54
Table 2-2 TaqMan probes.....	55
Table 2-3 Antibodies used in western blotting. ....	57
Figure 2-1 Antibiotic selection in MM1s cell lines.....	58
Table 2-4 Mutation impact categories.....	58
Figure 2-2 pCDH-CMV-MCS-EF1-Hygro-CRBN.....	60
Figure 2-3 Destination plate map.....	61
Figure 2-4 Plasmids used in the CRISPR screen. ....	63
Figure 2-5 Assessment of Cas9 activity.....	65
Table 3-1 Cell line characteristics. ....	72
Table 3-2 Acquired resistant cell line nomenclature.....	73
Figure 3-1 Viability assays demonstrating MM1s gaining resistance during long-term low dose IMiD/CELMoD exposure.....	75
Figure 3-2 Viability assays demonstrating H929 gaining resistance during long-term low dose IMiD/CELMoD exposure.....	76
Figure 3-3 Viability assays demonstrating response of MM1s resistant lines to other CRBN binding agents 1. ....	77
Figure 3-4 Viability assays demonstrating response of MM1s resistant lines to other CRBN binding agents 2. ....	78
Figure 3-5 Viability assays demonstrating response of H929 resistant lines to other CRBN binding agents 1. ....	79
Figure 3-6 Viability assays demonstrating response of H929 resistant lines to other CRBN binding agents 2. ....	80
Figure 3-7 CRBN mRNA levels.....	81

Figure 3-8 CRBN protein levels. ....	82
Figure 3-9 CRBN levels over time as the cells become resistant to IMiDs/CELMoDs. ....	83
Figure 3-10 The effect of IMiD/CELMoD treatment on Aiolos, Ikaros and IRF4 in the MM1s cell lines. ....	84
Figure 3-11 The effect of IMiD/CELMoD treatment on Aiolos and Ikaros in the H929 cell lines.....	85
Figure 3-12 The effect of IMiDs/CELMODs on IRF4 in the H929 cell lines.....	86
Table 3-3 Mutations in the resistant cell lines. ....	87
Figure 3-13 Mutations in CRBN. ....	87
Table 3-4 Allele frequency of each CRBN mutation in the resistant line and its matched control line.....	88
Figure 3-14 Copy number loss at the CRBN locus in the resistant cell lines. ...	89
Figure 3-15 Copy number loss at the COPS7B locus in the resistant cell lines. ....	90
Figure 3-16 Copy number loss at the COPS8 locus in the resistant cell lines. .	91
Figure 3-17 CRBN RNA expression in the resistant cell lines.....	92
Table 3-5 Functional enrichment analysis of transcripts with altered expression in the resistant cell lines.....	94
Figure 3-18 mRNA expression of TNFAIP3 and BIRC3 in the resistant cell lines. ....	95
Figure 3-19 Protein abundance of TNFAIP3 and BIRC3 in the resistant cell lines. ....	96
Figure 3-20 The effect of SM-164 on cell viability in the resistant cell lines. ....	97
Figure 3-21 Functional enrichment analysis of upregulated proteins in Iber-R-MM1s. ....	99
Figure 3-22 Functional enrichment analysis of downregulated proteins in Iber-R-MM1s. ....	100
Table 3-6 Functional enrichment analysis in the resistant cell lines.....	102
Figure 3-23 Functional enrichment analysis of proteins with increased phosphorylation in Iber-R-MM1s. ....	104
Figure 3-24 Functional enrichment analysis of proteins with decreased phosphorylation in Iber-R-MM1s. ....	105

Table 3-7 Functional enrichment analysis of proteins with altered phosphorylation in the resistant cell lines.....	107
Table 3-8 Proteome changes in CRBN-KO-MM1s compared to parental MM1s. ....	110
Figure 3-25 Functional enrichment analysis of proteins with reduced expression in CRBN-KO-MM1s.....	111
Figure 3-26 Functional enrichment analysis of proteins with increased expression in CRBN-KO-MM1s.....	112
Figure 3-27 CRBN re-expression in the resistant MM1s cell lines. ....	114
Figure 3-28 The effect of CRBN binders on viability in Iber-R-MM1s <sup>CRBN</sup> .....	115
Figure 3-29 CRBN levels in Iber-R-MM1s <sup>CRBN</sup> .....	115
Figure 3-30 Degradation of Aiolos and Ikaros in Iber-R-MM1s <sup>CRBN</sup> on exposure to IMiDs/CELMoDs. ....	116
Figure 3-31 Reduction in IRF4 in Iber-R-MM1s <sup>CRBN</sup> on exposure to IMiDs/CELMoDs. ....	117
Figure 3-32 Viability assays demonstrating the response of Len-R-MM1s to lenalidomide after removal of the selection pressure. ....	119
Figure 3-33 Viability assays demonstrating the response of Pom-R-MM1s to pomalidomide after removal of the selection pressure.....	120
Figure 3-34 Viability assays demonstrating the response of Iber-R-MM1s to iberdomide after removal of the selection pressure. ....	121
Figure 3-35 Viability assays demonstrating the response of resistant H929 lines to IMiDs/CELMoDs after removal of the selection pressure.....	122
Figure 3-36 Restoration of CRBN in the MM1s resistant lines.....	123
Figure 3-37 CRBN blots in the H929 resistant cell lines after removal of the selection pressure.....	123
Figure 4-1 Pathways targeted by library compounds.....	129
Figure 4-2 Expected patterns of compound screen data. ....	131
Figure 4-3 Results of compound screening in Ctrl-Iber-MM1s and Iber-R-MM1s. ....	133
Figure 4-4 12-point EC50 curves for compounds that demonstrated cross-resistance. ....	134
Figure 4-5 The effect of currently used anti-myeloma drugs in Ctrl-Iber-MM1s and Iber-R-MM1s.....	135

Figure 5-1 The CRISPR-Cas9 system. ....	138
Figure 5-2 The CRISPR screen workflow. ....	141
Figure 5-3 CRISPR screen results. ....	142
Figure 5-4 APOBEC3D knockout at the individual guide level. ....	143
Figure 5-5 Knockout of APOBEC3D at the mRNA level. ....	143
Figure 5-6 The effect of APOBEC3D knockout on CELMoD resistance. ....	144
Figure 5-7 APOBEC3D mRNA expression in the clonal lines. ....	145
Figure 5-8 The effect of iberdomide treatment on viability in the clonal cell lines. .....	145
Figure 5-9 Identification of novel vulnerabilities in the IMiD/CELMoD resistant setting. ....	147
Table 5-1 Potential novel vulnerabilities in the resistant state. ....	152
Figure 5-10 Functional enrichment analysis of potential vulnerabilities in the resistant setting. ....	154
Table 5-2 Available inhibitors to target potential vulnerabilities in the IMiD/CELMoD resistant state. ....	155
Figure 5-11 The effect on viability of selected inhibitors in the resistant cell lines. .....	156
Figure 6-1 The function of SETD2. ....	160
Figure 6-2 The abundance of SETD2 in the resistant cell lines. ....	162
Figure 6-3 Baseline expression of H3K36me3 and H3K36me2 in the resistant cell lines. ....	162
Figure 6-4 The chemical structures of EPZ-719 and EZM0414. ....	163
Figure 6-5 Representative 14-day cell growth assays with EPZ-719 treatment. .....	164
Figure 6-6 Day 14 cell counts after exposure to EPZ-719. ....	165
Figure 6-7 Response of the resistant cell lines to EMZ0414 treatment. ....	166
Figure 6-8 5-day cell viability assays with EPZ-719 and EZM0414 in the resistant cell lines. ....	167
Figure 6-9 Combination assays with EPZ-719 and iberdomide. ....	168
Figure 6-10 Synergy plots for EPZ-719 and iberdomide. ....	169
Figure 6-11 Cell proliferation assays with EPZ-719 at days 3-5. ....	170
Figure 6-12 Reduction in H3K36me3 with EPZ-719 treatment. ....	171
Figure 6-13 Conceptual scatter plot of RNA-Seq results. ....	173

Figure 6-14 Transcriptome changes with EPZ-719 treatment in Ctrl-Iber-MM1s and Iber-R-MM1s.....	173
Figure 6-15 Transcriptome changes with EPZ-719 treatment in Ctrl-Iber-H929 and Iber-R-H929.....	174
Table 6-1 Differentially altered transcripts with EPZ-719 treatment.....	175
Figure 6-16 Heat map showing transcripts altered with EPZ-719 treatment... ..	175
Table 6-2 Transcript changes after EPZ-719 treatment in the individual cell lines.....	176
Figure 6-17 Differentially decreased transcripts after EPZ-719 treatment in the resistant cell lines.....	177
Figure 6-18 Density binding plots showing concentration of H3K36me3 binding at each site in different pair wise comparisons.....	179
Figure 6-19 Bar chart showing the distribution of H3K36me3 binding across different genomic features in each condition.....	181
Figure 6-20 NCAM1/CD56 H3K36me3 binding tracks.....	182
Figure 6-21 EMP2 H3K36me3 binding tracks.....	183
Figure 6-22 TMSB15A H3K36me3 binding tracks.....	184
Figure 7-1 SCD levels in the resistant cell lines.....	189
Figure 7-2 Heat map showing log <sub>2</sub> FCs of SREBP pathway proteins in the resistant cell lines.....	190
Figure 7-3 The SREBP pathway.....	191
Figure 7-4 Viability assays demonstrating response of the resistant cell lines to PF-429242 treatment.....	192
Figure 7-5 Time course experiment with PF-429242 in the resistant cell lines.....	193
Figure 7-6 Clonal competition assay workflow.....	194
Figure 7-7 SCD clonal competition assay results.....	195
Figure 7-8 MBTPS1 clonal competition assay results.....	196
Figure 7-9 A schematic of de novo lipogenesis.....	197
Figure 7-10 Fraction of de novo synthesised fatty acids in the control and resistant cell lines.....	198
Figure 7-11 Proportion of lipogenic acetyl-CoA derived from labelled carbon in the control and resistant cell lines.....	199

Figure 7-12 Ratio of desaturated to saturated fatty acids in the control and resistant cell lines.....	200
Figure 7-13 mRNA expression of lipid genes in newly diagnosed and relapsed patient samples.....	201
Figure 7-14 Correlation of MBTPS1 and SCD mRNA expression at diagnosis with outcome.....	203
Figure 7-15 Summary diagram of the Myeloma XI trial.....	204
Table 7-1 Patient characteristics of samples from the Myeloma XI trial.....	205
Figure 7-16 Functional enrichment analysis of commonly upregulated proteins at relapse on lenalidomide.....	207
Figure 7-17 Functional enrichment analysis of commonly downregulated proteins at relapse on lenalidomide.....	208
Figure 7-18 The effect of opaganib on viability in the iberdomide resistant cell lines.....	210
Figure 7-19 Optimisation of viability assays with opaganib treatment in patient samples.....	211
Figure 7-20 The effect of opaganib treatment on the viability of ex vivo patient myeloma cells.....	212
Table 7-2 Patient characteristics of samples exposed to opaganib.....	213
Table 8-1 Key features of the resistant cell lines.....	219
Figure 9-1 Proliferation of the control and resistant cell lines.....	231
Figure 9-2 Raw CellTiter-Blue readings in the control and resistant cell lines.....	231
Table 9-1 Mutations present in the resistant cell lines.....	233
Table 9-2 Common differentially expressed genes in the resistant cell lines.....	235
Table 9-3 Common proteins with altered expression in the resistant cell lines.....	237
Table 9-4 Common sites with altered phosphorylation in the resistant cell lines.....	240
Figure 9-3 The effect of IMiDs/CELMoDs on the viability of the CRBN knockout MM1s cell lines.....	241
Figure 9-4 CRBN protein levels in the CRBN knockout cell lines.....	242
Figure 9-5 The effect of IMiD/CELMoD treatment on Aiolos, Ikaros and IRF4 levels in the CRBN knockout MM1s cell lines.....	242
Table 9-5 Hit compounds identified in the screen.....	246



Figure 9-6 Brunello library representation.....	247
Figure 9-7 Polybrene optimisation. ....	248
Figure 9-8 Cas9 mRNA levels.....	249
Figure 9-9 Assessing the activity of Cas9. ....	250
Figure 9-10 Calculation of the MOI for Brunello library virus.....	251
Figure 9-11 Cells did not regain sensitivity to iberdomide due to removal of selection pressure during the duration of the screen. ....	251
Figure 9-12 Optimisation of gRNA cassette PCR. ....	252
Figure 9-13 Pooling of the CRISPR screen samples. ....	253
Figure 9-14 Quality check of the pooled CRISPR screen samples.....	253
Figure 9-15 Correlation of biological replicates.....	255
Table 9-6 Details of transcripts altered with EPZ-719 treatment in both the MM1s and H929 cell lines.....	258
Figure 9-16 NCAM1/CD56 expression in the resistant cell line pairs.....	259
Figure 9-17 Viability assays showing the effect of GSK1940029 in the resistant cell lines. ....	260
Figure 9-18 Viability assays showing the effect of opaganib in the lenalidomide resistant cell lines.....	261
Figure 9-19 Viability assays showing the effect of opaganib in the pomalidomide resistant cell lines.....	262
Table 10-1 Buffers used in the ChIP protocol. ....	272

## Chapter 1 Introduction

---

Multiple myeloma is a malignant plasma cell dyscrasia which represents about 2% of all new cancer cases in the United Kingdom annually (1). The accumulating cancer cells in the bone marrow cause anaemia, immune paresis with associated infections, bone pain and fractures, high calcium levels and renal failure (2).

Outcomes for myeloma patients have improved significantly over the last 20 years, driven by the development of novel therapeutics (such as immunomodulatory agents (IMiDs), proteasome inhibitors (PIs) and anti-CD38 monoclonal antibodies), autologous stem cell transplantation (ASCT) and enhanced supportive care (2). More recently the treatment landscape has changed again with the development of immunotherapeutic agents such as bispecific antibodies and chimeric antigen receptor (CAR)-T cells. Most patients respond well to initial therapy but over time their disease will relapse, and a new line of treatment will be required. Eventually a treatment refractory state evolves, driven by drug-resistant subclones and protection from therapeutics and immune surveillance conferred by the malignant bone marrow (BM) niche (3-5).

IMiDs are a critical component of therapeutic combinations at all stages of disease and are also used as a single agent maintenance therapy after ASCT. At diagnosis most patients are sensitive to IMiD-based combination therapy; however about 5% are refractory and form an important group with difficult to manage disease (6). Patients who are initially IMiD-sensitive eventually acquire resistance and IMiD-refractory states are associated with shorter progression-free survival (PFS) and overall survival (OS) in response to subsequent therapies (7). Understanding and targeting IMiD resistance is therefore of key importance if we are to improve patient outcomes further.

In this introduction I will provide a brief overview of the pathogenesis and treatment of myeloma, as well as general concepts of drug resistance in cancer. This will be followed by an in depth discussion of our current understanding of IMiD resistance in myeloma.

## 1.1 Myeloma pathogenesis and treatment

### 1.1.1 The pathogenesis of myeloma

#### *The spectrum of clonal plasma cell disorders*

Myeloma is a malignancy of plasma cells. Plasma cells are long-lived, terminally differentiated B cells that reside in the bone marrow and secrete antigen-specific immunoglobulin, thereby forming a critical part of the immune response (2).

Myeloma evolves from the pre-malignant condition monoclonal gammopathy of unknown significance (MGUS). MGUS is a relatively common condition, found in nearly 3% of those over the age of 70. It can progress to smouldering myeloma and then to myeloma; the risk of progression from MGUS to myeloma is about 1% per year (4). Very rarely myeloma can evolve into plasma cell leukaemia, a condition in which cells are no longer reliant on the BM niche and can circulate in the blood stream (2). Together these conditions form a spectrum of clonal plasma cell disorders, which are diagnosed based on the size of the clonal population and the damage, or impending damage, to organs in the body (**Table 1-1**) (2).

Plasma cell disorder	Definition
MGUS	All 3 criteria must be met: Serum monoclonal protein <30g/L Clonal bone marrow plasma cells <10% Absence of end-organ damage using the CRAB criteria (hypercalcaemia, renal impairment, anaemia and bone lesions)
Smouldering myeloma	Both criteria must be met: Serum monoclonal protein (IgG or IgA) ≥30g/L, or urinary monoclonal protein ≥500mg/24 hours and/or clonal bone marrow plasma cells 10-60% Absence of myeloma defining events or amyloidosis
Myeloma	Both criteria must be met: Clonal bone marrow plasma cells ≥10% or biopsy-proven bony or extramedullary plasmacytoma Any one or more of the following myeloma-defining events: Evidence of end-organ damage using the CRAB criteria Hypercalcaemia: serum calcium >0.25mmol/L higher than the upper limit of normal or >2.75mmol/L Renal insufficiency: creatinine clearance <40ml per minute or serum creatinine >177µmol/L

	<p>Anaemia: Hb of &gt;20g/L below the lower limit of normal, or a Hb value of &lt;100g/L</p> <p>Bone lesions: one or more osteolytic lesions on skeletal XR, CT or PET-CT</p> <p>Clonal bone marrow plasma cells ≥60%</p> <p>Involved:uninvolved serum free light chain ratio of ≥100 (involved free light chain level must be ≥100mg/L)</p> <p>&gt; 1 focal lesion on MRI studies (at least 5mm in size)</p>
--	---

*Table 1-1 Diagnostic criteria for plasma cell disorders.*

CT, computer tomography; MGUS, monoclonal gammopathy of unknown significance; MRI, magnetic resonance imaging; PET-CT, positron emission tomography/computed tomography; XR, X-ray. Adapted from Rajkumar *et al* (8).

### ***The genetic evolution of myeloma***

Malignant plasma cell clones frequently make an excess of a specific immunoglobulin and also a surplus of light chains (2). Sequencing of the immunoglobulin heavy chain (IGH) variable region of myeloma cells has shown that the initial oncogenic events usually occur when plasma cells are developing in the germinal centres of lymph nodes (4). This is likely to happen during the processes of isotype class switching and somatic hypermutation which create the diversity seen in the antibody repertoire and are naturally mutation prone (4). Initiating myeloma events include translocation into the immunoglobulin locus in nearly half of patients, which places oncogenes under the influence of the strong enhancers of the immunoglobulin genes. Examples include Multiple Myeloma SET Domain (*MMSET*) and Fibroblast Growth Receptor 3 (*FGFR3*) (t(4;14)), Cyclin D3 (*CCND3*) (t(6;14)), Cyclin D1 (*CCND1*) (t(11;14)), MAF BZIP Transcription Factor (*MAF*) (t(14;16)) and MAF BZIP Transcription Factor B (*MAFB*) ((t14;20)) (9). In the remaining half of patients, hyperdiploidy is the initiating factor, characterised by trisomies of the odd-numbered chromosomes 3, 7, 9, 11, 15 or 17 (10). Irrespective of the initiating event, cyclin D1, D2 or D3 expression appears to be dysregulated in nearly all cases of myeloma, driving the cells through the G1/S cell cycle checkpoint and leading to dysregulated proliferation (11).

After these initiating events, which are found in both myeloma and its precursor conditions, acquired molecular lesions occur and promote disease progression. These events include copy number abnormalities (for example gain of 1q, loss of 1p and deletion of 17p (and with it TP53)), secondary translocations (for example into the *MYC* locus) and mutations in signalling pathway genes (for example TNF

(Tumour Necrosis Factor) Receptor Associated Factor 3 (*TRAF3*), CYLD Lysine 63 Deubiquitinase (*CYLD*) and Lymphotoxin Beta (*LTB*) in the Nuclear Factor Kappa B (NFκB) pathway) (12). Gain of 1q is one of the most common cytogenetic abnormalities observed in myeloma, occurring in around 40% of newly diagnosed patients (13). There are a number of potentially important genetic drivers located at 1q21, including *CKS1B* (CDC28 Protein Kinase Regulatory Subunit 1B), *MCL-1* (MCL1 Apoptosis Regulator, BCL2 Family Member), *IL-6R* (Interleukin 6 Receptor), *ADAR1* (Adenosine Deaminase RNA Specific) and *PDZK1* (PDZ Domain Containing 1). Many of these genes encode proteins that directly or indirectly result in activation of the Janus Kinase/Signal Transducer and Activator of Transcription 3 (JAK/STAT3) pathway (13).

Sequencing studies have been used to explore the mutational landscape of myeloma, comparing an individual's tumour cells to their normal cells and thus enabling identification of acquired somatic mutations (14). Several mutations have a high recurrence rate in myeloma and may play an important role in pathogenesis, progression and/or prognosis. This includes *KRAS* (KRAS Proto-Oncogene, GTPase), *NRAS* (NRAS Proto-Oncogene, GTPase), *TP53*, *DIS3* (DIS3 Homolog, Exosome Endoribonuclease And 3'-5' Exoribonuclease) and *FAM46C* (Family With Sequence Similarity 46 Member C) (14).

Myeloma is often stratified into risk groups based on these primary and secondary genetic alterations. High-risk disease is characterised by one or more adverse cytogenetic lesions, including t(4;14), t(14.16), t(14;20), 1q+, 17p-, or by distinct high-risk gene expression signatures such as the SKY92 and UAMS GEP70 profiles (15).

Myeloma is a heterogenous disease with great genetic diversity. Tumours can follow several evolutionary routes over the course of a patient's disease, with the tumour genomes of standard-risk patients showing fewer changes compared to those with high-risk disease (16). One study identified three different temporal patterns of tumour evolution: genetically stable, linearly evolving, or heterogeneous clonal mixtures with shifting predominant clones (16). This clearly demonstrates how the mutational landscape of myeloma can change during an individual's disease course. Whole exome sequencing was used to evaluate the genetics of paired samples taken at the time of diagnosis and relapse (following

induction therapy and lenalidomide maintenance or observation) (17). Patients achieving a complete response (CR) had predominately branching evolutionary patterns leading to relapse, whereas patients who achieved a partial response (PR) had a similar mutational and structural profile at diagnosis and relapse. Sixty-three % of the patients relapsing from CR had evidence of loss or gain of known recurrently mutated genes in comparison to only 25% of non-CR relapsing patients (17). This pattern was also seen for copy number alterations and structural variants, with 17p-, tMYC, 1q+, and loss of tumour suppressor gene regions (including *CDKN2C* (Cyclin Dependent Kinase Inhibitor 2C), *FAF1* (Fas Associated Factor 1), *FAM46C*, *RB1* (RB Transcriptional Corepressor 1) and *TRAF3*) being seen more frequently in the patients relapsing after CR (17). Therefore depth of response appears to be a key factor in genetic alterations at relapse compared to presentation.

### ***Epigenetic changes in myeloma***

Epigenetics describes heritable changes in gene expression that do not entail a change in DNA sequence. This includes alterations to DNA methylation, aberrant histone modifications and altered non-coding RNA expression (18).

The most common DNA modification in mammals is methylation of cytosine which has been most studied in the context of CpG dinucleotides (19). Myeloma is characterised by global DNA hypomethylation which is correlated with disease progression (20) and poor prognosis (21). However, there is also hypermethylation and silencing of tumour suppressor genes involved in the regulation of the cell cycle, DNA repair, apoptosis, and key signalling pathways (18). Furthermore, DNA methylation is now considered as a regulator of other epigenetic mechanisms, such as expression of microRNAs (18). The transcriptional consequences of DNA methylation are highly dependent on genomic context.

In eukaryotic cells DNA is complexed with proteins to form chromatin. The basic repeating structure of chromatin is the nucleosome, which consists of a histone octamer (comprised of 2 units of each of the core histones H2A, H2B, H3 and H4) around which ~147 base pairs of DNA are wrapped (18). Histone 1 links the nucleosomes together and is involved in the higher order of chromatin structure. The N-terminal domains of the core histone proteins can receive various post-

transcriptional modifications (including methylation, acetylation, phosphorylation, ubiquitination and sumoylation) that alter chromatin structure and therefore gene transcription and DNA replication and repair (18). In general, histone acetylation and phosphorylation are transcriptionally activating but histone methylation is more complicated and can be associated with activated or repressed transcription, depending on the amino acid modified, the state of methylation (mono, di or tri) and its genomic location (at promoters, enhancers and gene bodies) (18). A number of histone mark alterations are important in myeloma. For example, the histone H3 lysine 27 tri-methylation (H3K27me3) mark is a repressive transcriptional mark catalysed by the Polycomb Repressive Complex 2 (PRC2). Upregulation of the PRC2 catalytic subunit EZH2 (Enhancer of Zeste 2 Polycomb Repressive Complex 2 Subunit) has been observed in myeloma and correlates with poor prognosis (22).

Another important epigenetic mechanism influencing myeloma development is the expression of non-coding RNAs (ncRNAs). Although only 1–2% of the human genome consists of protein-encoding DNA, up to 75% is actively transcribed and produces ncRNA (23). Regulatory ncRNAs, such as microRNAs (miRNAs) and long non-coding RNAs (lncRNAs), are involved in regulating gene expression and chromatin based processes (18). For example, miR-21 is upregulated in myeloma, and its inhibition exerts anti-myeloma activity (24).

### ***The bone marrow niche***

In addition to oncogenic events intrinsic to the myeloma cell, the myeloma clone exists within a co-evolving bone marrow niche. This niche may promote disease progression, aid evasion of immune cell surveillance, and confer protection from anti-myeloma therapeutics (25). The bone marrow niche is complex and is composed of a cellular compartment, containing stromal cells, osteoblasts, osteoclasts, endothelial cells, and immune cells, and a non-cellular compartment, including the extracellular matrix and cytokines, growth factors and chemokines (26). The focus of the work in this thesis is directed towards the myeloma cell itself, but crosstalk between malignant plasma cells and the microenvironment is another important area of research.

## ***Epidemiology and prognosis***

In the UK there are nearly 6000 cases of myeloma each year, with over 3000 deaths per year (1). Myeloma incidence is strongly associated with age, and nearly half of all new diagnoses occur in people aged  $\geq 75$  years (1). Myeloma is more common in men than in women (58% vs 42%) and more common in the Black ethnic group (1). Increased risk has also been associated with obesity, immunodeficiency, autoimmune disease and a family history of the condition (1).

Survival rates are improving, and almost one third of patients with myeloma in England survive their disease for over 10 years (compared to less than 10% in the 1970s) (1).

## ***Clinical presentation***

Myeloma frequently presents with a high burden of symptoms. As the bone marrow becomes filled with malignant clonal myeloma cells the ability of the haemopoietic stem cells to produce new blood cells is reduced. This leads to anaemia, neutropenia and thrombocytopenia, which can present as fatigue, recurrent infections and easy bruising and bleeding (2). Another major feature of myeloma is destructive bone disease. Lytic skeletal lesions are frequently found at diagnosis and patients often present with bone pain and/or fractures (27). Hypercalcaemia caused by bone disease can lead to abdominal pain, constipation and confusion (27). In addition, many patients have multifactorial renal dysfunction, caused by hypercalcaemia, high light chains and use of pain medications such as non-steroidal anti-inflammatory drugs (28). In some cases precursor states (such as MGUS) may be detected incidentally and are then monitored for features that suggest progression and disease requiring intervention.

### **1.1.2 Treatment approaches in myeloma**

The variety of therapeutic options available to treat myeloma has rapidly expanded over the last decade. Active drug classes include corticosteroids, standard chemotherapeutic agents, PIs, IMiDs, histone deacetylase inhibitors (HDACs) and monoclonal antibodies (2). More recently, novel immunotherapies such as chimeric antigen receptor (CAR)-T therapies and bispecific antibodies have been developed, as well as antibody-drug conjugates (29). The table below



summarises the major treatment modalities currently used to treat myeloma (**Table 1-2**).

<b>Treatment modality</b>	<b>Examples</b>	<b>Mechanism of action</b>
Corticosteroids	Dexamethasone, prednisolone	Promote a broad range of anti-inflammatory and immunosuppressive activities (30).
Alkylating agents	Cyclophosphamide, melphalan, bendamustine	Bind to DNA and cross-links two stands, thus preventing DNA replication and inducing cell cycle arrest and cell death (31).
Anthracyclines	Doxorubicin, idarubicin	Inhibit topoisomerase II, intercalate into DNA, increase oxidative stress, damage chromatin, and promote anti-tumour immunity (32).
Proteasome inhibitors	Bortezomib, carfilzomib, ixazomib	Inhibit the proteasome, a large multi-protein complex within cells which degrades and processes intracellular proteins. In myeloma large amounts of monoclonal proteins are produced and secreted and inhibition of the proteasome leads to the accumulation of misfolded or unfolded proteins within the endoplasmic reticulum (ER), leading to ER stress and ultimately cell death (33).
Immunomodulatory drugs	Thalidomide, lenalidomide, pomalidomide	Bind to the cereblon component of a E3 ubiquitin ligase, leading to the ubiquitination and subsequent proteasomal degradation of novel substrates (e.g. Ikaros and Aiolos) (34).
Histone deacetylase inhibitors	Panobinostat	Inhibit histone deacetylases leading to hyperacetylation of histones, chromatin remodeling and gene expression changes (35).
Nuclear export inhibitors	Selinexor	Bind to exportin 1 (XPO1) which is involved in the nuclear transport of several proteins including tumour suppressors. Build up of tumour suppressors in the nucleus leads to subsequent cell cycle arrest and apoptosis (36).
Monoclonal antibodies	Daratumumab, isatuximab, elotuzumab	Bind to a myeloma cell surface maker (e.g. daratumumab binds to CD38) and initiate Fc-dependent immune effector mechanisms such as complement-dependent toxicity, antibody-dependent cellular cytotoxicity, and antibody-dependent cellular phagocytosis (37).

CAR-T therapy	Idecabtagene vicleucel (Ide-Cel), ciltacabtagene autoleucel (Cilta-cel)	Autologous or allogeneic T cells are transfected to express cell surface receptors that recognise one or more specific antigens on the surface of myeloma cells. This leads to T cell activation, immunological synapse formation, and cytotoxic granule-mediated myeloma cell apoptosis (29). For example, Ide-Cel is a BCMA targeting CAR-T cell.
Bispecific antibodies	Teclistamab, elranatamab	Antibodies that possess two antigen binding regions with different specificities; one region binds to an antigen on the myeloma cell and one region binds to an antigen on an immune effector cell. This leads to immunological synapse formation and myeloma cell death. For example, teclistamab binds to BCMA on the myeloma cell and CD3 on T cells (29).
Antibody-drug conjugates	Belantamab-mafodotin	Comprise of a monoclonal antibody directed to a myeloma cell surface protein coupled to a highly active cytotoxin by a linker molecule. This enables localised, high-concentration delivery of a potent toxin to the myeloma cells. For example, belantamab mafodotin is an anti-BCMA monoclonal antibody conjugated with monomethyl aurostatin F (29).

*Table 1-2 Current myeloma treatment modalities.*

This table summarises the current (FDA-approved) treatment modalities for myeloma, with examples and details regarding mechanism of action. BCMA, B cell Maturation Antigen, CAR, Chimeric Antigen Receptor.

At the present time in the UK, the initial treatment of myeloma patients is divided into those fit for autologous stem cell transplantation (ASCT) and those who would not tolerate this intensive procedure (2). Combination regimens, combining therapeutics from different classes, are given to reduce myeloma burden +/- ASCT (2). Those who have received ASCT are then eligible for lenalidomide (IMiD) maintenance until relapse (38). All patients also receive bone directed therapy, usually the bisphosphonate zoledronic acid, which has been shown to reduce skeletal-related adverse events (39).

The majority of patients respond well to initial therapy, but treatment is not curative. Over a variable period of time patients will relapse and although many

can be successfully retreated at relapse, the depth and length of each successive remission diminishes over time (**Figure 1-1**) (40).

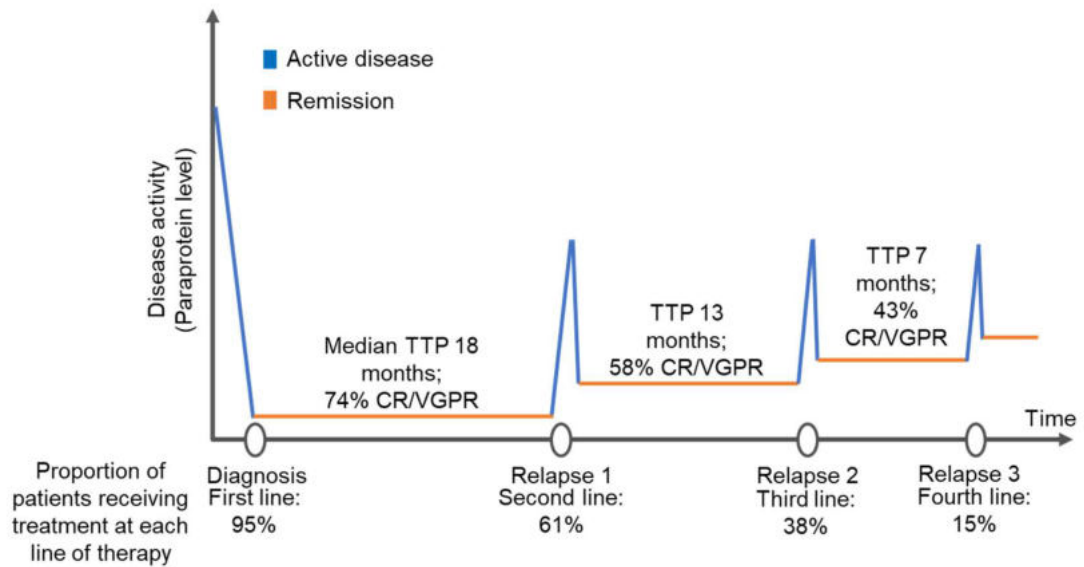


*Figure 1-1 Average response rates and remission times to sequential lines of therapy.*

Data from retrospective analysis of 4997 patient charts in Belgium, France, Germany, Italy, Spain, Switzerland and the UK (chart review performed in 2014). Only 38% of patients received 3rd line therapy which was reduced to 15% at 4th line. TTP, time to progression; CR, complete response; VGPR, very good partial response. Figure from Bird *et al* (2) with data from Yong *et al* (40).

IMiDs form part of many combination regimens. They are commonly used in triplet therapy together with a PI and dexamethasone. Given IMiDs work by binding to CRBN and targeting a new set of proteins for degradation by the proteasome it seems counter-intuitive that combination with a PI would be beneficial (41). However, in the clinical setting the combination of lenalidomide, bortezomib and dexamethasone was shown to have excellent activity in patients with both diverse prior therapies and adverse prognostic characteristics (42). Furthermore, a number of trials showed superiority of triplet therapy over duplet therapy (43-45). A reported mechanism that could potentially explain this synergy is that in pomalidomide treated cells there is ubiquitination and degradation of Methyl-CpG Binding Domain Protein 3 (MBD3), a critical member of the pluripotency repressor complex (46). This has been shown to lead to enrichment of embryonic stem (ES)/pluripotency genes and enhanced clonogenic growth of residual cells (46). Pre-exposure to the PI MG132 abrogated pomalidomide mediated loss of MBD3 and enrichment of ES genes; therefore concurrent use of

IMiDs and PIs may lead to synergistic effects by stopping the adverse effects of pomalidomide exposure on clonogenic growth of residual cells (46).

IMiDs are also being used in combination with immunotherapies. The POLLUX study showed that the addition of the monoclonal antibody daratumumab to lenalidomide and dexamethasone led to a significantly higher overall response rate, deeper responses, longer response durations (47) and prolonged PFS (48). Furthermore, the addition of IMiDs to treatment regimens of patients with daratumumab-refractory disease was shown to overcome resistance to both classes of drug (49). IMiDs are also being explored in combination with CAR-T therapies. There is a strong rationale for this approach as IMiDs enhance T cell proliferation and cytokine production via an interleukin (IL)-2 dependent mechanism (50). In addition, lenalidomide treatment has been shown to induce phosphorylation of CD28 (a co-stimulatory molecule of T cells), enhance the immunological synapse between CAR-T cells and their target tumour cells, increase IL-21 production and influence the balance of different T cell subsets (50).

## 1.2 Concepts of drug resistance in cancer

The well-established phenomenon of drug resistance describes a disease becoming tolerant to a pharmaceutical treatment. Just as bacteria can develop resistance to certain antibiotics, cancers can become resistant to a range of therapies. This can occur through several mechanisms including drug efflux, inhibition of DNA damage repair, cell death inhibition, changes in epithelial-mesenchymal transition, drug target alteration, drug inactivation or epigenetic changes (**Table 1-3**) (51). Another key concept is treatment leading to the enrichment of drug resistant cancer cells already present in the heterogeneous cancer cell population; a small proportion of cells may have unique stem cell properties and/or display drug resistance capabilities, enabling them to survive treatment and then expand (51).

<b>Drug resistance mechanism</b>	<b>Example</b>
Drug inactivation	Cytarabine (Ara-C) is a nucleoside drug that undergoes a three-step phosphorylation into the active metabolite Ara-C triphosphate. Down-regulation or mutations in this pathway can produce a decrease in the activation of cytarabine and lead to drug resistance.
Alteration of drug targets	Resistance to topoisomerase II-inhibiting drugs, such as amsacrine, can occur through mutations in the topoisomerase II gene.
Drug efflux	ATP-binding cassette transporters are found in the plasma membranes of healthy cells and stop toxins accumulating. Three members of this family, MDR1, MRP1 and BCRP, are implicated in many drug-resistant cancers; they have broad substrate specificity and can efflux many xenobiotics from cells.
DNA damage repair	The efficacy of DNA-damaging cytotoxic drugs depends on the failure of the cancer cell's DNA damage response (DDR) mechanisms. For example, platinum-containing drugs such as Cisplatin cause DNA crosslinks which can lead to apoptosis. However, resistance to these drugs often arises due to nucleotide excision repair and homologous recombination, which are the primary DDR mechanisms involved in reversing platinum damage.
Cell death inhibition	In many cancers BCL-2 family proteins, Akt and other anti-apoptotic proteins are highly expressed and down-stream transcription modulators such as NFκB and STAT are highly active, promoting cell survival.
Epithelial-Mesenchymal transition (EMT)	EMT, the mechanism by which solid tumors become metastatic, involves multiple processes including altered expression of receptors that influence cell-cell attachment and cell motility. In ERBB2 (HER2) positive breast cancer, tumours that express high levels of β1 integrins develop more resistance to antibody inhibitors such as trastuzumab.
Epigenetics	The DNA repair enzyme MGMT inhibits killing of tumour cells by alkylating chemotherapy agents. Melanoma cells can acquire resistance to fotemustine, and this has been associated with reactivation of MGMT secondary to changes in methylation of the <i>MGMT</i> gene.

*Table 1-3 Primary mechanisms of drug resistance in cancer cells.*

This table provides examples of the common mechanisms of drug resistance in cancer. Examples adapted from Housman *et al* (51). MRD1, Multiple Drug Resistance 1; MRP1, Multidrug Resistance Protein 1; BCRP, Breast Cancer Resistance Protein; BCL2, B cell Lymphoma 2; NFκB, Nuclear Factor Kappa B; STAT, Signal Transducer and Activator of Transcription; ERBB, Erb-B2 Receptor Tyrosine Kinase 2; MGMT, O-6-Methylguanine-DNA Methyltransferase.

## 1.3 An introduction to IMiDs/CELMoDs<sup>1</sup>

### 1.3.1 The development of IMiDs

IMiDs are a major class of drug treatment for myeloma. Thalidomide, the first-in-class IMiD, was synthesised in the 1950s and was found to be non-toxic in large doses in mice (52). In Europe and Canada it was sold without prescription and used as an anti-emetic and sleeping aid in pregnancy (52). However, there was a rapid increase in cases of babies born with phocomelia and it was withdrawn in 1961 (52). In the years that followed, thalidomide was found to have anti-inflammatory and anti-angiogenic properties and was used to treat inflammatory skin disorders such as lepromatous leprosy (53). In the 1990s, 5 patients with end-stage myeloma were treated with thalidomide on a compassionate use basis (52). One patient experienced a significant response and subsequently a phase II study was performed for patients with refractory disease. IMiDs in combination with dexamethasone were then investigated in newly diagnosed patients and became the standard of care at a time when treatment options for myeloma patients were very limited (52). Newer generation compounds were developed in the 2000s, including lenalidomide and then pomalidomide, which share common phthalimide and glutarimide moieties but have specific differences in the glutarimide ring (53).

### 1.3.2 The molecular target of IMiDs

Despite their demonstrated efficacy, the molecular target of IMiDs (and their mechanism of action as anti-myeloma agents) was not uncovered until the 2010s (34, 54). Work from several groups showed that IMiD activity against myeloma cells resulted from its ability to bind to a specific tri-tryptophan pocket of cereblon (CRBN), a substrate receptor of the cullin4-RING (CRL4) E3 ubiquitin ligase. Through acting as a molecular glue, a different set of proteins are designated for ubiquitination and subsequent degradation by the proteasome. In myeloma cells the critical neosubstrates are the B cell zinc-finger transcription factors Ikaros and Aiolos (34, 41, 55).

---

<sup>1</sup> Sections 1.3-1.5 are based on a review written as part of this PhD. Bird S, Pawlyn C. IMiD resistance in multiple myeloma: current understanding of the underpinning biology and clinical impact. *Blood*. 2023;142(2):131-40.

The rapid degradation of Ikaros and Aiolos is associated with decreased expression of IRF4 (Interferon Regulatory Factor 4) and c-MYC (MYC Proto-Oncogene, BHLH Transcription Factor), leading to growth inhibition and cell death (56). Both Ikaros and Aiolos belong to the Cys2-His2 zinc-finger protein family (57) and presence of this motif has also been found in subsequently identified IMiD neosubstrates such as Zinc-Finger Protein 91 (ZFP91) (58). The CRL4<sup>CRBN</sup> E3 ubiquitin ligase is maintained by the COP9 signalosome, a multiprotein complex that regulates cullin ring ubiquitin ligases by removing their activator NEDD8 (Neural Precursor Cell Expressed, Developmentally Down-Regulated Protein 8) (59) (**Figure 1-2**). In addition to its well-established role as a ubiquitin ligase for protein degradation, CRBN may also have other functions such as promoting maturation of proteins (60) and acting as a co-chaperone for Heat Shock Protein 90 (HSP90) (61).

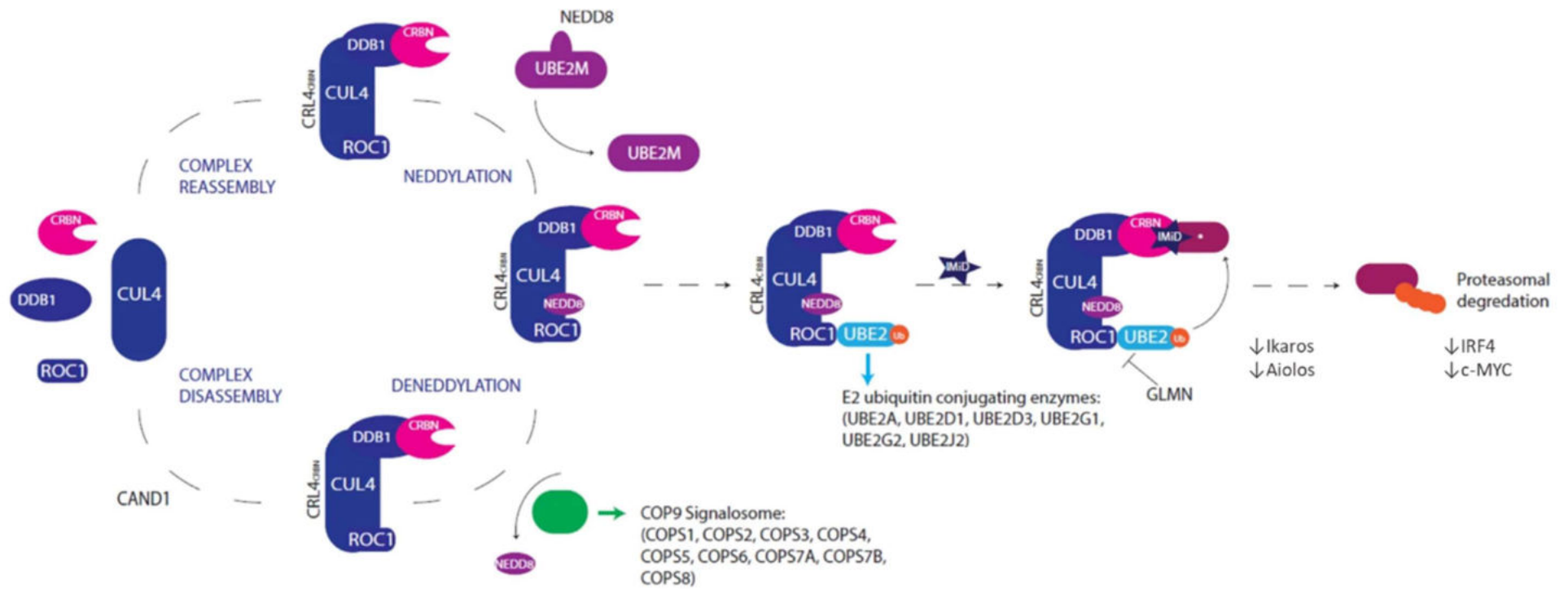


Figure 1-2 Components of the CRL4<sup>CRBN</sup> E3 ubiquitin ligase complex, COP9 signalosome and Ikaros/Aiolos/IRF4 axis.

Figure taken from Bird *et al* (62), which was adapted from Jones *et al* (63).



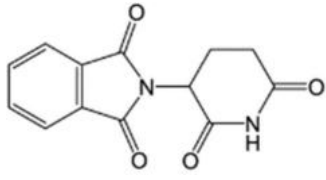
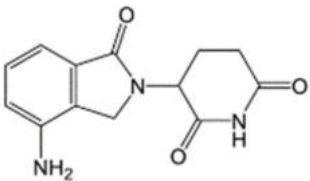
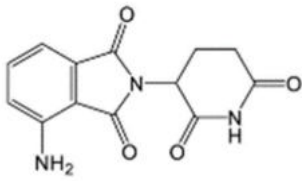
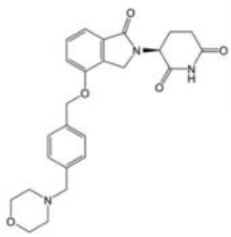
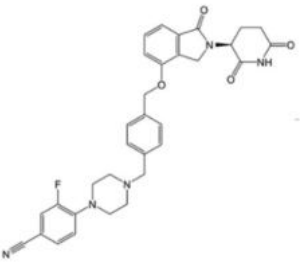
### 1.3.3 IMiD anti-myeloma activity

Direct IMiD-induced myeloma cell toxicity has been linked to a number of mechanisms in addition to decreased IRF4 and c-MYC, including inhibition of NFκB signalling, activation of caspases, increased expression of pro-apoptotic factors, decreased expression of anti-apoptotic factors and disruption of the phosphatidylinositol 3-kinase/protein kinase B (PI3K/PKB) signalling pathway (53). IMiDs also affect the interaction of myeloma cells with several components of the BM niche and have broad immunomodulatory effects including increased T cell priming, increased activity of natural killer (NK) and NK T cells and inhibition of T regulatory cells (53, 64). IMiD treatment leads to upregulation of interleukin-2 (IL-2) in T cells and interferon gamma (IFNγ) in NK cells and this is associated with the degradation of Ikaros and Aiolos, which are thought to act as transcriptional repressors in this cellular context (65). The action of IL-2 and IFNγ in the microenvironment leads to further immune cell expansion and immune-mediated myeloma cell destruction (65). IMiDs also have broad anti-angiogenesis effects associated with inhibition of Fibroblast Growth Factor 2 (FGF2) (53).

### 1.3.4 The development of CELMoDs

Further advancements in understanding the mechanism of action of CRBN binders led to the development of next generation cereblon E3 ligase modulators (CELMoDs), for example iberdomide (CC-220) and mezigdomide (CC-92480). CELMoDs are larger molecules with a higher CRBN binding affinity (66) and a different spectrum of neosubstrate degradation compared to IMiDs (**Table 1-4**). Patients who have become refractory to an earlier generation IMiD may respond to a later generation IMiD or CELMoD. For example, approximately one-third of patients who have become resistant to lenalidomide therapy still respond to pomalidomide (67). A recent analysis of the OPTIMISMM trial showed that in patients who had previously received lenalidomide, the combination of pomalidomide, bortezomib and dexamethasone (PVd) led to a significantly prolonged PFS compared with bortezomib and dexamethasone (Vd) alone (median 22.0 months versus 13.1 months,  $p = 0.03$ ) (68). Patients refractory to lenalidomide and pomalidomide can also respond to iberdomide and mezigdomide (69-71); a phase 1/2 trial of iberdomide in nearly 200 patients who

had received  $\geq 2$  prior lines of therapy, including lenalidomide or pomalidomide and a PI, found an overall response rate of  $\sim 30\%$  (72).

IMiD/CELMoD	Structure	Reported neosubstrates in myeloma cells	Cereblon-binding affinity IC <sub>50</sub> (μM)
Thalidomide		Ikaros, Aiolos, PLZF, RNF166, SALL4, TP63, ZFP91, ZNF276, ZNF653, ZNF692, ZNF827	
Lenalidomide		Ikaros, Aiolos, CK1α, FAM83F, RAB28, RNF166, SALL4, WIZ, ZFP91, ZNF276, ZNF653, ZNF692, ZNF827	1.5
Pomalidomide		Ikaros, Aiolos, ARID2, DTWD1, E4F1, FAM83F, GZF1, PATZ1, PLZF, RAB28, RNF166, SALL4, ZBTB39, ZFP91, ZNF98, ZNF198, ZNF276, ZNF517, ZNF582, ZNF653, ZNF654, ZNF692, ZNF787, ZNF827	1.2
Iberdomide		Ikaros, Aiolos, IKZF2, IKZF4, ZFP91, ZNF653, ZNF98, ZNF827	0.06
Mezigdomide		Ikaros, Aiolos, ZFP91	0.03

*Table 1-4 IMiDs/CELMoDs currently used in clinical practice.*

Table shows structure, known neosubstrates and IC<sub>50</sub> (as evaluated by protein competitive binding assay - displacing a Cy-5-labelled cereblon binding compound from CRBN). IC<sub>50</sub>, 50% inhibitory concentration. Table taken from Bird *et al* (62).

### **1.3.5 Response to sequential generations of IMiDs/CELMoDs**

The reasons underpinning response to sequential generations of IMiDs may relate to several factors. Over time, a reduction in the level of CRBN in malignant plasma cells commonly occurs (73, 74); longitudinal analysis of BM biopsy samples frequently shows decreased CRBN mRNA and protein levels in patients who acquire lenalidomide resistance (74). A CRBN binder with a higher binding affinity may be able to better 'utilise' the remaining CRBN to degrade neosubstrates and overcome resistance in the low CRBN state (66). Importantly, it is the function of IMiDs as molecular glues that enables this phenomenon; 1 IMiD molecule binds to 1 CRBN molecule but this can lead to the degradation of multiple neosubstrate molecules, amplifying the effect of very low levels of CRBN. In addition, CELMoDs are larger in size than IMiDs and this may increase physical interactions with CRBN (66). Furthermore, each CRBN binder may exhibit certain differences in the neosubstrate profile (75). For example, lenalidomide is the only IMiD that has clinical benefit in deletion 5q myelodysplastic syndrome (del 5q MDS) (76). Casein Kinase 1 Alpha (CK1 $\alpha$ ) is a unique neosubstrate of lenalidomide, and in the CK1 $\alpha$  haploinsufficient state present in del 5q MDS, further CRBN-mediated degradation of CK1 $\alpha$  leads to cell death by activation of p53 (76).

### **1.3.6 The use of IMiDs/CELMoDs in other malignancies**

Understanding the generation of resistance to IMiDs, and finding ways to target it, may also prove useful in the treatment of other malignancies. Lenalidomide has been shown to have efficacy, both as a single agent and in combination therapies, in chronic lymphocytic leukaemia (CLL) and several non-Hodgkin lymphomas (77). Furthermore, avadomide (CC-122) has potent anti-tumour and tumour microenvironment immunomodulatory effects in diffuse large B cell lymphoma (DLBCL) and there is early evidence of clinical efficacy (77, 78).

The mechanism of action of IMiDs has been exploited to develop additional molecular glues and also proteolysis-targeting chimeras (PROTACs), heterobifunctional molecules composed of two active domains and a linker which can induce degradation of a target protein via the ubiquitin-proteasome system (79). Targeted protein degradation has a large range of exciting therapeutic and experimental applications. For example, CAR-T therapy is increasingly being

used as a treatment for haematological malignancies but there is a risk of uncontrolled CAR-T cell activity which can lead to cytokine release syndrome (80). This has led to the development of on and off switches for CAR-T cells using degradation technology. For example, Jan *et al* developed degradation tags with enhanced sensitivity to lenalidomide to generate degradable CARs and also created a lenalidomide-inducible dimerization system to develop split CARs that require both lenalidomide and target antigen for activation (81).

## 1.4 Mechanisms of IMiD/CELMoD resistance

### 1.4.1 Concepts of resistance

Conceptually, IMiD resistance can be divided into factors intrinsic to the myeloma cell and extrinsic factors in the tumour microenvironment (**Figure 1-3**). Low CRBN protein levels are commonly, but not universally, seen in the resistant setting, including certain cell line models (82), mouse models (83) and patient samples (74). Decreased CRBN may be associated with genetic alteration, but alternative drivers of the low CRBN state and other mechanisms of resistance are currently not well understood. Given the mechanism of IMiD action, alterations in the CRL4<sup>CRBN</sup> E3 ubiquitin ligase complex, the COP9 signalosome and the Ikaros/Aiolos/IRF4 axis are likely targets for the generation of resistance (3). Indeed, genome wide CRISPR-Cas9 screens have identified CRBN and the proteins that directly regulate its expression and function as involved in IMiD resistance (84, 85). Similarly, a genome wide CRISPR study exploring resistance to PROTACs operating via CRBN found that the top individual loss of function events were those that disrupted the degradation machinery itself (86).

Resistance may also be generated by changes in the tumour microenvironment and could include failure of the usual function of IMiDs on immune cells including T cells and NK cells (65).

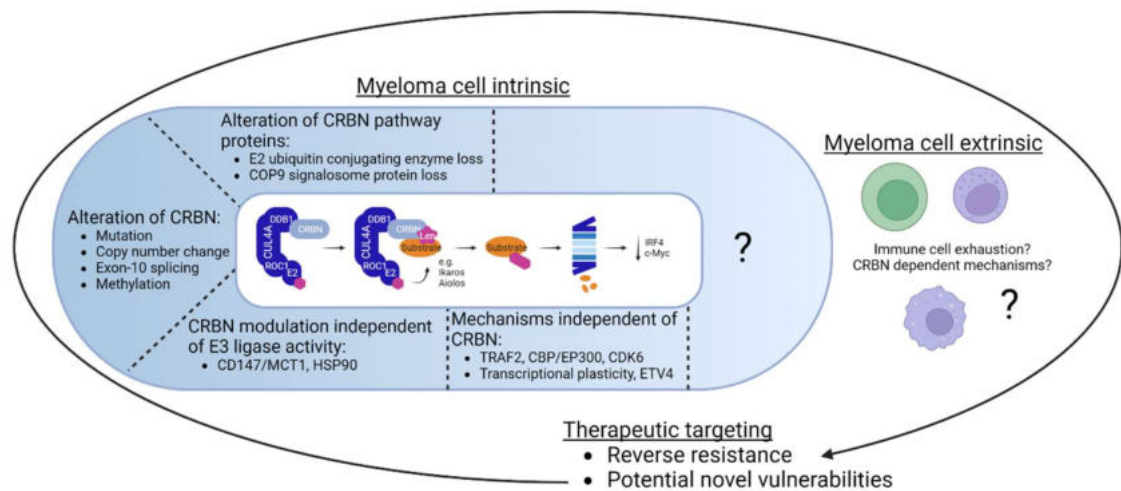


Figure 1-3 Concepts of IMiD resistance.

IMiD resistance can be divided into myeloma cell intrinsic factors and myeloma cell extrinsic factors. Myeloma cell intrinsic factors include genetic alteration of *CRBN* (including mutations, copy number changes and differential splicing), alterations of the E2 ubiquitin conjugating enzymes and the COP9 signalosome, and transcriptional plasticity. There are also changes in the tumour microenvironment, for example immune cell exhaustion. To target IMiD resistance we can consider reversing resistance or exploiting potential vulnerabilities that may develop alongside the generation of resistance. Figure taken from Bird *et al* (62).

#### 1.4.2 Myeloma cell intrinsic mechanisms of resistance

##### **Resistance associated with alteration of *CRBN***

Point mutations in *CRBN* are rare in patients with newly diagnosed myeloma (<1%) (87) but this increases to around 12% in patients treated with IMiDs (88). Select *CRBN* mutations found in patients have been modelled in the OCI-MY5 cell line (characterised by low expression of *CRBN* and IMiD resistance) (88). OCI-MY5 cells transduced with wild-type *CRBN* gained lenalidomide sensitivity, whereas those transduced with vectors containing *CRBN* mutants or empty vector remained resistant (88, 89).

A recent study performed whole genome sequencing and RNA sequencing on samples from patients with newly diagnosed, lenalidomide-refractory and pomalidomide-refractory myeloma to further explore the incidence of *CRBN* alterations, specifically in the IMiD refractory setting (90). Genetic alteration of *CRBN* occurred in nearly 30% of patients with relapsed/refractory myeloma if mutations, copy loss/structural variations and high exon-10 spliced *CRBN* transcripts were considered together (90). The splice variant lacking exon-10 is translated into a stable protein that can still bind to DDB1 (Damage Specific DNA Binding Protein 1)/CUL4A (Cullin 4A) but can no longer interact with IMiDs. In myeloma cell line models, high exon-10 splicing of *CRBN* was sufficient to stop

lenalidomide cytotoxicity (91). These genetic changes were associated with inferior outcomes with pomalidomide-based regimes in those already refractory to lenalidomide (90).

CRBN expression may also be controlled through epigenetic mechanisms. For example, deep bisulfite sequencing to evaluate CpG methylation at the single DNA molecule resolution was used to assess the role of promoter methylation in drug resistance in primary myeloma tumour samples (92). High levels of methylation in the *CRBN* promoter flanking region was found in 18 out of 27 samples from patients with IMiD resistance but in none of the matched control samples (92).

There are also several cell line models of acquired IMiD resistance which show decreased CRBN protein expression of unclear aetiology. Understanding how resistance is generated in these cases is important to allow identification of new mechanisms of resistance which can then be evaluated in patients. It is sometimes difficult to assess whether changes identified in the IMiD-resistant state are the *cause* or the *effect* of IMiD resistance, but either way they may represent useful targets. For example, acquired lenalidomide and pomalidomide resistant cell lines were created from two initially IMiD-sensitive cell lines (OPM2 and H929) by taking cells and culturing them with low doses of IMiDs over a period of several weeks (93). Both cell lines had low CRBN levels, genome wide increases in DNA methylation, and reductions in chromatin accessibility and gene expression (93). Furthermore, SMAD Family Member 3 (SMAD3) was identified as a commonly downregulated gene (93). The team showed that a combination of 5-azacytidine and the EZH2 inhibitor EPZ-6438 restored the observed accessibility changes, as well as SMAD3 expression, and re-sensitised the resistant cells to IMiDs (93). There is also early data supporting the presence of synergy between EZH2 inhibitors and pomalidomide in both in vitro and in vivo models (94).

A reduction in functional CRBN is also important because substrates have been shown to compete for access to it (75). A zinc-finger protein gene (*ZNF692*) was mutated such that the resultant protein could interact with CRBN but could not be degraded. This construct was expressed in the IMiD-sensitive MM1s cell line and resistance to lenalidomide was induced (75). Conversely, decreased levels of

non-essential substrates were shown to sensitise cells to lenalidomide (75). Therefore, in a given cell type the efficacy of an IMiD/CELMoD may be influenced by both the level of CRBN expression and the levels of alternative substrates (75).

### ***Resistance associated with alteration of CRBN pathway proteins***

In samples from patients, point mutations (88, 89) and copy number loss (95, 96) have been observed in CRBN pathway members. When compared to patients with newly diagnosed myeloma, those with IMiD-resistant disease show an increase in mutations in *Ikaros*, *Aiolos*, *IRF4* and *Cullin 4B (CUL4B)* (to ~10%) (88, 89). Four *Ikaros* mutations observed in patients have been modelled in cell lines and only those affecting the *Ikaros* degron sequence were found to induce IMiD resistance (89). A *CUL4B* knockout has been performed in IMiD-sensitive L363 cells and the knockout was more resistant to lenalidomide treatment, as confirmed by a clonal competition assay (89). Copy number loss is also likely to be important; the 2q37 chromosome region contains the COP9 signalosome members *COPS7B* and *COPS8* and copy loss here is significantly enriched between newly diagnosed patients (incidence 5.5%), lenalidomide refractory patients (incidence 10%) and lenalidomide-then-pomalidomide refractory states (incidence 16.4%) (95).

Modulators of the CRBN and *Ikaros/Aiolos/IRF4* axis may also be involved in the generation of resistance. For example, Runt-Related Transcription Factor 1 (*RUNX1*) and *RUNX3* compete with CRBN to bind to *Ikaros* and *Aiolos*, thus preventing their degradation (97). Inhibition of *RUNX1/3*, via genetic manipulation or small molecule, led to reversal of lenalidomide resistance in both myeloma cell lines and samples from patients (97).

Translocations involving the immunoglobulin  $\lambda$  (IgL) locus confer poor prognosis and it has been shown that *Ikaros* binds to the IgL enhancer at high levels (98). Data from the CoMMpaSS study (NCT01454297) showed that patients with t(IgL) had poor PFS and OS regardless of whether they received IMiD-containing therapy or not, in contrast to patients with non-t(IgL) disease who derived a clear benefit. This data suggests t(IgL) can lead to IMiD resistance, perhaps because the high level of bound *Ikaros* makes the locus relatively insensitive to IMiD-based depletion of *Ikaros* (98).



### ***Resistance associated with CRBN but independent of CRL4<sup>CRBN</sup> E3 ubiquitin ligase activity***

CRBN has been suggested to have important functions independent from its role in protein degradation. CRBN has been shown to promote the maturation of CD147 and Monocarboxylase Transporter 1 (MCT1) proteins, allowing the formation of an active CD147-MCT1 transmembrane complex, which promotes angiogenesis, proliferation, invasion, and lactate export (60). IMiDs outcompete CRBN binding to CD147 and MCT1, leading to mislocalisation and destabilisation of the complex (60). IMiD-sensitive myeloma cells lose CD147 and MCT1 expression, whereas IMiD-resistant cells retain their expression (60). A combination of cell-surface proteomics and functional CRBN interactome screens has shown that CRBN determines the chaperone activity of HSP90 by antagonising AHA1 (Activator of HSP90 ATPase Activity 1), and IMiDs disrupt the interaction of CRBN with HSP90 (61). One of the possible clients of the CRBN-AHA1-HSP90 axis is the amino acid transporter LAT1/CD98hc, which becomes destabilised and inactivated on IMiD treatment (61). Persistence of LAT1/CD98hc may be associated with resistance to IMiD treatment (61).

### ***Resistance independent of CRBN and its related proteins***

Although low CRBN expression often correlates with resistance, some samples from patients and myeloma cell lines show resistance to IMiDs despite normal CRBN levels and without currently identified genetic abnormalities in *CRBN* or its associated proteins (99). Resistance may be caused by activation of alternative signalling pathways that could upregulate IRF4, c-MYC or other pro-survival pathways (99).

A genome wide knockout CRISPR-Cas9 screen in the IMiD-sensitive cell line MM1s was performed in cells cultured with pomalidomide to allow identification of genes that when inactivated diminish the effects of IMiDs (84). Guide RNAs (gRNAs) targeting TNF Receptor-Associated Factor 2 (*TRAF2*) were enriched after IMiD selection and *TRAF2* knockout MM1s cells showed significant resistance to lenalidomide and pomalidomide treatment (100). *TRAF2* knockout had no effect on CRBN expression and there was persistent Ikaros and Aiolos degradation and reduction of IRF4 in response to IMiD treatment (100). *TRAF2* knockout cells showed strong activation of the non-canonical NFκB pathway and

the Extracellular Signal-Regulated Kinase (ERK) pathway and in vitro and in vivo murine xenograft studies showed that the Mitogen-Activated Protein Kinase Kinase (MEK) inhibitor AZD6244 could overcome IMiDs resistance in *TRAF2* knockout myeloma cells (100).

Further examples of IMiD resistance without low *CRBN* levels come from acquired IMiD-resistant cell line models. The XG1 myeloma cell line was cultured with low doses of lenalidomide to create the lenalidomide resistant line XG1LenRes (which displayed no genetic changes in *CRBN*) (101). XG1LenRes showed constitutive STAT3 (Signal Transducer And Activator of Transcription 3) activation and selective STAT3 inhibition led to re-sensitisation of the cell line to lenalidomide (101). The XG1LenRes cells also expressed a truncated *IRF4* that was not downregulated by lenalidomide. The IRF4/c-MYC axis was targeted with a selective inhibitor of CBP/EP300 (CREB binding protein/E1A Binding Protein P300) which directly suppresses *IRF4*, and this compound restored lenalidomide response in the XG1LenRes cells (101).

Transcriptional plasticity, with the expression of extra-lineage transcription factors, may also be important in the development of IMiD resistance. Resistance to IMiDs and loss of c-MYC repression can occur despite continued Ikaros and Aiolo degradation (102). Ikaros, Bromodomain Containing 4 (BRD4), lysine acetyl transferase P300 and Mediator Complex Subunit 1 (MED1) have been shown to colocalise within the myeloma genome (102). In the IMiD-sensitive cell line MM1s, exposure to lenalidomide reduced Ikaros, BRD4, P300 and MED1 at enhancer loci. However, in the resistant cell line RPMI8226, Ikaros was displaced but BRD4, P300 and MED1 were retained (102). A computational analysis showed strong enrichment of the GGAA motif, which is recognised by the Erythroblast Transformation Specific (ETS) family of transcription factors, at enhancers co-occupied by Ikaros and BRD4 (102). The ETS family transcription factor ETV4 (ETS Variant Transcription Factor 4) was expressed in IMiD-resistant but not IMiD-sensitive cell lines (102). Lenalidomide treatment induced global depletion of Ikaros but not ETV4 at BRD4-occupied enhancers in resistant cell lines (102). Knockout of *ETV4* in RPMI8226 cells sensitised them to lenalidomide, with c-MYC downregulation and cell death (102).

Although cell line models have provided useful insights into resistance generation, evaluation of patient samples is critical. Proteome analysis is particularly key because of the effect of IMiDs on protein degradation, but limited proteomic datasets are available to date. Proteomic and phosphoproteomic analysis was performed in 5 paired patient samples, pre-treatment and relapse on IMiD therapy (103). These patients did not show significantly reduced CRBN levels at relapse but did show an increase in Cyclin Dependent Kinase 6 (CDK6) (103). Overexpression of CDK6 in IMiD-sensitive myeloma cell lines led to reduced IMiD sensitivity and CDK6 inhibition (by palbociclib or degradation via a PROTAC) was found to be highly synergistic with IMiDs in vitro and in an MM1s xenograft mouse model (103).

### **1.4.3 Myeloma cell extrinsic mechanisms of resistance**

IMiDs and CELMoDs lead to profound changes in the composition and activity of immune cells in the microenvironment but resistance in this context needs further study. IMiD treatment leads to increased T cell proliferation, IL-2 and IFN- $\gamma$  secretion and NK and NKT cell activation (65). IMiDs also inhibit IL-6 production from monocytes and macrophages (65). However, IMiDs can lead to inhibitory immune responses, including increased T regulatory cells and myeloid derived suppressor cells (65). This may play a role in immune escape, although some studies reporting changes in these immune populations are in the context of combination treatment with IMiD and the immunosuppressive steroid dexamethasone (65). A loss of the IMiD induced IFN response in resistant myeloma cells may also contribute to immune escape; genes with a key role in modulating IFN response (including *NLRP4* (NLR Family Pyrin Domain Containing 4) and *NFKBIZ* (NFKB Inhibitor Zeta)) were differentially expressed in samples from patients who had developed resistance to lenalidomide compared to those who remained sensitive (104).

Mass cytometry before and after treatment with the CELMoD iberdomide has been used to evaluate T, B and NK cell subpopulations in the BM aspirates of 99 patients with heavily pre-treated disease (105). Treatment with iberdomide was associated with significant increases in effector T and NK cells, demonstrating innate and adaptive immune enhancement (105). In patients relapsing after prior therapy (including IMiDs), an increase in the markers of immune cell exhaustion

has been identified, including upregulation of Programmed Cell Death Protein 1 (PD-1) on the surface of T cells (65, 106, 107). These changes suggest an element of IMiD resistance may be related to immune cell exhaustion (65).

One mechanism to overcome the phenomenon of exhaustion in the clinic is the addition of the anti-CD38 antibody daratumumab, which enhances the adaptive immune response and contributes to enhanced efficacy in combination with IMiDs (108, 109). For example, the combination of daratumumab, lenalidomide and dexamethasone (DRd) led to an increased proportion of effector memory T cells, reduced immunosuppressive T regulatory cells and increased T cell repertoire clonality compared to lenalidomide and dexamethasone (Rd) alone (110). These combinations are now widely used in the clinic. Changes within key immune cell populations has also been assessed in the context of treatment with pomalidomide, daratumumab and low dose dexamethasone (POM-DARA-loDEX) (111). Although the effect of the individual agents is difficult to differentiate in the absence of single-agent treatment arms, there appeared to be reduction in absolute NK and B cell numbers, in keeping with the reported mechanism of action of daratumumab (111). In contrast, the proportion of activated and proliferating NK cells and CD8+ T cells increased with treatment, which correlated with the pomalidomide dosing schedule (111). Similar changes were observed in patients with lenalidomide-refractory disease, highlighting the importance of combining distinct therapeutic modalities in the treatment of relapsed myeloma but also the potential use of later generation IMiDs/CELMoDs in patients who are refractory to earlier generation compounds (111).

An alternative approach is to alter the function of checkpoints that regulate T cell function. PD-1 is an immunosuppressive protein critical to regulating immune system responses and its ligand PD-L1 is overexpressed on myeloma cells, leading to reduced proliferation of PD-1 positive T cells (112). The PD-1 inhibitor pembrolizumab was studied in early phase trials in combination with lenalidomide and showed good response rates (113). However, the phase 3 KEYNOTE 183 (114) and 185 (115) IMiD/pembrolizumab combination trials were stopped prematurely by the United States Food and Drug Administration because of a higher than expected number of deaths in the intervention arms.

## 1.5 Targeting the IMiD/CELMoD resistant state

### 1.5.1 Further exploration of resistance mechanisms

#### *Cell line models, drug screens and ex vivo primary samples*

The exploration of resistance generation has often been performed in cell line models due to the difficulty of keeping primary myeloma cells in culture for a prolonged period. Myeloma cell lines display differing levels of sensitivity to IMiD treatment, and these distinctions are not binary, with dose and time-course dependent responses (116). Several teams have generated lines with acquired resistance (82, 93, 116), which can then be explored through genetic sequencing, RNA-Seq analysis, whole proteome analysis, or more targeted approaches.

Cell line models have also allowed knockout genome wide CRISPR-Cas9 screens to be performed. As discussed earlier, the forward screens conducted to date predominately identified direct regulators of the degradation mechanism as important in IMiD resistance, as opposed to resistance pathways independent of CRBN. The opposite approach, genome wide CRISPR screening myeloma cells with acquired IMiD resistance, can be performed to identify genes that may reinduce sensitivity when knocked out. From one such screen DNA Topoisomerase II  $\beta$  (TOP2B) was identified as a putative candidate (117). CRISPR screening approaches could also be used to detect novel vulnerabilities in the acquired resistant setting, which may represent synthetic lethal targets in the low CRBN state.

Cell lines with acquired resistance have also been used in drug screening efforts to find more potent CRBN binders that may be able to overcome resistance to existing IMiDs/CELMoDs. Mezigdomide was discovered through a phenotypic screen of a CRBN modulator library in H929 with acquired resistance to lenalidomide (which had low levels of CRBN) (118, 119). Primary myeloma samples cannot be used for such large scale drug screens but efforts to maintain myeloma cell viability ex vivo, such as the myeloma drug sensitivity testing (My-DST) system, may help overcome this (120).

#### *Biomarkers of sensitivity and resistance*

Well validated biomarkers of sensitivity and resistance to IMiDs would be useful for prognosis and monitoring disease in the clinic. Furthermore, such biomarkers

could improve our understanding of the biology of IMiD resistance and provide potential future drug targets. Increased *CRBN* gene expression was significantly associated with longer PFS among 96 patients who received maintenance with thalidomide as part of the HOVON-65/GMMG-HD4 trial (121). However, there was no association between *CRBN* expression and survival in the bortezomib maintenance arm of the trial, suggesting an IMiD-specific effect (121). Several studies have also shown that a high level of CRBN protein expression is associated with good prognosis in patients treated with IMiDs (116, 122) but whether Ikaros, Aiolos and IRF4 expression correlates with IMiD response is not completely clear (99, 123, 124). As discussed previously, reduced abundance of CRBN, *CRBN* methylation changes and genetic alterations in *CRBN* (and CRBN pathway genes) have been identified in samples from patients relapsing on IMiDs. However, whether these changes can be used as predictive biomarkers of response is not certain. Data from the Myeloma XI trial also showed that mutations in *IRF4* and Early Growth Factor Response 1 (*EGFR1*) were associated with favourable OS in this IMiD-treated patient population (125) and the possible mechanisms behind this are being investigated.

Exploration of the myeloma cell surface proteome (the surfaceome), which determines malignant cell interaction with the BM microenvironment, has been carried out using glycoprotein cell surface capture (CSC) proteomics. The surfaceome was evaluated at baseline, in drug resistance and in response to acute drug treatment in OPM2 and H929 cell lines with acquired lenalidomide resistance (126). There was a common signature of increased CD33 and CD45 in resistance which, if validated, could potentially be used as a biomarker of resistance (126).

### **1.5.2 Overcoming resistance in the clinical setting**

Targeted approaches are needed in the clinic to improve outcomes for patients who are resistant to IMiDs. Based on the body of data described above, these can be divided into those aiming to overcome resistance whilst still targeting CRBN or those exploiting the IMiD-resistant state, by reversing resistance or by synthetic lethality. As discussed previously, newer generation IMiDs/CELMoDs may be able to overcome resistance to early generation compounds (99, 127). Several CELMoDs are currently in clinical trials, with iberdomide and

mezigdomide now moving into phase 3 trials (71, 72). In patients with *CRBN* mutations, it is important to understand whether a given mutation is likely to lead to resistance to selected IMiDs/CELMODs or all IMiDs/CELMoDs (as well as potential novel *CRBN*-directed glues and PROTACs). In patients with low *CRBN* levels, stronger binders may be able to use the lower levels of *CRBN* or stabilise *CRBN*. Recently, a new class of related compounds, known as monofunctional degradation activating compounds (MonoDACs) have been developed and entered into early phase trials (128). The MonoDAC CFT7455 was developed to induce potent, rapid and sustained degradation of Ikaros and Aiolos and have a high binding affinity to *CRBN*, in an attempt to overcome IMiD resistance (128). In comparison with mezigdomide, CFT7455 had different pharmacokinetics and pharmacodynamics that led to longer exposure, and it demonstrated superior efficacy in an H929 myeloma xenograft mouse model (128). In an open-label, multicentre, phase 1/2 clinical trial (NCT04756726) that included patients who were heavily pre-treated, early pharmacodynamic data showed deep degradation of Ikaros and Aiolos and evidence of single-agent activity (128).

Exploiting the IMiD-resistant state requires a different approach. Several novel pathways and their associated small molecule inhibitors have been discussed. The most promising, based on current data, are those targeting the MEK pathway (100), extra-lineage transcription factors such as ETV4 (102), and epigenetic regulators such as CBP/EP300 (101) and EZH2 (94).

## 1.6 Rationale and hypothesis

The generation of IMiD resistance is a critical challenge in the management of myeloma and although our understanding is growing there are still many unanswered questions. Even as the variety of myeloma therapeutics expands, for example the rapid adoption of T cell redirection therapies, IMiDs continue to be used in therapeutic combinations throughout the disease course and understanding resistance remains central to improving patient outcomes.

I hypothesise that generating myeloma cell line models with acquired IMiD/CELMoD resistance and interrogating these models with multiomics analyses will help us to uncover novel mechanisms of resistance generation and develop new ways to treat resistant disease.

## 1.7 Aims and objectives

My aim was to further our understanding of the generation of resistance to IMiDs and CELMoDs and find ways to treat resistant disease.

### 1.7.1 Objective 1: Generation and characterisation of cell line models of acquired IMiD/CELMoD-resistant disease

I developed and characterised cell line models of acquired IMiD/CELMoD-resistance by taking initially sensitive human myeloma cell lines and exposing them to low doses of IMiDs/CELMoDs over several weeks. Once resistant these cell lines were explored by whole exome sequencing, RNA-Seq and whole proteome analysis. Whilst cell line models of acquired resistance have previously been generated by other teams, I developed a large range of resistant models to enable me to look for commonalities. There is also limited proteomic and phosphoproteomic data in the literature exploring resistant cell line models. This work is the focus of Chapter 3.

### 1.7.2 Objective 2: Compound screening in an IMiD/CELMoD-resistant cell line

To identify pharmacological vulnerabilities that may develop alongside the acquisition of IMiD/CELMoD-resistance, I performed a compound screen in an IMiD/CELMoD-resistant cell line. Novel CELMoDs have been discovered through drug screens using cell lines with acquired IMiD resistance; for example mezigdomide was found in a phenotypic screen of a CRBN modulator library in H929 with acquired resistance to lenalidomide (118). However, drug screens of compounds targeting other pathways are limited. I therefore performed a drug screen using a library containing compounds which covered a broad range of signalling pathways known to be important in cancer development. The screen was carried out in a cell line with resistance to iberdomide which is a novel CELMoD currently in clinical trial. The screen will be discussed in Chapter 4.

### 1.7.3 Objective 3: Genome wide CRISPR screening in an IMiD/CELMoD-resistant cell line

I performed a genome wide knockout CRISPR screen in an IMiD/CELMoD-resistant cell line. The screen had two arms; in one arm the resistant line was treated with DMSO and in the other the resistant line was treated with



IMiD/CELMoD. This allowed me to uncover genes that when knocked out might lead to re-induction of sensitivity to IMiDs. In addition, I compared the effect on 'fitness' of knocking out a gene in the resistant cell line compared to the parental cell line (using publicly available data from DepMap). This allowed me to explore novel genetic vulnerabilities specific to, or enhanced in, the IMiD/CELMoD-resistant state. I performed this screen in a cell line with resistance to iberdomide (a novel CELMoD) and this will be discussed in Chapter 5.

#### **1.7.4 Objective 4: Validation of pathways and targets identified in objectives 1-3 in cell line models and patient samples**

Potential pathways and targets identified in the former objectives were then explored further in the cell line models and patient samples. Chapter 6 focuses on SET2 inhibition in IMiD/CELMoD resistance and Chapter 7 focuses on changes in lipid metabolism in the IMiD/CELMoD-resistant state.

## Chapter 2      Methods

---

### 2.1    General methods

#### 2.1.1   Cell lines and cell culture

Myeloma cells lines (MM1s and H929) were grown in RPMI1640 media containing GlutaMax (Gibco, Life Technologies) supplemented with 10% heat-inactivated fetal bovine serum (FBS, Gibco) and penicillin-streptomycin (Sigma). HEK293 cells were grown in DMEM media (Gibco, Life Technologies) supplemented with 10% FBS and penicillin-streptomycin. Cells were cultured at 37°C in a humidified gas chamber with 95% air and 5% carbon dioxide. Cell identity was confirmed using short tandem repeat (STR) typing (Eurofins), and cells were negative for mycoplasma (Mycoplasma Detection Kit, InvivoGen). Cells were counted by trypan blue exclusion assay using a haemocytometer or a Countess 3 FL Automated Cell Counter.

Resistant cell lines (Len-R-MM1s, Pom-R-MM1s, Iber-R-MM1s, Len-R-H929, Pom-R-H929, Iber-R-H929) were kept in culture with a low dose of their respective IMiD/CELMoD. Len-R-MM1s and Len-R-H929 were cultured with a final concentration of 1µM lenalidomide, Pom-R-MM1s with a final concentration of 0.1µM pomalidomide, Pom-R-H929 with a final concentration of 1µM pomalidomide and Iber-R-MM1s and Iber-R-H929 with a final concentration of 0.01µM iberdomide.

#### 2.1.2   Compounds

The compounds used in this thesis (except for those tested in the compound screen) are shown in the table below (**Table 2-1**).

Compound	Manufacturer
IMiDs/CELMoDs (lenalidomide, pomalidomide, iberdomide, mezigdomide)	ICR Cancer Therapeutics Unit Chemistry Department
A939572	Sigma Chemicals
Blasticidin	InvivoGen
Bortezomib	Cayman Chemical
CC-885	ICR Cancer Therapeutics Unit Chemistry Department
EPZ-719	ICR Cancer Therapeutics Unit Chemistry Department and MedChemExpress
EMZ0414	Advanced ChemBlocks
GSK1940029	MedChemExpress
Hygromycin	Sigma Chemicals
Lometrexol	Sigma Chemicals
Opaganib	Selleck Chemicals
PF-429242	MedChemExpress
Polybrene	Sigma Chemicals
Puromycin	InvivoGen
RGFP966	Cayman Chemical
SM-164	MedChemExpress
STM2457	MedChemExpress

*Table 2-1 Frequently used compounds.*

Compounds used in this thesis with manufacturer details.

### 2.1.3 EC50 assays

EC50 assays were performed in 96 well plates with serial dilutions of drug. Viability was measured using CellTiter-Blue (Promega) at a concentration of 1 in 100. Plates were incubated for 3 hours at 37°C and read on an Envision or Tecan plate reader (fluorescence excitation wavelength 544nm and fluorescence emission wavelength 590nm).

### 2.1.4 RNA extraction

Cells were spun down in a microfuge at 400 RCF for 5 minutes at 4°C. Supernatant was removed, and the pellet re-suspended in  $\beta$ -mercaptoethanol:RLT (ratio 10 $\mu$ L:1ml). For 1.5x10<sup>6</sup> cells, 350 $\mu$ L of  $\beta$ -mercaptoethanol:RLT was used. Samples were vortexed for 30 seconds and RNA extracted using the RNeasy Plus Mini Kit (Qiagen 74134) with a

QIASHredder (Qiagen 79656), according to the manufacturer's instructions. Samples were quantified using a Nanodrop and stored at -80°C.

### 2.1.5 Reverse transcription

Reverse transcription was performed using Applied Biosystems High-Capacity cDNA Reverse Transcription Kit (Thermo Fisher Scientific 4368814) as per the manufacturer's instructions and samples run on an Applied Biosystems Thermal Cycler Version 2.08 (cycling parameters 25°C for 10 minutes, 37°C for 120 minutes, 85°C for 5 minutes, 4°C ∞). cDNA was stored at -20°C.

### 2.1.6 Quantitative PCR

cDNA was diluted 1 in 10 prior to quantitative PCR (qPCR). Applied Biosystems TaqMan Fast Advanced Master Mix (Thermo Fisher Scientific 4444557) and appropriate TaqMan probes were used to carry out qPCR (**Table 2-2**). qPCR was performed using the Applied Biosystems 7500 Fast Real Time PCR system (cycling parameters: 95°C for 20 seconds, followed by 40 cycles of 95°C for 3 seconds and 60°C for 30 seconds).

Target	ID
APOBEC3D	Hs00537163_m1
CRBN	Hs00372266_m1
GAPDH (housekeeping control)	Hs99999905_m1
IRF4	Hs01056533_m1

*Table 2-2 TaqMan probes.*

TaqMan probes with ID numbers (purchased from Thermo Fisher Scientific).

To detect Cas9 mRNA expression the System Biosciences Cas9 RT-PCR Primer Set (SBI CAS9-PR-1) was used with Applied Biosystems SYBR Green qPCR Master Mix Buffer (Thermo Fisher Scientific 4309155). Cycling parameters: 50°C for 2 minutes, 95°C for 10 minutes, followed by 40 cycles of 95°C for 15 seconds and 60°C for 1 minute.

### 2.1.7 Preparation of protein samples

Cells were spun down in a microfuge at 400 RCF for 5 minutes at 4°C. Supernatant was removed and the cell pellet re-suspended in SDS 2% lysis buffer (150µL per 1.5x10<sup>6</sup> cells). SDS 2% contained TRIS pH 6.8 (final concentration 50mM), glycerol (final concentration 10%), SDS (final concentration 2%) and distilled H<sub>2</sub>O. Samples were heated to 95°C for 20 minutes

and then stored at -20°C. Protein was quantified using the Pierce BCA Protein Assay Kit (Thermo Fisher Scientific 23225) according to the manufacturer's instructions. After quantification, samples were diluted to equilibrate them using a standard curve. DTT/bromophenol blue 1:10 was then added and microcentrifuge tubes gently vortexed and heated for 10 minutes at 95°C.

### **2.1.8 Gel electrophoresis and western blotting**

Samples were loaded to a NuPAGE 4-12% Bis-Tris gel (Thermo Fisher Scientific NP0336BOX) and run with 1x MOPS (3-(N-morpholino)propanesulfonic acid) as running buffer. 20-30µg of protein (constant per experiment) was loaded alongside 10µL of Chameleon Duo Pre-stained Protein Ladder (LI-COR) or Precision Plus Protein Dual Color Standards (BIO-RAD). For blots of histone marks, 2µg of protein was loaded. Gels were run at 100V for 20 minutes and then the voltage increased to 150V for a further 60 minutes. For transfer, 1x Transfer Buffer and PVDF (polyvinylidene difluoride) membrane were used (membrane soaked in 100% methanol for 10 minutes before use) and the transfer was performed at 100V for 1 hour. Membranes were blocked with 5% BSA in TBS-T (Tris-Buffered Saline with 0.1% Tween) for 15 minutes. Primary antibody was added in 5% BSA (at a concentration of 1 in 1000) and incubated overnight at 4°C (**Table 2-3**). Membranes were washed in TBS-T for 15 minutes and secondary antibody added in 5% BSA (at a concentration of 1 in 10,000) and incubated for 1 hour at room temperature in the dark. Membranes were washed with TBS-T and imaged using the LI-COR Odyssey Fc imaging system.

Target	Antibody
Aiolos	Cell Signaling Technology 15103
APOBEC3D	Thermo Fisher Scientific PA5-88195
$\beta$ -actin	Sigma A5441
Cas9	Millipore MAC133; Abcam ab191468
CRBN	Sigma HPA045910
GAPDH	Cell Signaling Technology 5174
H3K36me2	Active Motif 61019
H3K36me3	Active Motif 61022
Ikaros	Cell Signaling Technology 14859
IRF4	Cell Signaling Technology 4964
SCD	Abcam ab19862
Goat anti-Mouse secondary	IRDye 800CW Goat anti-Mouse 926-32210
Goat anti-Rabbit secondary	IRDye 680RD Goat anti-Rabbit 926-68071

*Table 2-3 Antibodies used in western blotting.*

Antibodies used in this thesis with manufacturer.

### 2.1.9 DNA gels

One percent agarose (Invitrogen UltraPure Agarose Powder) gels were cast with 1 in 10,000 GelGreen Nucleic Acid Stain (10,000x stock). Gels were run with x1 TAE (Tris-acetate-EDTA) buffer at 110V for 70 minutes. DNA gels were visualised using the LI-COR Odyssey Fc imaging system or UVP Transilluminator. Gel extraction was performed using a Blue Light Transilluminator (Accuris) and the QIAquick Gel Extraction Kit (Qiagen 28704) as per the manufacturer's instructions.

### 2.1.10 Plasmid preparation

Plasmid expansion was performed using lysogeny broth or terrific broth with ampicillin at 1 in 1000 and the specified bacteria stab. The culture was incubated overnight in a shaking incubator (37.5°C, 225 RPM). MiniPrep (QIAprep Spin Miniprep Kit 27106) or MaxiPrep (Qiagen Plasmid Maxi Kit 12162) was performed as required according to the manufacturer's instructions. Plasmid sequence was then confirmed by Sanger sequencing (Source Bioscience).

### 2.1.11 Antibiotic selection

Plasmids used during the work presented in this thesis had different antibiotic selection markers, including blasticidin, puromycin and hygromycin. The doses

of these compounds needed for selection was assessed in 72-hour cell viability assays (**Figure 2-1**).

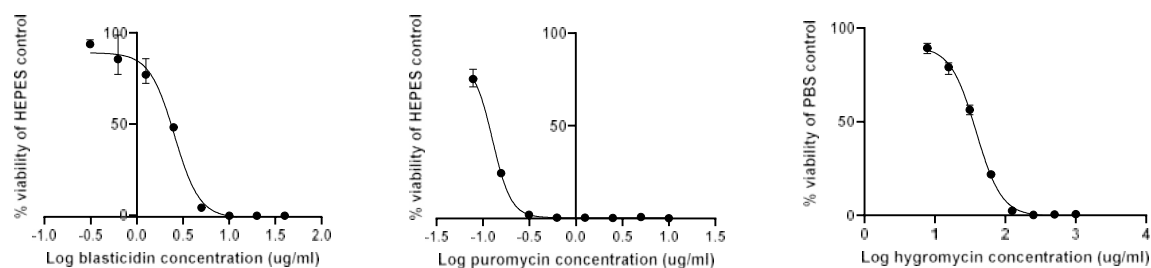


**Figure 2-1 Antibiotic selection in MM1s cell lines.**

Cell viability (CellTiter-Blue) assays were performed to optimise the dose of antibiotic needed for plasmid selection in the MM1s cell line at 72 hours. Doses selected for ongoing experiments were: blasticidin 20µg/ml, puromycin 2.5µg/ml and hygromycin 250µg/ml. N=1, graphs show mean and error bars represent range of 3 technical repeats.

## 2.2 Characterisation of the resistant cell lines

### 2.2.1 Whole exome sequencing

DNA was extracted from cell lines using the AllPrep DNA/RNA MiniKit (Qiagen 80204) according to the manufacturer's instructions and underwent whole exome sequencing at BGI (formerly Beijing Genomics Institute), China. Data analysis was performed in collaboration with Dr Harvey Che, Bioinformatician, Cancer Therapeutics, ICR. Samples were pre-processed and analysed using the ncore/sarek 2.7.1 pipeline following Genome Analysis Toolkit (GATK) best practices. MuTect2 was used to call short variants and variants were then annotated with Variant Effector Predictor (129) (**Table 2-4**). All cell lines were sequenced at >130X depth.

Mutation impact	Definition
Modifier	Usually describes non-coding variants or variants affecting non-coding genes where predictions are difficult or there is no evidence of impact.
Low	Assumed to be unlikely to change protein behaviour.
Moderate	A non-disruptive variant that might change protein effectiveness.
High	Likely to have a highly disruptive impact, causing protein truncation, loss of function or triggering nonsense mediated decay.

**Table 2-4 Mutation impact categories.**

The likely impact of a mutation was categorised as modifier, low, moderate or high impact (129).

### 2.2.2 RNA-Seq

RNA was extracted from cells using the AllPrep DNA/RNA MiniKit (Qiagen 80204) according to manufacturer's instructions and underwent RNA sequencing at BGI, China. Data processing was performed in collaboration with Dr Harvey Che. RNA-Seq analysis was processed by nf-core/rnaseq v3.2 (130). The following software were used in the pipeline: adaptor trimming (TrimGalore), quality control (MultiQC), pair-end reads mapping (STAR), genome assembly (GRCh38.p13), gene model (Gencode v36), gene expression quantification (ht-seq) and differential expression analysis (DESeq2).

### 2.2.3 Whole proteome analysis

Quantitative proteomics and phosphoproteomics of the cell lines was performed using mass spectrometry with a TMT-multiplexing approach. Two million cells of the resistant and control lines were harvested and washed twice with cold phosphate-buffered saline (PBS). Cell pellets were snap frozen on dry ice and stored at -80°C.

The 4 paired patient samples (sample taken at diagnosis and sample taken at relapse on lenalidomide from the same patient) had been stored as dry cell pellets or as viable cells in FBS with DMSO. The FBS stored samples were defrosted and then washed 3x with PBS to remove as much as the FBS as possible prior to processing.

Samples were processed by the ICR Proteomics Core Facility. The full method, provided by Dr Fernando Sialana, can be found in **Supplementary Methods Section 10.1** and is based on the SimPLIT workflow (131). In summary, cell pellets were lysed and then quantified. Aliquots containing 15µg or 60µg of total protein were used for proteomics or phosphoproteomics experiments respectively. Proteins were then digested, and the resultant peptides tandem mass tag (TMT) labelled. Peptides were then fractionated and phosphopeptides enriched. Liquid chromatography-mass spectrometry (LC-MS) was then performed. The SEQUEST-HT search engine was used to analyse the acquired mass spectra for protein identification and quantification. The spectra were searched against the UniProt-SwissProt proteomes of *Homo sapiens* protein entries, appended with contaminants. Normalised protein abundance values for



resistant versus control comparisons were performed using a moderated t-test in limma (implemented in Phantasus) (132).

## 2.2.4 Re-expression of CRBN in the IMiD-resistant cell lines

Re-expression of CRBN was performed using the pCDH-CMV-MCS-EF1a-Hygro plasmid (System Biosciences CD515B-1) with inserted CRBN (which led to stable expression of CRBN via the CMV promoter and conferred resistance to hygromycin, **Figure 2-2**).

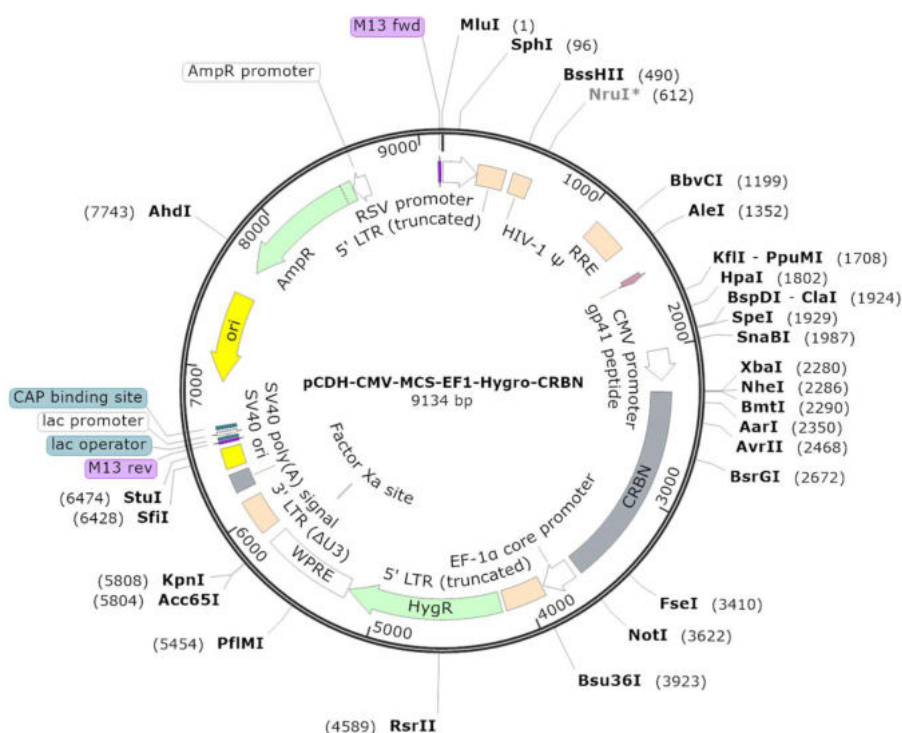


**Figure 2-2** pCDH-CMV-MCS-EF1a-Hygro-CRBN.

Plasmid map for pCDH-CMV-MCS-EF1a-Hygro-CRBN (created in SnapGene). Plasmid sequence was confirmed using Sanger sequencing.

Len-R-MM1s, Pom-R-MM1s and Iber-R-MM1s cell lines were transduced with virus in the presence of polybrene (final concentration 2µg/ml), aiming for one viral particle per cell. Twenty-four hours later, transduced cells were selected with hygromycin (final concentration 250µg/ml).

## 2.3 Compound screen

### 2.3.1 Preparation of compound list for screening, firing of compounds and cell plating

A list of compounds for screening was prepared from the Selleck Drugs and Tools (D&T) Compound set and the Epigenetic Probes set, which together contained

495 compounds. The compounds targeted a broad range of pathways known to be important in the development of cancer. The locations of compounds in the source plates were identified and ‘cherry pick’ lists were made in Excel. Source plates were prepared in low dead volume (LDV) plates with compounds re-suspended in DMSO at 320µM. Source plates were taken from nitrogen storage and spun at room temperature for 1 minute at 1000 RPM. The sealed foil lids were removed and replaced with DMSO saturated MicroClime Environmental lids (LabCyte LL-0310). An intermediate plate (LabCyte PP-0200) was prepared with 40µL of DMSO (Thermo Fisher Scientific BP231-100), and a MicroClime Environmental lid was added. 384 Clear Bottom Microplate destination plates (Corning 3701) were barcoded. The protocol was run using the LabCyte Echo and 24 compounds were fired into each destination plate (**Figure 2-3**). Each drug was fired in triplicate at 3 different concentrations: 800nM, 200nM and 80nM. Each destination plate also had bortezomib as a negative control and iberdomide as a differential control. Duplicates of each plate were generated; Ctrl-Iber-MM1s cells were added to one plate and Iber-R-MM1s cells added to the matching plate. Cells were only used if the viability was ≥98% on the day of the experiment. The total number of cells per well was 8000 in 40µL of media. Media only was aliquoted in the appropriate wells and all of the other wells contained cells (including outer wells). Plates were then centrifuged at 1000 RPM for 1 minute and incubated at 37°C until Day 5.

A1		2	3	4	5	6	7	8	9	10	11	12	13	14	15	16	17	18	19	20	21	22	23	24
B																								
C																								
D																								
E									Bort							Bort								
F																								
G																								
H									iber							iber								
I																								
J																								
K																								
L																								
M																								
N																								
O																								
P																								

*Figure 2-3 Destination plate map.*

Twenty-four compounds were fired into each destination plate. Each drug was fired in triplicate at 3 different concentrations: 800nM, 200nM and 80nM. Each destination plate also had bortezomib (bort) as a negative control and iberdomide (iber) as a differential control. Duplicates of each plate were generated. C = compound.

### 2.3.2 Viability assays using CellTiter-Blue

After 5 days of incubation, 5µL of CellTiter-Blue (Promega) was added to each well. Plates were spun at 1000 RPM for 1 minute and placed in an incubator at

37°C for 3 hours. Absorbance was then recorded using the Perkin Elmer Envision with the Alamar Blue High Gain filter.

### 2.3.3 Data analysis

Data analysis was performed in Excel, GraphPad Prism 9 and Vortex (a data visualisation and analysis tool from Dotmatics). Z primes were calculated for each plate using the formula  $Z \text{ prime} = 1 - ((3 * (\delta_p + \delta_n)) / (\mu_p - \mu_n))$ , where  $\delta_p$  is the standard deviation of the positive control,  $\delta_n$  is the standard deviation of the negative control,  $\mu_p$  is the mean of the positive control and  $\mu_n$  is the mean of the negative control. The Z prime is a statistical measure of the quality of a screening assay which takes into account both the assay signal dynamic range and the data variation associated with the signal measurements (133). Z primes of >0.4 were considered acceptable.

## 2.4 Genome wide knockout CRISPR screen

A genome wide loss-of-function CRISPR screen library was available within the Division of Cancer Therapeutics and was kindly provided by Dr Paul Clarke and Dr Marco Licciardello. Expansion of the plasmid pool had been performed and library representation confirmed by Dr Licciardello prior to lentivirus production (**Supplementary Figure 9-6**). Dr Licciardello also provided technical input and advice regarding the running of the screen.

### 2.4.1 Lentivirus production

On Day 1 HEK293T cells were seeded at 40% confluence in a T175 flask. On Day 2 the media was exchanged with 13ml OptiMEM 1 hour before transduction. 20µg of the plasmid of interest (e.g. pLEX\_311-Cas9v2 or Brunello plasmid pool on a lentiGuide-Puro backbone (**Figure 2-4**)), 10µg of pMD2.G and 15µg of psPAX2 were added to 4ml of OptiMEM. 100µl of Lipofectamine 2000 was also added to separate 4ml of OptiMEM. After a 5 minute incubation the tubes were mixed and incubated for a further 20 minutes. The 8ml was then added to the cells in a drip wise manner. Six hours later the media was changed to 30ml DMEM 10% FBS. On Day 5 the media was harvested and spun at 3000 RPM for 10 minutes at 4°C to pellet cell debris. The supernatant was then filtered through a 0.45µm low protein binding membrane and stored at -80°C. The presence of virus was confirmed using Lenti-X GoStix (Takara).

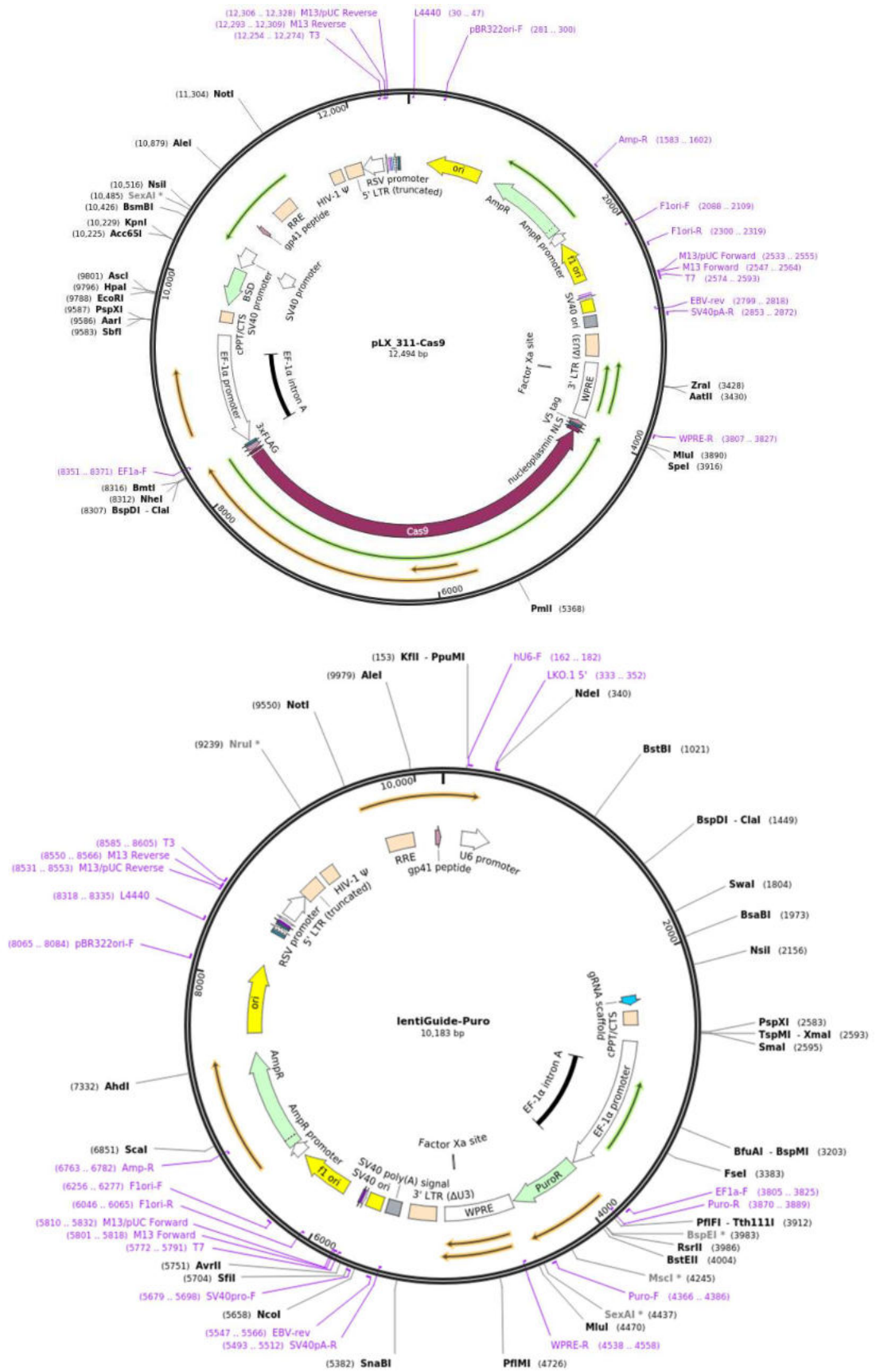


Figure 2-4 Plasmids used in the CRISPR screen.

Plasmid maps for pLEX\_311-Cas9v2/pLX\_311-Cas9 and the lentiGuide-Puro backbone of the Brunello plasmid pool (taken from Addgene).

### 2.4.2 Lentiviral multiplicity of infection calculation

Cells were seeded in 6-well plates ( $3 \times 10^6$  cells in 4ml media per well) with polybrene at a final concentration of  $2 \mu\text{g/ml}$  (for optimisation see **Supplementary Figure 9-7**). Cells were transduced with different amounts of virus leaving one well with untransduced cells. After 24 hours, cells were scraped and spun at 1200 RPM for 5 minutes. The cells from a given well were split equally between 2 separate wells and 1 of the 2 wells was treated with puromycin (final concentration  $1.25 \mu\text{g/ml}$ ). As soon as there were no cells in the untransduced puromycin treated control (Day 5), the wells were scraped, cells counted, and the percentage of infected cells calculated (number of cells in the well with puromycin divided by the number of cells in the well without puromycin  $\times 100$ ). The percentage of transduced cells was then converted to a multiplicity of infection (MOI) using the formula  $P(k) = e^{-m} m^k / k!$  where  $P(k)$  is the probability that any cell is infected with  $k$  particles,  $k$  is number of particles in a given cell and  $m$  is the MOI.

### 2.4.3 Introduction of Cas9 lentivirus

Cells were seeded in T25 flasks with media containing polybrene at a final concentration of  $2 \mu\text{g/ml}$  (for MM1s  $8 \times 10^6$  cells were seeded in 10ml of media per flask). Cells in each flask were transduced with varying amounts of virus. After 24 hours cells were scraped, spun at 1200 RPM for 5 mins and then split equally between two flasks. Blasticidin selection was commenced in only one of the two flasks (final concentration  $20 \mu\text{g/ml}$ ). Infection efficiency was calculated, and cells only kept in culture if infection efficiency was 10-50%.

### 2.4.4 Assessment of Cas9 activity

This assay allowed assessment of the activity of Cas9 in the transduced cells. Cas9-Iber-R-MM1s cells were seeded in a T25 flask ( $8 \times 10^6$  cells in 10ml media per flask) with polybrene at a final concentration of  $2 \mu\text{g/ml}$ . Cells were transduced with the amount of pXPR\_011 sgEGFP vector (**Figure 2-5**) virus required for an infection efficiency of 15-30%. The percentage of fluorescent cells was assessed by flow cytometry 8-10 days after infection. Uninfected Cas9-expressing cells were used as an EGFP negative control and wild type cells infected with the same amount of pXPR\_011 sgEGFP vector were used as an EGFP positive control.



For flow cytometry  $1 \times 10^6$  cells were spun down (1200 RPM for 5 minutes). Supernatant was removed and the cell pellet was re-suspended in 1000 $\mu$ L of PBS. The 1000 $\mu$ L was split between 2 flow tubes that were then spun. The supernatant was removed, and the cell pellet re-suspended in 600 $\mu$ L of PBS. DAPI (6 $\mu$ L) was added to one tube for each cell line. Samples were vortexed and analysed on a BD LSR II flow cytometer. Compensation controls (unstained, DAPI +ve and EGFP +ve) were run prior to sample analysis.

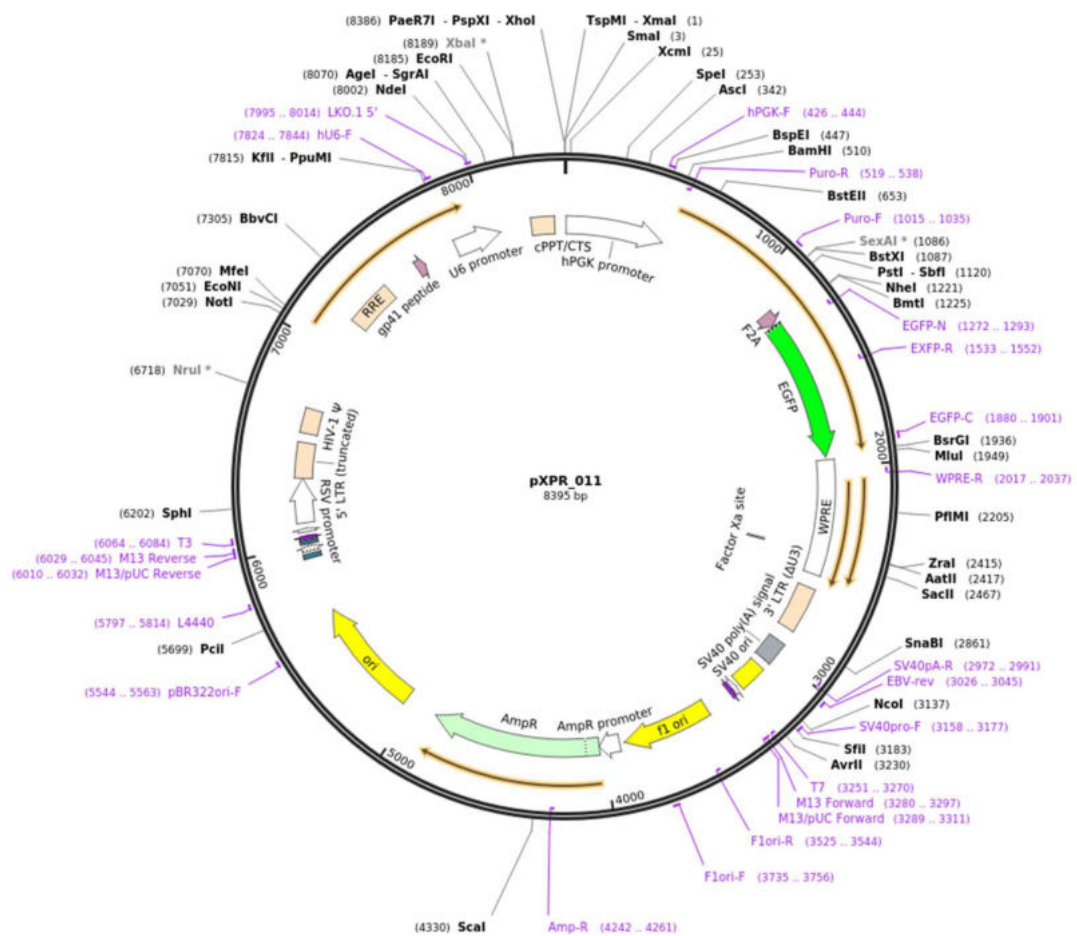


**Figure 2-5 Assessment of Cas9 activity.**

The pXPR\_011 sgEGFP plasmid was used to assess the activity of Cas9 (taken from Addgene).

### 2.4.5 Genome wide CRISPR screen with the Brunello library

The Brunello library contains 76,441 unique gRNAs targeting 19,114 genes. The following protocol assured 500x coverage (each gRNA is present in at least 500 unique cells) throughout the entire pipeline. A total of 108 million cells were needed to commence the screen. 18 million Cas9-Iber-R-MM1s cells were seeded in 6x T175 flasks with the quantity of Brunello lentivirus required (previously calculated, see **Supplementary Figure 9-10**) for an MOI of 0.3-0.5

(to ensure all of the transduced cells receive a maximum of one viral integrant) and a final concentration of 2µg/ml of polybrene. After 24 hours, the flasks were scraped, and the contents of each individual flask spun at 1200 RPM for 5 mins. The resulting cell pellets were re-suspended in media with puromycin at a final concentration of 1.25µg/ml. On Day 5 each flask was carefully scraped to retain all cells and the contents of all flasks pooled together. Cells were counted and an 80 million cell aliquot taken and stored as a T0 sample (cells spun down, washed with PBS and stored at -80°C as a dry cell pellet). 112 million cells were then split between 14 flasks (i.e. 8 million/flask) which were then split into two branches of 7 flasks each. One branch was treated with DMSO and one branch with iberdomide (final concentration 0.01µM). Drug treatment was continued for ~8 doublings, with cells split when confluent (every 5 days). At each split the cells for each branch were pooled before splitting again. At the end of the screen a cell pellet of 80 million was stored for each branch. Biological replicates were performed as independent infections of cells with the pooled gRNA library on distinct days.

#### **2.4.6 Genomic DNA extraction and PCR of gRNAs for next generation sequencing**

Genomic DNA (gDNA) was extracted from the stored cell pellets using the Blood and Cell Culture DNA Maxi Kit (Qiagen 13362) and an adapted version of the manufacturer's protocol (**Supplementary Methods 10.2.1**). PCR was then performed in 2 steps (**Supplementary Methods 10.2.2**). In summary, the first PCR was performed to amplify the gRNAs from the gDNA and the second PCR was performed to attach Illumina adaptors and to barcode the samples. The PCR#2 products from each sample were quantified on the LI-COR using GelGreen nucleic acid stain. Equimolar amounts of samples were pooled together, run on a gel, cut out using a scalpel and a Blue Light Transilluminator (Accuris), and extracted using the QIAquick Gel Extraction Kit (Qiagen 28104) as per the manufacturer's instructions (except a temperature of 30°C was used to melt the gel slices). Concentration of the resultant DNA was measured using a Qubit and quality assessed using the Agilent D1000 ScreenTape System.

## 2.5 14-day SETD2 inhibitor assays

Fourteen-day cell growth assays were performed with two different SETD2 (SET Domain Containing 2, Histone Lysine) inhibitors, EPZ-719 and EZM0414. Two million cells were seeded per condition on day 0. Cells were split at day 5 and day 10 and 2 million cells were re-seeded each time. At day 10 the number of cells present was divided by 2 million and the result was multiplied by the number of cells present at day 5. This number represented the total number of cells there would have been at day 10 if the cells had not been split at day 5. On day 14 the number of cells present was divided by 2 million and the result was multiplied by the calculated total number of cells at day 10 if splitting had not occurred. This gave the total number of cells at day 14 that would be present if the cells had not required splitting during the experiment.

## 2.6 Paired RNA-Seq and ChIP-Seq for exploration of SETD2 sensitivity in the resistant cell lines

### 2.6.1 RNA-Seq

RNA was extracted from cells using the AllPrep DNA/RNA MiniKit (Qiagen 80204) according to the manufacturer's instructions. RNA sequencing was carried out at BGI (China). Data processing was performed using Galaxy, with the following pipeline: HISAT2 to align reads to the genome (hg38), htseq-counts to count reads and DESeq2 to make comparisons.

### 2.6.2 ChIP-Seq

#### *Fixation of cells*

Twenty million cells per condition were collected and spun for 5 minutes at 300 RCF. Cells were washed 2x with 20ml of room temperature PBS. The pellet was then re-suspended in 18.8ml of room temperature PBS and 1250 $\mu$ l of freshly opened 16% methanol-free formaldehyde (Thermo Fisher Scientific) was added. After careful mixing the sample was rotated for 10 minutes at room temperature. The formaldehyde was then quenched by adding 6ml of cold glycine (Thermo Fisher Scientific) and the cell suspension rotated for 5 minutes at room temperature. Cells were then collected by centrifugation at 800 RCF for 5 minutes at 4<sup>o</sup>C and washed x2 with 15ml of ice-cold PBS. Cell pellets were then snap-



frozen in liquid nitrogen and stored at  $-80^{\circ}\text{C}$ . At this point associated proteins are cross-linked to the chromatin.

### ***Processing ChIP-Seq samples***

The full method for processing ChIP samples can be found in **Supplementary Methods 10.3.1**. In summary, cells were lysed and the nuclei isolated using buffers containing 1% Triton X-100. Chromatin is insoluble under these conditions and was recovered by centrifugation. The samples then underwent sonication using a Covaris E220 to fragment the chromatin (to ~200-600 base pair fragments). Prior to immunoprecipitation a drosophila spike-in control was added to each sample. By 'spiking in' a small amount of exogenous chromatin it would then be possible to normalise the signal from experimental samples to this control in the final sequencing data, allowing robust inter-sample comparisons (134). Immunoprecipitation was performed using the H3K36me3 antibody (Diagenode C15410192) to capture the histone mark of interest and its bound DNA. Antibody-antigen (and DNA) complexes were affinity captured on magnetic beads, and wash steps performed to remove non-antibody-bound chromatin. A tagmentation approach (which uses a Tn5 transposase to integrate library preparation) was used and PCR amplification was performed directly from bead-bound immunoprecipitated chromatin. The library was then purified, and size selected using Kappa Pure beads (Roche KK8000) (to ensure unwanted DNA fragments such as unligated primers or primer dimers were removed).

A total input control was used in this experiment and the full method is described in **Supplementary Methods 10.3.2**. Briefly, after the sonication step, a small amount of each sample was taken and did not undergo immunoprecipitation. The crosslinks between the protein and DNA were reversed using Proteinase K, and Phenol:Chloroform:Isoamylalcohol was used to extract the DNA. The same tagmentation approach and library purification and size selection methods were then followed.

The samples were pooled and run on a S1 flow cell by the ICR's Genomics Facility. Deconvoluted FASTQ files for each sample were produced.

## **Data analysis**

The ChIP analysis was performed using a pipeline built in Nextflow from the Institut Curie NGS/Bioinformatics core facility (<https://github.com/bioinfo-pf-curie/ChIP-seq>). The outputs of this pipeline included FastQC, BigWig tracks and peak data. Visualisations were created in R with help from Dr Alan Mackay, ICR.

## **2.7 Labelled glucose experiments**

### **2.7.1 Labelling with $^{13}\text{C}_6$ -glucose**

Myeloma cells were incubated with media containing labelled  $^{13}\text{C}_6$ -glucose (final concentration 2mg/ml) for 24 hours or 48 hours.  $1 \times 10^6$  cells were seeded in 6 well plates for each condition and harvested at the specified timepoint.

### **2.7.2 Methanol quenching and extraction**

Quenching solution (60% methanol with 0.85% (w/v) ammonium bicarbonate (pH=7.4)) and extraction solution (100% methanol) were pre-cooled to  $-40^\circ\text{C}$  on dry ice. The pre-cooled quenching solution was then added to the harvested cell suspension and gently mixed. For  $1 \times 10^6$ - $1 \times 10^7$  cells, 5 volumes of quenching solution was added. The suspension was then centrifuged at 1000 RCF for 1 minute at  $4^\circ\text{C}$  and the supernatant removed. The cell pellet was re-suspended with 0.5ml of extraction solution. The sample was vortexed and centrifuged at 800 RCF for 3 minutes at  $4^\circ\text{C}$  and the supernatant collected. The extraction was repeated by adding another 0.5ml of extraction solution. The supernatant was pooled and centrifuged at 15,000 RCF for 1 minute at  $4^\circ\text{C}$ . The supernatant was collected and dried under  $\text{N}_2$  flow. The samples were then kept at  $-80^\circ\text{C}$ .

### **2.7.3 Sample preparation, GC-MS and data analysis**

Final sample processing, gas chromatography-mass spectrometry (GC-MS) analysis and initial data processing were carried out by Mr Yitao Xu in Professor Hector Keun's laboratory at Imperial College London. A full description of the method, provided by Mr Yitao Xu, can be found be **Supplementary Methods Section 10.4**. In summary, after methanol quenching and extraction, a dual phase extraction was performed to separate and enrich non-polar metabolites (such as fatty acids) for further analysis. Then GC-MS analysis was performed, and metabolites identified using an in-house library. Two parameters that describe fatty acid synthesis were estimated: 1) the proportion of lipogenic acetyl-

CoA that is derived from a  $^{13}\text{C}$  tracer (parameter D) and 2) the fraction of fatty acids that are de novo synthesised during the incubation ( $g(t)$ ) (135).

## **2.8 Processing patient samples**

Bone marrow aspirates from patients were received in the laboratory as part of an ethically approved research study (Royal Marsden Clinical Committee for Research approval number CCR5106). CD138+ve cells were extracted using a magnetic bead system with a Robosep, following the manufacturer's protocol. In summary, bone marrow aspirate samples were diluted 5-fold in PBS and filtered using a Cell Tech 70 $\mu\text{M}$  reversible strainer. The cells were then centrifuged at 300 RCF for 10 minutes (brakes 1, acceleration 9). The plasma was then carefully removed without disturbing the buffy coat/red cell pellet. The pellet was then resuspended to the original volume of the bone marrow aspirate with PBS. An equal amount of 1x EasySep RBS Lysis Buffer was added to the sample which was then processed on the Robosep. After magnetic bead selection there was a CD138+ve fraction (containing myeloma cells) and CD138-ve fraction (containing stromal cells). These fractions can then be stored or used in experiments.

## Chapter 3 Generation and Characterisation of Models to Explore Acquired IMiD/CELMoD Resistance

---

### 3.1 Introduction

Immortal cell lines are commonly used in the laboratory setting in place of primary tumour cells. Cell lines are cost effective, easy to use, mitigate ethical concerns regarding the use of human or animal material, and critically provide an unlimited source of material. However, how closely myeloma cell lines reflect disease in patients is questionable. Whilst the majority of myeloma cells reside in the bone marrow, cell lines are derived from patient cells that were circulating in the bloodstream as plasma cell leukaemia (or in effusions at other sites), and therefore no longer rely on the bone marrow niche (136). Sarin *et al* recently used transcriptional correlation profiling to compare the similarity of 66 myeloma cell lines to 779 newly diagnosed patient tumours and showed that the lines differed significantly with respect to patient tumour representation (with the median R ranging from 0.35 to 0.54) (136).

Whilst there have been efforts to culture primary myeloma cell samples from patients in a variety of in vitro co-culture systems, there is no consistent approach to support these cells to proliferate or survive long-term ex vivo (137). Patient-derived xenograft (PDX) mouse models can be employed, however establishing models can be difficult (138) and there are still limitations on cell numbers. Therefore, performing large drug screens and genome wide CRISPR screens, which both require tens of millions of cells, in patient samples is not possible. We sought to create cell line models and selected two initially IMiD-sensitive cell lines MM1s and H929. These cell lines were both in the “top” 20 cell lines that best correlated with patient tumour representation (136) and had different initiating genetic backgrounds (**Table 3-1**) (139).

Cell line name	Sex	Ancestry	Clinical heavy chain	Clinical light chain	Translocation
MM1s	Female	Africa	IgA	Lambda	t(14;16) and t(8;14)
H929	Female	Europe	IgA	Kappa	t(4;14)

*Table 3-1 Cell line characteristics.*

Table describing the background of the two major cell lines used throughout this thesis. The cell lines have different initiating genetic backgrounds. Data available from the Keats Lab website (139).

Developing drug-resistant cell lines is a long-established practice; one of the first publications of an anti-cancer drug-resistant in vitro model was published in 1970 (140). Drug-resistant lines are developed by exposing a carefully selected cell line to the drug of choice. This is commonly done through continuous exposure to a low concentration of drug or a high concentration pulsatile exposure (141). Models can also be broadly divided into ‘clinically relevant’ models which attempt to mimic the conditions patient cancer cells experience (e.g. with clinically relevant doses of drug), and high-level laboratory models which are developed to understand potential mechanisms of toxicity and resistance (140). There are also novel methods of generating resistance such as culturing cells under hypoxic conditions with a single treatment of drug (100).

When making a drug resistant cell line there are several other important factors to consider, including the long-term stability of resistance. Some cell lines may be stably resistant and can be grown in the absence of drug. However, others may need to be grown continuously in the drug, either at the dose used during the selection process or at a lower maintenance dose, to ensure consistency of experiments (140). In most selection strategies the whole population of cells remains as one group and there will be competing sub-populations of clonal cells, somewhat reflecting the heterogeneity observed in patient tumours. It is also possible to explore clonal variation in resistance by single cell seeding (140). Furthermore, treating the same cell line with the same drug may lead to a heterogenous range of drug-resistant models (140).

## 3.2 Results

### 3.2.1 Generation of IMiD/CELMoD-resistant cell lines

The Myeloma Biology and Therapeutics laboratory had previously developed acquired IMiD/CELMoD-resistant MM1s cell lines. To expand the range of tools available I generated a further set of cell lines, using the same method, with a second IMiD-sensitive myeloma cell line H929. H929 has a different initiating genetic background and would therefore allow identification of common or distinct resistance generation mechanisms. Cells were cultured in low doses of lenalidomide, pomalidomide and iberdomide (final concentration in media of 1 $\mu$ M, 0.1 $\mu$ M and 0.01 $\mu$ M respectively, ~10x the GI50 concentration for each drug in the parental lines), each with a paired DMSO control (**Table 3-2**). The controls were cultured in DMSO for the duration of the resistance generation experiment. Lenalidomide and pomalidomide are both approved IMiDs that are used standardly in the clinic and iberdomide is a CELMoD currently in clinical trials.

Cell line name	Description
Len-R-MM1s	MM1s cells cultured in, and resistant to, lenalidomide
Ctrl-Len-MM1s	Matched DMSO control line for Len-R-MM1s
Pom-R-MM1s	MM1s cells cultured in, and resistant to, pomalidomide
Ctrl-Pom-MM1s	Matched DMSO control line for Pom-R-MM1s
Iber-R-MM1s	MM1s cells cultured in, and resistant to, iberdomide
Ctrl-Iber-MM1s	Matched DMSO control line for Iber-R-MM1s
Len-R-H929	H929 cells cultured in, and resistant to, lenalidomide
Ctrl-Len-H929	Matched DMSO control line for Len-R-H929
Pom-R- H929	H929 cells cultured in, and resistant to, pomalidomide
Ctrl-Pom-H929	Matched DMSO control line for Pom-R-H929
Iber-R-H929	H929 cells cultured in, and resistant to, iberdomide
Ctrl-Iber-H929	Matched DMSO control line for Iber-R-H929

*Table 3-2 Acquired resistant cell line nomenclature.*

Cells were cultured over a period of several weeks and gradually acquired resistance to the IMiD/CELMoD they were cultured in and exhibited a degree of cross-resistance to other CRBN binders. During the development period, when possible, cells were stored in viable aliquots (in FBS with DMSO), RLT and protein lysis buffer.

### ***Viability curves over the period of resistance generation***

The cell lines became resistant over several weeks. Len-R-MM1s took ~12 weeks to become maximally resistant, whilst Pom-R-MM1s and Iber-R-MM1s were maximally resistant by ~8 weeks (**Figure 3-1**).

Len-R-H929 was maximally resistant by ~10 weeks. Pom-R-H929 was still not resistant at week 16 so the dose of pomalidomide was increased (from 0.1  $\mu$ M to 1  $\mu$ M final concentration in the media) and cells then became maximally resistant 4 weeks later (week 20). Iber-R-H929 was maximally resistant at ~10 weeks (**Figure 3-2**).

### ***Cross-resistance to other IMiDs/CELMoDs***

Resistant cell lines were assessed for cross-resistance to other CRBN binders including IMiDs, CELMoDs and G1 To S Phase Transition 1 (GSPT1) degraders. Exposure to a GSPT1 degrader usually leads to the degradation of GSPT1 (which is ubiquitinated and subsequently degraded by the proteasome). There are selective GSPT1 degraders, such as CC-90009, and compounds that degrade Ikaros, Aiolos and GSPT1, such as CC-885.

The 3 resistant MM1s cell lines showed cross-resistance to the IMiDs (lenalidomide and pomalidomide), CELMoDs (iberdomide, mezigdomide) and GSPT1 degrader (CC-885) tested (**Figure 3-3, Figure 3-4**). Pom-R-H929 and Iber-R-H929 also showed this pattern. However, Len-R-H929 exhibited full resistance to lenalidomide and pomalidomide, some sensitivity to iberdomide and mezigdomide and full sensitivity to CC-885 (**Figure 3-5, Figure 3-6**). It therefore appears that CELMoDs can partially overcome resistance in Len-R-H929 and GSPT1 degraders may be able to fully overcome IMiD resistance in this line.

No resistance to other commonly used anti-myeloma agents (such as bortezomib and dexamethasone) or agents that are sensitive to drug efflux pumps (such as doxorubicin) was seen. This is explored in detail in Chapter 4.

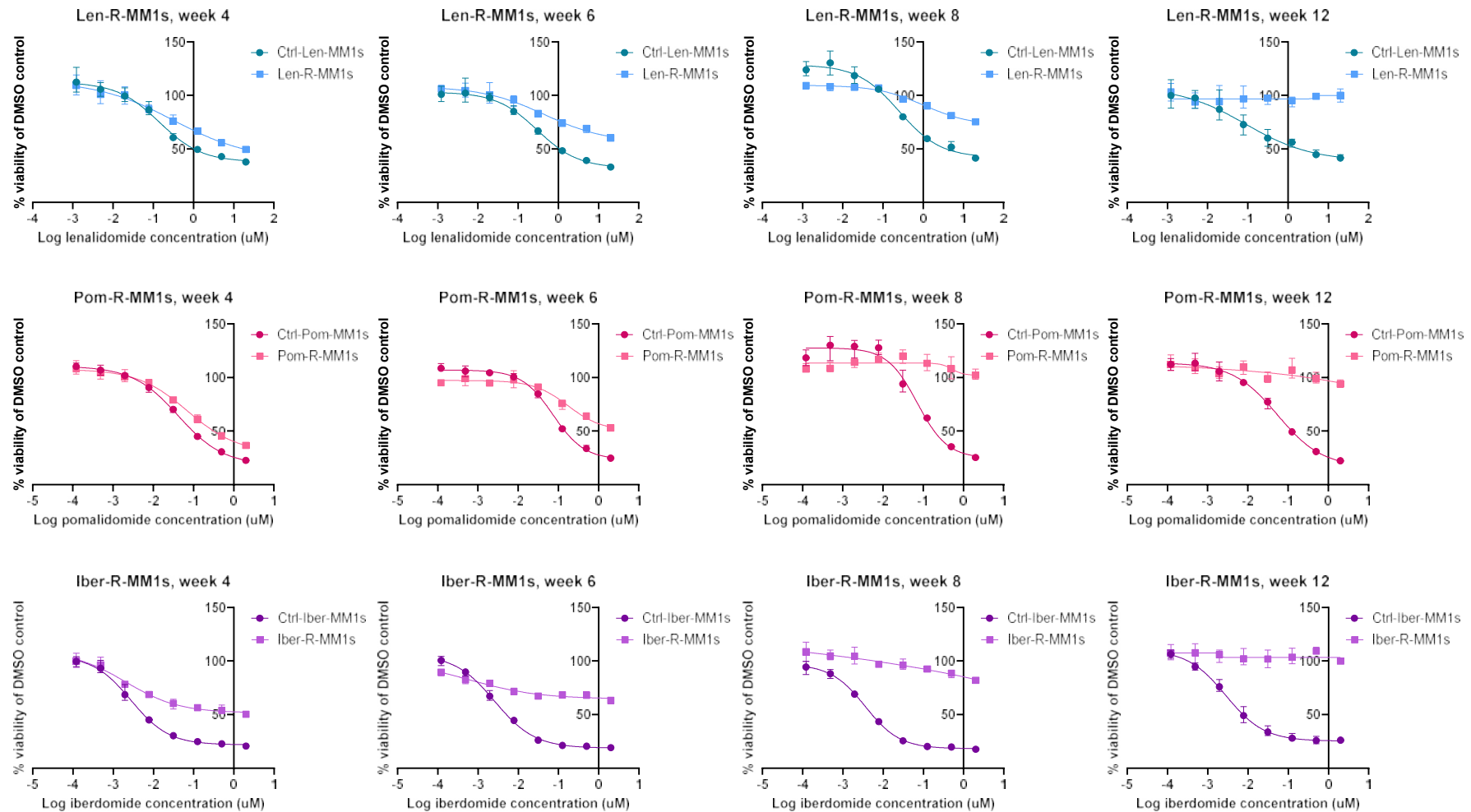


**Figure 3-1 Viability assays demonstrating MM1s gaining resistance during long-term low dose IMiD/CELMoD exposure.**

Plots show results of cell viability assays (using CellTiter-Blue) after 5 days incubation with IMiD/CELMoD at the indicated week after commencing exposure to lenalidomide/pomalidomide/iberdomide. Results for each cell line are normalised to DMSO treatment control. Mean and range of 3 technical replicates shown.



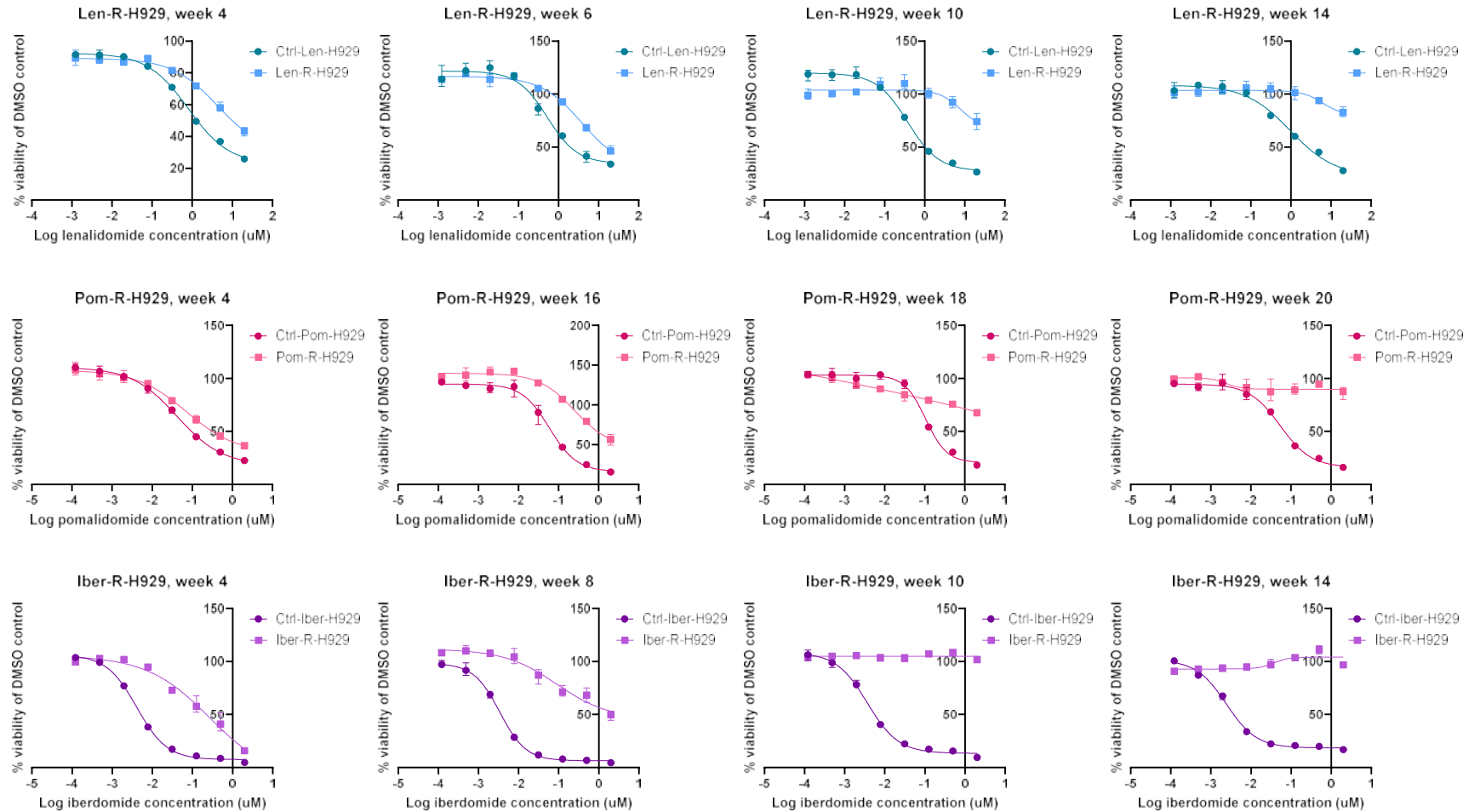


**Figure 3-2 Viability assays demonstrating H929 gaining resistance during long-term low dose IMiD/CELMOd exposure.**

Plots show results of cell viability assays (using CellTiter-Blue) after 5 days incubation with IMiD/CELMOd at the indicated week after commencing exposure to lenalidomide/pomalidomide/iberdomide. Results for each cell line are normalised to DMSO treatment control. Mean and range of 3 technical replicates shown.

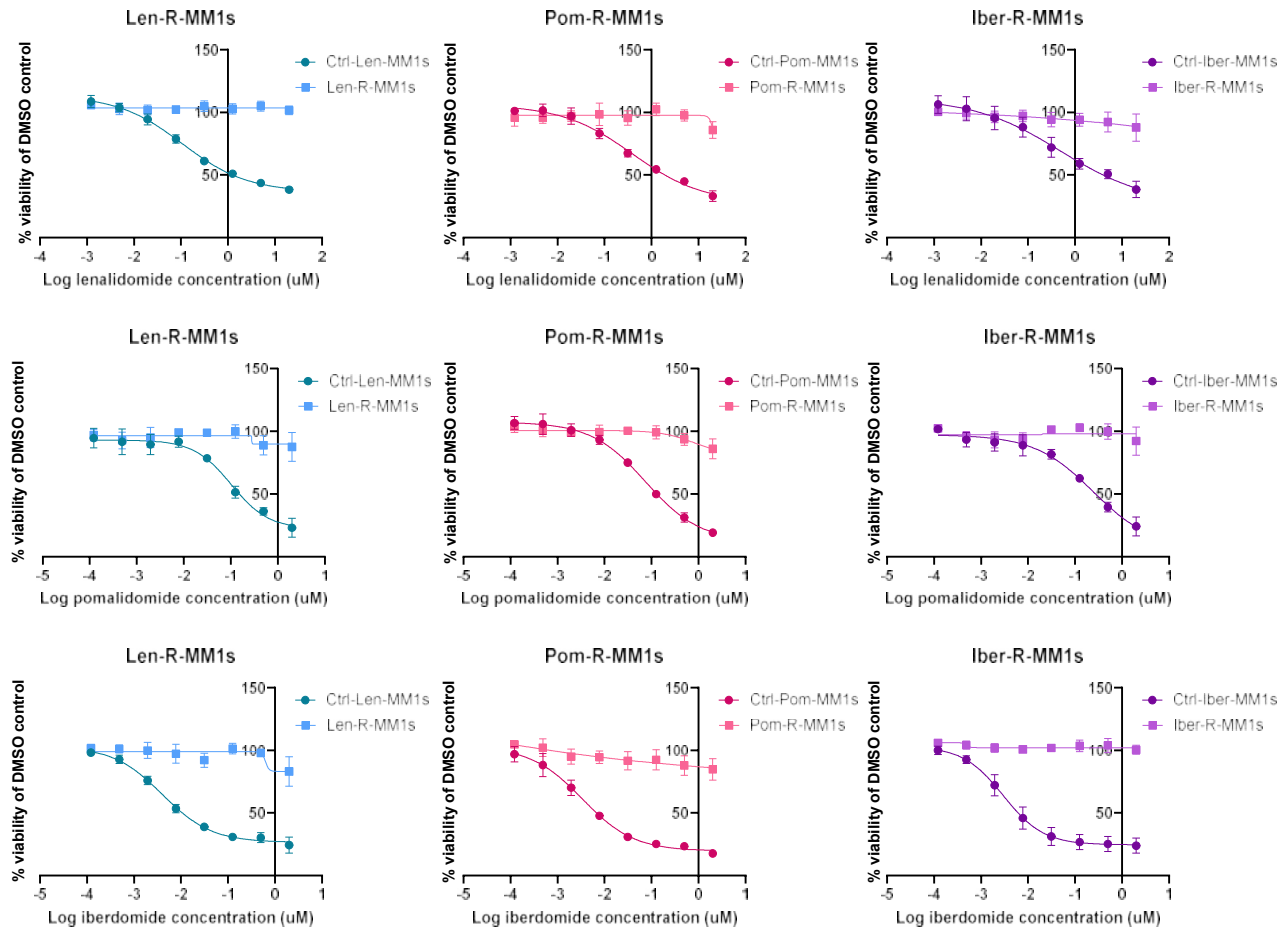


*Figure 3-3 Viability assays demonstrating response of MM1s resistant lines to other CRBN binding agents 1.*

Effect of lenalidomide, pomalidomide and iberdomide on the viability of control and resistant MM1s cell lines (assessed by CellTiter-Blue assay after 5 days of incubation). Mean and standard error of the mean (SEM) shown, n=3.

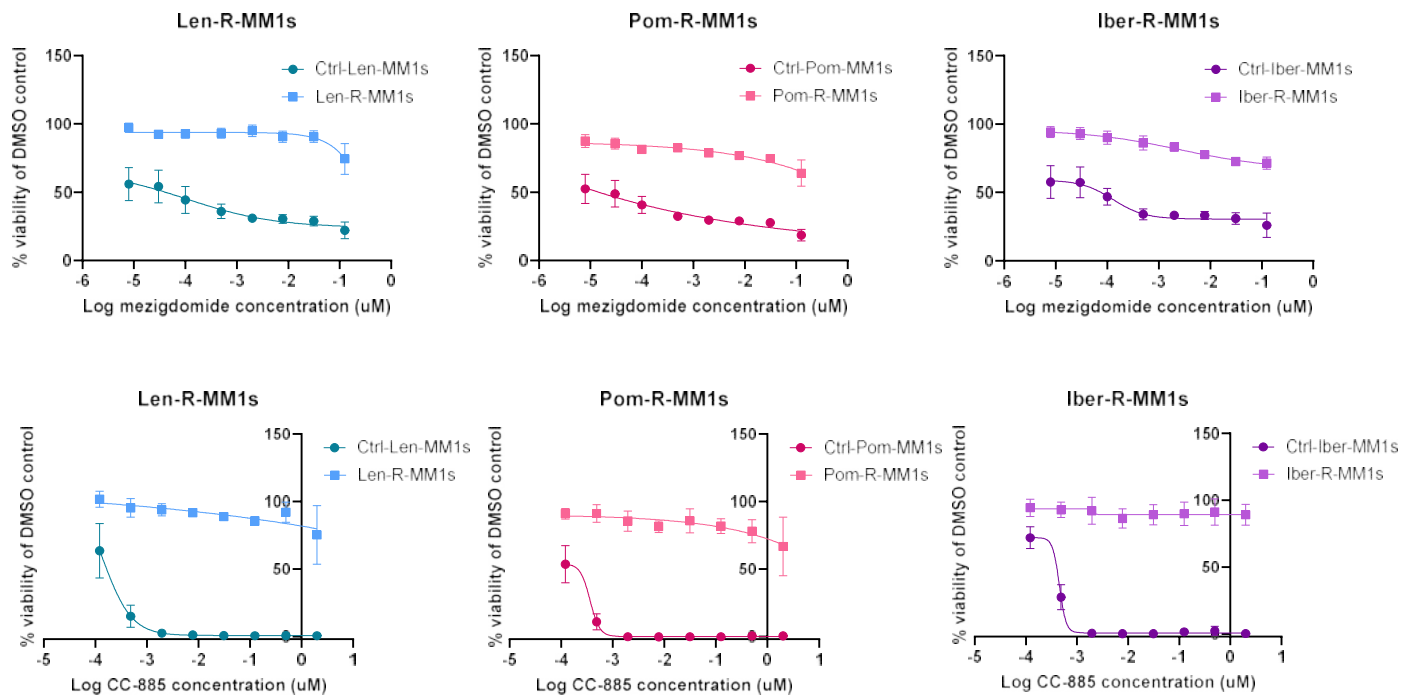
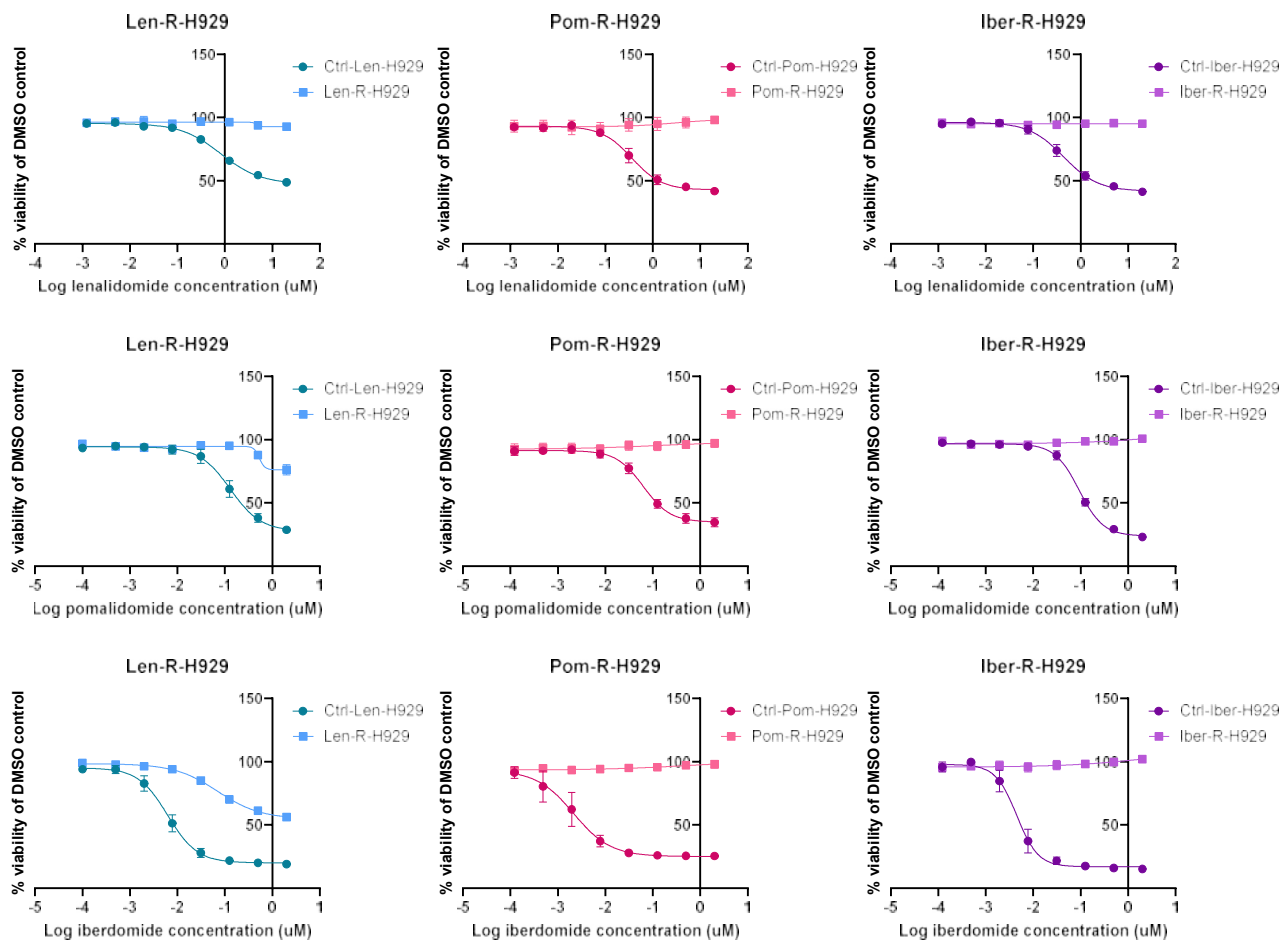


Figure 3-4 Viability assays demonstrating response of MM1s resistant lines to other CRBN binding agents 2.

Effect of mezigdomide and CC-885 on the viability of control and resistant MM1s cell lines (assessed by CellTiter-Blue assay after 5 days of incubation). Mean and SEM shown, n=3.



*Figure 3-5 Viability assays demonstrating response of H929 resistant lines to other CRBN binding agents 1.*

Effect of lenalidomide, pomalidomide and iberdomide on the viability of control and resistant H929 cell lines (assessed by CellTiter-Blue assay after 5 days of incubation). Mean and SEM shown, n=3.

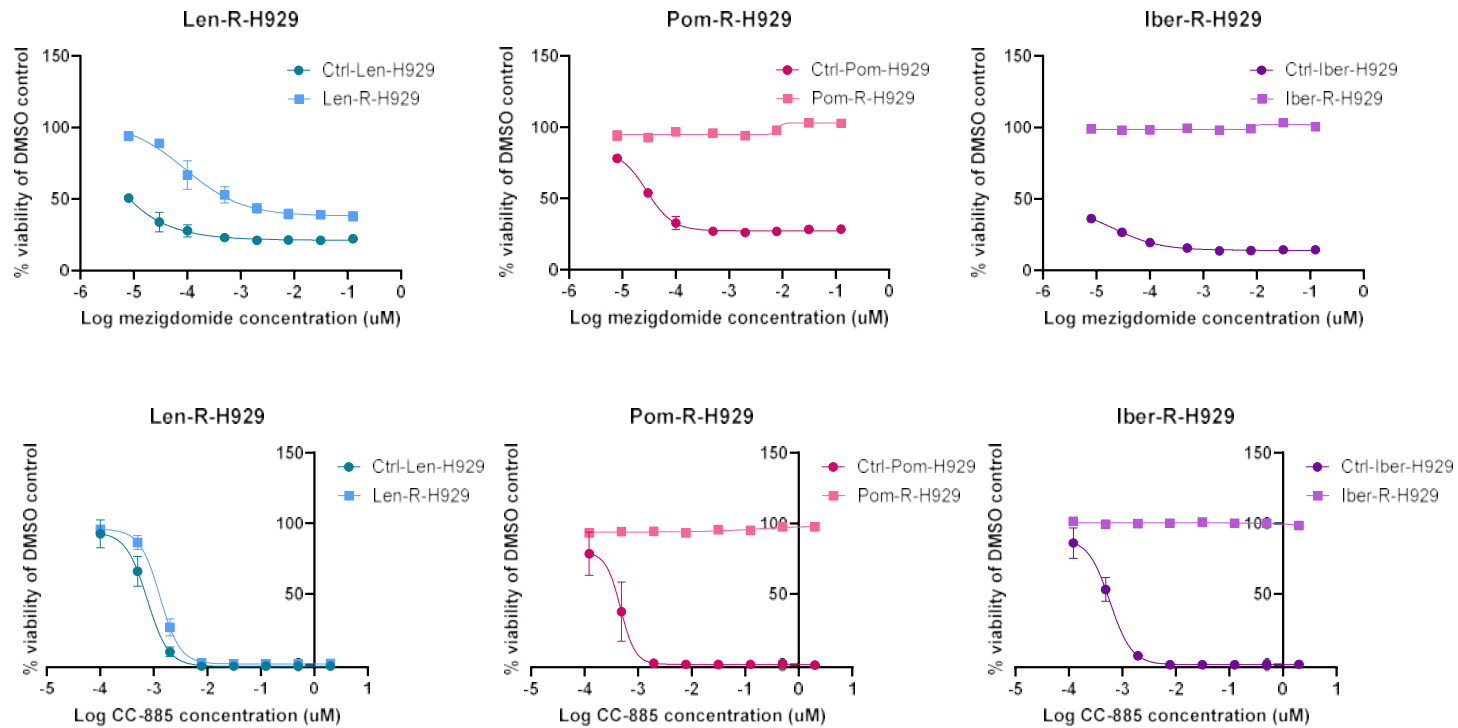


Figure 3-6 Viability assays demonstrating response of H929 resistant lines to other CRBN binding agents 2.

Effect of mezigdomide and CC-885 on the viability of control and resistant H929 cell lines (assessed by CellTiter-Blue assay after 5 days of incubation). Mean and SEM shown, n=3.

### ***Proliferation rate in the resistant cell lines***

There was no significant difference in proliferation rate between the resistant cell lines and their control lines at 5 days, the time point at which the IMiD/CELMoD assays are performed (**Supplementary Figure 9-1**). However, there was a trend to increased proliferation in the Pom-R-H929 cell line compared to its control. Of note, the raw readings of CellTiter-Blue were lower in the resistant lines, both at day 0 and day 5. This suggests that although the cell proliferation rate is not changing (controlled to the baseline reading) there may be some differences in how the resistant cells process the redox dye (resazurin) into the fluorescent end product (resorufin) compared to their sensitive counterparts (**Supplementary Figure 9-2**).

### ***Cereblon levels at maximal resistance***

As discussed previously, IMiDs/CELMoDs bind to CRBN, and the generation of resistance is frequently associated with a reduction in CRBN levels. In keeping with this the resistant cell lines all showed a reduction in CRBN at the mRNA level (**Figure 3-7**) and at the protein level (by western blotting and quantitative proteomics (**Figure 3-8**)). However, the reduction in CRBN in Len-R-H929 was modest. This may explain the difference in response to CRBN binders shown in **Figure 3-5** and **Figure 3-6**, as there may have been sufficient CRBN remaining for the more potent degraders to be effective.

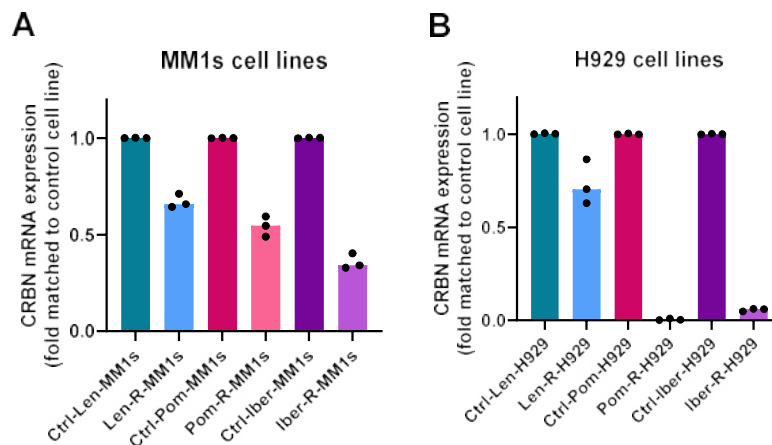


**Figure 3-7** *CRBN mRNA levels.*

Quantitative RT-PCR showed *CRBN* was reduced at the mRNA level in the A) MM1s and B) H929 resistant cell lines, albeit to varying extents. Individual points represent independent experiments (n=3), and the bar represents the median.

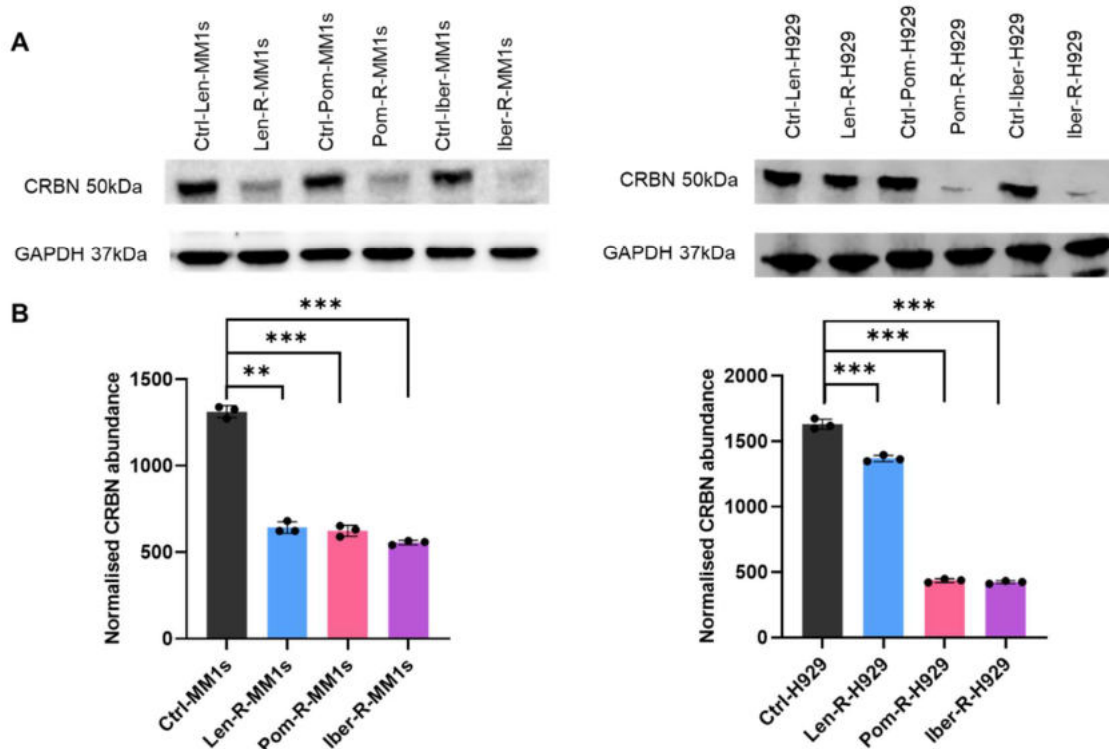


*Figure 3-8 CRBN protein levels.*

CRBN levels were reduced at the protein level, as shown by A) western blotting (representative blot of n=2) and B) quantitative proteomics (n=3). Quantitative proteomic data was analysed by a limma moderated t-test in Phantasus (v1.19.3). \*\* p<0.01, \*\*\*p<0.001. Graphs show mean and SEM.

In the resistant lines, CRBN expression was gradually lost over time (**Figure 3-9**). A more in depth time course was performed for Iber-R-MM1s (alongside its control line) as this line went on to be used in the subsequent compound screen (Chapter 4) and genome wide CRISPR screen (Chapter 5). Len-R-MM1s took ~12 weeks to become fully resistant and CRBN levels fell gradually over this time. Pom-R-MM1s become maximally resistant at 8 weeks but CRBN levels continued to fall after this time point. Iber-R-MM1s became fully resistant by ~8 weeks and at this time point CRBN became undetectable. Len-R-H929 was maximally resistant by ~10 weeks and there was only a moderate reduction in CRBN levels. Pom-R-H929 was still not resistant at week 16 so the dose of pomalidomide was increased (0.1µM to 1µM final concentration in the media) and then the cells became maximally resistant 4 weeks later (week 20), which coincided with CRBN becoming non-detectable. Iber-R-H929 was maximally resistant at ~10 weeks at which point there were very low levels of CRBN. Unfortunately no samples could be stored before week 10 because there were such low numbers of viable cells. In summary, acquisition of resistance in most of the cell lines appeared to correlate well with reduction in CRBN but there was variation.

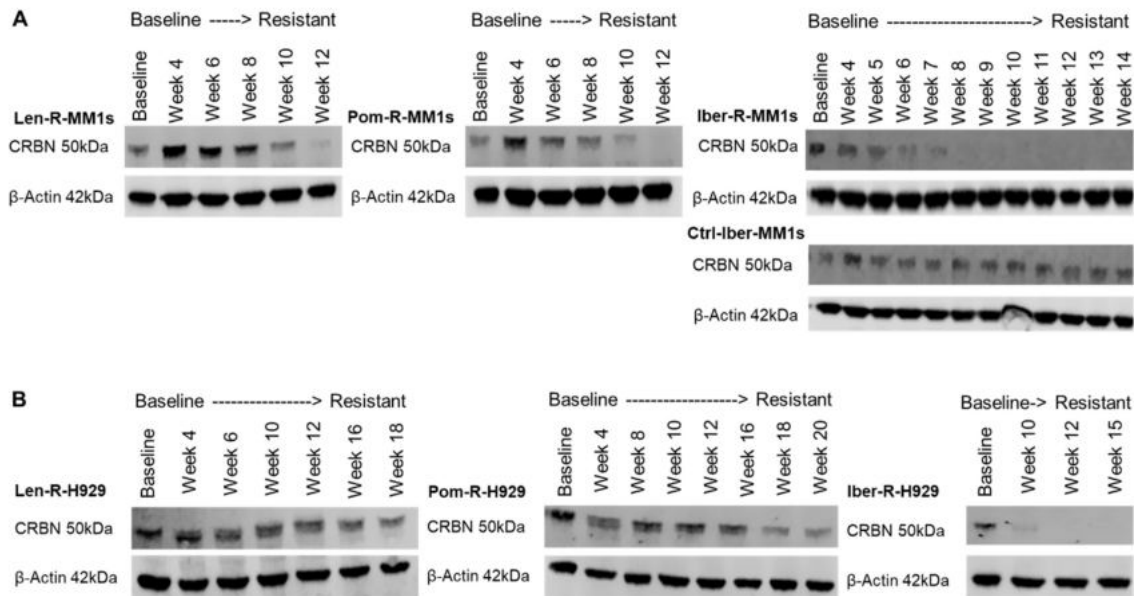


**Figure 3-9** CRBN levels over time as the cells become resistant to IMiDs/CELMoDs.

CRBN levels over time were explored by western blotting in A) the MM1s lines and B) the H929 cell lines. The resistant cell lines showed a reduction in CRBN as cells were cultured with lenalidomide/pomalidomide/iberdomide for the number of weeks indicated in the blots. However, Ctrl-Iber-MM1s showed no reduction in CRBN.

**The effect of IMiD treatment on Aiolos, Ikaros and IRF4 levels in the resistant lines**

The functional ability of the resistant cell lines to degrade known neosubstrates when exposed to IMiDs/CELMoDs was then explored. In the MM1s control lines there was a reduction in Aiolos and Ikaros with IMiD/CELMoD treatment due to their degradation. As Aiolos and Ikaros function as transcription factors for IRF4, there was also a rapid decrease in mRNA levels of *IRF4*. In the resistant lines these well characterised effects of IMiD/CELMoD treatment were abrogated (Figure 3-10).



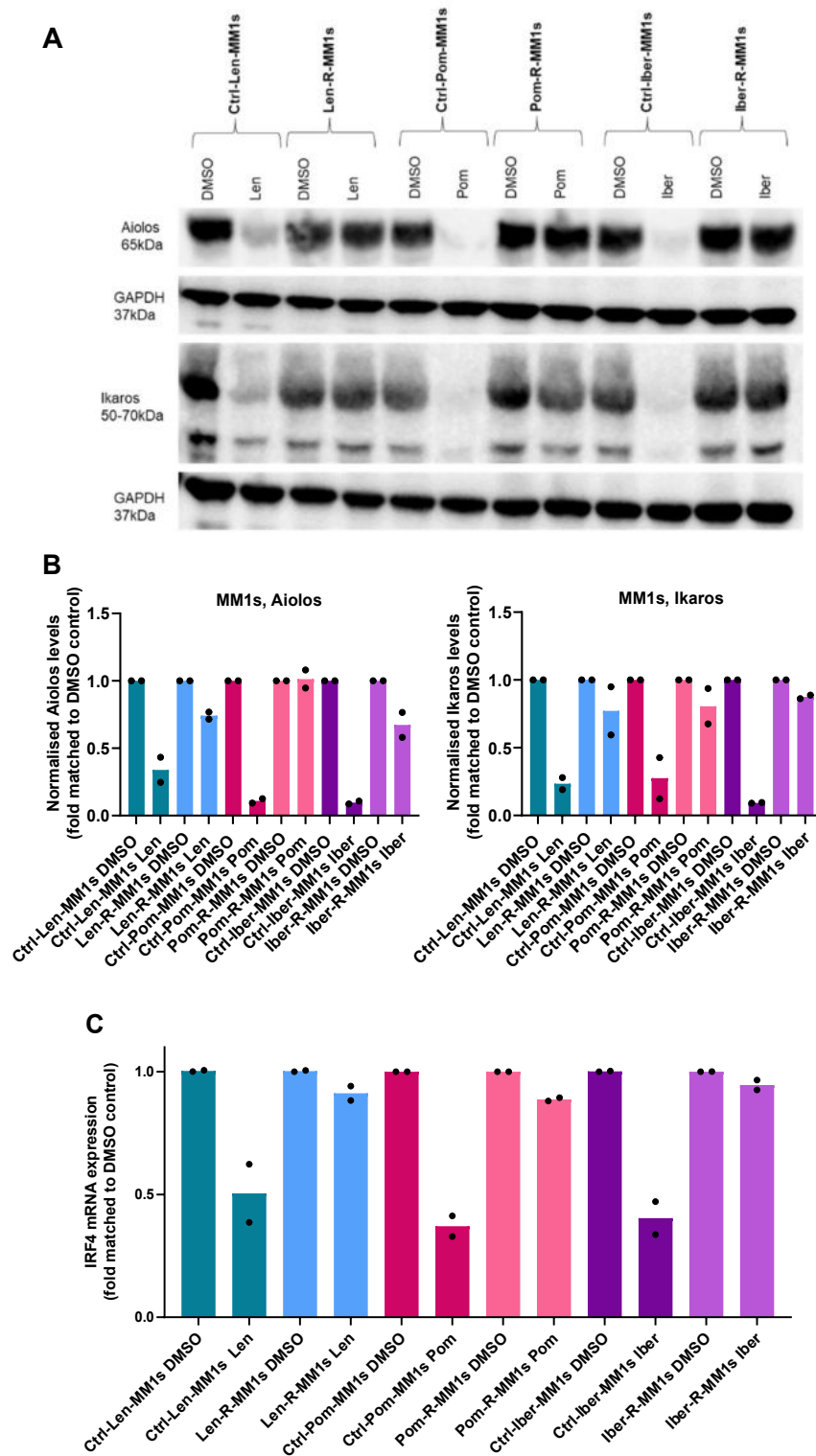


**Figure 3-10** The effect of IMiD/CELMOd treatment on Aiolos, Ikaros and IRF4 in the MM1s cell lines.

Aiolos and Ikaros were degraded in the control lines with IMiD/CELMOd treatment, but this effect was abrogated in the resistant lines; A) is a representative western blot and B) shows quantification of western blots (individual points represent independent experiments (n=2) and the bar represents the median). C) *IRF4* mRNA expression (by quantitative RT-PCR) was reduced in the control lines with IMiD/CELMOd treatment but this effect was reduced in the resistant cell lines. Individual points represent independent experiments (n=2), and the bar represents the median. Len, lenalidomide; pom, pomalidomide; iber, iberdomide.

In the H929 control lines there was a reduction in the level of Aiolos and Ikaros with IMiD/CELMoD treatment due to degradation. This effect was greatly reduced in the resistant lines (but less so in Len-R-H929 which appears to retain some functional CRBN) (**Figure 3-11**). This did not lead to a change in *IRF4* expression at 24 hours, but at 48 hours there was a small reduction in *IRF4* mRNA with iberdomide in the Ctrl-Iber-H929 line that was not seen in its resistant partner (**Figure 3-12**).

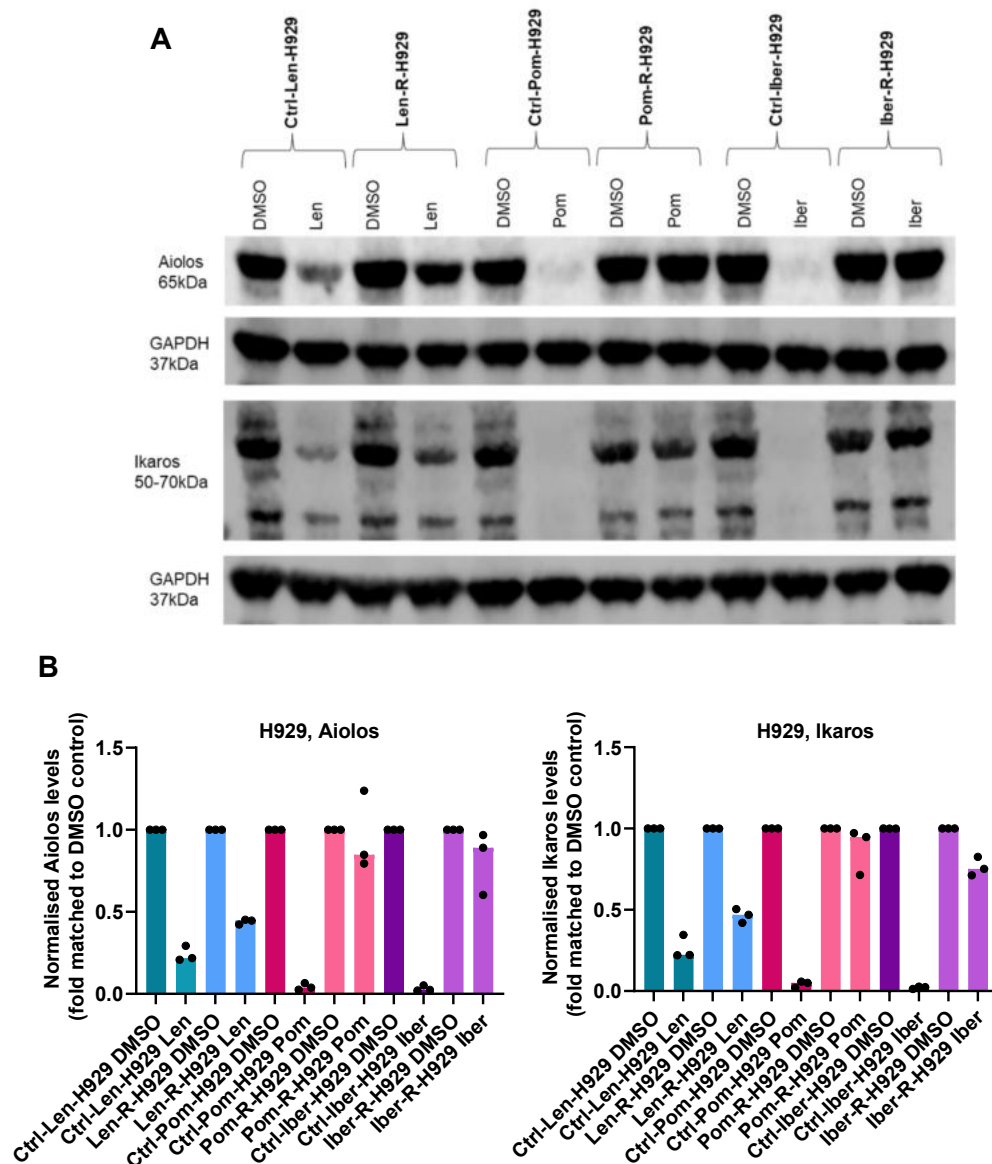


**Figure 3-11** The effect of IMiD/CELMoD treatment on Aiolos and Ikaros in the H929 cell lines.

Aiolos and Ikaros were degraded in the control lines with IMiD/CELMoD treatment, but this effect was abrogated in the resistant lines; A) is a representative western blot and B) shows quantification of western blots (individual points represent independent experiments (n=3) and the bar represents the median).

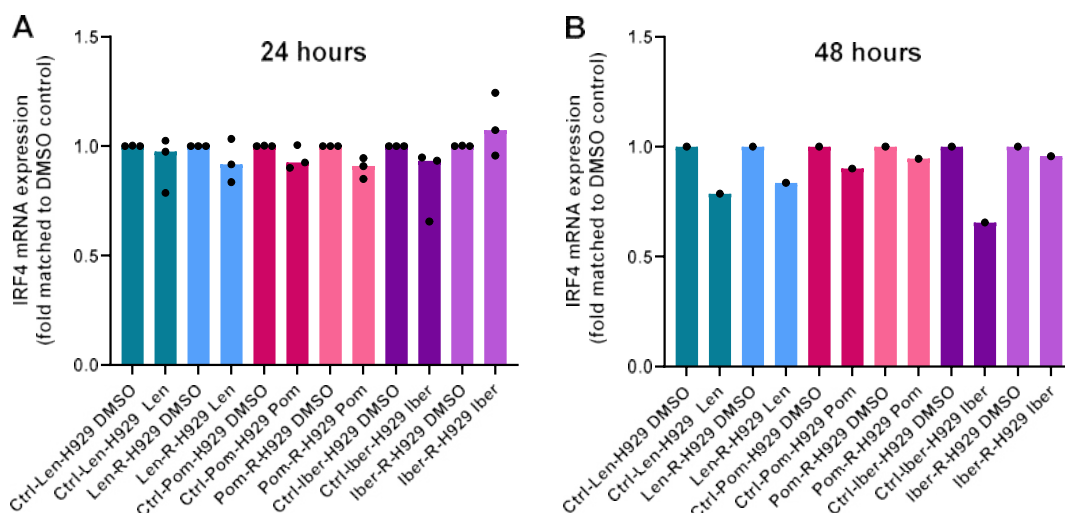


**Figure 3-12** The effect of IMiDs/CELMODs on *IRF4* in the H929 cell lines.

Quantitative RT-PCR showed no reduction in *IRF* mRNA at the 24-hour time point (A). At the 48-hour time point (B) there was a small reduction in *IRF4* mRNA in the Ctrl-Iber-H929 line with iberdomide. Individual points represent independent experiments, and the bar represents the median.

### 3.2.2 Whole exome sequencing of the resistant cell lines

Whole exome sequencing (WES) was carried out to explore whether IMiD resistance might be due to mutations affecting *CRBN* or other key *CRBN* pathway members (**Figure 1-2**). Each of the resistant cell lines had several mutations that were likely to highly impact on protein function. It is important to note that the control cell lines also gained some high impact mutations compared to the parental MM1s and H929 cell lines (data not shown), as has previously been observed during long-term cell culture (142). The high impact gene mutations for each of the resistant cell lines (present in resistant line but not its DMSO control line) are shown in the table below (**Table 3-3**).

Cell line	Mutated genes (with a predicted high impact on the resultant protein)
Len-R-MM1s	AC004997.1, CASTOR1, DSCAM, FNDC7, KATNBL1, MKI67, PADI3, PLXNA3, SLC38A8, SYNC, WASL, ZNF746
Pom-R-MM1s	ABCA2, AL109761.1, APBA1, ATP6V1F, CD22, CRBN, DGKK, FNDC7, KATNBL1, KIF13B, LAMA3, MKI67, MMP28, PKD1L1, RIPK4, RYR2, SLC4A10, SPPL2B, SPTA1, THBS3, TIGD4, TXNL1, UBR2
Iber-R-MM1s	ABCA2, APBA1, CD22, DSCAM, ELL2, FNDC7, MKI67, MYO1H, PKD1L1, SPTA1, SYNC, THBS3, TXNL1
Len-R-H929	ACADVL, TTN, TXNRD3
Pom-R-H929	ABCB11, ANKRD36, C5, CCNT1, CRBN, DIP2B, IFI16, LAMC3, MAG, MPP1, MTRES1, MYH1, NBEA, SLC4A1AP, TACC2, YAP1, ZBTB41
Iber-R-H929	CCNT1, CRBN, MTRES1

*Table 3-3 Mutations in the resistant cell lines.*

This table lists the mutations observed in each cell line. For the full name of each gene see **Supplementary Table 9-1**.

### **Genetic changes in CRBN and its regulators**

CRBN mutations were identified in 3 of the acquired IMiD-resistant cell lines. Pom-R-MM1s had a mutation which created a splice site variant (C to G at position 3154076 chr3) and both Pom-R-H929 and Iber-R-H929 had a mutation which created an early stop codon (G to A at position 3174138 chr3) (**Figure 3-13**). These mutations were predicted (by Ensembl Variant Effector Predictor) to have a high impact on the resultant protein. The allele frequency (AF) for these mutations is shown in **Table 3-4**. No high impact mutations in other IMiD pathway genes (**Figure 1-2**) were observed in any of the cell lines.

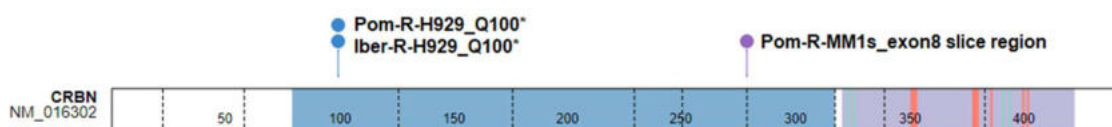


*Figure 3-13 Mutations in CRBN.*

Pom-R-H929 and Iber-R-H929 had an early stop codon mutation and Pom-R-MM1s had a splice site mutation. LON substrate binding domain (blue), thalidomide binding domain (purple), tri-tryptophan IMiD binding pocket (red), zinc ion binding site (green). Image created using ProteinPaint (<https://proteinpaint.stjude.org>).

Cell line	Mutation in CRBN	AF in the resistant line (%)	AF in the control line (%)
Pom-R-MM1s	3154076 - C to G	26.3	3.0
Pom-R-H929	3174138 - G to A	80.3	1.1
Iber-R-H929	3174138 - G to A	63.6	1.8

*Table 3-4 Allele frequency of each CRBN mutation in the resistant line and its matched control line.*

The table shows the allele frequency (AF) of each mutation in the resistant line and its matched control line. AF is calculated by dividing the number of times the allele of interest (i.e. the mutated CRBN) is observed in the population by the total number of copies of all the alleles at that particular genetic locus in the population.

### ***Copy number loss at the CRBN, COPS7B and COPS8 loci***

Copy number loss at the CRBN locus was also explored as this has been associated with IMiD resistance in the literature (143). Pom-R-H929 had the largest copy number loss at this locus, with Len-R-H929 showing copy number loss a lesser degree (**Figure 3-14**). Copy number loss was also explored at the COPS7B (**Figure 3-15**) and COPS8 (**Figure 3-16**) loci. COPS7B and COPS8 are COPS9 signalosome members which are essential for maintenance of the CRL4 E3 ubiquitin ligase and copy number loss at their loci has also been associated with IMiD resistance in patients (90, 95). There was not a large degree of copy number loss at either of these loci in any of the resistant cell lines.

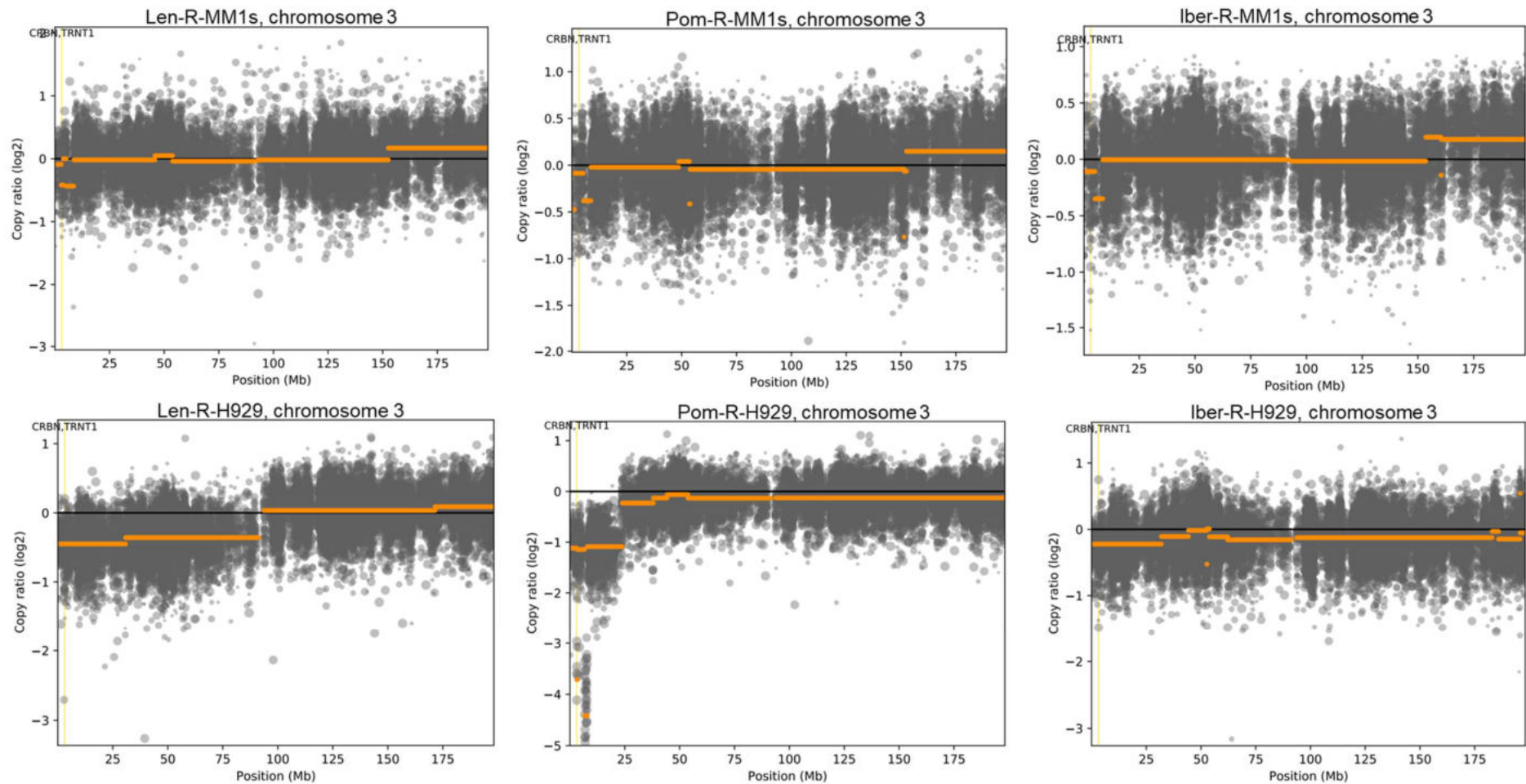
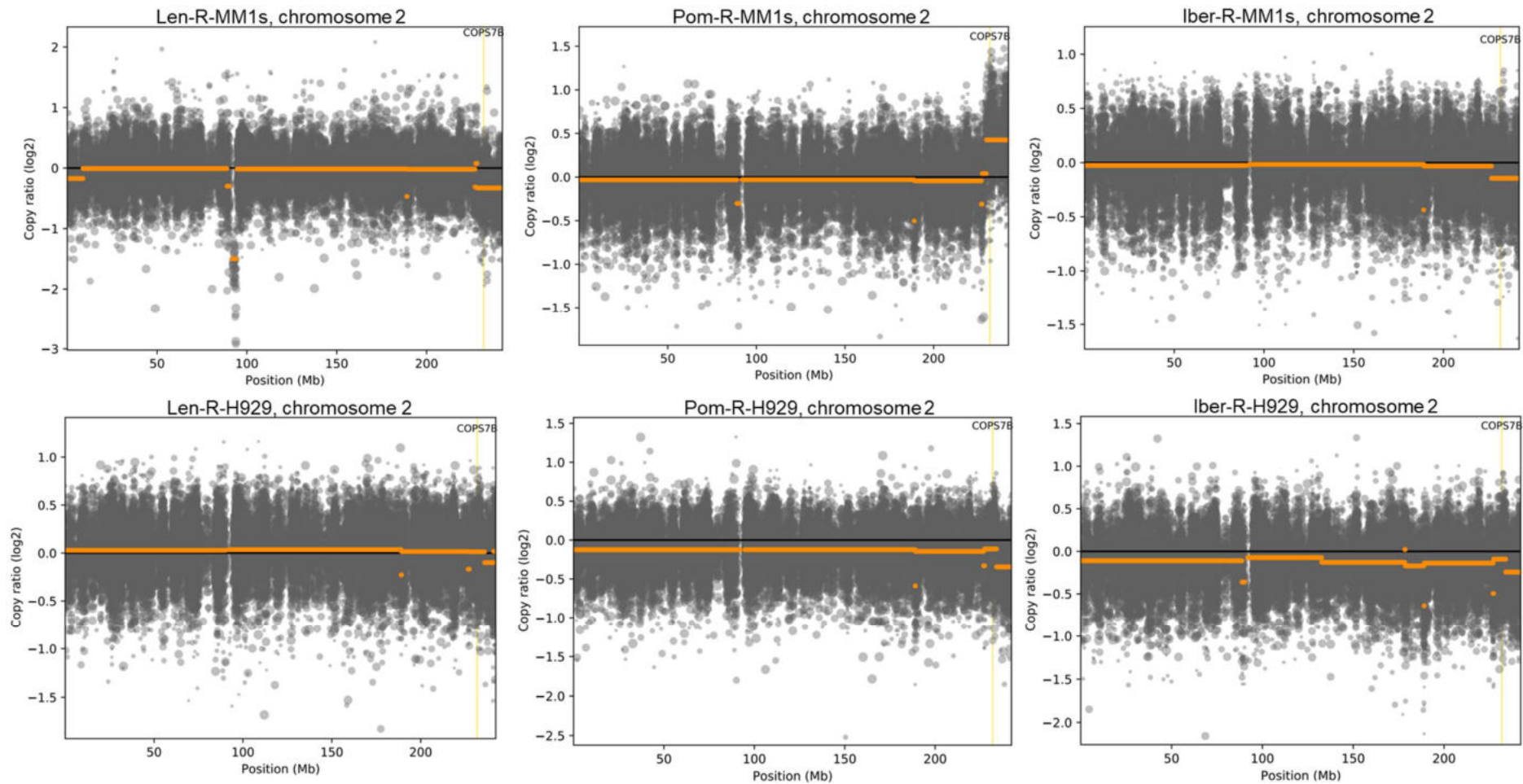


Figure 3-14 Copy number loss at the *CRBN* locus in the resistant cell lines.

Copy number loss was observed in Pom-R-H929, and to a lesser degree in Len-R-H929. Plots were generated by CNVkit; the grey circles represent individual bins (segments of the sequence), and the orange line indicates copy number change. The yellow vertical line shows the position of *CRBN* on chromosome 3 (144).





*Figure 3-15 Copy number loss at the COPS7B locus in the resistant cell lines.*

There was not a large degree of copy number loss at *COPS7B* in any of the resistant cell lines. Plots were generated by CNVKit; the grey circles represent individual bins (segments of the sequence), and the orange line indicates copy number change. The yellow vertical line shows the position of *COPS7B* on chromosome 2 (144).

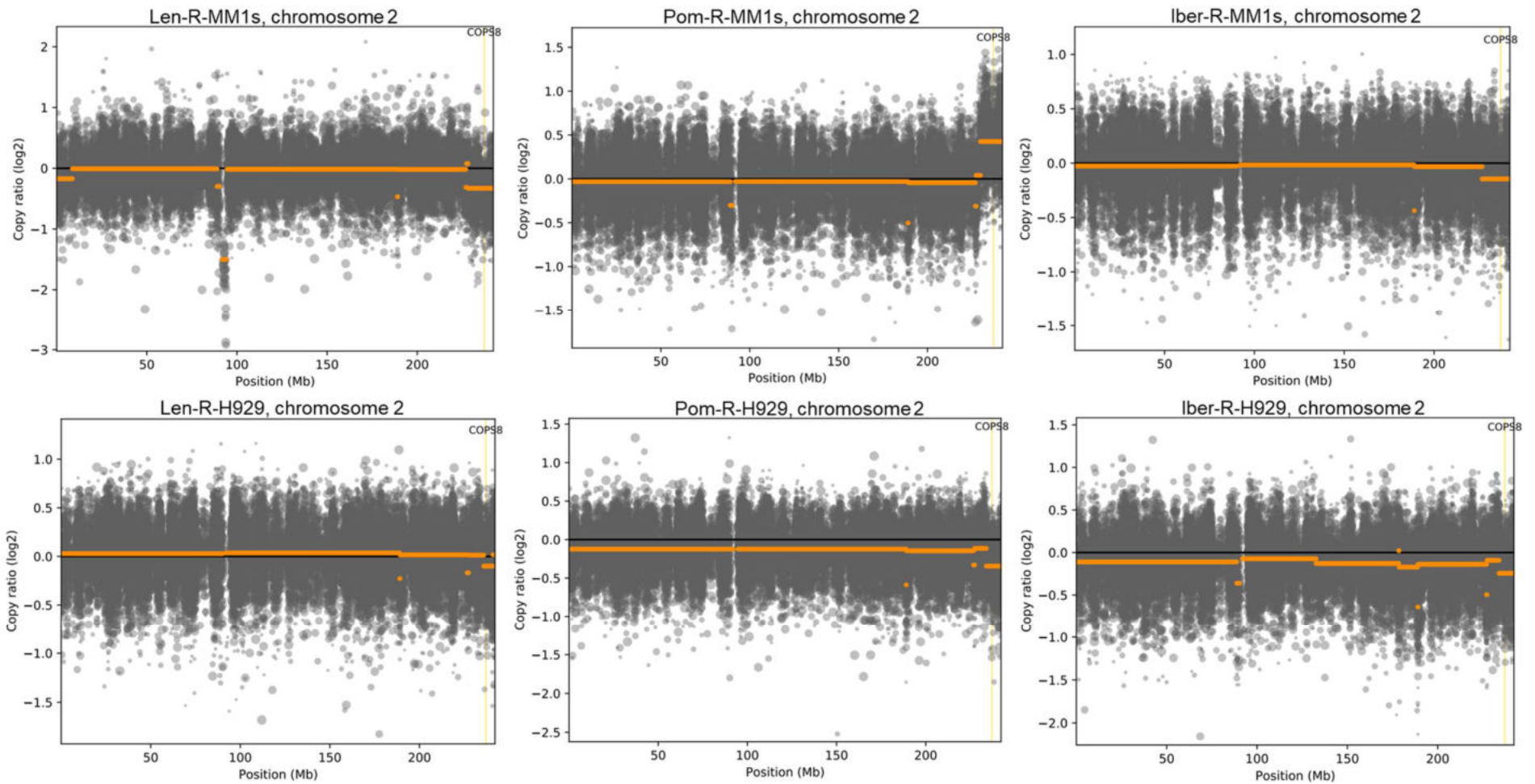


*Figure 3-16 Copy number loss at the COPS8 locus in the resistant cell lines.*

There was not a large degree of copy number loss at COPS8 in any of the resistant cell lines. Plots were generated by CNVKit; the grey circles represent individual bins (segments of the sequence), and the orange line indicates copy number change. The yellow vertical line shows the position of COPS8 on chromosome 2 (144).



### **Mutations in other genes**

All 3 MM1s cell lines had developed a mutation in Fibronectin Type III Domain Containing 7 (*FNDC7*), a protein coding gene on Chromosome 1 that has limited information available about its function, and Marker of Proliferation Ki-67 (*MKI67*), which is involved in chromosome segregation and regulation of mitotic nuclear division. As well as sharing the same *CRBN* mutation, Pom-R-H929 and Iber-R-H929 also both had mutations in Cyclin T1 (*CCNT1*) and Mitochondrial Transcription Rescue Factor 1 (*MTRES1*).

### **3.2.3 RNA-Seq analysis in the resistant cell lines**

#### ***CRBN* expression**

In order to identify key gene expression differences in the resistant setting, baseline RNA-Seq analysis was performed on the resistant lines and their control lines. *CRBN* mRNA was significantly reduced in all of the resistant cell lines (**Figure 3-17**), in keeping with the RT-PCR data shown above (**Figure 3-7**).

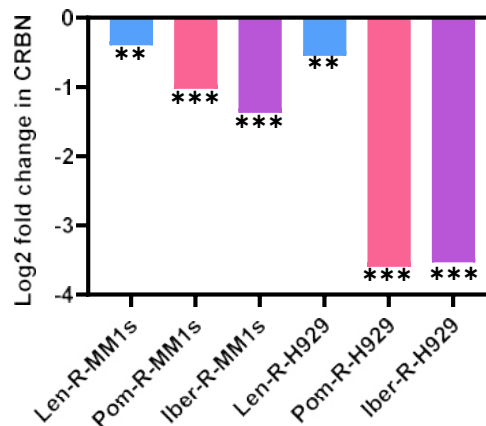


*Figure 3-17 CRBN RNA expression in the resistant cell lines.*

*CRBN* was reduced at the mRNA level in the resistant cell lines. Each resistant cell line was compared to its matched control line using DESeq2. \*\* adj p<0.01, \*\*\* adj p<0.001.

### **Differential gene expression in the resistant cell lines**

#### ***Commonly altered transcripts in the resistant lines***

The transcriptomes of each IMiD-resistant cell line and its control line were compared. Genes for which mRNA expression was increased or decreased (log2 fold change +/- 0.2, adjusted p value of <0.05) in the resistant line compared to its control were selected. The sets of genes this generated per line were then compared using Venn diagrams. No genes were commonly upregulated in all 6

cell lines, but 17 genes were commonly upregulated in 5 of the lines (**Supplementary Table 9-2**). *CRBN* was the only gene commonly down regulated in all 6 cell lines but 10 genes were commonly downregulated in  $\geq 5$  lines (**Supplementary Table 9-2**), including two genes from the NF $\kappa$ B pathway, Baculoviral IAP Repeat Containing 3 (*BIRC3*) and TNF Alpha Induced Protein 3 (*TNFAIP3*).

*Functional enrichment analysis of altered transcripts in the resistant lines*

Functional enrichment analysis (using g:Profiler) was performed for each cell line individually, exploring the most upregulated and downregulated transcripts (**Table 3-5**). No common pathways between cell lines were observed.

Cell line	Number of upregulated transcripts in the resistant line (adj p<0.05)	Enriched pathways in upregulated transcripts
Len-R-MM1s	55	N/A
Pom-R-MM1s	1147	Aldosterone-regulated sodium reabsorption (KEGG)
Iber-R-MM1s	259	Cell adhesion molecules (KEGG), Attachment and entry (REAC)
Len-R-H929	2236	N/A
Pom-R-H929	4230	Viral protein interaction with cytokine and cytokine receptor (KEGG), Interactions of natural killer cells in pancreatic cancer (WP)
Iber-R-H929	4264	N/A
Cell line	Number of downregulated transcripts in the resistant line (adj p<0.05)	Enriched pathways in downregulated transcripts
Len-R-MM1s	33	Interleukin-10 signaling (REAC), IL1 and megakaryocytes in obesity (WP)
Pom-R-MM1s	1692	Lacto series sphingolipid metabolism (WP)
Iber-R-MM1s	370	Biosynthesis of amino acids (KEGG), Response of EIF2AK1 (HRI) to heme deficiency (REAC)
Len-R-H929	2466	N/A
Pom-R-H929	4507	N/A
Iber-R-H929	3991	N/A

*Table 3-5 Functional enrichment analysis of transcripts with altered expression in the resistant cell lines.*

Functional enrichment analysis was performed on upregulated and downregulated transcripts in the resistant cell lines. Analysis was performed on statistically significantly altered transcripts (adj p<0.05), with the top 100 transcripts by fold change analysed if the set size was >100. Analysis performed with g:Profiler and results for KEGG, Reactome (REAC) and WikiPathways (WP) shown (145).

### ***The NFκB pathway in the resistant cell lines***

Two of the 27 genes with common differential expression in the resistant cell lines, *BIRC3* and *TNFAIP3*, are members of the NFκB signalling pathway, which is known to be important in myeloma pathogenesis (146). These genes were significantly upregulated in 5 of the 6 resistant cell lines (**Figure 3-18**).

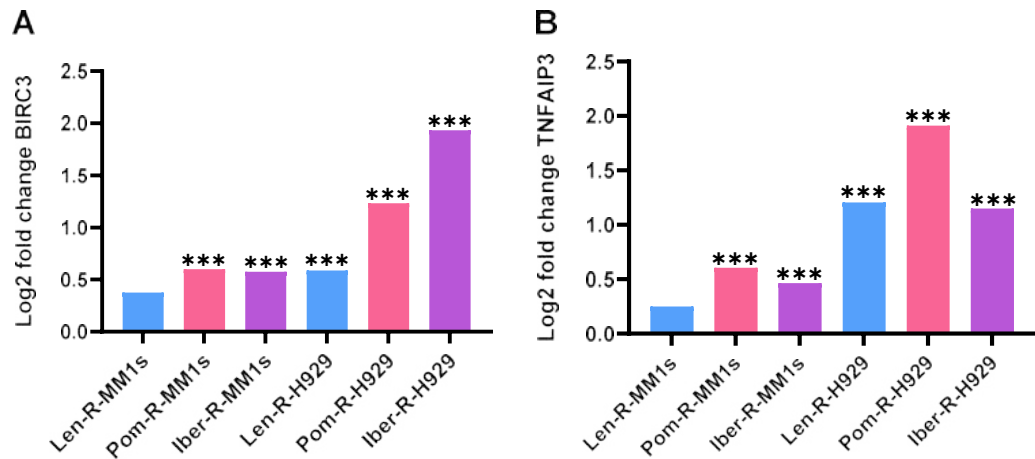


**Figure 3-18** mRNA expression of *TNFAIP3* and *BIRC3* in the resistant cell lines.

Each resistant cell line was compared to its matched control line using DESeq2; A) shows mRNA changes in *BIRC3* and B) shows mRNA changes in *TNFAIP3*. N=3, \*\*\* adj p<0.001.

Quantitative proteomics was used to explore *TNFAIP3* and *BIRC3* at the protein level. *BIRC3* was expressed at very low abundance in the MM1s lines and was not detected in the H929 lines. There was a small increase in *BIRC3* in the resistant MM1s cell lines, which reached statistical significance in Pom-R-MM1s and Iber-R-MM1s (**Figure 3-19**). *TNFAIP3* protein abundance was unchanged in the MM1s resistant lines but was significantly increased in the H929 resistant lines, which was confirmed on western blot (**Figure 3-19**).

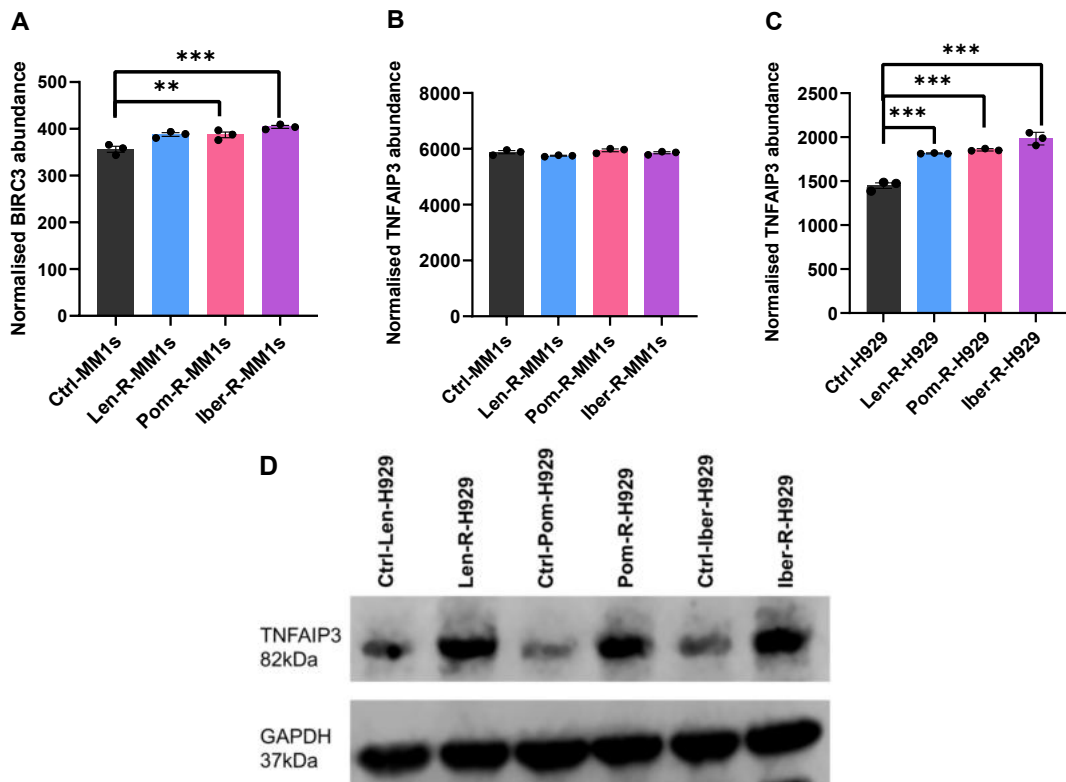


**Figure 3-19 Protein abundance of TNFAIP3 and BIRC3 in the resistant cell lines.**

Each resistant cell line was compared to control (Ctrl-Iber-MM1s for MM1s resistant lines and Ctrl-Iber-H929 for H929 resistant lines). Quantitative proteomic data for A) BIRC3 in the MM1s cells, B) TNFAIP3 in the MM1s lines and C) TNFAIP3 in the H929 lines was analysed by a limma modified t-test in Phantasus (v1.19.3). Bar shows mean and error bars represent SEM, n=3, \*\* adj p<0.01, \*\*\* adj p<0.001. D) is a representative western blot of TNFAIP3 in the H929 lines (n=2).

These data suggest that the NF $\kappa$ B pathway is altered in the resistant setting. There are several compounds that inhibit IAPs (inhibitor of apoptosis proteins) such as BIRC3. SM-164 is a SMAC (second mitochondrial-derived activator of caspases) mimetic which inhibits all 3 IAPs: cIAP1, cIAP2 (otherwise known as BIRC3) and XIAP. The MM1s cell lines were not sensitive to SM-164. However, the IMiD/CELMoD-resistant H929 lines appeared to be cross-resistant to SM-164 treatment, perhaps because they have higher levels of cIAP2/BIRC3 (**Figure 3-20**). This suggests that cIAP2/BIRC3 does not represent a good therapeutic target in the resistant cells.

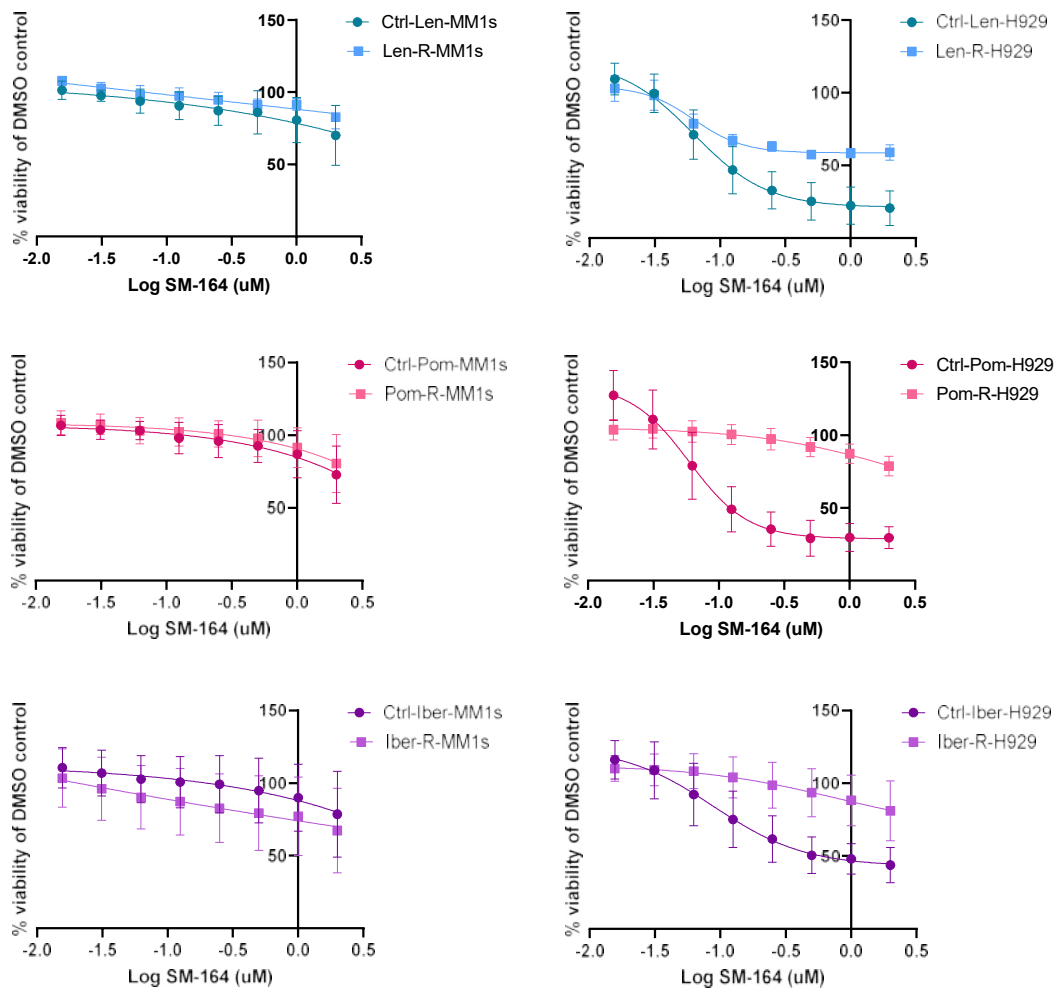


**Figure 3-20** The effect of SM-164 on cell viability in the resistant cell lines.

SM-164 did not affect viability in the MM1s cell lines in a 3-day CellTiter-Blue viability assay. The control H929 lines were sensitive to SM-164, but the resistant H929 lines exhibited cross-resistance. Mean and SEM shown, n=3.

### 3.2.4 Proteome and phosphoproteome analysis in the resistant cell lines

The resistant cell lines and one representative control line (Ctrl-Iber-MM1s and Ctrl-Iber-H929) underwent whole proteome evaluation. This was performed using a TMT-multiplexing approach. The proteomes of the resistant lines were heterogeneous but reduction in CRBN was confirmed in all of the resistant lines (Figure 3-8).

#### Proteome analysis in the resistant cell lines

##### Commonly altered proteins in the resistant lines

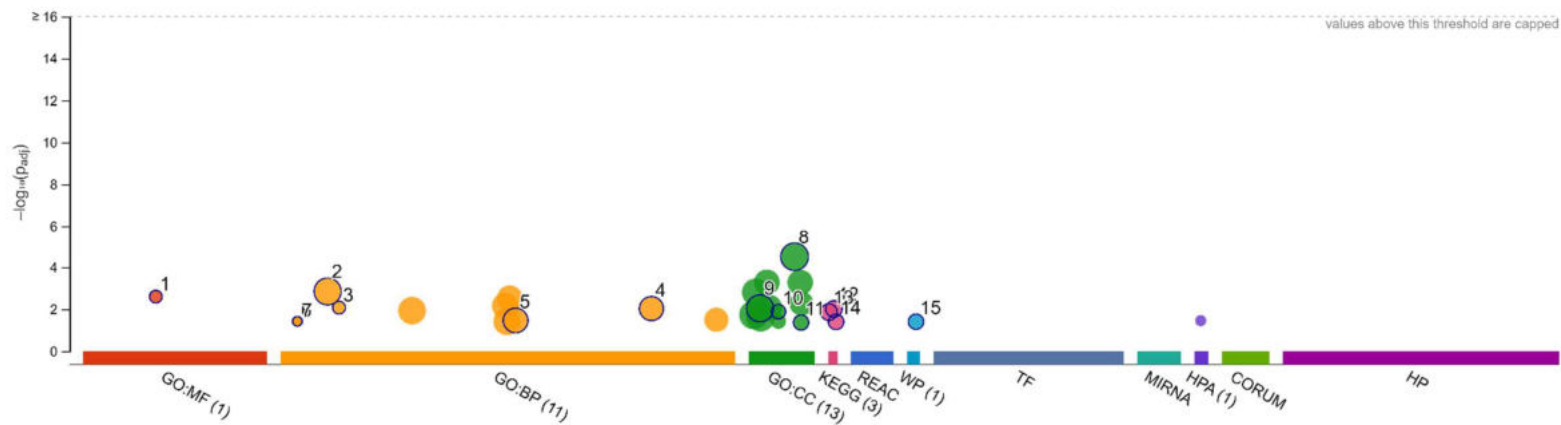
The proteomes of each IMiD-resistant cell line and its control line were compared. Proteins for which abundance was increased or decreased (log<sub>2</sub> fold change +/- 0.2, adjusted p value <0.05) in the resistant line compared to its control were

selected. The sets of proteins this generated for each line were then compared using Venn diagrams. Family With Sequence Similarity 169 Member A (FAM169A) was the only protein upregulated in all of the resistant lines, and only two proteins (Carbonic Anhydrase 8 and MX Dynamin Like GTPase 1) were upregulated in 5 lines. Fourteen proteins were commonly upregulated in  $\geq 4$  of the 6 resistant cell lines (**Supplementary Table 9-3**). Only two proteins, CRBN and Stearoyl-Co-A Desaturase (SCD), were downregulated in all 6 cell lines. Two further proteins, Prolyl 4-Hydroxylase Subunit Alpha 1 (P4HA1) and Sulfite Oxidase (SUOX), were downregulated in 5 cell lines and 20 proteins were commonly downregulated in  $\geq 4$  of the 6 pairs (**Supplementary Table 9-3**). There was common alteration in a number of proteins involved in lipid synthesis including HMG-CoA Reductase (HMGCR), Stearoyl-CoA Desaturase (SCD), Acyl-CoA Synthetase Long Chain Family Member 4 (ACSL4), Fatty Acid Synthase (FASN) and Farnesyl Diphosphate Synthase (FDPS).

#### *Functional enrichment analysis of altered proteins in the resistant lines*

Functional enrichment analysis (carried out in g:Profiler) was performed on proteins that were upregulated or downregulated in each resistant line compared to control (with an adj  $p < 0.05$ ). Where this criterion described many proteins only the top 100 upregulated or downregulated proteins were evaluated. The full g:Profiler results for Iber-R-MM1s are shown (**Figure 3-21, Figure 3-22**), with a table summarising the analyses of the other cell lines (**Table 3-6**).

There were common changes in lipid synthesis pathways (including the Sterol regulatory element binding protein (or SREBP) pathway, fatty acid metabolism and cholesterol biosynthesis) in proteins with significantly downregulated expression in 5 out of the 6 resistant cell lines. This will be discussed in greater depth in Chapter 7.

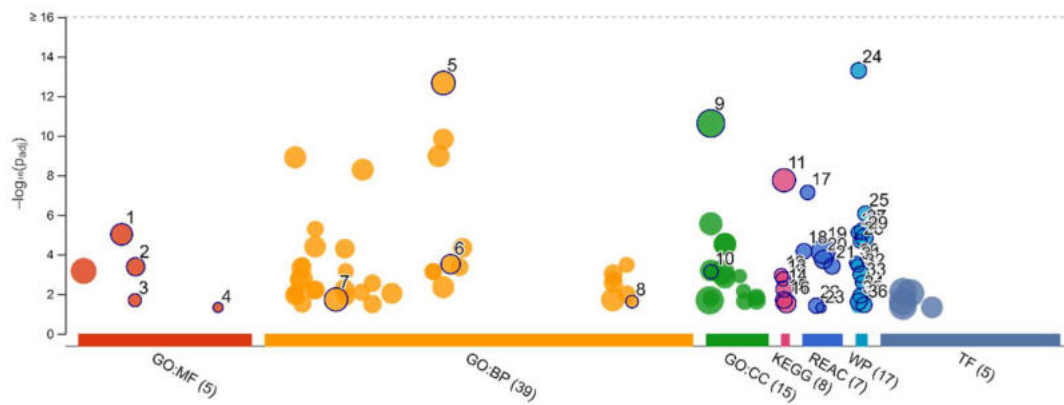


ID	Source	Term ID	Term Name	Padj (query_1)
1	GO:MF	GO:0032395	MHC class II receptor activity	$2.533 \times 10^{-3}$
2	GO:BP	GO:0007275	multicellular organism development	$1.434 \times 10^{-3}$
3	GO:BP	GO:0009445	putrescine metabolic process	$8.478 \times 10^{-3}$
4	GO:BP	GO:1901701	cellular response to oxygen-containing compound	$9.420 \times 10^{-3}$
5	GO:BP	GO:0051240	positive regulation of multicellular organismal pro...	$3.465 \times 10^{-2}$
6	GO:BP	GO:0002469	myeloid dendritic cell antigen processing and pres...	$3.816 \times 10^{-2}$
7	GO:BP	GO:0002491	antigen processing and presentation of endogeno...	$3.816 \times 10^{-2}$
8	GO:CC	GO:0071944	cell periphery	$3.166 \times 10^{-3}$
9	GO:CC	GO:0012505	endomembrane system	$9.111 \times 10^{-3}$
10	GO:CC	GO:0042613	MHC class II protein complex	$1.315 \times 10^{-2}$
11	GO:CC	GO:0098553	luminal side of endoplasmic reticulum membrane	$4.342 \times 10^{-2}$
12	KEGG	KEGG:04672	Intestinal immune network for IgA production	$9.799 \times 10^{-3}$
13	KEGG	KEGG:00330	Arginine and proline metabolism	$1.380 \times 10^{-2}$
14	KEGG	KEGG:05310	Asthma	$4.037 \times 10^{-2}$
15	WP	WP:WP5284	Cell interactions of the pancreatic cancer microenv...	$3.971 \times 10^{-2}$

Figure 3-21 Functional enrichment analysis of upregulated proteins in Iber-R-MM1s.

The top 100 upregulated proteins (by fold change) underwent functional enrichment analysis in g:Profiler (145). Driver GO terms and all KEGG, Reactome and WikiPathways pathways are highlighted.





ID	Source	Term ID	Term Name	Padj (query_1)
1	GO:MF	GO:0016491	oxidoreductase activity	$9.719 \times 10^{-6}$
2	GO:MF	GO:0019842	vitamin binding	$4.188 \times 10^{-4}$
3	GO:MF	GO:0019215	intermediate filament binding	$2.054 \times 10^{-2}$
4	GO:MF	GO:0090433	palmitoyl-CoA ligase activity	$4.777 \times 10^{-3}$
5	GO:BP	GO:0044281	small molecule metabolic process	$2.172 \times 10^{-13}$
6	GO:BP	GO:0045333	cellular respiration	$3.087 \times 10^{-4}$
7	GO:BP	GO:0010941	regulation of cell death	$1.895 \times 10^{-2}$
8	GO:BP	GO:1903069	regulation of ER-associated ubiquitin-dependent ...	$2.428 \times 10^{-2}$
9	GO:CC	GO:0005737	cytoplasm	$2.406 \times 10^{-11}$
10	GO:CC	GO:0005751	mitochondrial respiratory chain complex IV	$7.481 \times 10^{-4}$
11	KEGG	KEGG:01100	Metabolic pathways	$1.783 \times 10^{-8}$
12	KEGG	KEGG:00100	Steroid biosynthesis	$1.150 \times 10^{-3}$
13	KEGG	KEGG:00900	Terpenoid backbone biosynthesis	$1.716 \times 10^{-3}$
14	KEGG	KEGG:01212	Fatty acid metabolism	$5.715 \times 10^{-3}$
15	KEGG	KEGG:01230	Biosynthesis of amino acids	$1.992 \times 10^{-2}$
16	KEGG	KEGG:04714	Thermogenesis	$2.924 \times 10^{-2}$
17	REAC	REAC:R-HSA-19...	Cholesterol biosynthesis	$7.355 \times 10^{-8}$
18	REAC	REAC:R-HSA-24...	Activation of gene expression by SREBF (SREBP)	$6.935 \times 10^{-5}$
19	REAC	REAC:R-HSA-14...	Metabolism	$7.086 \times 10^{-5}$
20	REAC	REAC:R-HSA-89...	Metabolism of steroids	$1.787 \times 10^{-4}$
21	REAC	REAC:R-HSA-16...	Regulation of cholesterol biosynthesis by SREBP (S...	$3.890 \times 10^{-4}$
22	REAC	REAC:R-HSA-75...	Fatty acyl-CoA biosynthesis	$3.873 \times 10^{-2}$
23	REAC	REAC:R-HSA-43...	Intracellular metabolism of fatty acids regulates in...	$4.997 \times 10^{-2}$
24	WP	WP:WP4718	Cholesterol metabolism with Bloch and Kandutsch...	$5.103 \times 10^{-14}$
25	WP	WP:WP5333	Cholesterol metabolism	$8.596 \times 10^{-7}$
26	WP	WP:WP197	Cholesterol biosynthesis pathway	$7.673 \times 10^{-6}$
27	WP	WP:WP5304	Cholesterol metabolism	$6.585 \times 10^{-6}$
28	WP	WP:WP5193	Cholesterol synthesis disorders	$2.153 \times 10^{-5}$
29	WP	WP:WP5329	Cholesterol biosynthesis pathway in hepatocytes	$1.437 \times 10^{-5}$
30	WP	WP:WP4190	Mevalonate arm of cholesterol biosynthesis pathw...	$2.670 \times 10^{-4}$
31	WP	WP:WP4724	Omega-9 fatty acid synthesis	$3.718 \times 10^{-4}$
32	WP	WP:WP4313	Ferroptosis	$9.851 \times 10^{-4}$
33	WP	WP:WP357	Fatty acid biosynthesis	$2.600 \times 10^{-3}$
34	WP	WP:WP5312	Metabolic pathways of fibroblasts	$1.209 \times 10^{-2}$
35	WP	WP:WP1982	Sterol regulatory element-binding proteins (SREBP...	$2.426 \times 10^{-2}$
36	WP	WP:WP4290	Metabolic reprogramming in colon cancer	$3.563 \times 10^{-2}$

**Figure 3-22 Functional enrichment analysis of downregulated proteins in Iber-R-MM1s.**

The top 100 downregulated proteins (by fold change) underwent functional enrichment analysis in g:Profiler (145). Driver GO terms and all KEGG, Reactome and WikiPathways pathways are highlighted.

<b>Cell line</b>	<b>Number of upregulated proteins in the resistant line (adj p&lt;0.05, those included in the analysis capped at 100)</b>	<b>Enriched pathways in upregulated proteins</b>
Len-R-MM1s	59	Selenium micronutrient network
Pom-R-MM1s	1168	2q37 copy number variation syndrome
Iber-R-MM1s	761	Cell interactions of the pancreatic cancer microenvironment
Len-R-H929	2543	N/A
Pom-R-H929	2158	Kit receptor signaling pathway
Iber-R-H929	2173	B cell receptor signaling pathway
<b>Cell line</b>	<b>Number of downregulated proteins in the resistant line (adj p&lt;0.05, those included in the analysis capped at 100)</b>	<b>Enriched pathways in downregulated proteins</b>
Len-R-MM1s	40	Cholesterol metabolism with Bloch and Kandutsch-Russell pathways, Sterol regulatory element-binding proteins (SREBP) signaling, Cholesterol metabolism, Mevalonate arm of the cholesterol biosynthesis pathway, Omega-9 fatty acid synthesis, Cholesterol biosynthesis pathway, Cholesterol synthesis disorders, Cholesterol biosynthesis pathway in hepatocytes, Fatty acid biosynthesis, Cholesterol metabolism, Mevalonate pathway
Pom-R-MM1s	990	Amino acid metabolism in triple-negative breast cancer cells, MFAP5 effect on permeability and motility of endothelial cells via cytoskeleton rearrangement, Neuroinflammation and glutamatergic signaling
Iber-R-MM1s	409	Cholesterol metabolism with Bloch and Kandutsch-Russell pathways, Cholesterol metabolism, Cholesterol biosynthesis pathway, Cholesterol biosynthesis pathway in hepatocytes, Cholesterol synthesis disorders, Mevalonate arm of cholesterol biosynthesis pathway, Omega-9 fatty acid synthesis,

		Ferroptosis, Mevalonate pathway, Fatty acid biosynthesis, Metabolic pathways of fibroblasts, Electron transport chain: OXPHOS system in mitochondria, Mitochondrial complex IV assembly, Sterol regulatory element-binding proteins (SREBP) signaling, Metabolic reprogramming in colon cancer, SREBF and miR33 in cholesterol and lipid homeostasis
Len-R-H929	2431	Omega-9 fatty acid synthesis, Cholesterol metabolism with Bloch and Kandutsch-Russel
Pom-R-H929	2324	Omega-9 fatty acid synthesis, Cholesterol metabolism with Bloch and Kandutsch-Russell pathways, Exercise-induced circadian regulation
Iber-R-H929	2299	Omega-9 fatty acid synthesis, Cholesterol metabolism with Bloch and Kandutsch-Russell pathways, Ethylmalonic encephalopathy

*Table 3-6 Functional enrichment analysis in the resistant cell lines.*

Functional enrichment analysis was performed on upregulated and downregulated proteins in the resistant cell lines. Analysis was performed on proteins with adj  $p < 0.05$ , with the top 100 proteins by fold change analysed if the set size was  $> 100$ . Analysis performed with g:Profiler and results for WikiPathways shown (145).

### ***Phosphoproteome analysis in the resistant cell lines***

Matched phosphoproteomics was also performed in the cell lines and ~7000 phosphosites were detected.

### ***Commonly altered protein phosphosites in the resistant lines***

The protein phosphosites in each IMiD-resistant cell line and its control line were compared. Sites with increased or decreased phosphorylation ( $\log_2$  fold change  $\pm 0.2$ , adjusted  $p$  value  $< 0.05$ ) in the resistant line compared to its control were selected. The sets of sites this generated per line were then compared by Venn diagrams. There were 2 sites with commonly increased phosphorylation in  $\geq 4$  of the 6 pairs (Ras GTPase-Activating-Like Protein IQGAP2 [S16] and Msx2-Interacting Protein [S847]) and 2 sites with commonly decreased phosphorylation in  $\geq 4$  of the 6 pairs (Heat Shock Protein Beta-1 [S15] and Heat Shock Protein Beta-1 [S82]). There were 44 sites with commonly increased phosphorylation in  $\geq 3$  of the 6 pairs and 67 sites with commonly decreased phosphorylation in  $\geq 3$  of the 6 pairs.

the 6 pairs (**Supplementary Table 9-4**). Interestingly, there were 2 sites in FASN (S207 and T2204) with significantly decreased phosphorylation in all three of the resistant H929 lines (FASN was a commonly downregulated protein in the proteomics). There was also a site of decreased phosphorylation in another protein involved in fatty acid synthesis, Acetyl-Coenzyme A Synthetase, Cytoplasmic (ACSS2 [S30]). Furthermore, there were 12 sites with decreased phosphorylation in MKI67 in all 3 of the resistant MM1s lines and WES analysis had identified MKI67 mutations in each of these lines (**Table 3-3**).

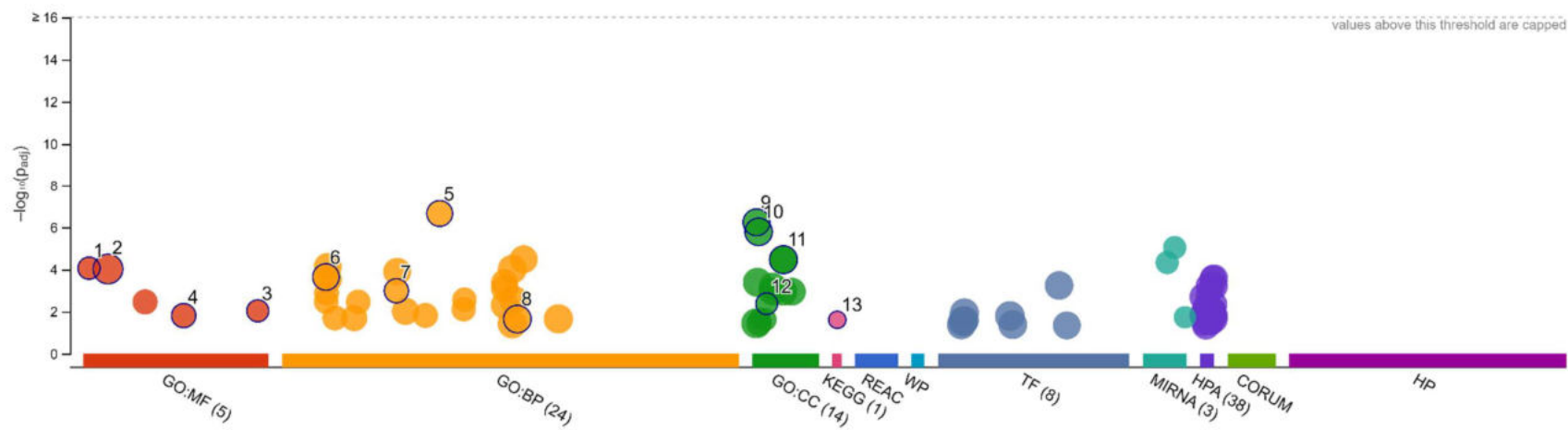
#### *Functional enrichment analysis of proteins with altered phosphorylation in the resistant lines*

Functional enrichment analysis (carried out in g:Profiler) in each of the resistant cell lines was performed on **proteins** containing sites of significantly (adj  $p < 0.05$ ) increased or decreased phosphorylation (compared to control). If the set size was  $>100$ , the 100 proteins containing phosphosites with the largest changes in phosphorylation were examined. The full g:Profiler results for Iber-R-MM1s are shown (**Figure 3-23**, **Figure 3-24**), with a table summarising the analysis in the other cell lines (**Table 3-6**). Four of the six resistant lines showed alterations in the Rho GTPase cycle/signalling by Rho GTPases pathways.



Figure 3-23 Functional enrichment analysis of proteins with increased phosphorylation in Iber-R-MM1s.

Pathway analysis was performed on the 100 proteins containing a phosphosite with the largest increase in phosphorylation (adj p<0.05) in g:Profiler (145). Driver GO terms and all KEGG, Reactome and WikiPathways pathways are highlighted.



ID	Source	Term ID	Term Name	Padj (query_1)
1	GO:MF	GO:0003712	transcription coregulator activity	$8.668 \times 10^{-5}$
2	GO:MF	GO:0005515	protein binding	$9.488 \times 10^{-5}$
3	GO:MF	GO:0140297	DNA-binding transcription factor binding	$9.204 \times 10^{-3}$
4	GO:MF	GO:0044877	protein-containing complex binding	$1.548 \times 10^{-2}$
5	GO:BP	GO:0035556	intracellular signal transduction	$2.198 \times 10^{-7}$
6	GO:BP	GO:0006996	organelle organization	$2.284 \times 10^{-4}$
7	GO:BP	GO:0022402	cell cycle process	$1.030 \times 10^{-3}$
8	GO:BP	GO:0051171	regulation of nitrogen compound metabolic proces...	$2.260 \times 10^{-2}$
9	GO:CC	GO:0005654	nucleoplasm	$5.748 \times 10^{-7}$
10	GO:CC	GO:0005829	cytosol	$1.631 \times 10^{-6}$
11	GO:CC	GO:0043232	intracellular non-membrane-bounded organelle	$3.419 \times 10^{-5}$
12	GO:CC	GO:0030055	cell-substrate junction	$4.224 \times 10^{-3}$
13	KEGG	KEGG:04370	VEGF signaling pathway	$2.459 \times 10^{-2}$

Figure 3-24 Functional enrichment analysis of proteins with decreased phosphorylation in Iber-R-MM1s.

Pathway analysis was performed on the 100 proteins containing a phosphosite with the largest decrease in phosphorylation (adj p<0.05) in g:Profiler (145). Driver GO terms and all KEGG, Reactome and WikiPathways pathways are highlighted.

	<b>Number of phosphorylation sites with increased phosphorylation (adj p&lt;0.05)</b>	<b>Number of unique proteins</b>	<b>Enriched pathways in proteins with increased phosphorylation</b>
Len-R-MM1s	74	33	N/A
Pom-R-MM1s	577	335	RHO GTPase cycle; Signaling by Rho GTPases; Signaling by Rho GTPases, Miro GTPases and RHOBTB3; RHO GTPase cycle
Iber-R-MM1s	456	271	RHO GTPase cycle; Signaling by Rho GTPases; Signaling by Rho GTPases, Miro GTPases and RHOBTB3; RAC1 GTPase cycle; CDC42 GTPase cycle
Len-R-H929	1546	822	N/A
Pom-R-H929	1185	539	N/A
Iber-R-H929	1003	498	Signaling by Rho GTPases; RHO GTPase cycle; Signaling by Rho GTPases, Miro GTPases and RHOBTB3
	<b>Number of phosphorylation sites with decreased phosphorylation (adj p&lt;0.05)</b>	<b>Number of unique proteins</b>	<b>Enriched pathways in proteins with decreased phosphorylation</b>
Len-R-MM1s	67	25	N/A
Pom-R-MM1s	612	332	Apoptotic cleavage of cellular proteins; Signaling by Rho GTPases, Miro GTPases and RHOBTB3; RHO GTPase cycle; Apoptotic execution phase; Apoptotic cleavage of cell adhesion proteins; Apoptosis; VEGFA-VEGFR2 Pathway; Signaling by VEGF; Programmed Cell Death; RHOBTB1 GTPase cycle; Semaphorin interactions; RHOBTB GTPase Cycle; RHOB GTPase cycle; Signal Transduction; Cell death signaling via NRAGE, NRIF and NADE

Iber-R-MM1s	303	175	N/A
Len-R-H929	1259	697	HDR through MMEJ (alt-NHEJ)
Pom-R-H929	897	539	RHO GTPase cycle; Signaling by Rho GTPases; Signaling by Rho GTPases, Miro GTPases and RHOBTB3
Iber-R-H929	1001	560	Signal Transduction; RHO GTPase cycle; Interactions of Tat with host cellular proteins; Signaling by Rho GTPases; Signaling by Rho GTPases, Miro GTPases and RHOBTB3

**Table 3-7 Functional enrichment analysis of proteins with altered phosphorylation in the resistant cell lines.**

Functional enrichment analysis in each of the resistant cell lines was performed on proteins containing sites of significantly (adj  $p < 0.05$ ) increased or decreased phosphorylation (compared to control). If the set size was  $> 100$ , the 100 proteins containing phosphosites with the largest changes in phosphorylation were examined. Analysis performed with g:Profiler (145) and results for Reactome shown.

### 3.2.5 Generation and characterisation of knockout CRBN cell lines

To determine if the transcriptome and proteome changes observed in the cell lines with acquired IMiD/CELMoD resistance were predominately driven by decreased CRBN or by alternate pathway modulation, *CRBN* knockout cell lines were analysed. The Myeloma Biology and Therapeutics lab had previously used CRISPR-Cas9 to generate MM1s cell lines with *CRBN* genetically knocked out. Two different knockout models were generated, Clone A (homozygous deletion chr3:3172863-3179679) and Clone B (homozygous deletion chr3:3179660-3183271). The models were resistant to IMiDs and CELMoDs (**Supplementary Figure 9-3**), had no CRBN on western blotting (**Supplementary Figure 9-4**) and did not show degradation of Ikaros and Aiolos (or reduction in *IRF4* mRNA levels) with IMiD/CELMoD treatment (**Supplementary Figure 9-5**). These models were used to enable comparison of acute knockout of *CRBN* with the gradual reduction of CRBN seen in the cell lines with acquired resistance. Clone A CRBN-KO-MM1s underwent RNA-Seq and whole proteome analysis.

#### **RNA-Seq analysis**

Parental MM1s and Clone A CRBN-KO-MM1s were analysed by RNA-Seq (performed in biological triplicate). Using a log<sub>2</sub> fold change threshold of 0.2 and adj  $p < 0.05$  there were 640 upregulated transcripts and 533 downregulated



transcripts. Functional enrichment analysis (g:Profiler) of the one hundred most upregulated transcripts did not highlight any enriched pathways and the same analysis of the hundred most downregulated transcripts highlighted limited pathways (KEGG showed enrichment of Glycerolipid metabolism and Reactome and WikiPathways showed no enriched pathways).

There were 27 commonly changed transcripts in the acquired resistant lines (changed in  $\geq 5$  of the 6 resistant lines, **Supplementary Table 9-2**) and 8 of these were altered in CBRN-KO-MM1s. *CRBN* and *CKLF Like MARVEL Transmembrane Domain Containing 7 (CMTM7)* were also downregulated in the *CRBN* knockout line. *BIRC3* and *Formin Binding Protein 1 (FNBP1)* were also upregulated in the knockout line. *Dedicator Of Cytokines 4 (DOCK4)*, *ST8 Alpha-N-Acetyl-Neuraminide Alpha-2,8-Sialyltransferase 2 (ST8SIA2)* and *Sulfotransferase Family 1A Member 3 (SULT1A3)* were upregulated in the resistant lines but downregulated in CBRN-KO-MM1s. *Long Intergenic Non-Protein Coding RNA 665 (LINC00665)* was downregulated in the resistant lines but upregulated in the knockout. Therefore, it would appear that low *CRBN* levels are not the only cause of the transcriptome changes seen in the acquired resistant lines.

### **Whole proteome analysis**

Whole proteome analysis of parental MM1s and Clone A CBRN-KO-MM1s was performed in duplicate. The top 10 most upregulated and downregulated proteins in the knockout (with adj  $p < 0.05$ ) are shown below (**Table 3-8**).

Symbol	Full name	Description	Unique peptides	log2FC
<b>Upregulated proteins in CBRN-KO-MM1s</b>				
MGST1	Microsomal Glutathione S-Transferase 1	Catalyses the conjugation of glutathione to electrophiles and the reduction of lipid hydroperoxides	2	1.91
TNFSF9	TNF Superfamily Member 9	Cytokine that belongs to the tumor necrosis factor ligand family	1	1.90
MYO1F	Myosin IF	Actin-based motor molecule with ATPase activity	4	1.81

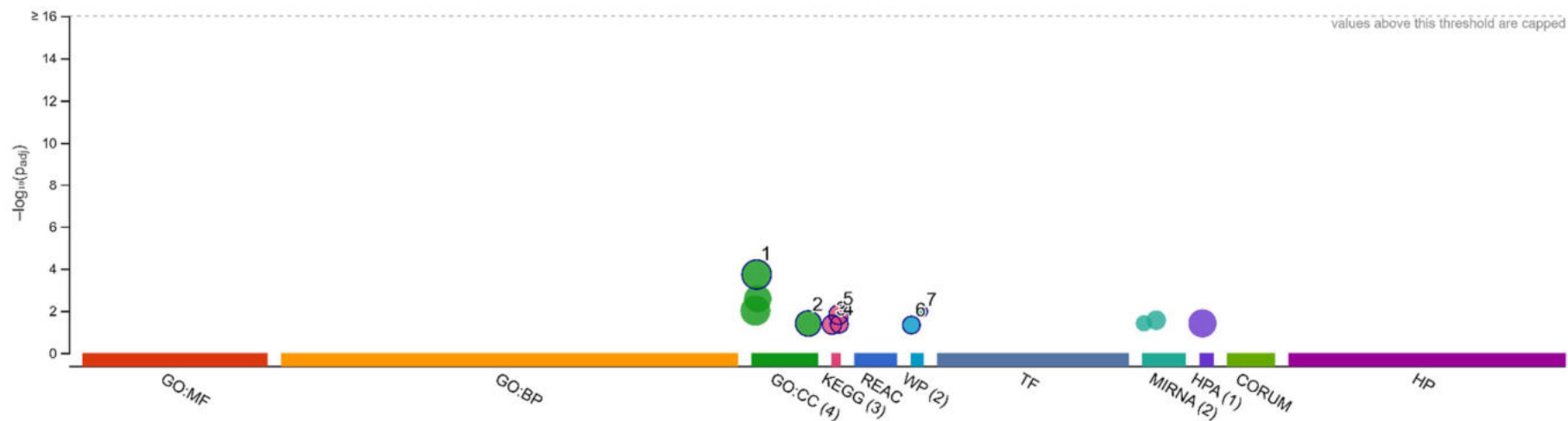
ADGRE5	Adhesion G Protein-Coupled Receptor E5	Receptor potentially involved in adhesion and signaling processes early after leukocyte activation	2	1.72
RASGRP3	RAS Guanyl Releasing Protein 3	Guanine nucleotide exchange factor for Ras and Rap1	3	1.64
GSN	Gelsolin	Calcium-regulated, actin-modulating protein	4	1.51
IL4I1	Interleukin 4 Induced 1	Secreted L-amino-acid oxidase that acts as a key immunoregulator	2	1.45
TLR7	Toll Like Receptor 7	Member of the Toll-like receptor family	1	1.44
UBA7	Ubiquitin Like Modifier Activating Enzyme 7	Activates ubiquitin	8	1.41
PTPRS	Protein Tyrosine Phosphatase Receptor Type S	Cell surface receptor that binds to glycosaminoglycans	1	1.38
<b>Downregulated proteins in CRBN-KO-MM1s</b>				
GCFC2	GC-Rich Sequence DNA-Binding Factor 2	Involved in pre-mRNA splicing	3	-3.47
GYPC	Glycophorin C (Gerbich Blood Group)	Integral membrane glycoprotein	2	-3.29
SULT1A3/ SULT1A4	Sulfotransferase Family 1A Member 3/4	Sulfotransferase enzymes	3	-2.85
CMBL	Carboxymethylenebut enolidase Homolog	Cysteine hydrolase	1	-2.47
TP53I11	Tumor Protein P53 Inducible Protein 11	Predicted to be involved in negative regulation of proliferation	1	-2.44
CRBN	Cereblon	Substrate recognition component of an E3 protein ligase complex	4	-2.24
PFKP	Phosphofructokinase, Platelet	Member of the phosphofructokinase A protein family	1	-1.98
C1orf198	Chromosome 1 Open Reading Frame 198	Unknown function	1	-1.70
BRSK1	BR Serine/Threonine Kinase 1	Serine/threonine-protein kinase that plays a key role in	1	-1.64

			polarisation of neurons and centrosome duplication		
ABLIM3	Actin Binding LIM Protein Family Member 3		Member of the actin-binding LIM family of proteins	1	-1.59

*Table 3-8 Proteome changes in CRBN-KO-MM1s compared to parental MM1s.*

Quantitative proteomic data was analysed by a limma modified t-test in Phantasus (v1.19.3). The top 10 most downregulated and upregulated proteins in the CRBN-KO-MM1s (with adj p<0.05) are described (147).

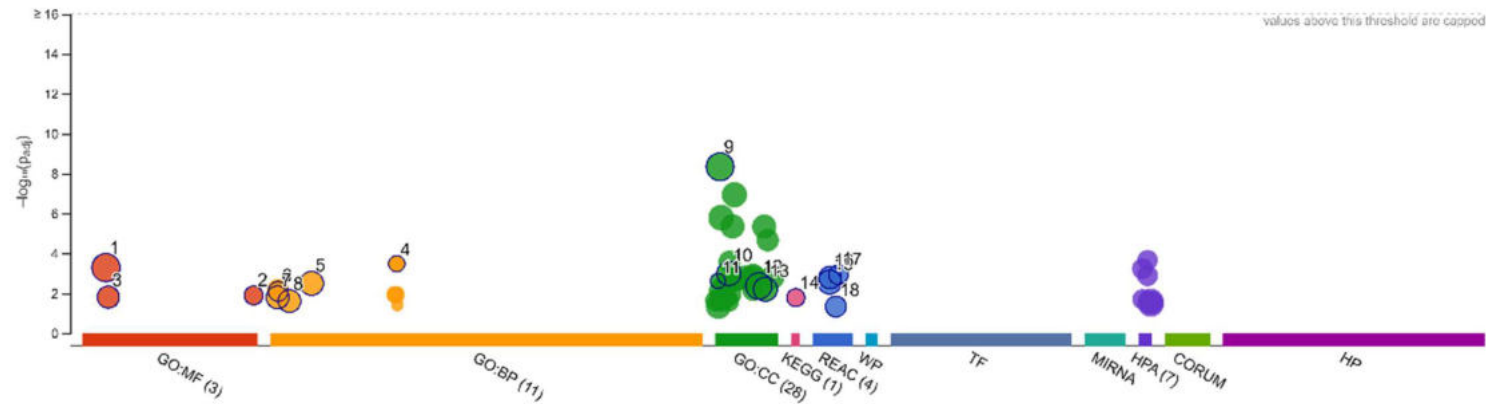
Functional enrichment analysis was then performed on proteins with the largest changes in expression in CRBN-KO-MM1s compared to parental MM1s (**Figure 3-25, Figure 3-26**). Notably lipid metabolism pathways were not enriched in the downregulated proteins. This is important because 5 of the 6 acquired resistant cell lines showed enrichment of these pathways. Therefore, changes in lipid metabolism proteins are not replicated by acute loss of CRBN expression and are likely to be influenced by complementary pathways.



ID	Source	Term ID	Term Name	p <sub>adj</sub> (query_1)
1	GO:CC	GO:0005737	cytoplasm	$1.886 \times 10^{-4}$
2	GO:CC	GO:0120025	plasma membrane bounded cell projection	$3.954 \times 10^{-2}$
3	KEGG	KEGG:00230	Purine metabolism	$4.532 \times 10^{-2}$
4	KEGG	KEGG:05230	Central carbon metabolism in cancer	$4.259 \times 10^{-2}$
5	KEGG	KEGG:05160	Hepatitis C	$1.515 \times 10^{-2}$
6	WP	WP:WP3651	Pathways affected in adenoid cystic carcinoma	$4.713 \times 10^{-2}$
7	WP	WP:WP4931	Direct reversal repair	$1.060 \times 10^{-2}$

Figure 3-25 Functional enrichment analysis of proteins with reduced expression in CRBN-KO-MM1s.

Functional enrichment analysis was performed on statistically significantly altered (adj p<0.05) proteins with the most decreased expression in CRBN-KO-MM1s compared to parental MM1s (n=100) using g:Profiler (145). Driver terms in GO and all KEGG, Reactome and WikiPathways pathways are highlighted.



ID	Source	Term ID	Term Name	P <sub>adj</sub> (query_1)
1	GO:MF	GO:0005515	protein binding	$5.189 \times 10^{-4}$
2	GO:MF	GO:1901981	phosphatidylinositol phosphate binding	$1.278 \times 10^{-2}$
3	GO:MF	GO:0008289	lipid binding	$1.559 \times 10^{-2}$
4	GO:BP	GO:0032648	regulation of interferon-beta production	$3.304 \times 10^{-4}$
5	GO:BP	GO:0006955	immune response	$3.184 \times 10^{-3}$
6	GO:BP	GO:0001818	negative regulation of cytokine production	$8.020 \times 10^{-3}$
7	GO:BP	GO:0001775	cell activation	$1.611 \times 10^{-7}$
8	GO:BP	GO:0002684	positive regulation of immune system process	$2.460 \times 10^{-2}$
9	GO:CC	GO:0005737	cytoplasm	$4.567 \times 10^{-9}$
10	GO:CC	GO:0030054	cell junction	$1.017 \times 10^{-3}$
11	GO:CC	GO:0002102	podosome	$2.426 \times 10^{-3}$
12	GO:CC	GO:0071944	cell periphery	$4.322 \times 10^{-3}$
13	GO:CC	GO:0095088	bounding membrane of organelle	$6.240 \times 10^{-3}$
14	KEGG	KEGG:04611	Platelet activation	$1.661 \times 10^{-2}$
15	REAC	REAC:R-HSA-16...	Immune System	$2.727 \times 10^{-3}$
16	REAC	REAC:R-HSA-16...	Innate Immune System	$1.614 \times 10^{-3}$
17	REAC	REAC:R-HSA-76...	Platelet activation, signaling and aggregation	$1.174 \times 10^{-2}$
18	REAC	REAC:R-HSA-67...	Neutrophil degranulation	$4.600 \times 10^{-2}$

Figure 3-26 Functional enrichment analysis of proteins with increased expression in CRBN-KO-MM1s.

Functional enrichment analysis was performed on statistically significantly altered (adj p<0.05) proteins with the most increased expression in CRBN-KO-MM1s compared to parental MM1s (n=100). Driver terms in GO and all KEGG, Reactome and WikiPathways pathways are highlighted.

### 3.2.6 Re-expression of CRBN in the resistant cell lines

The resistant cell lines had a lower level of CRBN than their matching control lines (**Figure 3-8**) but whether this was the sole driver of resistance, or whether other altered pathways might be contributing, was not confirmed. A rescue experiment was therefore conducted to explore whether re-expression of CRBN would lead to re-sensitisation to IMiDs/CELMoDs. CRBN was stably re-expressed in Len-R-, Pom-R- and Iber-R-MM1s using a lentiviral system (with an empty vector control). CRBN re-expression led to partial re-sensitisation to IMiDs/CELMoDs (**Figure 3-27**). The level of CRBN in the resistant cell lines after transduction with the stable *CRBN* expression plasmid was less than that of parental MM1s and the control lines (**Figure 3-27**). The reasons behind this were not confirmed but could be related to the activity of the promoter driving CRBN expression. The partial re-sensitisation to IMiDs/CELMoDs observed in the transduced cell lines could be related to the low level of CRBN expression or could indicate the importance of complementary pathways.

The Iber-R-MM1s<sup>CRBN</sup> line was then explored in more detail. This cell line showed partial restoration of sensitivity to a panel of IMiDs, CELMoDs and GSPT1 degraders (**Figure 3-28**), and the degree of re-sensitisation correlated with CRBN binding potency. Restoration of CRBN level to about half that of Ctrl-Iber-MM1s was confirmed (**Figure 3-29**). When Iber-R-MM1s<sup>CRBN</sup> was exposed to IMiDs/CELMoDs there was degradation of Aiolos and Ikaros (**Figure 3-30**) and *IRF4* mRNA expression was reduced (**Figure 3-31**), in keeping with partial restoration of CRBN function.

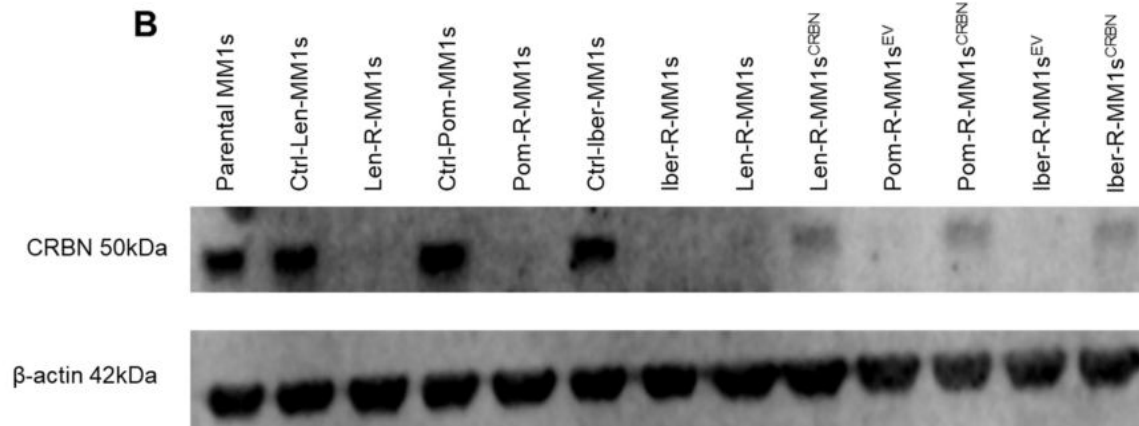
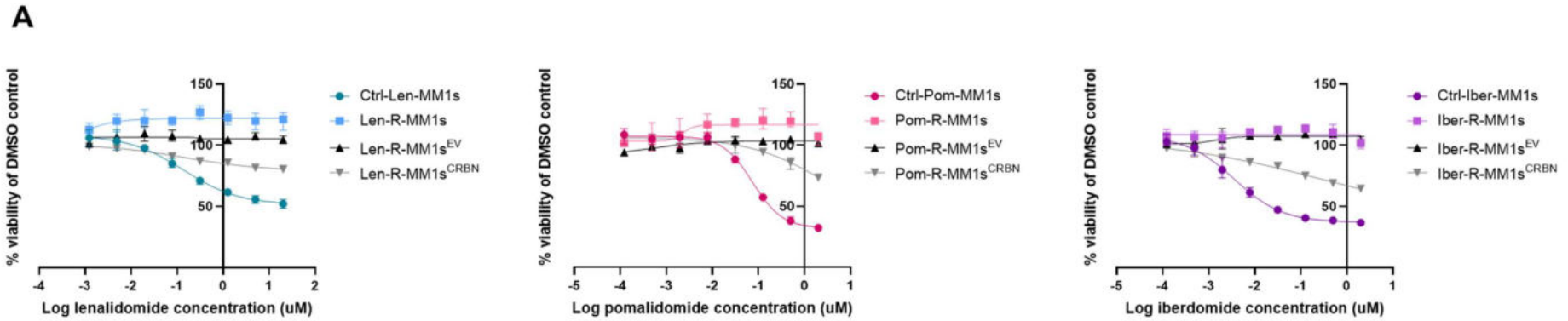


*Figure 3-27 CRBN re-expression in the resistant MM1s cell lines.*

CRBN was re-expressed in the resistant MM1s cell lines and this led to partial re-sensitisation to IMiDs/CELMoDs. Data shows n=1, EC<sub>50</sub> curves show mean and range of technical triplicates. The superscript EV denotes cell lines transduced with empty vector and CRBN denotes cell lines transduced with the CRBN expression plasmid.

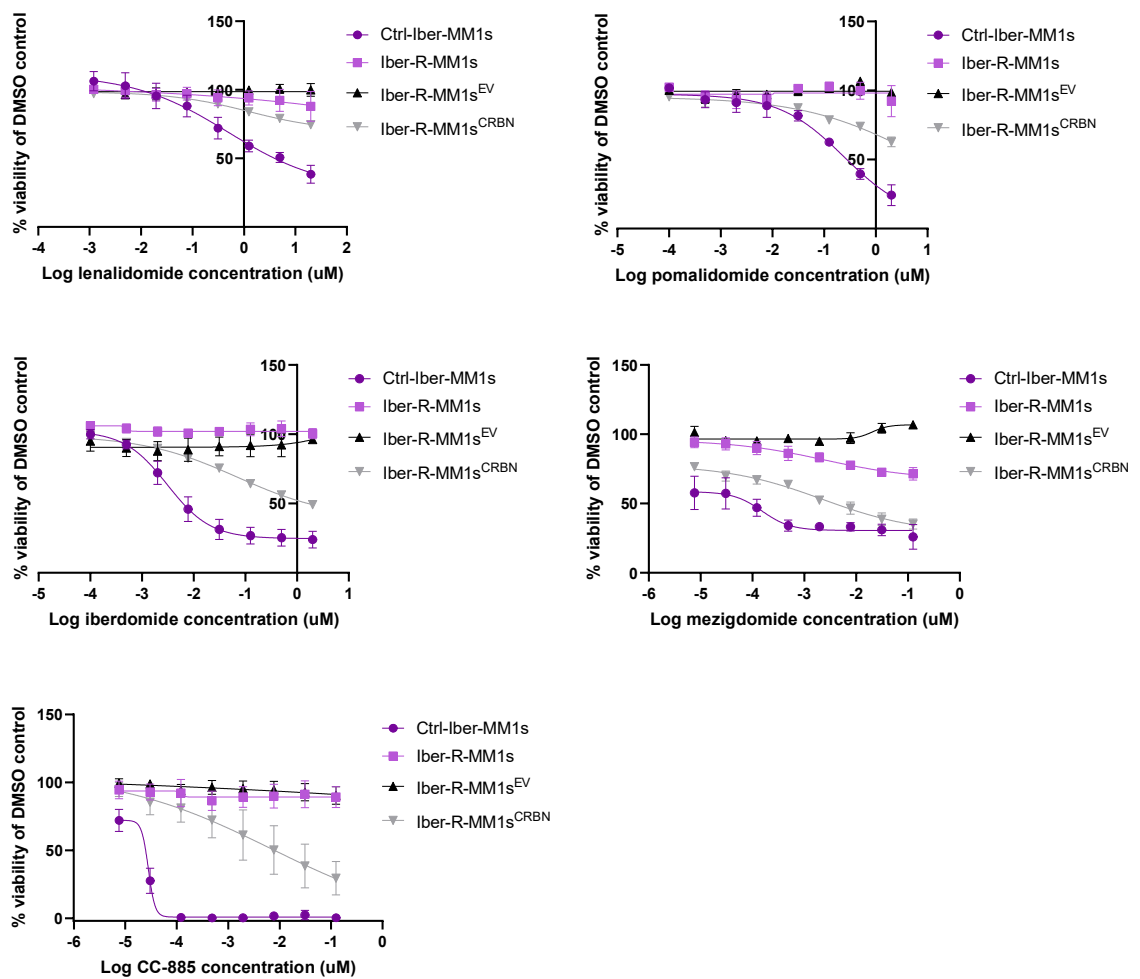


**Figure 3-28** The effect of CRBN binders on viability in Iber-R-MM1s<sup>CRBN</sup>.

Viability at day 5 was assessed in a CellTiter-Blue assay. N=3, mean and SEM shown. The superscript EV denotes transduction with empty vector and CRBN denotes transduction with a CRBN expression plasmid.

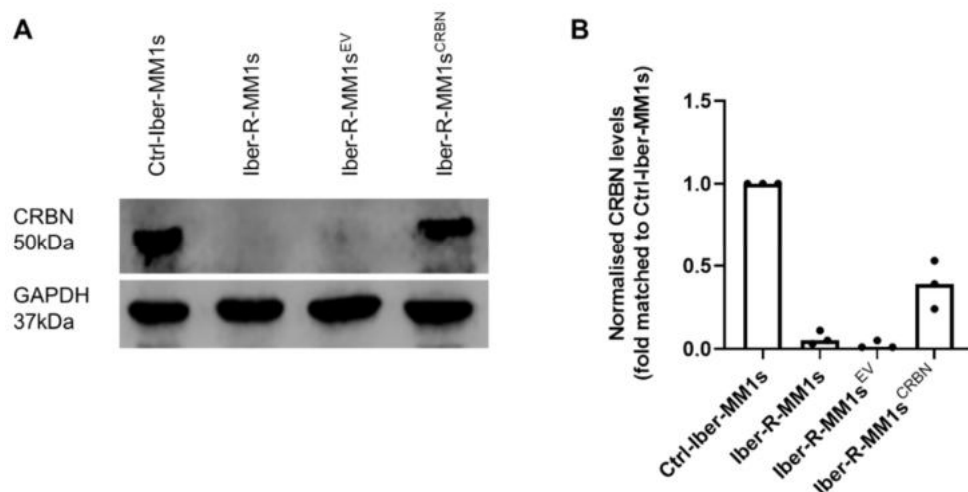


**Figure 3-29** CRBN levels in Iber-R-MM1s<sup>CRBN</sup>.

A) Representative western blot of CRBN levels (n=3), which is then quantified in B). Individual points represent independent experiments, and the top of the bar represents the median. The superscript EV denotes transduction with empty vector and CRBN denotes transduction with a CRBN expression plasmid.



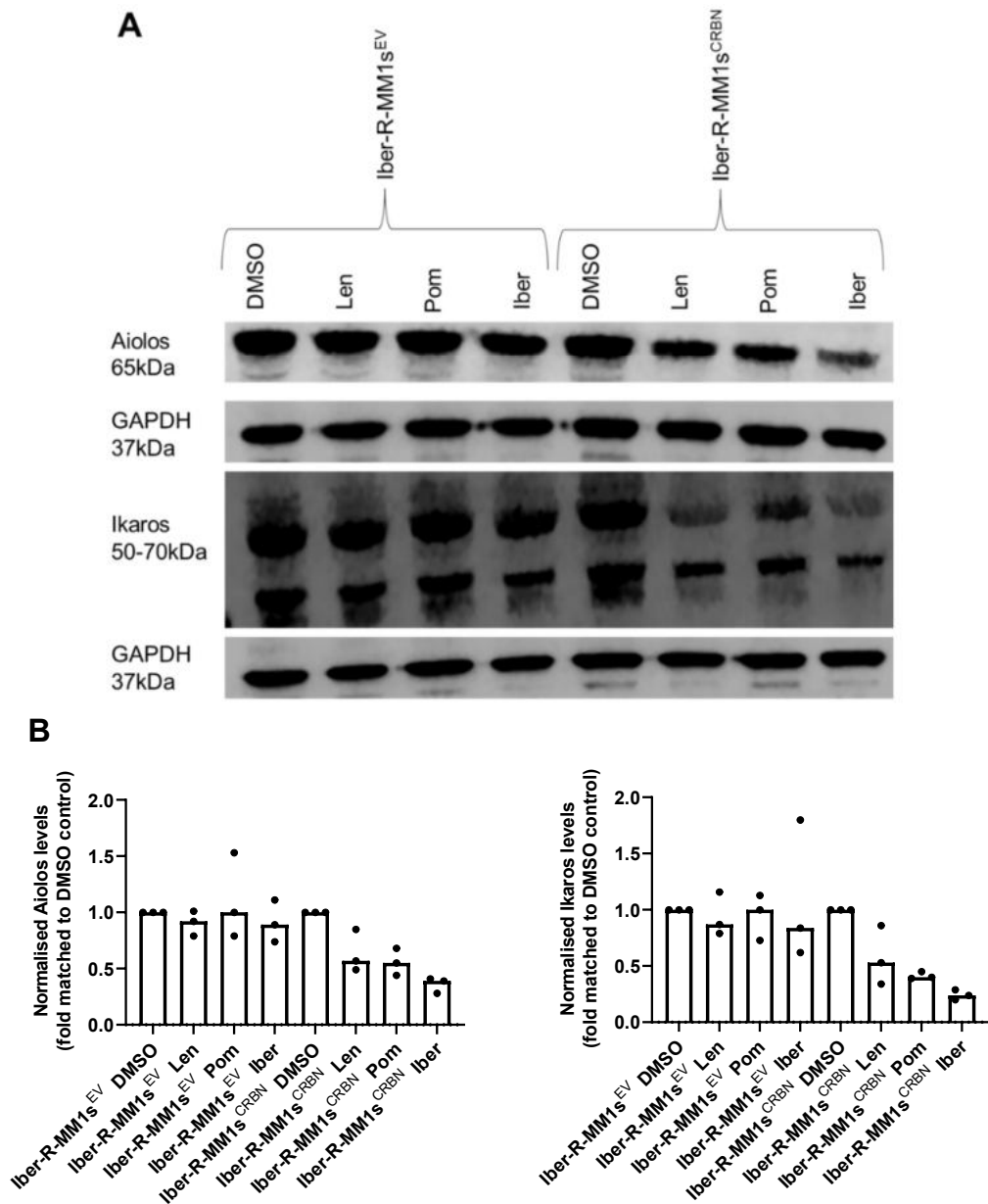


**Figure 3-30 Degradation of Aiolos and Ikaros in Iber-R-MM1s<sup>CRBN</sup> on exposure to IMiDs/CELMoDs.**

Aiolos and Ikaros were degraded in Iber-R-MM1s<sup>CRBN</sup>, in contrast to Iber-R-MM1s<sup>EV</sup>. A) Shows a representative western blot with B) quantification (individual points represent independent experiments (n=3) and the bar represents the median).

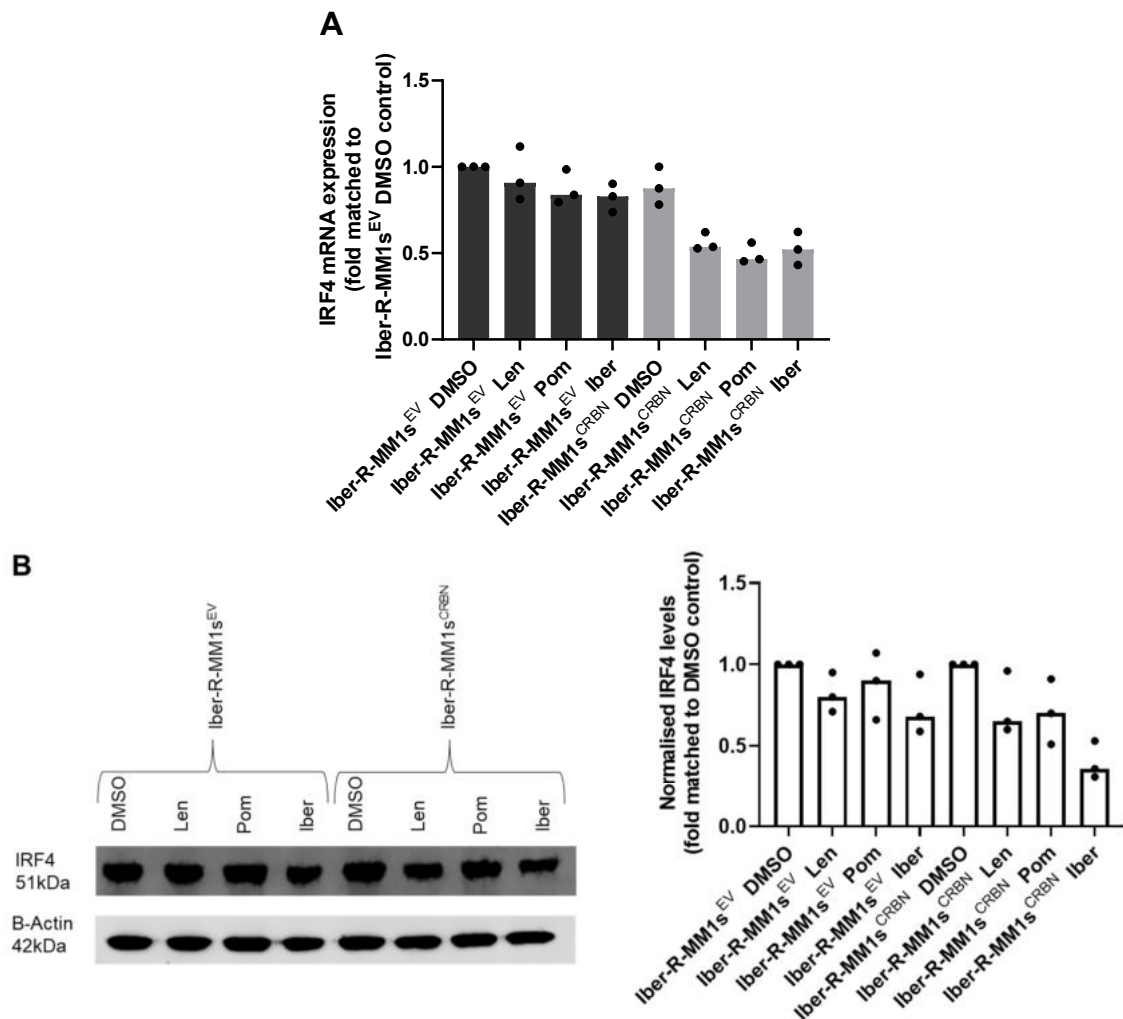


**Figure 3-31 Reduction in IRF4 in Iber-R-MM1s<sup>CRBN</sup> on exposure to IMiDs/CELMoDs.**

A) There was reduced *IRF4* mRNA expression with IMiD/CELMoD treatment in Iber-R-MM1s<sup>CRBN</sup> by quantitative RT-PCR. Individual points represent independent experiments (n=3), and the bar represents the median. B) IRF4 was also reduced at the protein level. A representative western blot is shown alongside blot quantification (individual points represent independent experiments (n=3) and the bar represents the median).

### 3.2.7 The effect of removing selection pressure on the resistant cell lines

It was important to assess if the resistant cell lines remained resistant when the selection pressure was removed or if they would regain sensitivity. Restoration of sensitivity might indicate reversible epigenetic changes or potentially the effects of clonal competition. The resistant cell lines were therefore grown out of IMiD/CELMoD for several weeks. Serial viability experiments were carried out and expression of CRBN monitored. The MM1s resistant lines regained partial sensitivity, Len-R-MM1s by 16 weeks (**Figure 3-32**), Pom-R-MM1s by 14 weeks (**Figure 3-33**) and Iber-R-MM1s by 20 weeks (**Figure 3-34**). Interestingly, the control lines appeared to become less sensitive to IMiD/CELMoD treatment over

time, which might be due to high passage number. The H929 resistant lines did not regain sensitivity by 28 weeks, at which point the experiment was stopped (**Figure 3-35**). The same reduction in drug sensitivity developed in the control H929 lines.

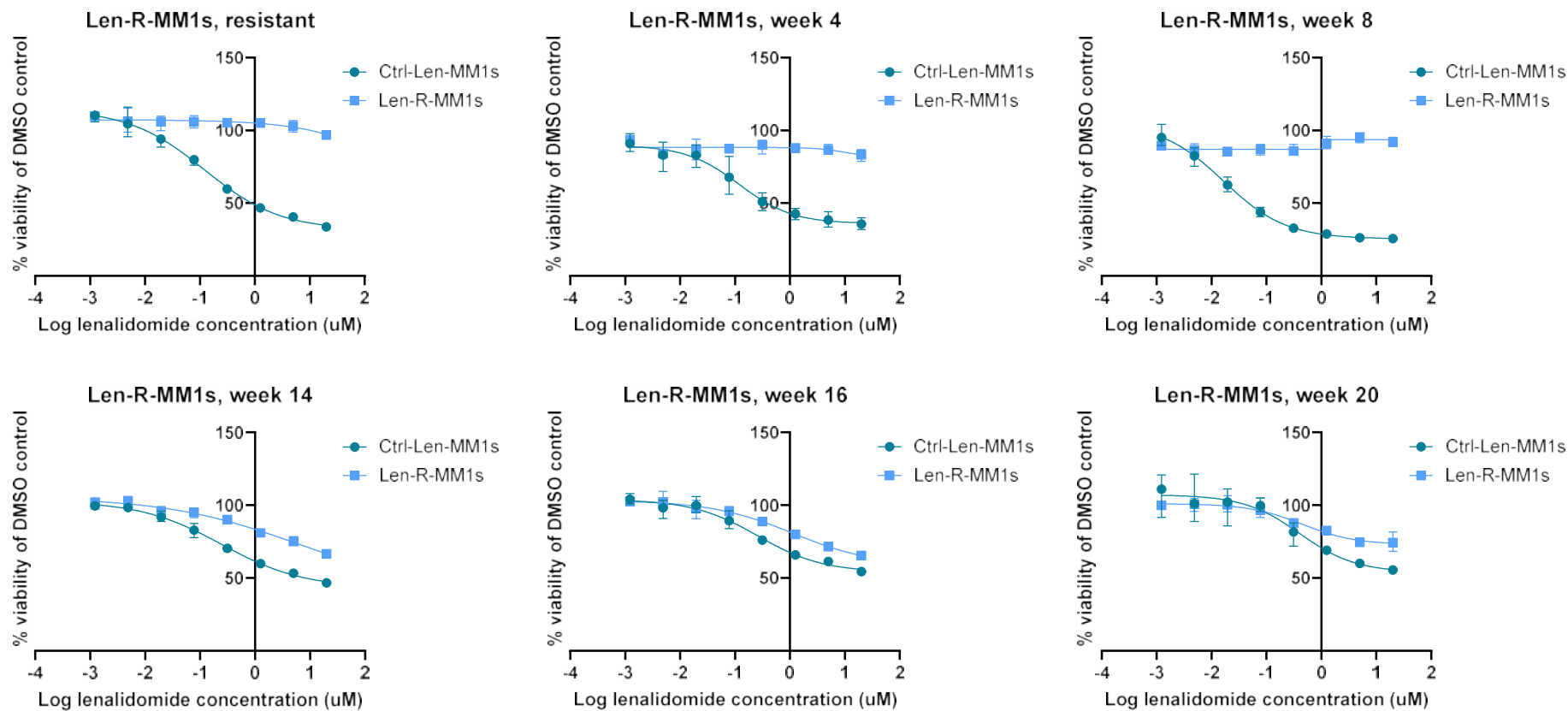


*Figure 3-32 Viability assays demonstrating the response of Len-R-MM1s to lenalidomide after removal of the selection pressure.*

Serial EC50 assays (CellTiter-Blue) showed that Len-R-MM1s regained sensitivity to IMiDs about 16 weeks after the selection pressure was removed. Graphs show mean and range of 3 technical triplicates.

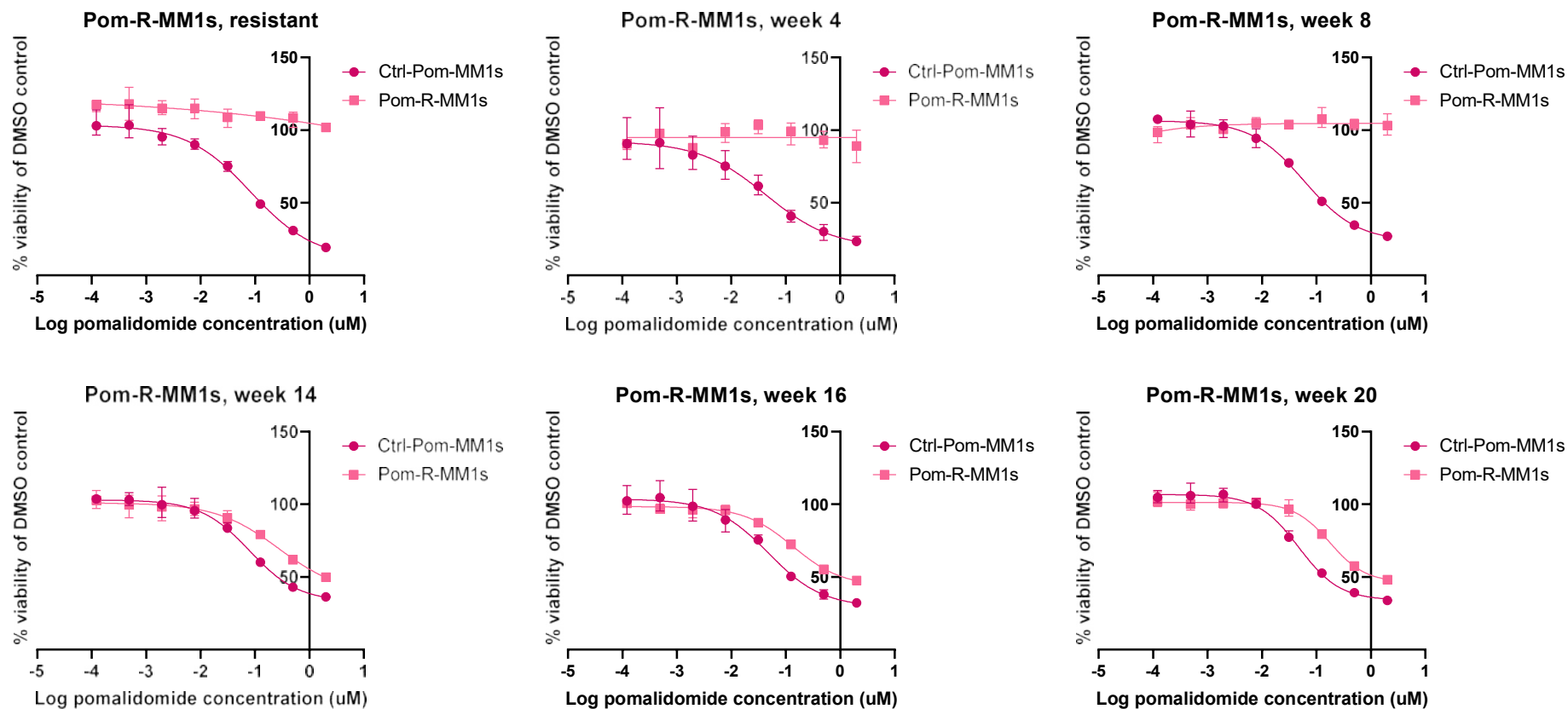


*Figure 3-33 Viability assays demonstrating the response of Pom-R-MM1s to pomalidomide after removal of the selection pressure.*

Serial EC50 assays (CellTiter-Blue) showed that Pom-R-MM1s regained sensitivity to IMiDs about 14 weeks after the selection pressure was removed. Graphs show mean and range of 3 technical triplicates.

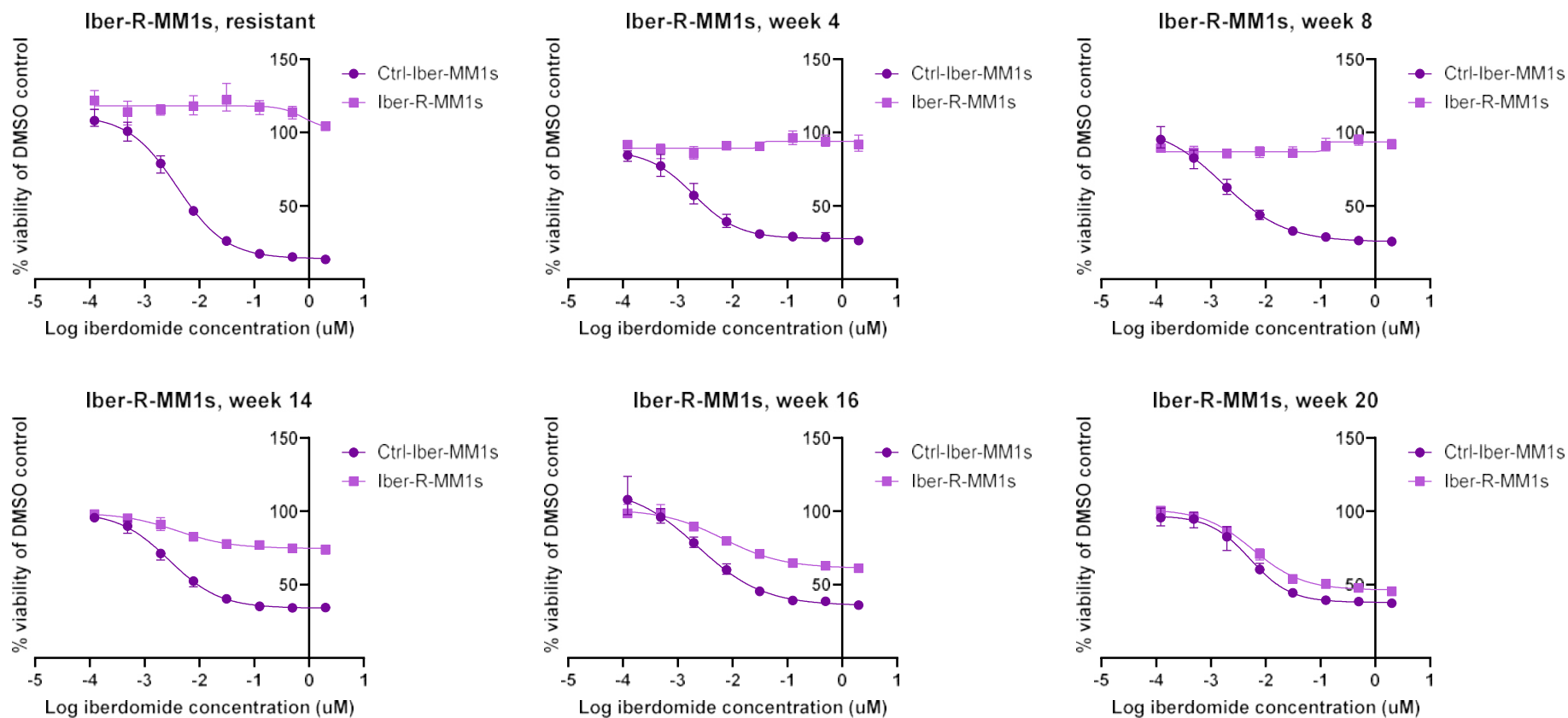


*Figure 3-34 Viability assays demonstrating the response of Iber-R-MM1s to iberdomide after removal of the selection pressure.*

Serial EC50 assays (CellTiter-Blue) showed that Iber-R-MM1s regained sensitivity to IMiDs about 20 weeks after the selection pressure was removed. Graphs show mean and range of 3 technical triplicates.

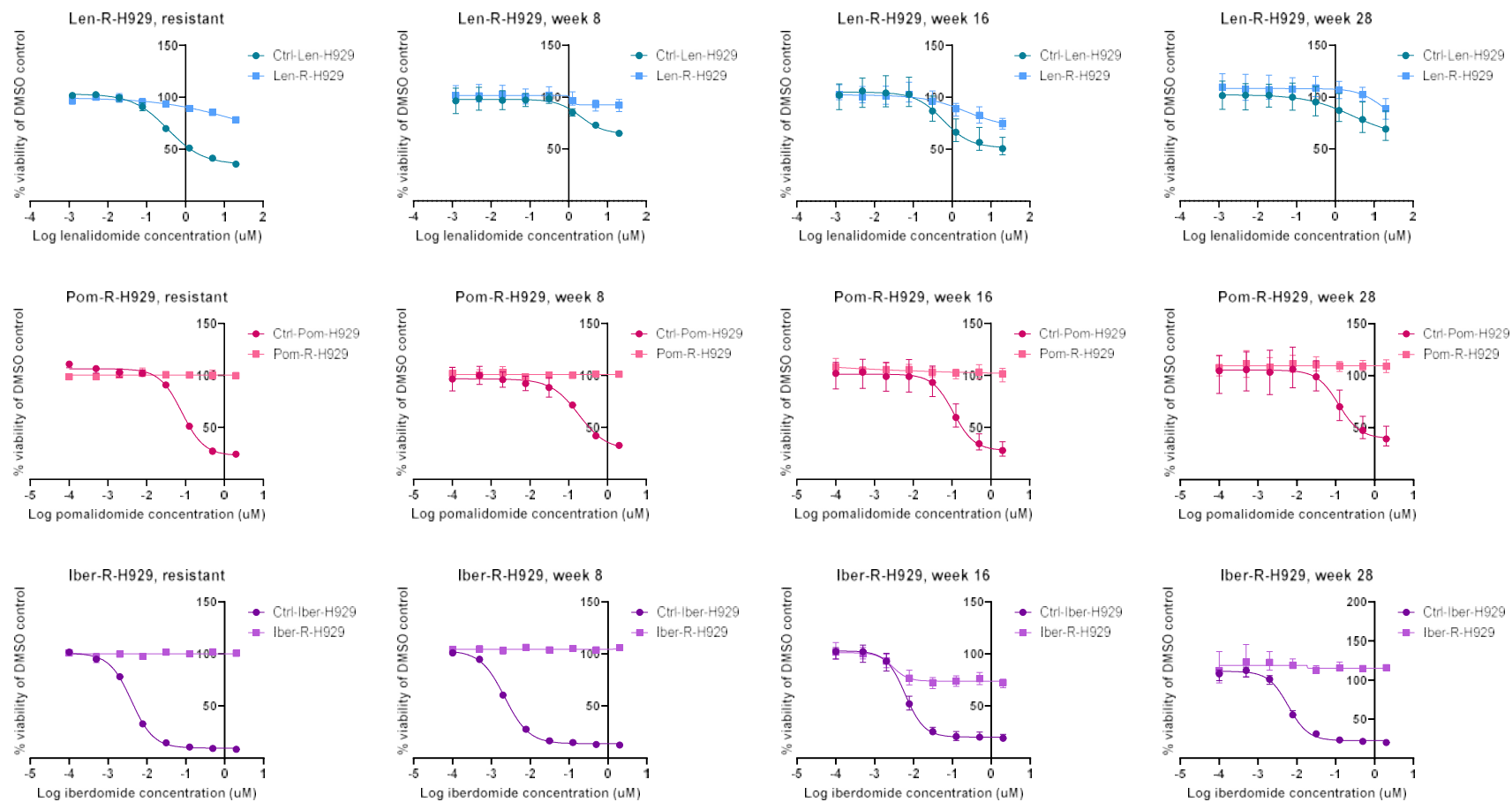


**Figure 3-35 Viability assays demonstrating the response of resistant H929 lines to IMiDs/CELMoDs after removal of the selection pressure.**

Serial EC50 assays (CellTiter-Blue) showed that none of the H929 resistant cell lines regained sensitivity by week 28 at which point the experiment was stopped. Graphs show mean and range of 3 technical triplicates.

The MM1s lines showed re-expression of CRBN as the cells were cultured out of drug. This began at week 14, and Iber-R-MM1s showed an increase in CRBN expression over a 6 week period (**Figure 3-36**). This time course suggested a strong correlation between the return of CRBN expression and the return of IMiD/CELMoD sensitivity.

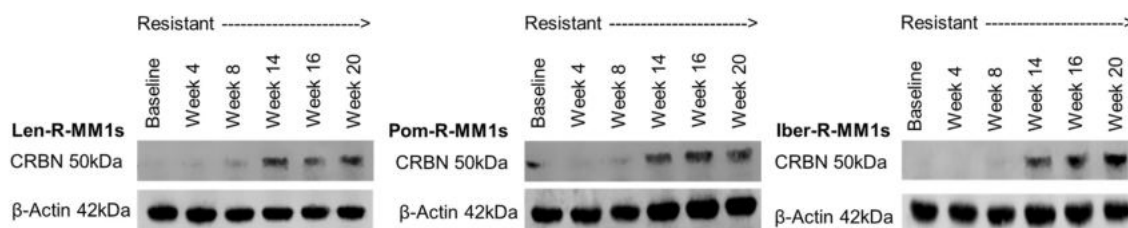


*Figure 3-36 Restoration of CRBN in the MM1s resistant lines.*

By week 14 all of the resistant MM1s cell lines showed some restoration of CRBN expression. This increased gradually in Iber-R-MM1s over a period of 6 weeks.

Len-R-H929 had the smallest reduction in CRBN expression of all the resistant cell lines, and an increase in CRBN levels was not observed when the line was cultured out of drug. Pom-R-H929 did not regain CRBN expression by week 28. Iber-R-H929 gradually regained CRBN expression over time. It is interesting that this cell line remained resistant to IMiDs/CELMoDs despite restoration of CRBN expression (**Figure 3-37**).

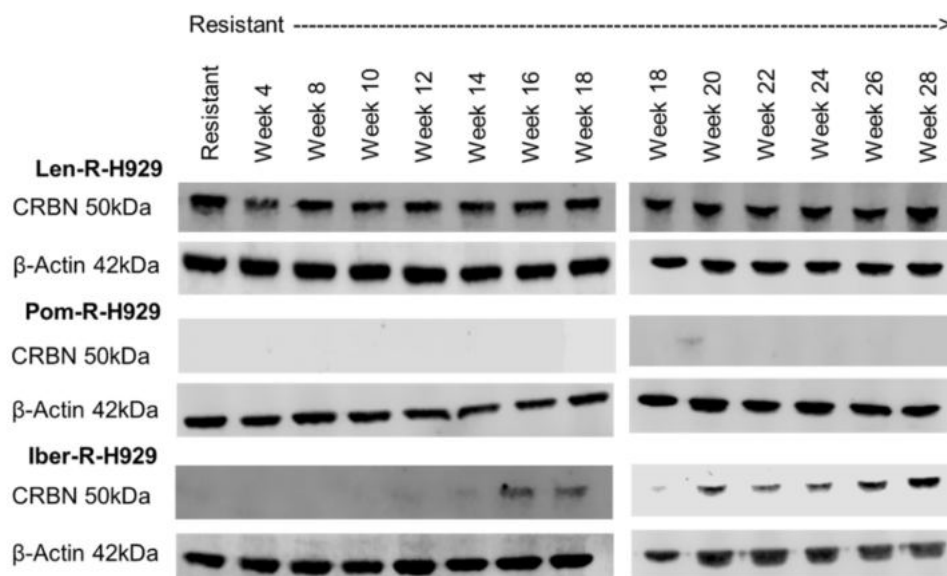


*Figure 3-37 CRBN blots in the H929 resistant cell lines after removal of the selection pressure.*

In Len-R-H929 the level of CRBN remained the same when the cells were cultured without IMiD. Pom-R-H929 did not regain CRBN expression after 28 weeks. Iber-R-H929 showed an increase in CRBN over time, starting at week 16. Note the week 18 time point on each blot is from the same protein sample.



### 3.3 Discussion

The Myeloma Biology and Therapeutics laboratory had previously generated 3 IMiD/CELMoD-resistant cell lines using the myeloma cell line MM1s, which has the t(14;16) and t(8;14) translocations (139). I then generated a second set of acquired resistant cell lines using the H929 cell line which has t(4;14) (139). Both t(14;16) and t(4;14) confer high-risk disease in myeloma patients (139). Utilising multiple acquired IMiD/CELMoD-resistant cell line models with different initiating genetic backgrounds allowed exploration of both common and distinct mechanisms of resistance throughout the work presented in this thesis.

Characterisation of the resistant cell lines demonstrated that they were resistant to the IMiD/CELMoD with which they were generated and showed cross-resistance to other CRBN binders (except for Len-R-H929, in which resistance could be overcome by CELMoDs and GSPT1 degraders). The lines all showed reduction in CRBN (although this was modest in Len-R-H929) and the normal effects of IMiD/CELMoD treatment (e.g. Aiolos and Ikaros degradation) were abrogated. In most of the cell line models the time course of reduction in CRBN expression correlated well with the generation of resistance.

The reduction in CRBN observed in the acquired resistant cell lines could be related to genetic alterations in *CRBN*, epigenetic changes, or altered RNA translation that occurred in the cells due to IMiD/CELMoD exposure. However, an alternate hypothesis is that culturing the cells with IMiD/CELMoD led to the selection of cells with pre-existing low levels of CRBN expression (for any of the above reasons) that already existed within the initial heterogeneous cell population.

WES showed that 3 of the acquired IMiD-resistant cell lines (Pom-R-MM1s, Pom-R-H929 and Iber-R-H929) had *CRBN* mutations predicted to have a high impact on function; Pom-R-MM1s had a splice site mutation and Pom-R-H929 and Iber-R-H929 had an early stop codon. Interestingly, the early stop codon mutation in the H929 lines has also been found in IMiD-resistant patients (148). The nature of these mutations is such that a reduction in the level of functional CRBN protein would be expected. However, the VAF in Pom-R-MM1s was only 26% and therefore this may not be the only factor contributing to resistance in this cell line (in which CRBN protein levels are very low). There were no high impact mutations

in other IMiD pathway genes in the acquired resistant cell lines. Copy number loss at the *CRBN*, *COPS7B* and *COPS8* loci was also explored and Pom-R-H929 showed copy number loss in *CRBN*. This is interesting because Pom-R-H929 also has an early stop codon mutation. One possible explanation is that in Pom-R-H929 there are two different populations, one with copy number loss at the *CRBN* locus and one with a stop codon mutation in *CRBN*. There was also copy number loss in *CRBN* in Len-R-H929, although to a smaller degree than in Pom-R-H929. This may explain the more modest reduction in *CRBN* protein expression observed in this cell line. Genetic changes in *CRBN* and IMiD pathway genes are thought to account for resistance generation in nearly 1/3<sup>rd</sup> of patients (89-91, 95) and therefore having cell line models both with and without genetic alterations in *CRBN* is important to enable replication of the diverse patient state for further study.

All three MM1s resistant cell lines developed high impact mutations in *MKI67*, with Pom-R-MM1s exhibiting a frameshift mutation and Len-R-MM1s and Iber-R-MM1s both exhibiting the same early stop codon mutation. *MKI67* encodes a nuclear protein that is expressed by proliferating cells (149). It is involved in regulation of chromosome segregation and regulation of mitotic nuclear division (147). High *MKI67* expression, as measured by immunohistochemistry on bone marrow biopsies, is associated with reduced PFS and OS in newly diagnosed myeloma patients (149). There was no difference in proliferation between control and resistant cell lines (**Supplementary Figure 9-1**) and no high impact mutation in *MKI67* occurred in any of the H929 resistant cell lines.

The RNA-Seq analysis showed a reduction in *CRBN* mRNA levels in all of the resistant cell lines. High exon-10 splicing of the *CRBN* transcript has been associated with IMiD resistance in patients (91), but unfortunately this could not be evaluated in this RNA-Seq dataset due to the library preparation used. However, the RNA-Seq analysis highlighted several genes that are commonly differentially expressed in the acquired resistant cell lines. Of particular interest were *TNFAIP3* and *BIRC3*, which are both members of the NFκB pathway. This pathway is known to have a critical role in the survival and proliferation of myeloma cells (150). *TNFAIP3* is an inhibitor of the NFκB pathway and has both ubiquitin ligase and deubiquitinase activities (151). *BIRC3* also has ubiquitin

ligase activity and is a multifunctional protein which regulates caspases, apoptosis and NFκB signalling (it acts as a positive regulator of the canonical pathway and suppresses constitutive activation of the non-canonical pathway) (152). The resistant H929 cell lines showed a degree of resistance to the SMAC mimetic SM-164 compared to their control lines. Of note, steps in the NFκB pathway are frequently regulated by phosphorylation but this was not highlighted as altered in the resistant setting in the phosphoproteomics analysis. Further exploration of changes in the NFκB pathway in the IMiD/CELMoD-resistant state was not undertaken in this thesis due to the absence of supportive data from other experiments (Chapters 4 and 5).

Whole proteome analysis of the resistant cell lines identified key changes in lipid metabolism in the resistant state. Lipid pathways, including SREBP, fatty acid metabolism and cholesterol biosynthesis, were commonly enriched in 5 out of the 6 resistant lines when functional enrichment analysis was performed on downregulated proteins. Moreover there were only 2 commonly downregulated proteins in all of the resistant cell lines, CRBN and SCD. SCD is an enzyme that catalyses the rate-limiting step in the formation of monounsaturated fatty acids.

Phosphoproteomic analysis showed enrichment of Rho GTPase pathways in 4 of the resistant cell lines. Members of the Rho GTPase family are part of the Ras superfamily and they are involved in multiple cellular processes including organisation of actin and microtubule cytoskeletons, regulation of gene expression, vesicle trafficking, cell cycle progression, cell morphogenesis, cell polarity and cell migration (153). Rho GTPases are regulated by cycling between GTP- and GDP-bound states and also by post-translational modifications such as lipid alterations, phosphorylation, ubiquitination and SUMOylation (153). Exploring this further would be of interest but was not prioritised during the available time.

CRBN expression is thought to be critical for the function of IMiDs/CELMoDs. In the acquired resistant cell lines the protein levels of CRBN are greatly reduced and therefore restoring CRBN levels was explored. CRBN was re-expressed using a lentiviral system in Len-R-MM1s, Pom-R-MM1s and Iber-R-MM1s. CRBN was not re-expressed in the H929 lines due to time constraints. CRBN was found to be present at a relatively low level after transduction compared to parental

MM1s/the control lines. However, even at this low expression level, partial sensitivity to IMiDs/CELMoDs was restored. It is interesting to consider whether IMiD sensitivity would be fully restored if *CRBN* expression was returned to the parental MM1s level. This could potentially be achieved by using a more active promoter to drive *CRBN* expression or inserting multiple copies of the *CRBN* construct. However, it may be that changes in complementary pathways have developed alongside the reduction in *CRBN* expression that maintain resistance even when *CRBN* expression is restored.

The effect of removing the selection pressure was also explored in the resistant cell lines. The MM1s lines regained expression of *CRBN* and sensitivity to IMiDs/CELMoDs in roughly the same time frame. However, the H929 resistant cell lines did not follow this pattern, and none regained sensitivity after 28 weeks of culture without drug. Interestingly, Iber-R-H929 did regain expression of *CRBN* by week 16. To understand this disparity it would be important to assess if the *CRBN* is functional and if the *CRBN* gene has any mutations. As the cell lines were cultured out of selection pressure for many weeks, the control lines became progressively less sensitive to IMiD/CELMoD treatment. This may be related to high passage number.

Overall, the work in this chapter demonstrates that reduction in *CRBN* is a key feature in the generation of IMiD/CELMoD resistance, as has been suggested in the literature previously. However, I also found changes in lipid synthesis proteins and/or pathways in all of the acquired resistant cell lines, which is a novel finding. The resistant cell lines were otherwise heterogenous, with only a small number of commonly altered transcripts and proteins. Whilst it is important to acknowledge the differences between the resistant cell line models, future work focused on understanding and targeting the common changes to maximise potential applicability across a range of patients. Lipid pathway changes will be further explored in Chapter 7.

## Chapter 4 Identification of Pharmacological Sensitivities in IMiD/CELMoD Resistance

---

### 4.1 Introduction

Conceptually there are two possible approaches to specifically target IMiD-resistant disease in patients; either the resistance driver must be reversed so that the original agent can be continued, or a novel acquired vulnerability must be identified and targeted. This chapter and Chapter 5 explore these two approaches using both pharmacological and genetic methods, building on the previous work in Chapter 3 which identified genetic re-expression of CRBN as a mechanism to reverse resistance. I initially focused on targeting acquired vulnerabilities by performing a compound screen.

Targetable acquired vulnerabilities have been observed in other cancers. For example, *BRAF(V600E)* mutant melanomas inevitably become resistant to BRAF and MEK inhibitors, frequently due to reactivation of the mitogen activated protein kinase (MAPK) pathway (154). Resistance to these inhibitors is associated with increased levels of reactive oxygen species (ROS) (154). Treatment with the histone deacetylase inhibitor vorinostat suppressed SLC7A11 (Solute Carrier Family 7 Member 11), leading to a lethal increase in the already elevated levels of ROS and selective apoptotic death of drug-resistant tumour cells (154). Another example of exploiting an acquired vulnerability comes from the study of cisplatin resistance. Three cell lines (from liver, lung and cervical carcinomas) with acquired cisplatin resistance were developed and found to have increased intracellular hypoxia (155). The team then constructed a hypoxia-amplifying DNA repair-inhibiting liposomal nanomedicine (HYDRI NM), which consisted of a platinum(IV) prodrug with 2 payloads, glucose oxidase (which consumes oxygen) and hypoxia-activatable tirapazamine (which causes DNA cleavage and topoisomerase poisoning) (155). In both patient-derived organoids and xenograft tumours, HYDRI NM suppressed the growth of cisplatin-resistant tumours (155).

I used a high-throughput drug screening approach to try and identify vulnerabilities. High-throughput screening (HTS) has developed rapidly in the last couple of decades due to improvements in automated equipment, which allows multiple compounds to be tested in parallel. HTS requires relatively simple and

automation-compatible assay designs, robotic-assisted sample handling and automated data processing (156). HTS is commonly used in the pharmaceutical industry to identify 'hit' compounds that can then be used as a starting point for chemical optimisation (156). It can also be used to identify new indications for compounds that have already been approved for clinical use, allowing the possibility of providing targeted treatment at a fraction of the development cost (157). HTS assays are commonly performed in microplates and compounds can be tested at a single concentrations or multiple concentrations.

A pharmacological screening approach in an IMiD/CELMoD-resistant cell line was undertaken to identify whether the process of resistance generation could have caused changes in signalling pathways that might lead to differential drug responses. A compound might reduce viability in the control line but not the IMiD/CELMoD-resistant line, thus the IMiD/CELMoD-resistant line would show cross-resistance to the compound. For example, this was seen with SM-164 in the H929 cell lines (**Figure 3-20**) and gave us an indication that the NFκB pathway was altered in the resistant setting. Therefore, cross-resistance provides an insight into mechanisms of IMiD/CELMoD resistance which can then be explored further. In contrast, a compound could reduce viability in the IMiD/CELMoD-resistant line but not the control line. This pharmacological sensitivity in the IMiD/CELMoD-resistant state would be interesting mechanistically and could potentially be used as a treatment for IMiD/CELMoD-resistant patients.

The screen was performed using an in-house drug screening library, which included a Selleck drug library (474 compounds) and a curated Epigenetic library (20 compounds). Together these libraries targeted a broad range of signalling pathways known in be important in cancer development (**Figure 4-1**).

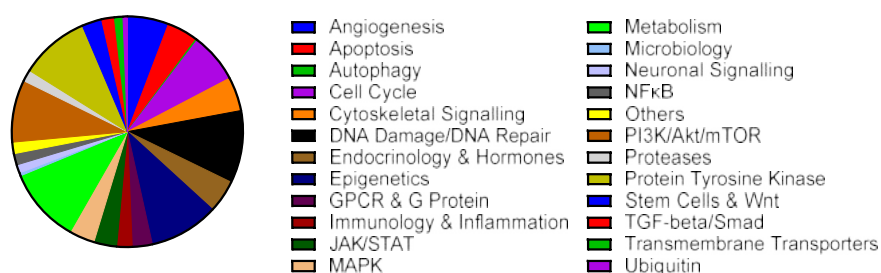


**Figure 4-1 Pathways targeted by library compounds.**

This pie chart describes the signalling pathways targeted by the compounds within the library. Signalling pathway data was taken from the Selleck website ([www.selleckchem.com](http://www.selleckchem.com)).

## 4.2 Results

### 4.2.1 Drug screening with the Selleck and Epigenetics libraries

To identify pharmacological sensitivities in the IMiD/CELMoD-resistant state, a drug screen in Iber-R-MM1s and Ctrl-Iber-MM1s was performed. This cell line was selected because iberdomide is one of the more potent, novel CELMoDs and it is in advanced clinical trials. In addition, this cell line did not have a *CRBN* mutation and therefore the screen might be able to highlight alternative mechanisms of IMiD/CELMoD resistance.

The 494 available compounds were tested at 3 concentrations: 800nM, 200nM and 80nM. These concentrations were selected to cover the expected active ranges of the included compounds. The effect of the compounds on cell line viability was measured at day 5 in a CellTiter-Blue assay. Cell numbers and the experimental protocol for large scale screening in a 384 well plate format had been optimised previously by Dr Laura Chan and Dr Hannah Wang (Translational Cancer Discovery Team, ICR). The compounds were fired using an acoustic liquid dispenser in technical triplicate at each concentration within the plate and the screen was repeated in biological triplicate. Each screening plate also had iberdomide and the proteasome inhibitor bortezomib as controls; iberdomide should reduce viability in the control cell line only and bortezomib had previously been confirmed to reduce viability equally in both lines. Data was anticipated to fall into the patterns shown in **Figure 4-2**.

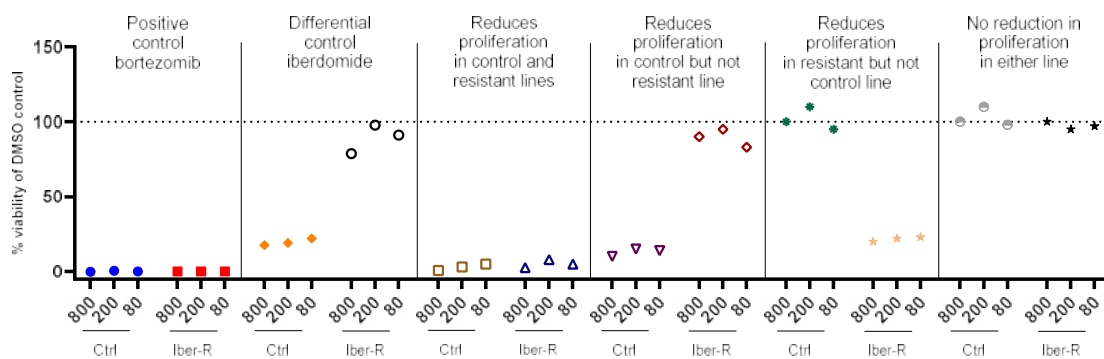
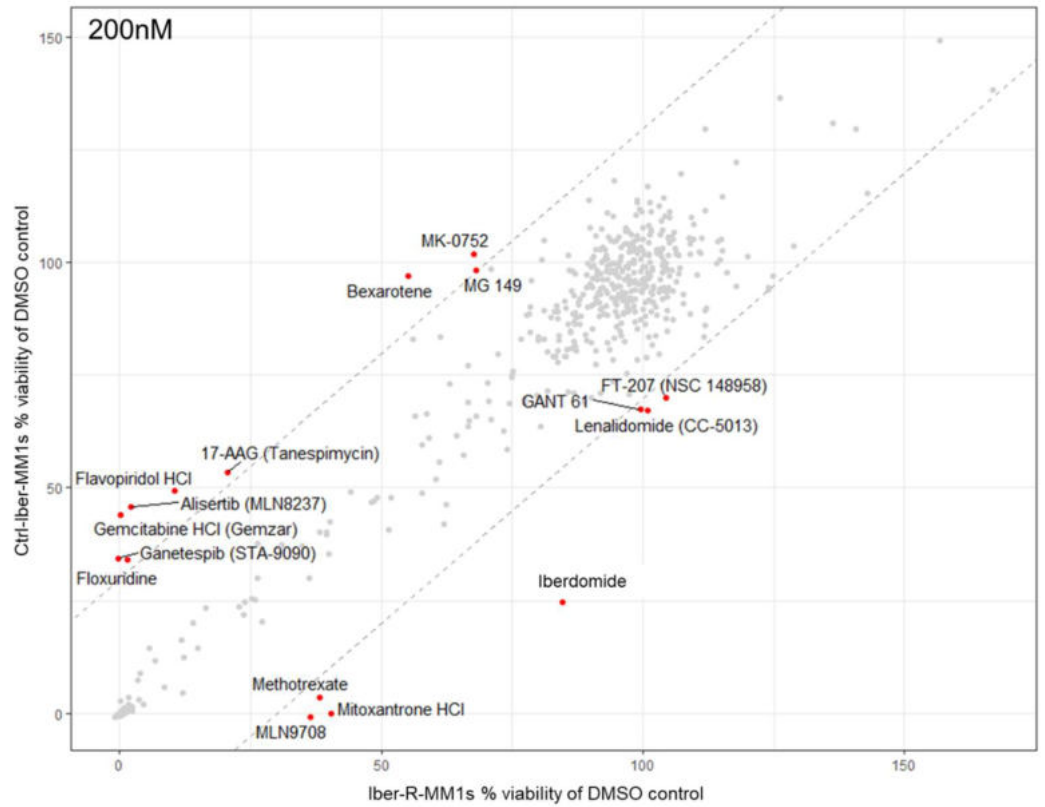
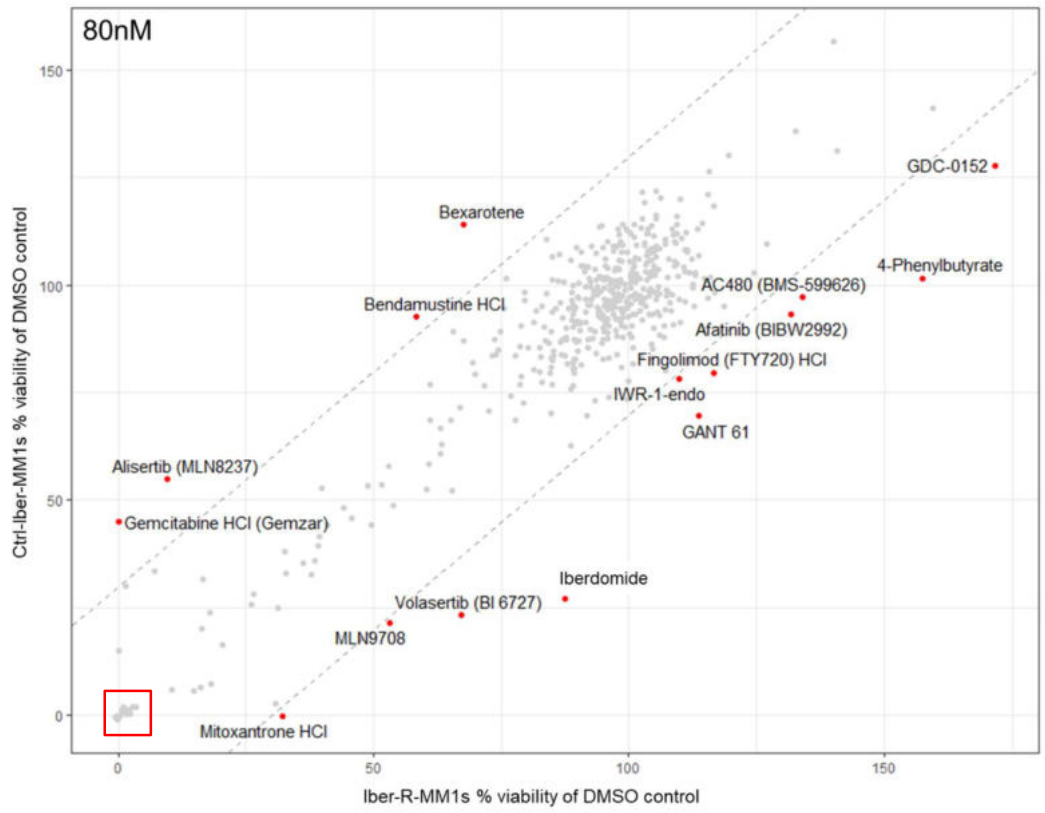


**Figure 4-2** *Expected patterns of compound screen data.*

Cell viability (CellTiter-Blue) assays compared the response of Ctrl-Iber-MM1s and Iber-R-MM1s to 3 doses (800nM, 200nM and 80nM) of different compounds (shown as a percentage of DMSO treatment control). Compounds may reduce proliferation in both the control and resistant cell lines, indicating no cross-resistance to IMiDs. Compounds may reduce proliferation in the control line but not in the resistant cell line, suggesting cross-resistance to IMiDs. Compounds may selectively reduce proliferation in the resistant cell line, suggesting exploitation of a novel vulnerability.

Compounds at each concentration were analysed separately using Dotmatics Vortex. The median viability (as a percentage of DMSO control) for each compound was plotted, with Ctrl-Iber-MM1s on the y-axis and Iber-R-MM1s on the x-axis (**Figure 4-3**). Hits were defined as compounds that led to a  $\geq 30\%$  difference in viability between the 2 cell lines (lines at  $y=x\pm 30$ ) or a  $\geq 80\%$  reduction in viability in both cell lines at 80nM. The latter was included in case there was a differential response at a lower dose that would otherwise be masked using this screening approach.





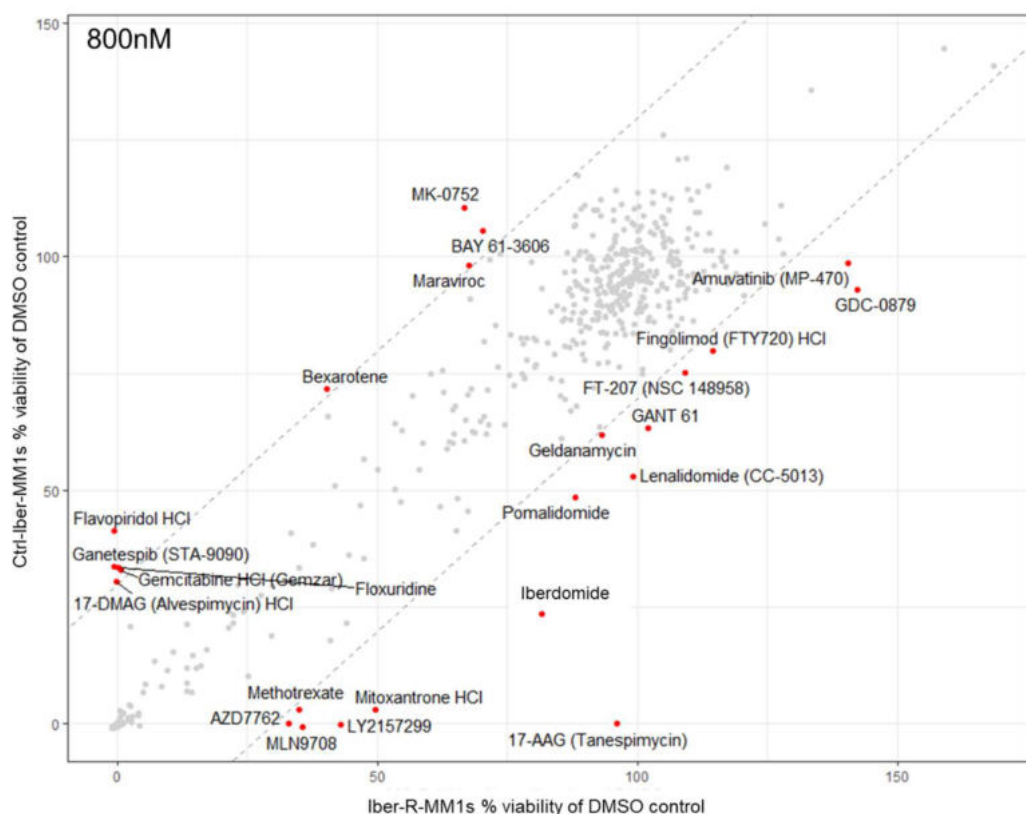


**Figure 4-3 Results of compound screening in Ctrl-Iber-MM1s and Iber-R-MM1s.**

The median % viability (CellTiter-Blue assay) compared to DMSO control for each compound was plotted, with Ctrl-Iber-MM1s on the y-axis and Iber-R-MM1s on the x-axis. Hits were defined as compounds that led to a  $\geq 30\%$  difference in viability between the 2 cell lines (lines at  $y=x\pm 30$ ) or a  $\geq 80\%$  reduction in viability in both cell lines at 80nM (compounds highlighted by the red box).

#### 4.2.2 Secondary screen of hit compounds

Primary hits (62 compounds, **Supplementary Table 9-5**) were then further assessed in 12-point dilution assays (highest concentration 800nM, dilution factor of 3). The secondary screen was performed in biological triplicate and iberdomide and bortezomib were used as controls on each plate. Except for lenalidomide and pomalidomide, no compounds were validated to show a differential response in the control and resistant lines (**Figure 4-4**). This indicated that the screen design was able to identify differential responses, but the only observed cross-resistance was to other IMiDs and there were no compounds in the library that exploited a novel vulnerability in the resistant setting.

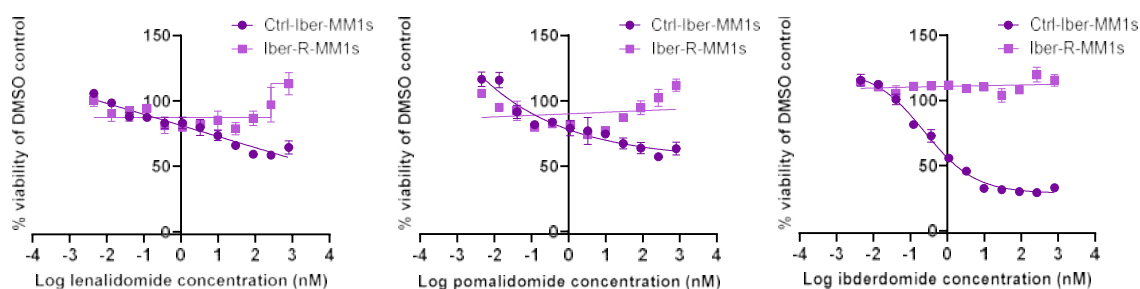


*Figure 4-4 12-point EC50 curves for compounds that demonstrated cross-resistance.*

Lenalidomide and pomalidomide showed cross-resistance in Iber-R-MM1s, indicating the screen design was able to identify differential compound responses in the control and resistant cell lines. Graphs show median and 95% confidence interval (n=3).

It was also important to highlight the compounds that are very active (cause a reduction in viability of  $\geq 80\%$ ) against sensitive and resistant myeloma cells at low concentrations ( $\leq 80\text{nM}$ ) (**Supplementary Table 9-5**). Whilst there was no differential response between the sensitive and resistant cell lines (confirmed on the secondary screen at lower concentrations) these compounds might still be of benefit to patients with IMiD-resistant myeloma as they were active in the resistant as well as sensitive setting. Thirty compounds met these criteria, including conventional chemotherapies (e.g. gemcitabine, doxorubicin, epirubicin, daunorubicin), heat-shock protein inhibitors, histone deacetylase inhibitors, vascular disrupting agents, kinesin spindle inhibitors, and pathway targeting agents such as QNZ (an NF $\kappa$ B inhibitor), YM155 (a Survivin/BIRC5 suppressant), GSK461364 (a Polo-Like Kinase 1 (PLK1) inhibitor), GSK2126458 (a dual PI3K/mTOR inhibitor), KX2-391 (an Src inhibitor) and INK 128 (an mTOR inhibitor).

A number of compounds currently used in clinical practice to treat myeloma were present in the list of 62 compounds, including the anthracycline chemotherapeutic agent doxorubicin (used as part of DT-PACE treatment (dexamethasone, thalidomide, cisplatin, doxorubicin, cyclophosphamide and etoposide)), bendamustine (an alkylating agent), panobinostat (an HDAC inhibitor), KPT-330/selinexor (a nuclear export inhibitor) and MLN9708/ixazomib (a PI). Bendamustine and MLN9708/ixazomib did not validate as compounds with a differential response in the two lines. However, the other compounds did validate as compounds that led to a large reduction in viability at low concentrations in both cell lines (**Figure 4-5**). Importantly, doxorubicin had comparable activity in

the control and resistant lines; doxorubicin is sensitive to the presence of drug efflux pumps, so IMiD/CELMoD resistance in Iber-R-MM1s is unlikely to be due to the presence of increased efflux pumps. Other important anti-myeloma agents were present in the initial screen but did not meet the definition of a hit (a differential response in the two cell lines or a  $\geq 80\%$  reduction in viability in a 5-day CellTiter-Blue assay at 80nM), such as dexamethasone and cyclophosphamide.

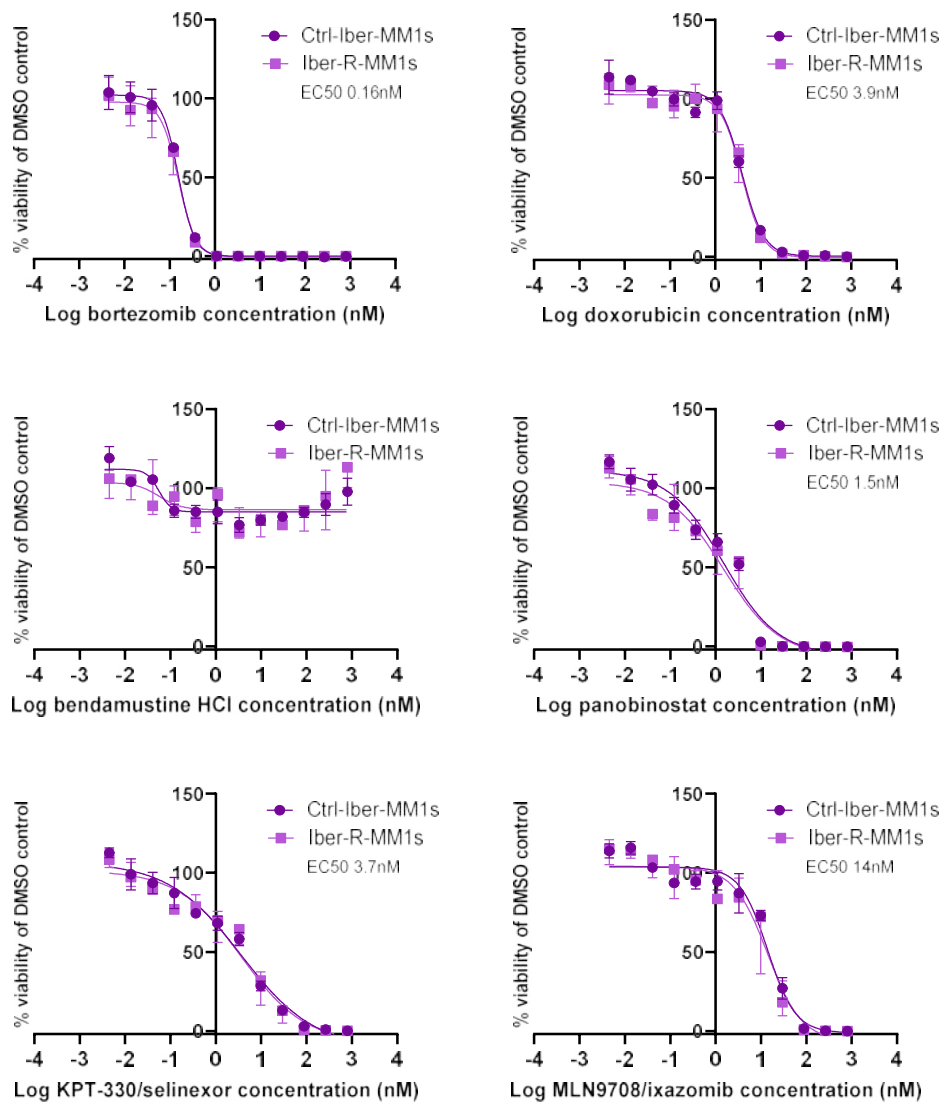


**Figure 4-5** The effect of currently used anti-myeloma drugs in Ctrl-Iber-MM1s and Iber-R-MM1s.

In a 5 day cell CellTiter-Blue viability assay bortezomib, doxorubicin, panobinostat, KPT-330/selinexor and MLN9708/ixazomib reduced viability equally in the Ctrl-Iber-MM1s and Iber-R-MM1s cell lines at low concentrations. Bendamustine did not validate as an agent with differential action in the two cells lines and did not lead to a reduction in viability at 800nM. Graphs show median and 95% confidence interval (n=3). EC50 is the concentration of compound that led to half the maximal reduction in viability.

### 4.3 Discussion

A drug screen of nearly 500 compounds was performed in Iber-R-MM1s and its control line. Lenalidomide and pomalidomide were present in the screen and Iber-R-MM1s showed cross-resistance to these drugs. This had been observed in my previous work and helped to confirm validity of the screen. However, no other compounds showed cross-resistance and no compounds appeared to be exploiting a novel pharmacological sensitivity in the resistant setting. The two cell lines were equally sensitive to low concentrations of a number of established anti-myeloma agents including bortezomib, doxorubicin, panobinostat, KPT-330/selinexor and MLN9708/ixazomib. They were also equally sensitive to low concentrations ( $\leq 80\text{nm}$ ) of several chemotherapeutic agents, heat shock protein inhibitors, vascular disrupting agents, kinesin spindle protein inhibitors and a number of pathway inhibitors (including NF $\kappa$ B and mTOR inhibitors), in keeping with the literature (150, 158-161).

These data suggest that the mechanism of resistance generated in the cell lines is very specific to IMiDs/CELMoDs and is not reflective of a pan-resistant state. It also appears that there are not many novel vulnerabilities in key pathways that are commonly altered in cancer (**Figure 4-1**). Limitations of the screening approach included using 800nM as the highest concentration for every compound and exploring all compounds in 5-day assays; for any given compound this concentration and exposure time may not be optimal. However, the practicality of performing such a screen requires these factors to be uniform. For example, compounds that target epigenetic changes often take several days to have their maximal effect (162). In addition, the screen contained predominately older compounds which targeted well known pathways; novel compounds that were not tested could affect viability differentially. Another inherent limitation of any screening approach is that libraries can only consist of existing compounds. An alternative is to take a genome wide approach and use genetic manipulation of potential targets. This would include all possible vulnerabilities, even those that do not yet have a pharmacological inhibitor. The compound screen described here would also not be able to identify compounds that might restore sensitivity to IMiDs/CELMoDs. This would need to be done through combination compound assays that would be more difficult to perform and analyse. Therefore, a genome wide genetic approach was taken forwards, as described in Chapter 5.

## Chapter 5 Reversing IMiD/CELMoD Resistance and Identifying Genetic Vulnerabilities in the IMiD/CELMoD-Resistant State

---

### 5.1 Introduction

In tandem with the pharmacological approach taken in Chapter 4, and given the limitations discussed in Section 4.3, a genome wide genetic approach was also undertaken. This aimed to identify targets that might reinduce sensitivity to IMiDs/CELMoDs and also explore novel vulnerabilities in the IMiD/CELMoD-resistant state to complement the compound screen.

A CRISPR screening approach was chosen after consideration of both CRISPR and RNA interference (RNAi) screening methods. CRISPR technology acts at the DNA level to permanently silence (knockout) a gene whereas RNA interference (RNAi) reduces the expression of a gene by selective inactivation of its corresponding mRNA by double-stranded RNA (dsRNA). The dsRNA can be in the form of small interfering RNAs (siRNAs) or short hairpin RNAs (shRNAs), which lead to degradation of target mRNA, or microRNAs (miRNAs) which also suppress translation (163). For this experiment, I wanted permanent knockout of each gene to completely stop protein expression and eliminate any confounding effects of residual protein. Therefore, a CRISPR screening approach was selected.

CRISPR-Cas9 gene editing has revolutionised biological research. CRISPR-Cas9 consists of two key molecules, the endonuclease Cas9 and a guide RNA (gRNA) (**Figure 5-1**). Cas9 induces a double-strand break in DNA at a specific genomic location designated by the gRNA. The gRNA is a specifically designed sequence of about 20 base pairs which is located within a longer RNA scaffold. The scaffold binds to DNA and the guide sequence ensures Cas9 cuts at the correct location.

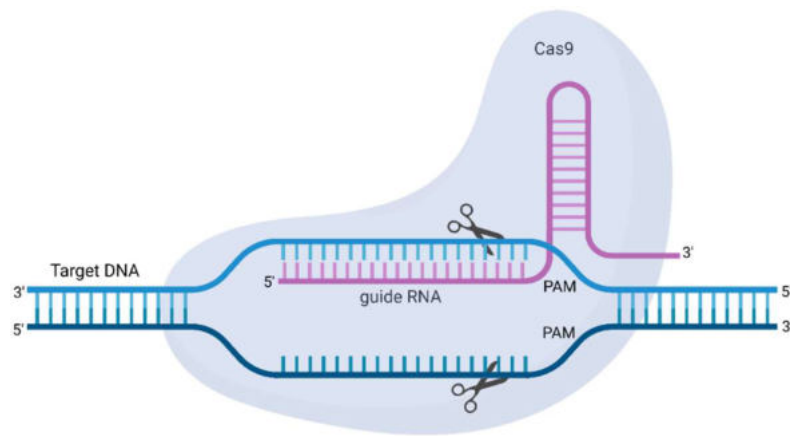


*Figure 5-1 The CRISPR-Cas9 system.*

Cas9 is directed to its target sequence by a guide RNA which can be synthesised as a single strand. To enable cutting, a protospacer adjacent motif (PAM) must be about 2-6 nucleotides downstream of the DNA sequence targeted by the guide. The exact PAM sequence depends upon the bacteria used to produce the Cas9. Repair following DNA cutting may occur via non-homologous end joining or homology directed repair (164). Image created using BioRender.

The cell then recognises that the DNA is damaged and tries to repair it. This repair can occur via two pathways. The primary pathway is non-homologous end joining, which commonly results in random insertions or deletions of DNA. This can lead to frameshift mutations and subsequent loss-of-function of the specified gene (knockout) (164). The less common pathway is homology directed repair, in which a homologous piece of DNA is used as a repair template. This leads to a more accurate repair, which can be exploited in the laboratory to specifically edit DNA (164). The barcoded nature of the gRNAs, coupled with the availability of next generation sequencing (NGS), allows pooled screens to be carried out (165). Therefore, we can look for genetic vulnerabilities on a genome wide scale.

In pooled screens, cells are transduced with a lentiviral gRNA library and in each individual cell only one gene is knocked out. Cells are then exposed to specific selection criteria, such as a drug treatment, and there is often a control comparator arm. After a specified number of cell doublings, the gRNAs are amplified from the transduced cells' genomic DNA and guide abundance is quantified by NGS. Guides that are enriched in the treatment arm (as compared to the untreated control) may indicate that a given gene is required for a drug's cytotoxic activity, whereas depleted guides identify essential genes or genes that are protective against a drug's activity (165).

This type of knockout CRISPR screen is one of the most commonly performed. However, other types of screens have been developed such as CRISPR

interference (CRISPRi) and CRISPR activation (CRISPRa) screens. CRISPRi uses a catalytically inactive Cas9 (dCas9) fused to a transcriptional repressor. When a guide targets the dCas9 to a gene promoter or exon this can repress transcription by steric interference and the transcriptional repressor can further reduce gene expression by genetically silencing the locus (without permanently knocking it out) (165). In a CRISPRa screen dCas9 is fused to transcriptional activator to activate expression of specific target genes (165).

CRISPR systems are rapidly improving, but challenges remain. One major concern is off-target effects, in which Cas9 acts on untargeted genomic sequences. This is often gRNA dependent as Cas9 can tolerate up to 3 mismatches between the gRNA and genomic DNA sequence (166). However, *in silico* tools to aid gRNA design are improving and minimising these effects (166). CRISPR screens are less susceptible to off-target effects than RNAi screens (167).

The genome wide knockout CRISPR screen was performed in Iber-R-MM1s, the cell line used in the compound screen in Chapter 4. Iber-R-MM1s cells were transduced with the Brunello library and then treated with iberdomide or DMSO. This design allowed me to identify any genes that when knocked out restored sensitivity to CELMoDs. In a separate analysis, I could also compare the effect of knockout of a given gene on the fitness of Iber-R-MM1s cells and parental MM1s (using publicly available CRISPR screen data from DepMap). This would enable exploration of genetic vulnerabilities in the IMiD/CELMoD resistant state which complements the compound screen in Chapter 4.



## 5.2 Results

### 5.2.1 Genome wide loss-of-function CRISPR screen in Iber-R-MM1s

The CRISPR screen was performed in Iber-R-MM1s, and key optimisation experiments are described in detail in **Supplementary Results Section 9.3**. In summary, a two-vector system was employed. Iber-R-MM1s cells were initially transduced to stably express Cas9 and Cas9 activity was confirmed (**Supplementary Figure 9-9**). These cells were then transduced with Brunello plasmid pool lentivirus, which targets >19,000 protein-coding genes with ~4 gRNAs per gene. It is critical that a maximum of one gene is knocked out per cell, and this required careful optimisation (**Supplementary Figure 9-10**).

The cells were then split into two branches and a sample of cells taken to provide a baseline sample for confirmation of library representation and to allow downstream comparisons. The screen commenced with 108 million cells to enable at least 500 cells per gRNA after antibiotic selection of transduced cells. One branch of cells was cultured with DMSO, and one branch cultured with iberdomide. Drug exposure was continued for eight doublings, providing sufficient time for good resolution of negatively selected genes. Cell samples were collected from each branch at the end of the experiment and, along with the baseline sample, genomic DNA (gDNA) was extracted. PCR was then used to amplify the gRNA sequences from the gDNA (optimisation shown in **Supplementary Figure 9-12**). NGS of the amplicons was performed and the frequency of read counts for a given gRNA in the DMSO and iberdomide experimental conditions compared. This allowed identification of genes that when knocked out in the resistant cells **restored sensitivity** to iberdomide (**Figure 5-2**). Using the baseline cell sample and the sample from the DMSO branch at the end point of the experiment, it was also possible to model the effect of knockout of a given gene on cell fitness.

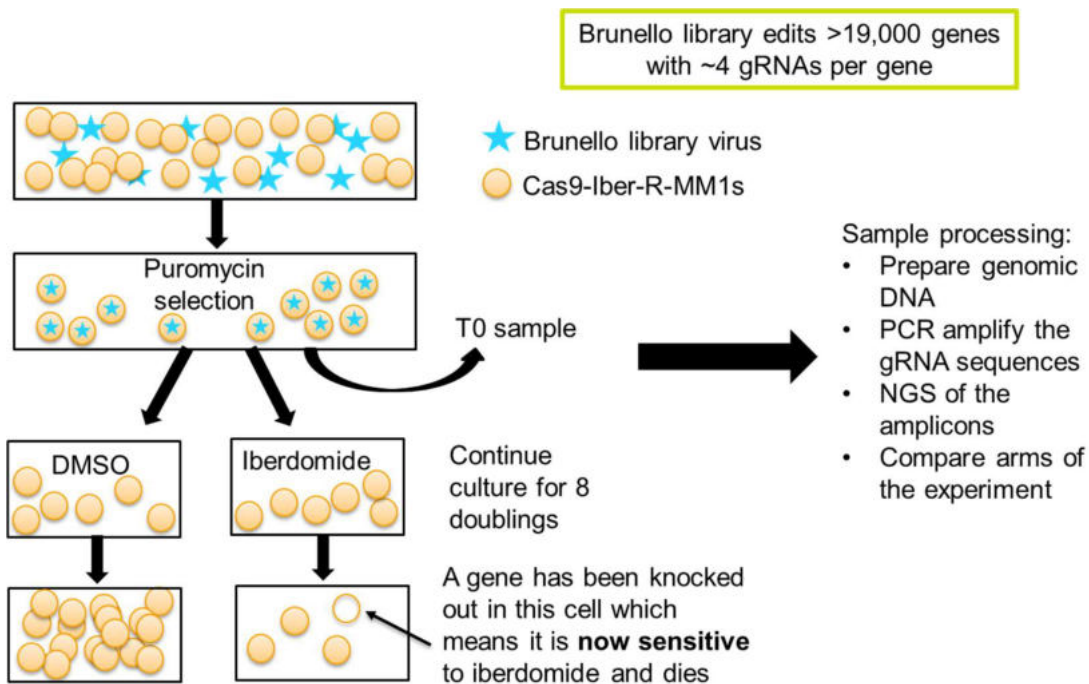


*Figure 5-2 The CRISPR screen workflow.*

The CRISPR screen flow is depicted, with initial transduction of Cas9-Iber-R-MM1s with the Brunello plasmid pool, followed by puromycin selection, treatment with DMSO or iberdomide and sample processing steps.

### 5.2.2 Identifying ways to reverse IMiD/CELMOd resistance

The CRISPR screen data was analysed using MAGeCKFlute, an integrative analysis pipeline for pooled CRISPR functional genetic screens (168). This pipeline calculates beta scores for each gene in the two arms of the experiment which can then be compared. The beta score describes how a gene is selected; a lower score in the iberdomide arm compared to the DMSO arm would indicate a possible re-induction of sensitivity to IMiDs (**Figure 5-3**). APOBEC3D (Apolipoprotein B mRNA Editing Enzyme Catalytic Subunit 3D) showed the greatest negative selection with iberdomide compared to DMSO of all the genes (i.e. the greatest difference between the beta score in the DMSO arm and the beta score in the iberdomide arm, excluding ZDHHC23 (Zinc Finger DHHC-Type Palmitoyltransferase 23) which was not selected for in the iberdomide treatment arm).

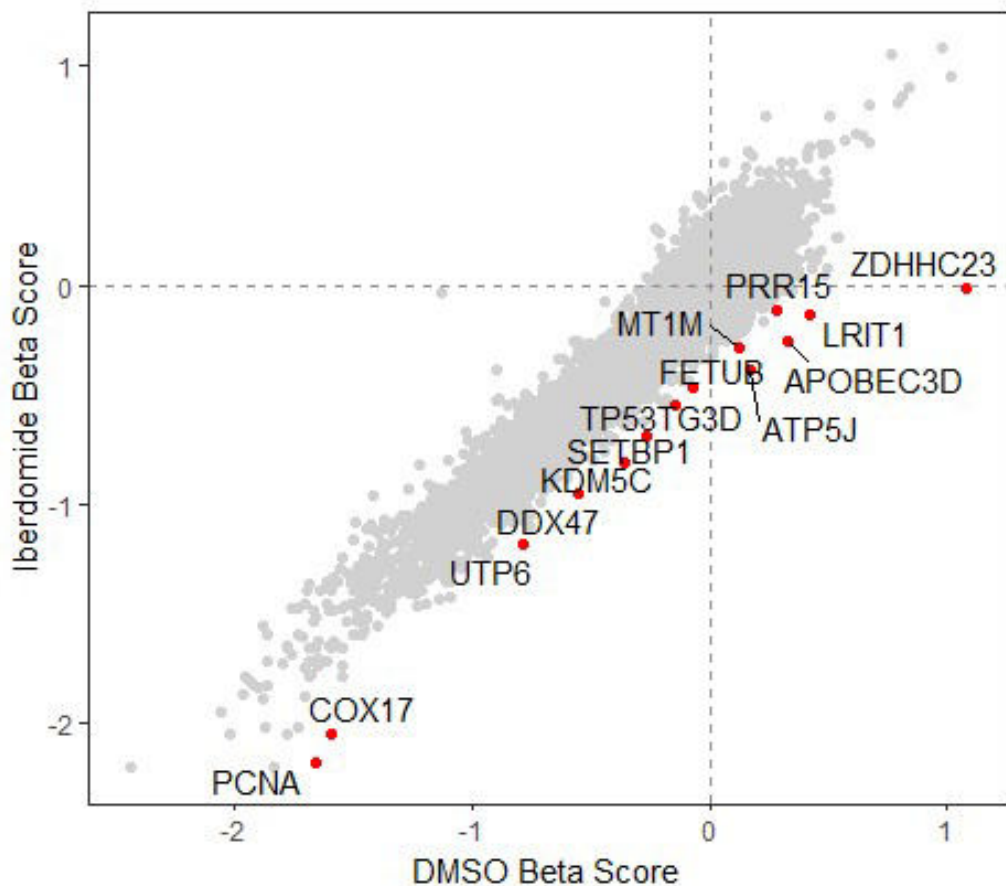


*Figure 5-3 CRISPR screen results.*

Beta scores were generated for genes in each arm of the experiment and compared. The beta score describes how the gene is selected; a positive beta score indicates positive selection, and a negative beta score indicates negative selection. Genes with a difference of 0.4 between the beta score in the DMSO arm and the beta score in the iberdomide arm are labelled. PCNA (Proliferating Cell Nuclear Antigen), COX17 (Cytochrome C Oxidase Copper Chaperone COX17), UTP6 (UTP6 Small Subunit Processome Component), DDX47 (DEAD-Box Helicase 47), KDM5C (Lysine Demethylase 5C), SETBP1 (SET Binding Protein 1), TP53TG3D (TP53 Target 3D), FETUB (Fetuin B), ATP5J (ATP Synthase Peripheral Stalk Subunit F6), MT1M (Metallothionein 1M), APOBEC3D (Apolipoprotein B mRNA Editing Enzyme Catalytic Subunit 3D), LRIT1 (Leucine Rich Repeat, Ig-Like And Transmembrane Domains 1), PRR15 (Proline Rich 15) and ZDHHC23 (Zinc Finger DHHC-Type Palmitoyltransferase 23).

### **Exploration of APOBEC3D**

To explore knockout of *APOBEC3D* further, normalised counts for each individual gRNA were assessed at T0 (the baseline sample),  $T_{\text{finalDMSO}}$  and  $T_{\text{finaliberdomide}}$ . *APOBEC3D* knockout had no effect on cell fitness (**Figure 5-4 A**). However, *APOBEC3D* guides appeared to be negatively selected for in the iberdomide arm, suggesting possible reinduction of sensitivity to IMiDs (**Figure 5-4 B and C**).

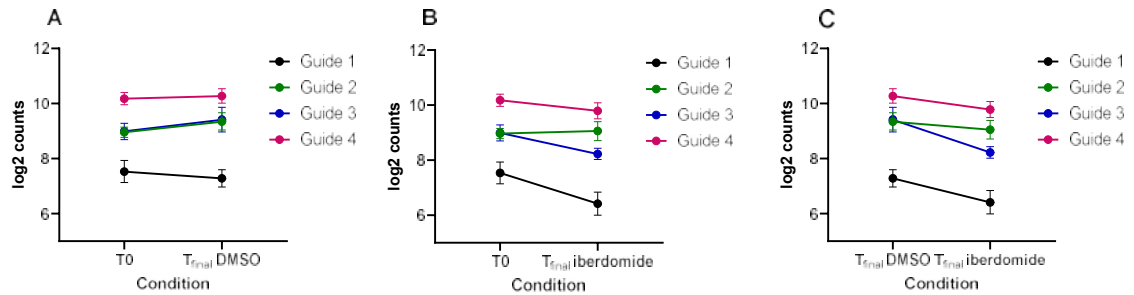


**Figure 5-4** *APOBEC3D* knockout at the individual guide level.

A) Comparing T<sub>0</sub> and T<sub>final</sub>DMSO, *APOBEC3D* knockout did not have an effect on cell fitness. B) Comparing T<sub>0</sub> and T<sub>final</sub>iberdomide, *APOBEC3D* knockout had a negative effect of cell fitness. C) *APOBEC3D* guides appeared to be negatively selected for in the T<sub>final</sub>iberdomide arm as compared to the T<sub>final</sub>DMSO arm. N=5, graphs show mean and SEM.

In an attempt to validate this finding, *APOBEC3D* was then knocked out in Cas9-Iber-R-MM1s (alongside an empty vector control) to see if this led to restoration of sensitivity to IMiD/CELMoD therapy. This was done using a pool of the same guides present in the Brunello library. A reduction in *APOBEC3D* mRNA level was confirmed (**Figure 5-5**) but there was no validated antibody available for protein level assessment.

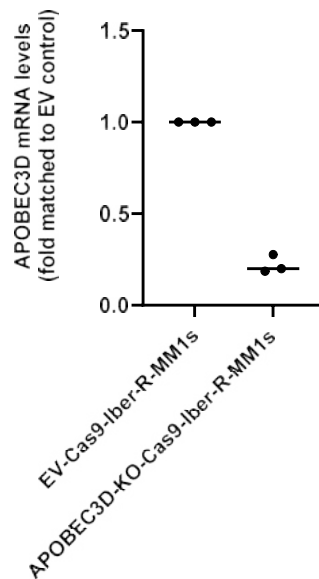


**Figure 5-5** Knockout of *APOBEC3D* at the mRNA level.

*APOBEC3D*-KO-Cas9-Iber-R-MM1s showed a reduction in *APOBEC3D* mRNA compared to an empty vector (EV) control. Individual points represent independent experiments, and the horizontal bar represents the median (n=3).

EV-Cas9-Iber-R-MM1s and *APOBEC3D*-KO-Cas9-Iber-R-MM1s were exposed to iberdomide, and there was no evidence of restoration of CELMoD sensitivity with *APOBEC3D* knockout (**Figure 5-6**).

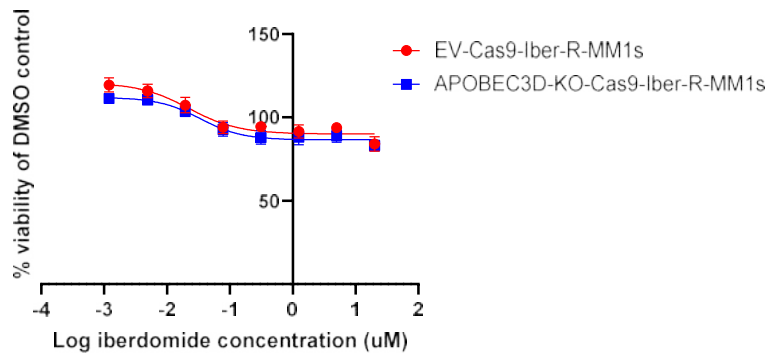


*Figure 5-6 The effect of APOBEC3D knockout on CELMoD resistance.*

The two cell lines were exposed to varying concentrations of iberdomide in a 5-day cell viability assay (CellTiter-Blue). There was no restoration of CELMoD sensitivity with *APOBEC3D* knockout. N=4, graph shows mean and error bars represent SEM.

It was possible that the lack of difference in CELMoD response between the bulk cell populations of EV-Cas9-Iber-R-MM1s and APOBEC3D-KO-Cas9-Iber-R-MM1s was because the restoration of sensitivity was subtle in the *APOBEC3D* knockout cells and thus could not be detected in the heterogenous population. Single cell clones were therefore cultured to see if a change in IMiD/CELMoD sensitivity could be detected in a clonal population of cells with no/very low APOBEC3D expression (based on mRNA levels in the first instance given the lack of a specific antibody).

The single cells took 8-10 weeks to recover and proliferate. Twelve EV-Cas9-Iber-R-MM1s and 12 APOBEC3D-KO-Cas9-Iber-R-MM1s clones were selected for further exploration. All of the APOBEC3D-KO clones showed reduced *APOBEC3D* mRNA expression to varying extents; clones 1,2,3,5,7,11 and 12 had very low/no expression (**Figure 5-7**).

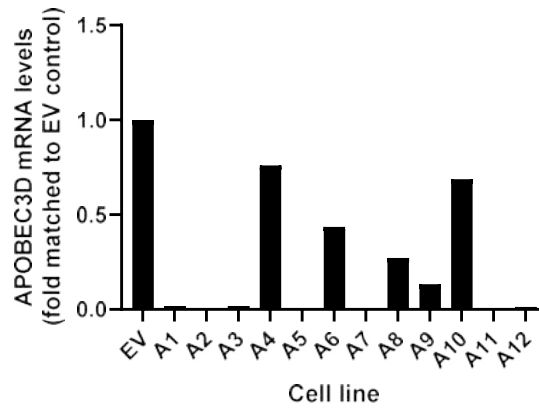


**Figure 5-7** *APOBEC3D* mRNA expression in the clonal lines.

*APOBEC3D* mRNA levels in the *APOBEC3D*-KO-Iber-R-MM1s clones were compared to the average of the empty vector (EV) clones. The *APOBEC3D*-KO lines all showed a reduction in *APOBEC3D* expression to varying extents, highlighting the heterogeneity in the initial population. mRNA levels were quantified by RT-PCR, n=1 shown. A1-12 are clonal populations derived from *APOBEC3D*-KO-Cas9-Iber-R-MM1s.

The clonal lines were exposed to iberdomide in a 5-day cell viability assay. Unfortunately, at this time point many of the EV-Cas9-Iber-R-MM1s had regained sensitivity to iberdomide (note the cells had to be kept out of selection pressure because possible reinduction of sensitivity was being explored) (**Figure 5-8**). Without an appropriate control the experiment could not be continued; the *APOBEC3D*-KO lines may have regained sensitivity to iberdomide secondary to removal of the selection pressure and not loss of *APOBEC3D* expression. When the selection pressure was removed in my previous work, Iber-R-MM1s had regained sensitivity by ~ 20 weeks. It is interesting that the recovering single cells regained sensitivity much sooner than this.

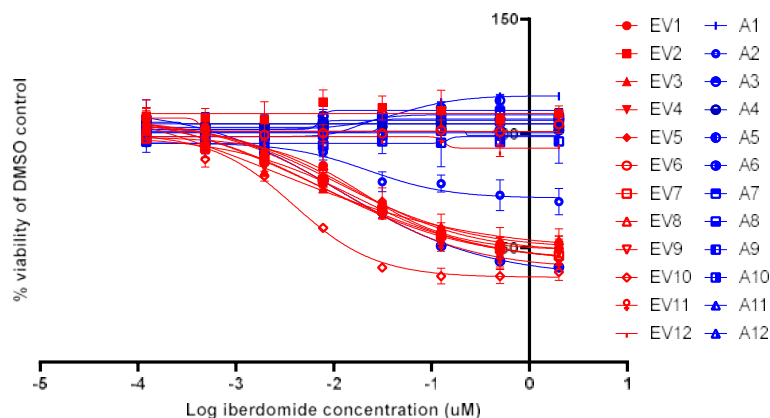


**Figure 5-8** The effect of iberdomide treatment on viability in the clonal cell lines.

Clonal populations (from single cells) were exposed to iberdomide for 5 days and viability assessed in a CellTiter-Blue assay. Several of the empty vector clones had regained sensitivity to iberdomide. N=2, graph shows mean and error bars represent SEM. EV1-12 are clonal populations seeded from EV-Cas9-Iber-R-MM1s; A1-12 are clonal populations from *APOBEC3D*-KO-Cas9-Iber-R-MM1s.

### 5.2.3 Identifying novel vulnerabilities in the IMiD/CELMoD-resistant setting

#### *The Chronos algorithm*

As well as finding mechanisms to reverse resistance to IMiDs/CELMoDs, the CRISPR screen data was also used to look for novel vulnerabilities in the IMiD/CELMoD-resistant setting. In the first approach, we are trying to uncover ways to restore sensitivity to IMiDs/CELMoDs and enable these drugs to have ongoing efficacy. In the second approach, we are looking for vulnerabilities that may have developed alongside the generation of IMiD/CELMoD resistance which can then be targeted. This is similar to concept behind the pharmacological screen (Chapter 4) but uses a genome wide approach not limited to compounds available within the library.

To do this Chronos was employed, an algorithm that infers gene knockout fitness effects based on a model of cell proliferation dynamics after CRISPR gene knockout (169). The algorithm calculates a gene effect score for each gene; a lower score means a gene is more likely to be dependent, with a score of 0 indicating that a gene is not essential and a score of -1 representing the median of all common essential genes. The gene effect scores for the Iber-R-MM1s line were then compared to publicly available gene effect scores for parental MM1s (available via the Broad Institute DepMap portal and calculated in the same way from CRISPR screen data). A novel dependency was defined as a score of  $<-1$  in Iber-R-MM1s and  $>-0.5$  in parental MM1s. These criteria selected 47 genes that may represent novel vulnerabilities in the resistant setting (**Figure 5-9**).

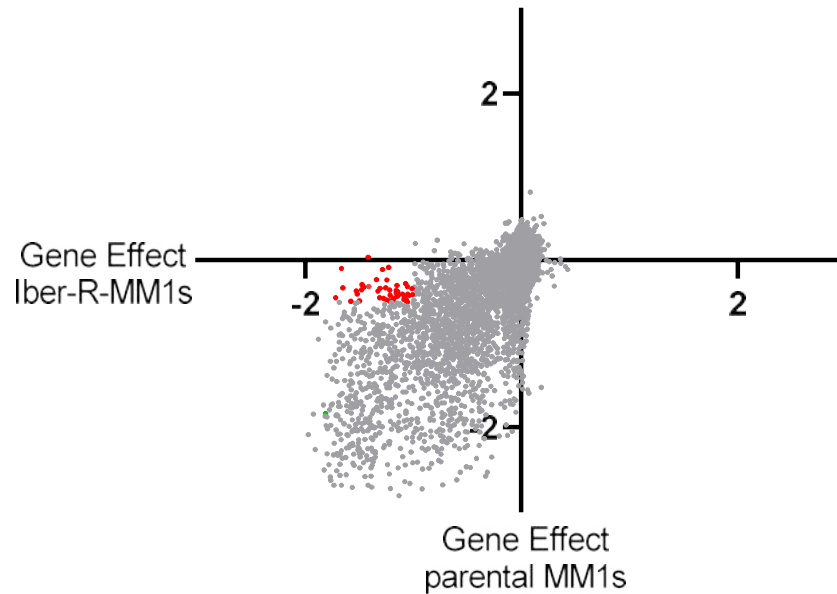


**Figure 5-9 Identification of novel vulnerabilities in the IMiD/CELMoD resistant setting.**

The Chronos algorithm was used to calculate gene effect scores for each gene in the Iber-R-MM1s cell line. These scores were then compared to those for parental MM1s using data from the DepMap portal that had been generated using the same method. A lower score means that a gene is more likely to be dependent in a given cell line. This graph shows the gene effect scores for Iber-R-MM1s on the x axis and parental MM1s on the y axis. For example, *IRF4* has a score of -1.8 in both cell lines and therefore is essential in both cell lines. Potential novel dependencies were defined as a score of <-1 in the resistant line and >-0.5 in parental MM1s. This identified 47 genes which are highlighted in red.

The 47 genes are briefly discussed in the table below (**Table 5-1**).

Gene symbol	Name	Gene effect in Iber-R-MM1s	Gene effect in parental MM1s	Description
MRPL52	Mitochondrial Ribosomal Protein L52	-1.66	-0.10	Component of the mitochondrial large ribosomal subunit.
LIPT2	Lipoyl(Octanoyl) Transferase 2	-1.42	0.04	Involved in essential redox reactions.
MRPL20	Mitochondrial Ribosomal Protein L20	-1.65	-0.33	Component of the mitochondrial large ribosomal subunit.
PTPMT1	Protein Tyrosine Phosphatase Mitochondrial 1	-1.72	-0.45	Lipid phosphatase.
PRMT1	Protein Arginine Methyltransferase 1	-1.47	-0.29	Arginine methyltransferase.



NSMCE4A	NSE4 Homolog A, SMC5-SMC6 Complex Component	-1.28	-0.11	Component of the SMC5-SMC6 complex.
HSD17B10	Hydroxysteroid 17-Beta Dehydrogenase 10	-1.53	-0.37	Mitochondrial dehydrogenase involved in pathways of fatty acid, branched-chain amino acid and steroid metabolism.
RNASEK	Ribonuclease K	-1.23	-0.08	Endoribonuclease.
VAR2	Valyl-TRNA Synthetase 2, Mitochondrial	-1.46	-0.32	Mitochondrial aminoacyl-tRNA synthetase.
GART	Phosphoribosylglycinamide Formyltransferase	-1.48	-0.35	Involved in de novo purine synthesis.
LIN52	Lin-52 DREAM MuvB Core Complex Component	-1.52	-0.40	Exists in quiescent cells where it represses cell cycle-dependent genes.
DHPS	Deoxyhypusine Synthase	-1.34	-0.23	Required for the formation of hypusine, a unique amino acid.
MBTPS1	Membrane Bound Transcription Factor Peptidase, Site 1	-1.41	-0.32	Serine protease, known substrates are SREBP1, SREBP2, BDNF, GNPTAB, ATF6 and ATF6B.
INO80	INO80 Complex ATPase Subunit	-1.58	-0.49	ATPase component of the INO80 chromatin remodeling complex.
HDAC3	Histone Deacetylase 3	-1.50	-0.49	Responsible for the deacetylation of lysine residues on core histones.
METTL3	Methyltransferase 3, N6-Adenosine-Methyltransferase Complex Catalytic Subunit	-1.24	-0.24	Methylates adenosine residues of some RNAs and regulates various processes including the circadian clock, differentiation of embryonic and hematopoietic stem cells, cortical neurogenesis, response to DNA damage,

				differentiation of T-cells and primary miRNA processing.
MRPL48	Mitochondrial Ribosomal Protein L48	-1.31	-0.33	Component of the mitochondrial large ribosomal subunit.
COG4	Component Of Oligomeric Golgi Complex 4	-1.33	-0.37	Plays a role in SNARE-pin assembly and Golgi-to-ER retrograde transport.
ATIC	5-Aminoimidazole-4-Carboxamide Ribonucleotide Formyltransferase /IMP Cyclohydrolase	-1.25	-0.33	Catalyses the last two steps of purine biosynthesis.
MEAF6	MYST/Esa1 Associated Factor 6	-1.31	-0.45	Component of the NuA4 histone acetyltransferase complex which is involved in transcriptional activation of select genes.
TMED10	Transmembrane P24 Trafficking Protein 10	-1.22	-0.36	Cargo receptor involved in protein vesicular trafficking and quality control in the endoplasmic reticulum and Golgi.
ISCA1	Iron-Sulfur Cluster Assembly 1	-1.15	-0.30	Involved in the maturation of mitochondrial 4Fe-4S proteins.
MTHFD1	Methylenetetrahydrofolate Dehydrogenase, Cyclohydrolase And Formyltetrahydrofolate Synthetase 1	-1.28	-0.46	Involved in the pathway of tetrahydrofolate interconversion, which is part of one-carbon metabolism.
TUBGCP2	Tubulin Gamma Complex Component 2	-1.21	-0.42	Enables gamma-tubulin binding activity.
SEL1L	SEL1L Adaptor Subunit Of	-1.16	-0.36	Required for the retrotranslocation of misfolded

	SYVN1 Ubiquitin Ligase			proteins from the endoplasmic reticulum lumen to the cytosol, where they are degraded by the proteasome in a ubiquitin-dependent manner.
C19orf25	Chromosome 19 Open Reading Frame 25	-1.07	-0.28	Unknown function.
MED12	Mediator Complex Subunit 12	-1.25	-0.48	Component of the Mediator Complex, a coactivator involved in the regulated transcription of nearly all RNA polymerase II-dependent genes.
UQCRB	Ubiquinol-Cytochrome C Reductase Binding Protein	-1.15	-0.38	Part of the mitochondrial electron transport chain which drives oxidative phosphorylation.
ITPK1	Inositol-Tetrakisphosphate 1-Kinase	-1.16	-0.39	Kinase that can phosphorylate various inositol polyphosphates.
ZBTB8OS	Zinc Finger And BTB Domain Containing 8 Opposite Strand	-1.05	-0.32	Component of the tRNA-splicing ligase complex.
VPS52	VPS52 Subunit Of GARP Complex	-1.22	-0.49	Component of the GARP complex that is involved in retrograde transport from early and late endosomes to the trans-Golgi network.
HNRNPA1	Heterogeneous Nuclear Ribonucleoprotein A1	-1.14	-0.42	Involved in the packaging of pre-mRNA into hnRNP particles, transport of poly(A) mRNA from the nucleus to the cytoplasm and may modulate splice site selection.
NDUFA1	NADH:Ubiquinone Oxidoreductase Subunit A1	-1.18	-0.46	Accessory subunit of the mitochondrial membrane respiratory chain NADH dehydrogenase (Complex I).

ARMC5	Armadillo Repeat Containing 5	-1.19	-0.47	Involved in foetal development, T-cell function, and adrenal gland growth homeostasis.
SETD2	SET Domain Containing 2, Histone Lysine Methyltransferase	-1.15	-0.43	Histone methyltransferase that specifically trimethylates Lys-36 of histone H3.
FPGS	Folypolyglutamate Synthase	-1.19	-0.49	Catalyses conversion of folates to polyglutamate derivatives, allowing concentration of folate compounds in the cell and the intracellular retention of these cofactors. These are important substrates for folate-dependent enzymes that are involved in one-carbon transfer reactions (required for purine, pyrimidine, and amino acid synthesis.)
DHX9	DExH-Box Helicase 9	-1.10	-0.41	Multifunctional ATP-dependent nucleic acid helicase that unwinds DNA and RNA in a 3' to 5' direction.
GADD45GIP1	GADD45G Interacting Protein 1	-1.01	-0.34	Acts as a negative regulator of G1 to S cell cycle phase progression by inhibiting cyclin-dependent kinases.
IRF2	Interferon Regulatory Factor 2	-1.05	-0.40	Specifically binds to the upstream regulatory region of type I IFN and IFN-inducible MHC class I genes and represses those genes.
RMI1	RecQ Mediated Genome Instability 1	-1.08	-0.44	Component of the RMI complex, which is involved in the processing of homologous recombination intermediates to limit DNA crossover formation in cells.

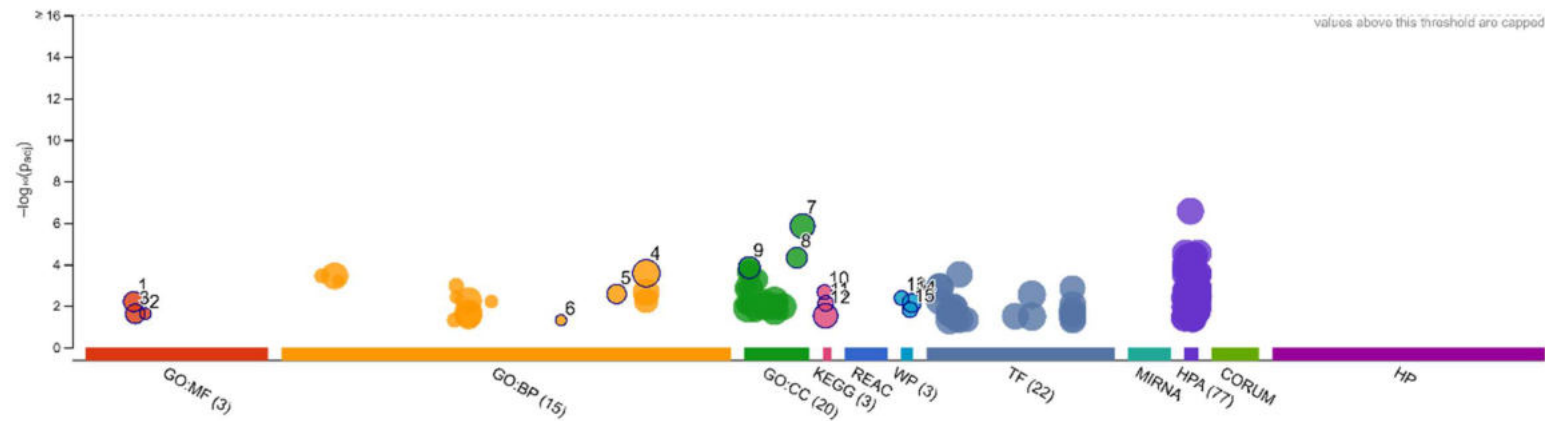
NDUFB11	NADH:Ubiquinone Oxidoreductase Subunit B11	-1.09	-0.47	Accessory subunit of the mitochondrial membrane respiratory chain NADH dehydrogenase (Complex I).
PFN1	Profilin 1	-1.04	-0.42	Binds to actin and affects the structure of the cytoskeleton.
SCD	Stearoyl-CoA Desaturase	-1.07	-0.47	Stearoyl-CoA desaturase that introduces the first double bond into saturated fatty acyl-CoA substrates.
KRT18	Keratin 18	-1.07	-0.47	Involved in the uptake of thrombin-antithrombin complexes by hepatic cells.
RPIA	Ribose 5-Phosphate Isomerase A	-1.01	-0.41	Involved in a sub pathway of the pentose phosphate pathway, which is itself part of carbohydrate degradation.
TRMT5	TRNA Methyltransferase 5	-1.07	-0.48	Involved in mitochondrial tRNA methylation.
PFDN5	Prefoldin Subunit 5	-1.05	-0.50	Binds specifically to cytosolic chaperonin and transfers target proteins to it. Represses the transcriptional activity of MYC.

*Table 5-1 Potential novel vulnerabilities in the resistant state.*

The table describes the 47 genes that may represent novel vulnerabilities in the IMiD/CELMOd resistant state. Descriptions taken from GeneCards (147).

Functional enrichment analysis of these genes highlighted mitochondrial genes, folate pathways (including one-carbon metabolism), and broad metabolic pathways (**Figure 5-10**). Metabolism changes, predominately lipid metabolism changes, were seen in the resistant lines on whole proteome evaluation (**Section 3.2.4**). Stearoyl-CoA desaturase (SCD) was significantly down-regulated in all the resistant cell lines at the protein level and appeared as a novel vulnerability in the Chronos analysis of the CRISPR screen data (**Table 5-1**). SCD transcription is regulated by Sterol Regulatory Element-Binding Transcription Factor 1 (SREBP1) which is activated by Membrane Bound Transcription Factor Peptidase Site 1 (MBTPS1), which also appeared in the list of 47 genes. Therefore, knockout of *SCD* or *MBTPS1* may represent a novel vulnerability in

the IMiD/CELMoD resistant setting which could be related to baseline changes in metabolism.



ID	Source	Term ID	Term Name	Padj (query_1)
1	GO:MF	GO:0016741	transferase activity, transferring one-carbon groups	$6.325 \times 10^{-7}$
2	GO:MF	GO:0019238	cyclohydrolase activity	$2.384 \times 10^{-7}$
3	GO:MF	GO:0016874	ligase activity	$2.426 \times 10^{-7}$
4	GO:BP	GO:1901576	organic substance biosynthetic process	$2.696 \times 10^{-4}$
5	GO:BP	GO:0140053	mitochondrial gene expression	$2.688 \times 10^{-3}$
6	GO:BP	GO:0070901	mitochondrial tRNA methylation	$4.963 \times 10^{-2}$
7	GO:CC	GO:1902494	catalytic complex	$1.429 \times 10^{-6}$
8	GO:CC	GO:0098798	mitochondrial protein-containing complex	$4.818 \times 10^{-5}$
9	GO:CC	GO:0005759	mitochondrial matrix	$1.427 \times 10^{-4}$
10	KEGG	KEGG:00670	One carbon pool by folate	$2.181 \times 10^{-3}$
11	KEGG	KEGG:01523	Antifolate resistance	$7.599 \times 10^{-3}$
12	KEGG	KEGG:01100	Metabolic pathways	$3.034 \times 10^{-2}$
13	WP	WP:WP4259	Disorders of folate metabolism and transport	$4.204 \times 10^{-3}$
14	WP	WP:WP411	mRNA processing	$7.216 \times 10^{-3}$
15	WP	WP:WP241	One-carbon metabolism	$1.549 \times 10^{-2}$

Figure 5-10 Functional enrichment analysis of potential vulnerabilities in the resistant setting.

Functional enrichment analysis (g:Profiler, (145)) of the 47 genes highlighted mitochondrial genes, folate pathways and metabolic pathways. Driver terms in GO and all KEGG, Reactome and WikiPathways pathways are highlighted.

### ***Targeting vulnerabilities with available inhibitors***

Chemical inhibitors of the proteins encoded by the 47 genes were sought. Seven had available specific inhibitors and six had a mechanism of action that suggested a response might be expected in a standard 5-day cell viability assay (**Table 5-2**). SETD2 (SET Domain Containing 2, Histone Lysine) inhibitors were explored in 14-day viability assays based on previous data (170) and in keeping with the slower changes generally seen in response to epigenetics inhibitors. This data is described in Chapter 6.

<b>Protein</b>	<b>Compound</b>
SCD	A939572
METTL3	STM2457
GART	Lometrexol
HDAC3	RGFP966
PRMT1	MS023
MBTSP1	PF-429242
SETD2	EPZ-719, EZM0414

*Table 5-2 Available inhibitors to target potential vulnerabilities in the IMiD/CELMoD resistant state.*

Specific inhibitors were available for 7 of the possible novel vulnerabilities.

The first 6 inhibitors were initially tested in Iber-R-MM1s and Iber-R-H929, alongside their respective controls (**Figure 5-11**). The MBTSP1 inhibitor PF-429242 reduced viability to a greater extent in Iber-R-H929 compared to Ctrl-Iber-H929. However, a differential response was not observed between the two MM1s cell lines, in which the compound only affected viability at the highest concentration in both Iber-R-MM1s and Ctrl-Iber-MM1s. The SCD inhibitor A939572 did not reduce viability in the control or resistant MM1s or H929 cell lines. The other compounds had a similar effect on viability in the IMiD/CELMoD resistant and sensitive settings. The effect of PF-429242 will be further explored in Chapter 7.



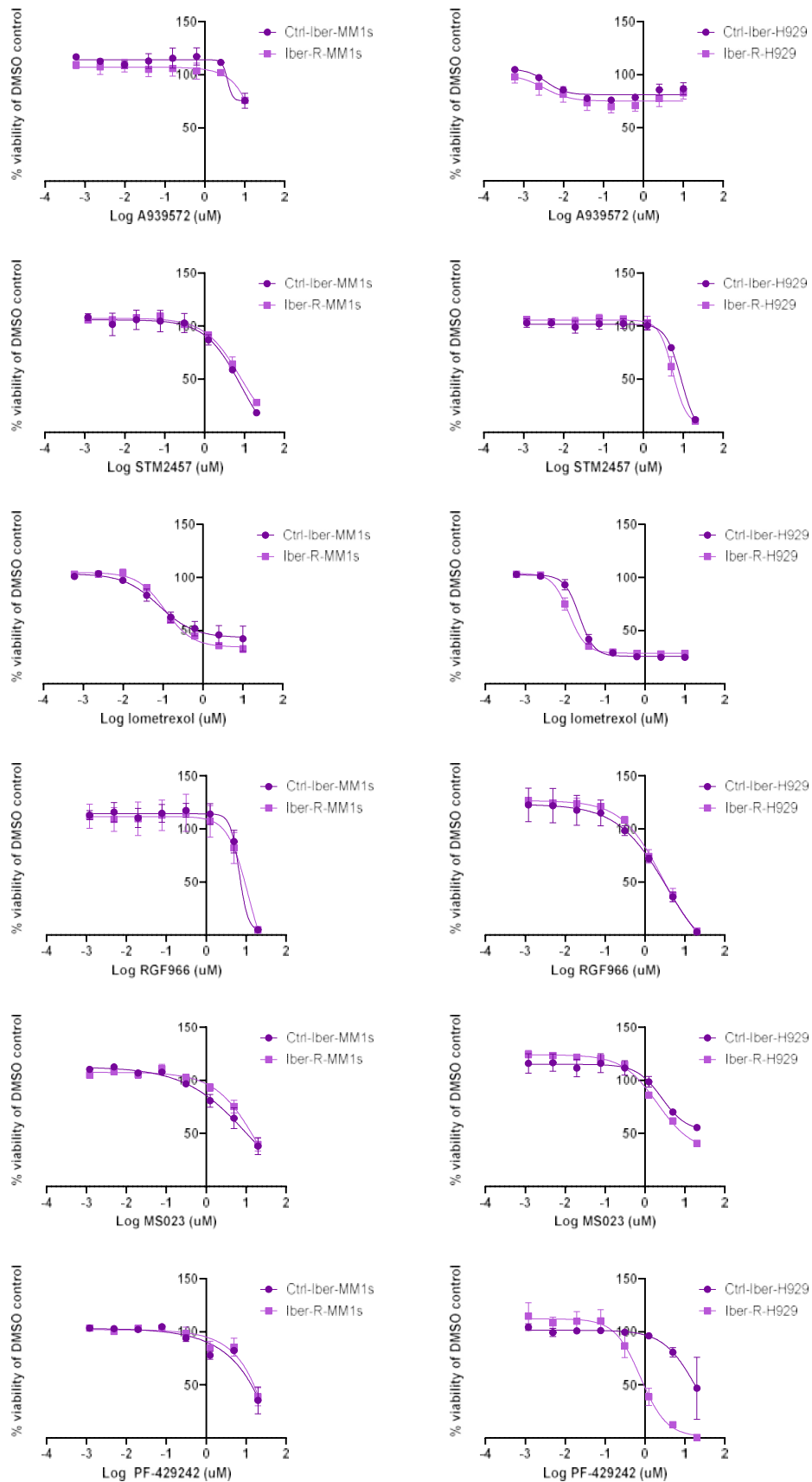


**Figure 5-11** The effect on viability of selected inhibitors in the resistant cell lines.

Iber-R-MM1s and Iber-R-H929 (with their respective controls) were exposed to A939572, STM2457, lometrexol, RGF966, MS023 and PF-429242 in 5-day viability assays (CellTiter-Blue). PF-429242 caused a greater reduction in proliferation in Iber-R-H929 compared to its control. N=2, graphs show mean and SEM.

### 5.3 Discussion

A genome wide knockout CRISPR screen was performed to answer two critical questions: 1) are there one or more genes that when knocked out restore sensitivity to IMiDs/CELMODs? and 2) are there novel vulnerabilities associated with the IMiD/CELMoD-resistant state?

Comparing the relative quantities of each gRNA in the DMSO control arm and the iberdomide arm of the screen allowed me to answer the first question. Guides that were negatively selected for in the iberdomide arm to a greater extent than the DMSO arm suggested a possible re-induction of IMiD/CELMoD sensitivity. The MAGeCKFlute pipeline used this data to calculate a beta score for each gene in each arm of the experiment. APOBEC3D showed the greatest negative selection with iberdomide treatment compared to control, although this difference was small. At the individual guide level there was a small decrease in guide count in the iberdomide arm compared to the control arm. However, this did not translate to re-induction of iberdomide sensitivity in a mixed pool of APOBEC3D-KO-Cas9-Iber-R-MM1s cells. Clonal populations with very low levels of APOBEC3D expression were explored, but unfortunately the results were confounded by cells losing CELMoD resistance because of removal of the selection pressure. Additional potential target genes from this analysis were not explored as they had an even smaller difference in negative selection between the iberdomide and DMSO arms than APOBEC3D and so the likelihood of their validation appeared low.

A possible mechanism of *APOBEC3D* knockout leading to restoration of IMiD/CELMoD sensitivity is difficult to hypothesise. The Apolipoprotein B mRNA-Editing Enzyme Catalytic Polypeptides (APOBECs) form a large family of cytosine deaminases involved in innate and adaptive immunity (171). However, the APOBEC3s can also deaminate the host genome and generate oncogenic mutations with specific signatures. These mutational signatures are some of the most common in cancer and are observed in many different tumour types (171). APOBEC3 mutations are important for initial tumour formation but also may occur during tumour evolution and lead to sub-clonal mutations and tumour heterogeneity which can promote drug resistance (171). Whilst APOBEC3s are closely linked to drug resistance, and inhibiting APOBEC3s could potentially

reduce the occurrence of resistance, it is difficult to understand how knockout could reverse pre-existing resistance.

Next, I wanted to consider novel vulnerabilities in the IMiD/CELMoD-resistant state. The DMSO arm of the screen allowed me to look at the effect on fitness of knockout of each individual gene. Using the Chronos algorithm gene effect scores were calculated for Iber-R-MM1s and compared to parental MM1s using publicly available data. This allowed the identification of potential novel vulnerabilities in the resistant setting. The analysis highlighted 47 genes, some of which were involved in common pathways, such as mitochondrial gene expression, folate pathways (including one-carbon metabolism) and metabolic pathways. These pathways are interesting for further exploration.

In comparison to the drug screen performed in Chapter 4, the CRISPR screen allowed me to identify a broader range of targets. For example, all of the compounds tested in this chapter were not present in the compound library. However, a limitation of this approach was that the MM1s parental gene effect scores came from publicly available CRISPR screens. To make a more direct comparison, it might have been better to carry out the screen in Ctrl-Iber-MM1s in exactly the same way as Iber-R-MM1s, and then compare the Chronos results for the two cell lines. However, the time and costs involved in CRISPR screening meant this was not feasible. It would also be interesting to perform the screen in an IMiD/CELMoD-resistant H929 cell line, but despite attempts it was not possible to express Cas9 in the H929 lines.

*SCD* and *MBTPS1* knockout appeared to be novel vulnerabilities in the IMiD/CELMoD-resistant setting and whole proteome analysis of the resistant lines, discussed in Chapter 3, highlighted enrichment of the SREBP pathway (on analysis of proteins with reduced expression). SREBP transcription factors are cleaved and activated by MBTPS1 and SREBP is a key controller of SCD expression (172). Therefore, it is possible that changes in lipid metabolism in the resistant lines lead to novel vulnerabilities that can then be targeted. The MBTPS1 inhibitor PF-429242 reduced viability more in the Iber-R-H929 cell line than its control, but this effect was not seen in MM1s. Treatment with the SCD inhibitor A939572 did not lead to a reduction in viability in either the control or resistant lines, which might be related to its cellular uptake or efficacy. Overall,

this data provided a strong rationale for exploring lipid metabolism changes in the resistant setting further, as these alterations could be targetable and potentially provide treatment options for resistant patients. This will be explored in Chapter 7.

## Chapter 6 SETD2 Inhibition in IMiD/CElMoD Resistance

### 6.1 Introduction

A potential new dependency in the IMiD/CElMoD-resistant setting was SETD2 (as shown in Chapter 5, Section 5.2.3). This is of particular interest because SETD2 inhibitors are currently being explored in early phase clinical trials in haematological malignancies (173).

SETD2 is a histone methyltransferase and is the only enzyme known to be capable of trimethylation of histone 3 lysine 36 (H3K36) (**Figure 6-1**). SETD2 can also methylate non-histone proteins such as  $\alpha$ -tubulin (trimethylation of which promotes proper chromosome segregation), actin, STAT1 (Signal Transducer And Activator Of Transcription 1) and the catalytic unit of the Polycomb Complex (174). SETD2 is important in transcriptional regulation, RNA splicing, DNA damage repair and B cell development and differentiation (173).



*Figure 6-1 The function of SETD2.*

SETD2 and NSD2/MMSET (Multiple Myeloma SET Domain Containing Protein) are both H3K36 methyltransferases but SETD2 is the only known enzyme capable of generating H3K36me<sub>3</sub>. Image created using BioRender.

SETD2 inhibition has been shown to reduce proliferation of myeloma cell lines and Diffuse Large B-cell Lymphoma (DLBCL) cell lines (173). These findings have also been confirmed in cell line derived xenograft models (173). The SETD2 inhibitor EZM0414 is currently being investigated in a phase 1 clinical trial in patients with relapsed/refractory myeloma and DLBCL (NCT05121103). This is expected to be completed in 2024/2025 and is likely to include ~100 participants in total.

Data to date has focussed attention on the t(4;14) subgroup of myeloma patients, as this translocation is a potential biomarker for response to SETD2 inhibition. The t(4;14) translocation is found in ~15% of newly diagnosed myeloma patients (and the H929 cell line) and is associated with high-risk disease. The

translocation leads to over-expression of Fibroblast Growth Factor Receptor 3 (FGFR3) and Multiple Myeloma SET Domain Containing Protein (MMSET or NSD2) (175). The overexpression of MMSET/NSD2 leads to increased dimethylation of H3K36 and dysregulation of gene expression (170). Early data suggests that t(4;14) myeloma cells lines may be more sensitive to SETD2 inhibition than other lines and therefore this could be a good drug candidate for patients with this high-risk genetic background (170). If there was also evidence that IMiD/CELMoD-resistant patients may be sensitive this would open up a second target population. Given this context, pharmacological inhibition of SETD2 in the acquired IMiD/CELMoD-resistant setting was explored.

## 6.2 Results

### 6.2.1 SETD2 expression in the IMiD/CELMoD resistant cell lines

The CRISPR screen highlighted knockout of *SETD2* as a potential novel vulnerability in the resistant setting (Section 5.2.3). In order to explore this further, other data sets that had been generated during the work presented in this thesis were examined. There was no difference in the abundance of SETD2 in the resistant lines compared to control on proteomic analysis (Section 3.2.4) (**Figure 6-2**).

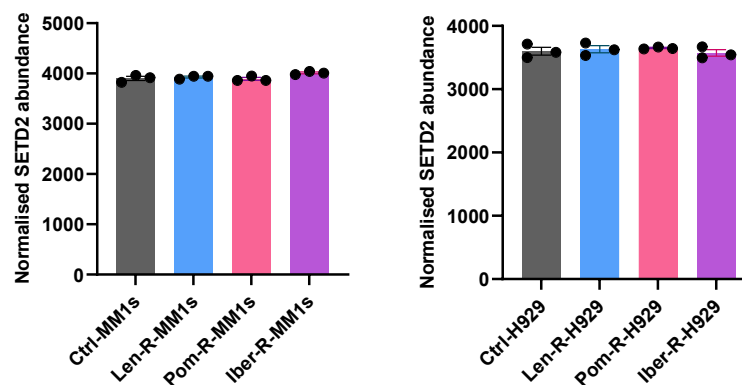


*Figure 6-2 The abundance of SETD2 in the resistant cell lines.*

There was no difference in the normalised abundance of SETD2 in the control and resistant lines (assessed by limma t-test in Phantasus (132)). N=3, graph shows mean and SEM.

Western blotting showed there was also no difference in the global baseline levels of H3K36me2 or H3K36me3 (**Figure 6-3**).

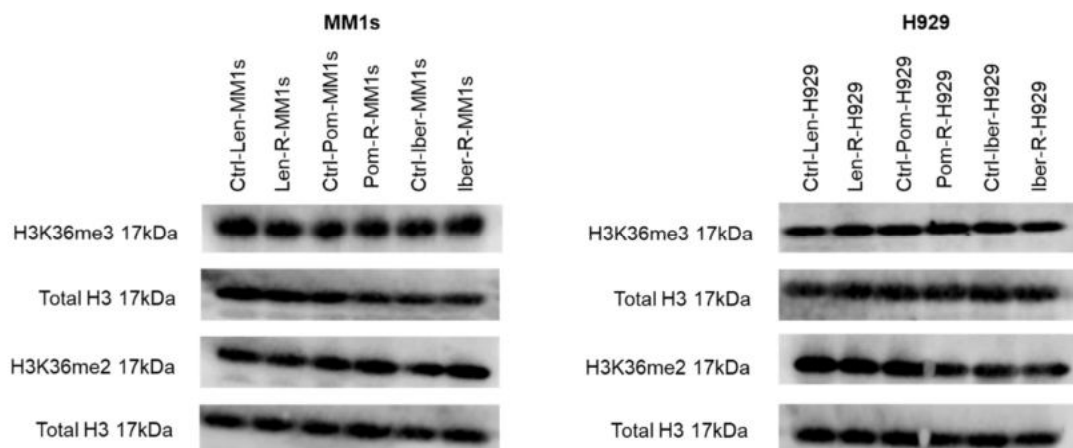


*Figure 6-3 Baseline expression of H3K36me3 and H3K36me2 in the resistant cell lines.*

There was no difference in the baseline expression of H3K36me3 or H3K36me2 in the control and resistant cell lines. This is a representative blot, n=2.

## 6.2.2 The effect of SETD2 inhibitors in the IMiD/CELMoD-resistant cell lines

Two SETD2 inhibitors, EPZ-719 and EZM0414, were explored in the resistant cell lines (**Figure 6-4**). As these drugs are epigenetic modulators, 14-day cell growth assays were performed, in keeping with assays described in the literature (173). Initial work was performed using EPZ-719 as the clinical compound EZM0414 was not commercially available at the time this work was commenced. However, key experiments were later confirmed with EZM0414. EZM0414 has an improved absorption, distribution, metabolism, excretion and toxicity (ADMET) profile compared to earlier chemical leads (176).

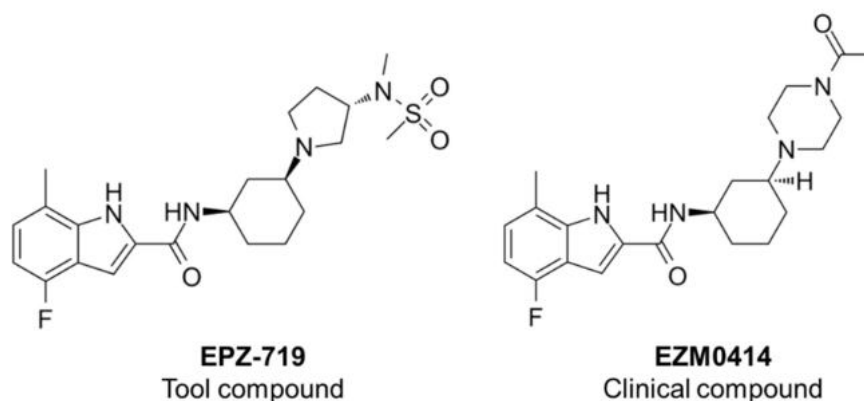


*Figure 6-4 The chemical structures of EPZ-719 and EZM0414.*

EPZ-719 (**Figure 6-5, Figure 6-6**) and EZM0414 (**Figure 6-7**) reduced viability to a greater extent in the resistant MM1s and H929 cell lines compared to controls (with Ctrl-Iber-MM1s or Ctrl-Iber-H929 respectively being used as the control line in all experiments given the scale of the experimental workload). The differential effect of EPZ-719 was particularly pronounced in Pom-R-H929 and Iber-R-H929. The effect of both compounds was concentration dependent.



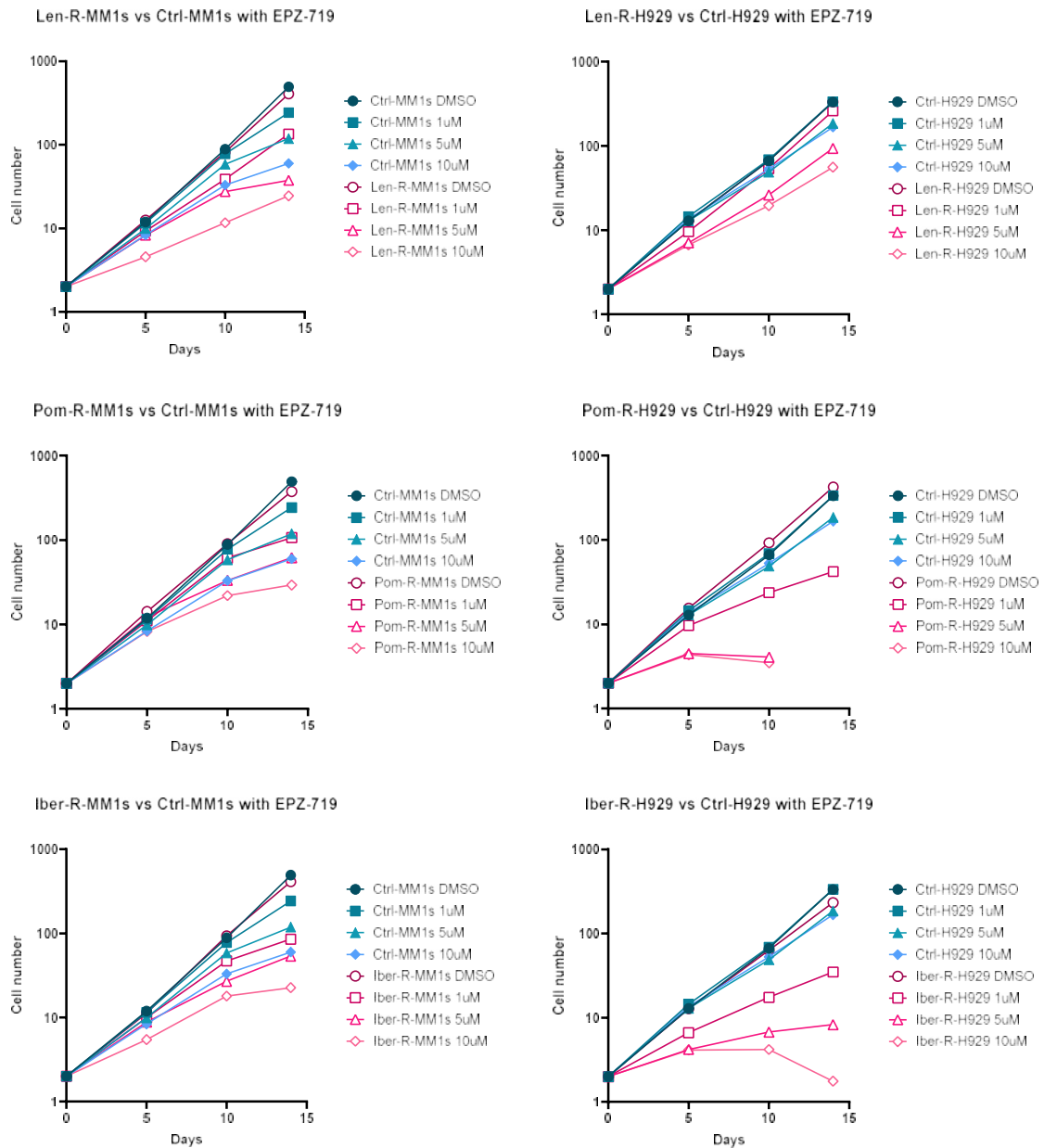
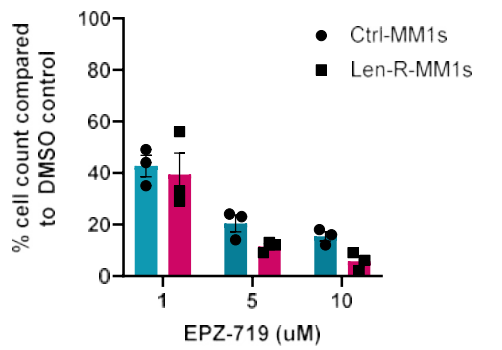
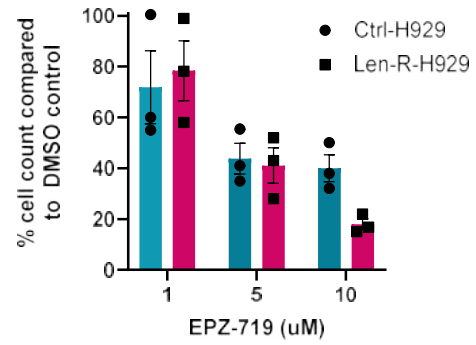


**Figure 6-5 Representative 14-day cell growth assays with EPZ-719 treatment.**

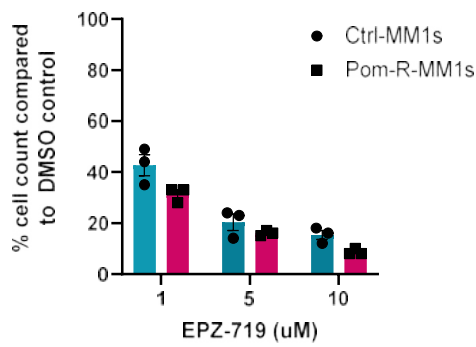
Graphs show the differential effect of EPZ-719 on cell proliferation in control and resistant cell lines. Cells were manually counted (Trypan-Blue exclusion assay) and split at day 5 and day 10. EPZ-719 was used at 1, 5 and 10 μM with a DMSO control matching the highest concentration. The method for cell number calculation is described in Method Section 2.5.



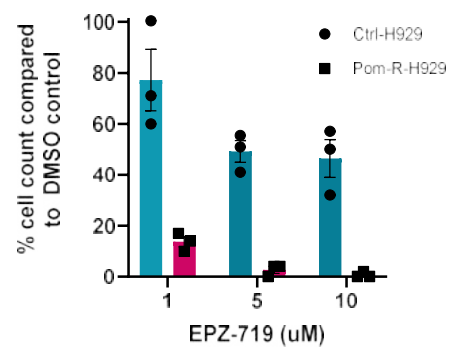
Source of Variation	% of total variation	P value
Concentration x Cell line	0.8861	0.8186
Concentration	77.65	<0.0001
Cell line	5.902	0.1479



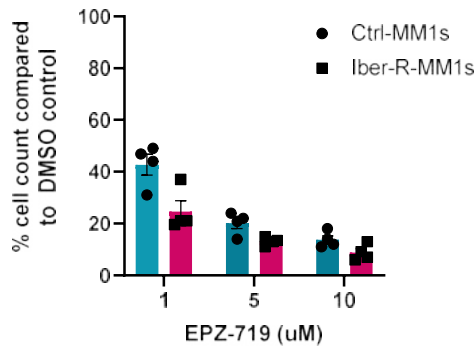
Source of Variation	% of total variation	P value
Concentration x Cell line	6.175	0.3443
Concentration	65.24	0.0042
Cell line	1.618	0.4441



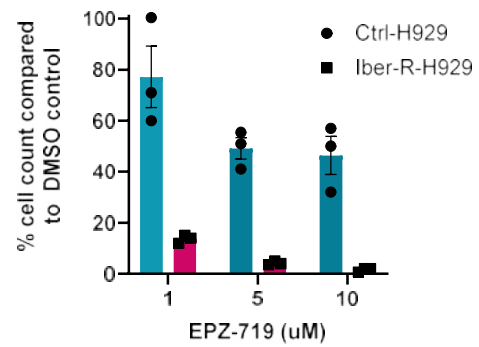
Source of Variation	% of total variation	P value
Concentration x Cell line	1.510	0.4424
Concentration	80.63	<0.0001
Cell line	9.880	0.0128



Source of Variation	% of total variation	P value
Concentration x Cell line	1.963	0.3908
Concentration	11.17	0.0128
Cell line	78.12	<0.0001



Source of Variation	% of total variation	P value
Concentration x Cell line	5.645	0.0673
Concentration	62.26	<0.0001
Cell line	17.22	0.0010



Source of Variation	% of total variation	P value
Concentration x Cell line	2.310	0.2733
Concentration	10.89	0.0255
Cell line	77.99	<0.0001

**Figure 6-6 Day 14 cell counts after exposure to EPZ-719.**

Day 14 cell counts for each resistant line (and control) with EPZ-719 treatment at 3 concentrations (1, 5 and 10 $\mu$ M) are shown. Individual points represent independent experiments (n=3), the bar represents the mean and error bars show SEM. A two-way ANOVA (with matching of replicates) was performed.

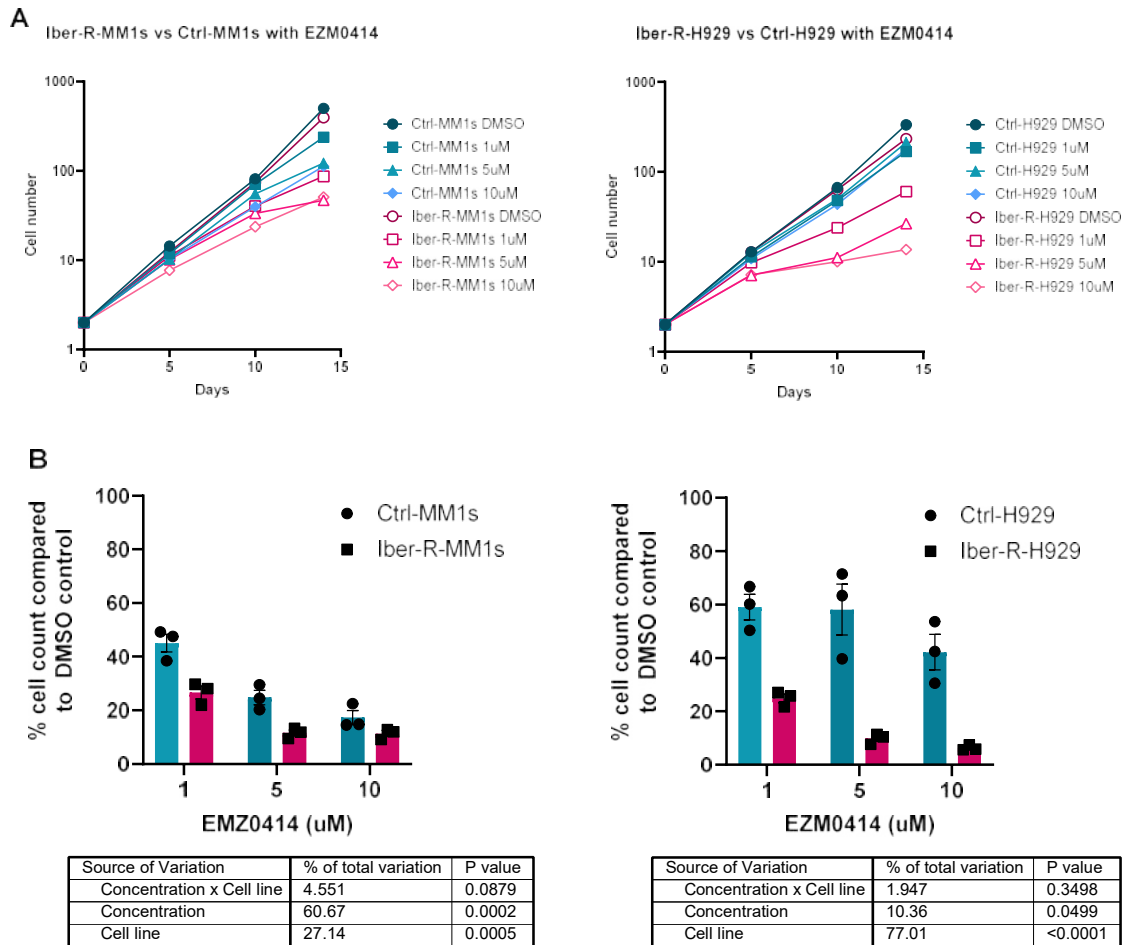


**Figure 6-7 Response of the resistant cell lines to EZM0414 treatment.**

A) Representative 14-day cell growth assays with EZM0414 treatment in Iber-R-MM1s and Iber-R-H929 (and their respective controls) show the differential effect of treatment in the IMiD/CElMoD sensitive and resistant settings. B) Day 14 cell counts for each resistant line (and respective control) with EZM0414 at 3 concentrations (1, 5 and 10 $\mu$ M) are shown. Individual points represent independent experiments (n=3), top of bar represents the mean and error bars show SEM. A two-way ANOVA (with matching of replicates) was performed.

As Pom-R-H929 and Iber-R-H929 showed an early reduction in cell proliferation with SETD2 inhibition by day 5, these lines could be explored in a plate-based assay with multiple different concentrations of inhibitor. The two lines showed reduced viability with both EPZ-719 and EZM0414 compared to Ctrl-H929 at day 5 with low concentrations of drug (~0.3 $\mu$ M) (**Figure 6-8**).

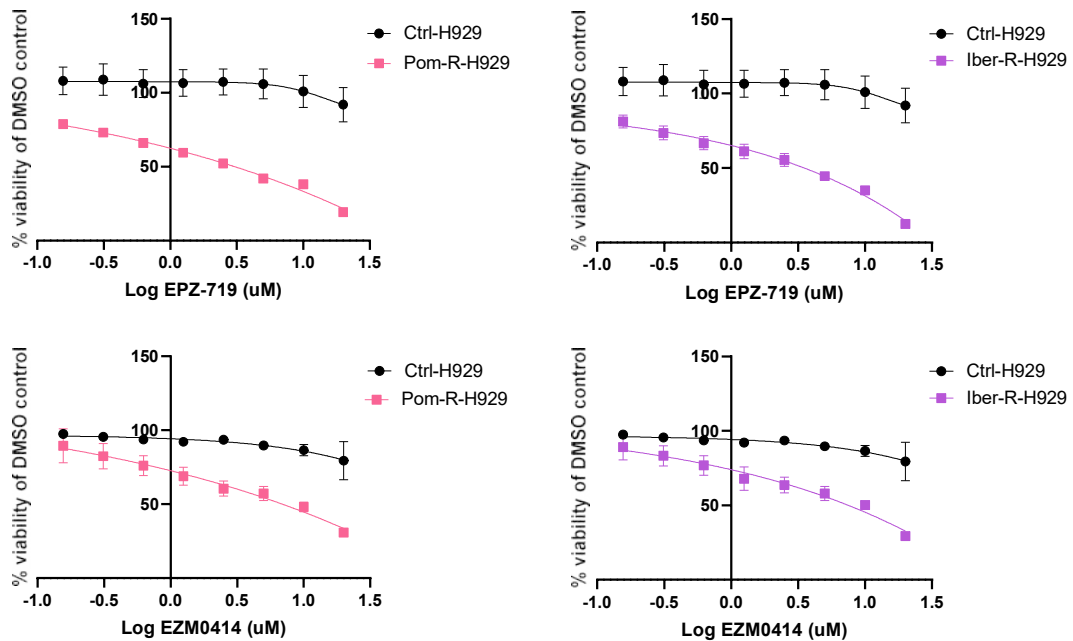


*Figure 6-8 5-day cell viability assays with EPZ-719 and EZM0414 in the resistant cell lines.*

Reduction in cell viability was seen as early as day 5 in Pom-R-H929 and Iber-R-H929 with EPZ-719 and EZM0414 in a CellTiter-Blue assay. Pom-R-H929 and Iber-R-H929 showed a much greater reduction in viability than the control line. Graphs show mean and SEM (n=3). The highest concentration of both compounds was 20µM (with 2-fold dilutions).

### **Combination treatment with EPZ-719 and iberdomide**

The combination of SETD2 inhibition and treatment with iberdomide was then explored as EZM0414 had previously been shown to have synergistic activity with several common myeloma therapies (including dexamethasone, lenalidomide and pomalidomide) in cell line models with t(4:14) (173). Cells were initially treated with DMSO or 3 different concentrations of EPZ-719 (1, 5 and 10µM) for 5 days and then continued to be exposed to the same dose of DMSO/EPZ-719 and varying doses of iberdomide (**Figure 6-9**) for a further 5 days. SynergyFinder (version 3.0) (177) was used to explore the interaction of the two drugs and the ZIP model was employed (178). Synergy describes the combination of two agents producing a combined effect greater than the expected sum of their additive effects (as opposed to antagonism when the combined effect of compounds is less than would be expected) (179). Iberdomide and EPZ-719 are synergistic in Ctrl-Iber-MM1s and are additive, trending towards synergistic, in Ctrl-Iber-H929 (**Figure 6-10**). The mechanism underlying this would be an interesting area for further exploration. EPZ-719 treatment does not restore sensitivity to iberdomide in the resistant lines (in keeping with the MAGeCKFlute analysis of the CRISPR

screen, **Figure 5-3**) and therefore there was no synergy between EPZ-719 and iberdomide in this setting (**Figure 6-10**).

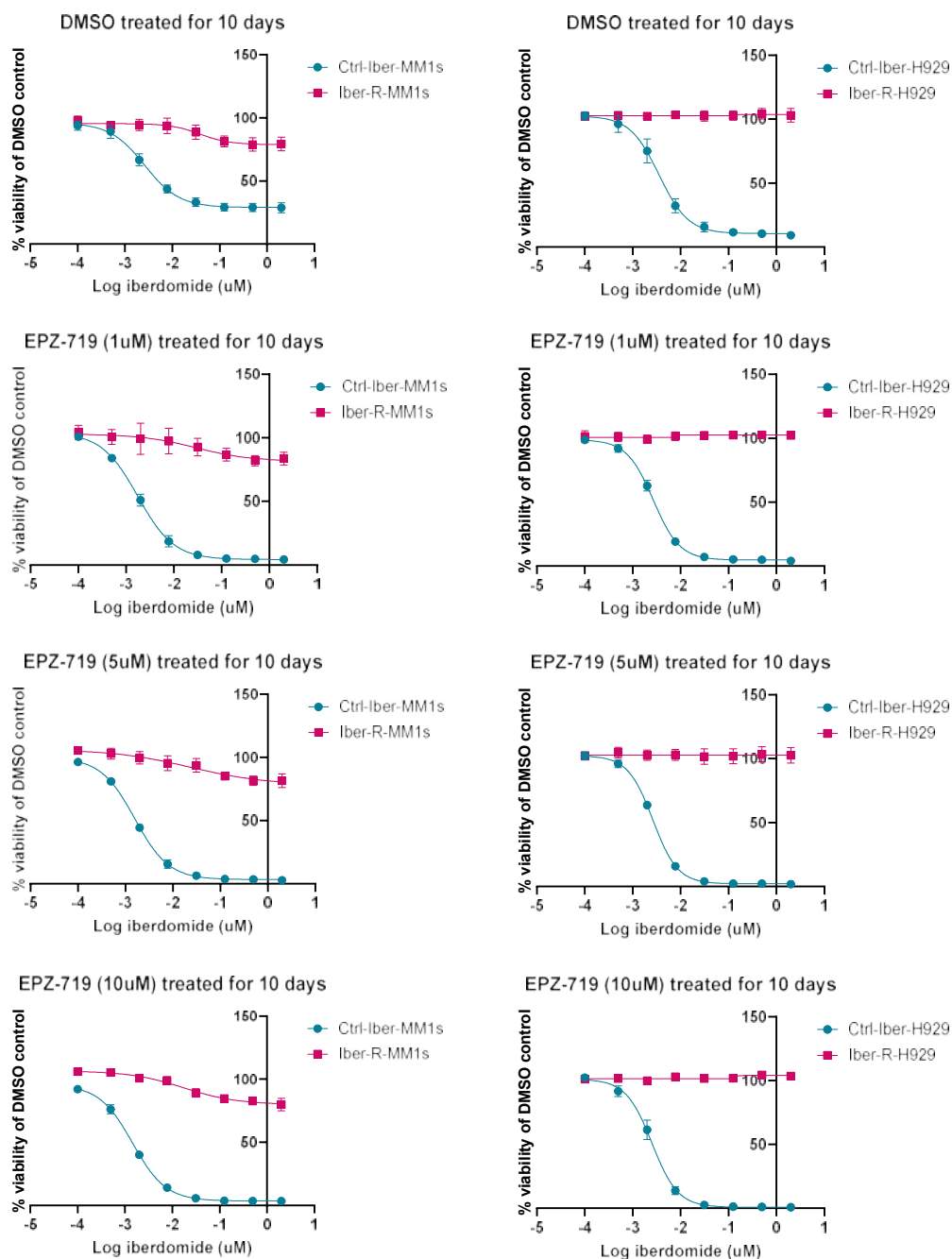


**Figure 6-9** Combination assays with EPZ-719 and iberdomide.

Cells were treated with DMSO or EPZ-719 for 5 days and then cultured with the same concentration of DMSO/EPZ-719 and varying doses of iberdomide in an 8-point EC50 cell viability assay (CellTiter-Blue). Graphs show mean and SEM (n=3). The y-axis shows the % viability of DMSO control for iberdomide treatment for each cell line and therefore the effect of EPZ-719 as a single agent cannot be inferred from these graphs. However, synergy can be observed; the reduction in viability in Ctrl-Iber-MM1s with the highest dose of iberdomide was ~70% in cells treated with DMSO for 10 days but was ~100% in cells treated with 1µM EPZ-719 for 10 days.

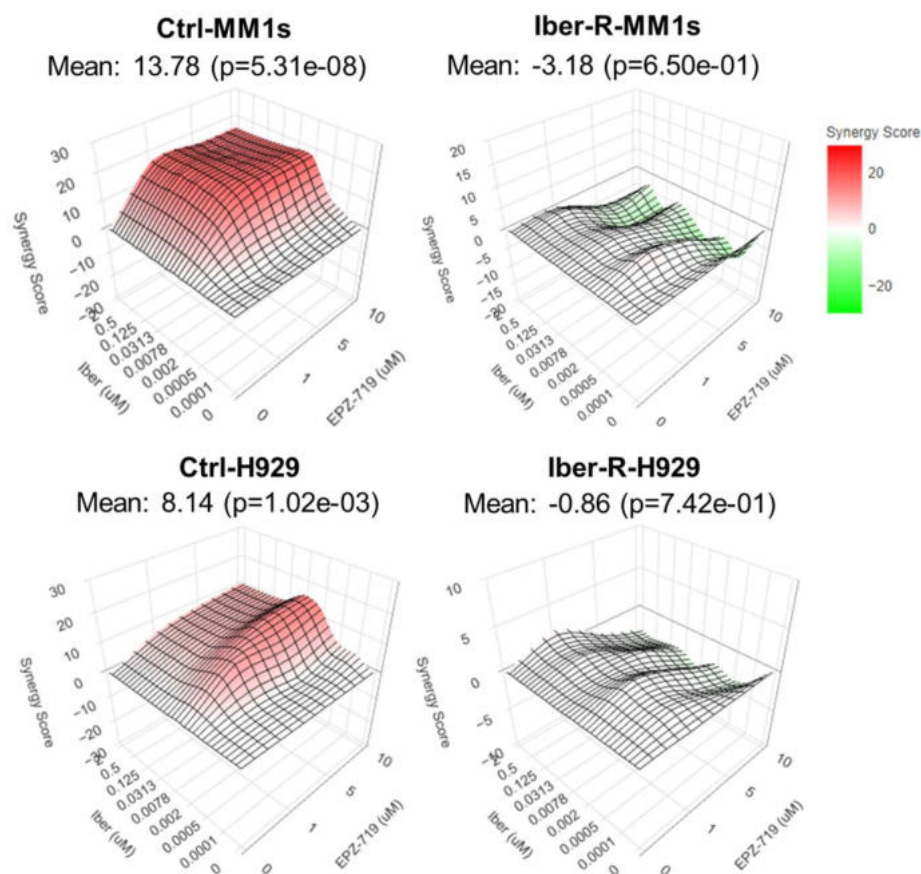


*Figure 6-10 Synergy plots for EPZ-719 and iberdomide.*

Synergy between EPZ-719 and iberdomide in Ctrl-MM1s, Iber-R-MM1s, Ctrl-H929 and Iber-R-H929 was explored using the ZIP model in SynergyFinder (177). A score  $< -10$  indicates the interaction between two drugs is likely to be antagonistic, a score between  $-10$  and  $10$  indicates the interaction is likely to be additive, and a score  $> 10$  indicates the interaction is likely to be synergistic.

### 6.2.3 Paired ChIP-Seq and RNA-Seq analysis

To explore the reasons underpinning greater sensitivity to SETD2 inhibition in the IMiD/CELMoD resistant cell lines compared to their matched control lines, paired ChIP-Seq and RNA-Seq was performed in Iber-R-MM1s and Iber-R-H929 (and their matched control lines Ctrl-Iber-MM1s and Ctrl-Iber-H929).

#### *Preliminary experiments*

The optimal exposure time of cells to EPZ-719 prior to harvesting for ChIP-Seq and RNA-Seq was explored. A concentration of  $1\mu\text{M}$  was used as this was the lowest dose tested in the 14-day cell growth assays. It was important to select a time point at which EPZ-719 could alter the methylation state of H3K36 but at which there was not a significant effect on viability (to ensure the identification of early changes in gene expression directly driven by methylation alteration, rather than downstream changes associated with cell death).

Exposure to 1 $\mu$ M EPZ-719 for 3-5 days caused limited changes in cell viability, except in Iber-R-H929 which did show a slight reduction (**Figure 6-11**). A global change in H3K36me3 was observed after 3 days of drug exposure on western blotting (**Figure 6-12**), confirming EPZ-719 was changing the histone mark at this time point and concentration. Therefore cells were exposed to 1 $\mu$ M of EPZ-719 for 3 days prior to harvesting. The full ChIP-Seq and RNA-Seq experimental methodology can be found in **Methods Section 2.6** and **Supplementary Methods Section 10.3**.

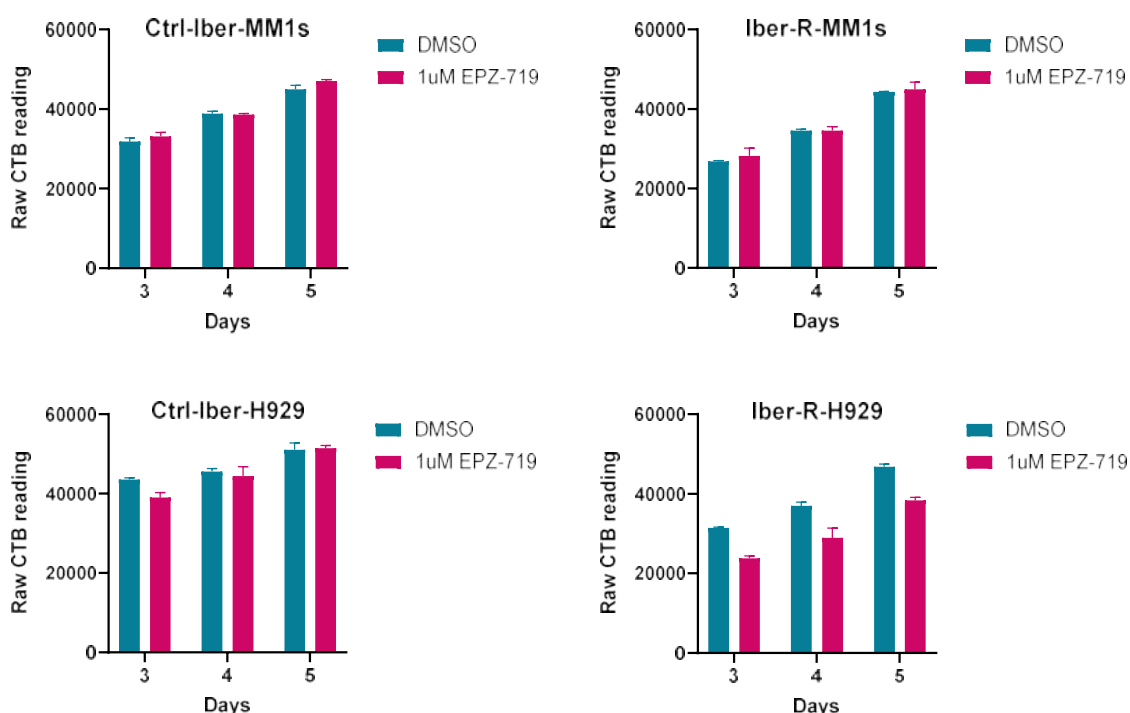


*Figure 6-11 Cell proliferation assays with EPZ-719 at days 3-5.*

The effect of exposure to EPZ-719 for 3-5 days on cell viability was explored in CellTiter-Blue assays. At 3 days there appeared to be a small reduction in viability in Iber-R-H929 with exposure to 1 $\mu$ M of EPZ-719 but no decrease in viability in the other cell lines. Graphs show mean and range of 3 technical triplicates (n=1).



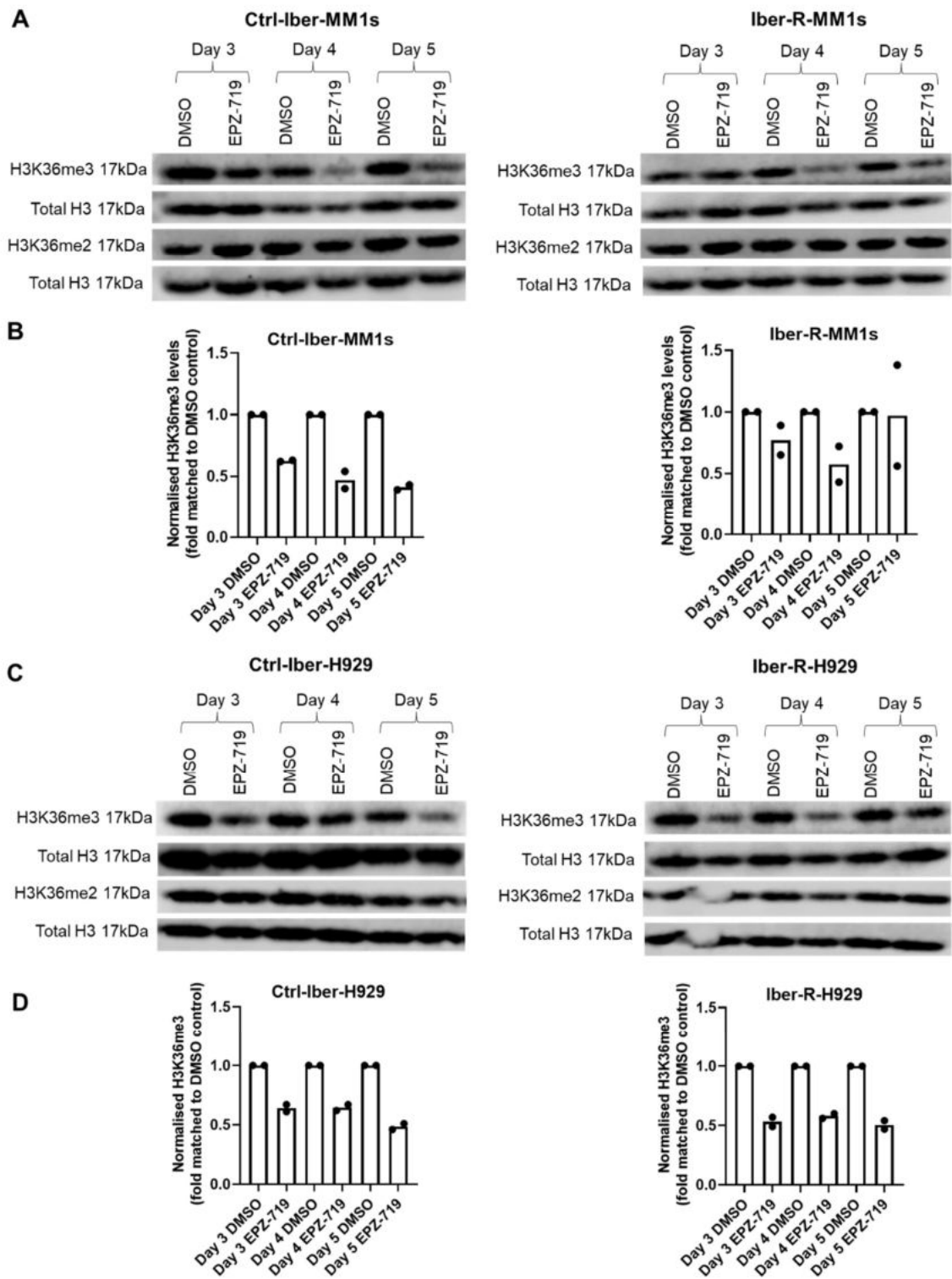


**Figure 6-12 Reduction in H3K36me3 with EPZ-719 treatment.**

Western blots showed a reduction in global H3K36me3 with 1 $\mu$ M EPZ-719 treatment by day 3. A) Representative blots in the MM1s cell lines with B) quantification. C) Representative blots in the H929 cell lines with D) quantification. Graphs show individual experiments, (n=2).

### **RNA-Seq differences at baseline**

Ctrl-Iber-MM1s, Iber-R-MM1s, Ctrl-Iber-H929 and Iber-R-H929 were exposed to 1 $\mu$ M of EPZ-719 or DMSO for 3 days prior to harvesting. The transcriptomes of



each cell line in each condition were then explored. Considering just the DMSO treated samples allowed evaluation of baseline differences in the control and resistant cell lines. In keeping with the previous RNA-Seq analysis discussed in Chapter 3, the resistant lines (compared to control) had a statistically significant decrease in *CRBN* levels (log<sub>2</sub>FC -0.41, adj p<0.001 in Iber-R-MM1s compared to Ctrl-Iber-MM1s and log<sub>2</sub>FC -3.8, adj p<0.001 in Iber-R-H929 compared to Ctrl-Iber-H929), and an increase in *BIRC3* (log<sub>2</sub>FC 0.33, adj p<0.01 in Iber-R-MM1s compared to Ctrl-Iber-MM1s and log<sub>2</sub>FC 1.3, adj p<0.001 in Iber-R-H929 compared to Ctrl-Iber-H929) and *TNFAIP3* (log<sub>2</sub>FC 0.24, adj p<0.01 in Iber-R-MM1s compared to Ctrl-Iber-MM1s and log<sub>2</sub>FC 1.6, adj p<0.001 in Iber-R-H929 compared to Ctrl-Iber-H929).

### ***Transcriptome changes with EPZ-719***

The transcriptome changes in response to EPZ-719 treatment in each cell line were then assessed. The fold changes in the abundance of each transcript with EPZ-719 treatment (compared to DMSO) for Ctrl-Iber-MM1s were plotted on the x-axis and for Iber-R-MM1s were plotted on the y-axis (**Figure 6-14**). The same procedure was also carried out for the H929 lines (**Figure 6-15**). Transcripts that demonstrated altered expression with EPZ-719 treatment (defined as  $\geq 3$  standard deviations from the mean log<sub>2</sub> fold change) might be commonly changed in the IMiD/CELMoD resistant and sensitive setting, potentially indicating the mechanism of SETD2 activity in myeloma (**Figure 6-13**). There may also be transcripts that are differentially changed in the two settings, which might explain why the resistant cell lines were more sensitive to SETD2 inhibition. Venn diagrams were then used to assess the overlap between the MM1s and H929 lines and identify commonly changed transcripts.

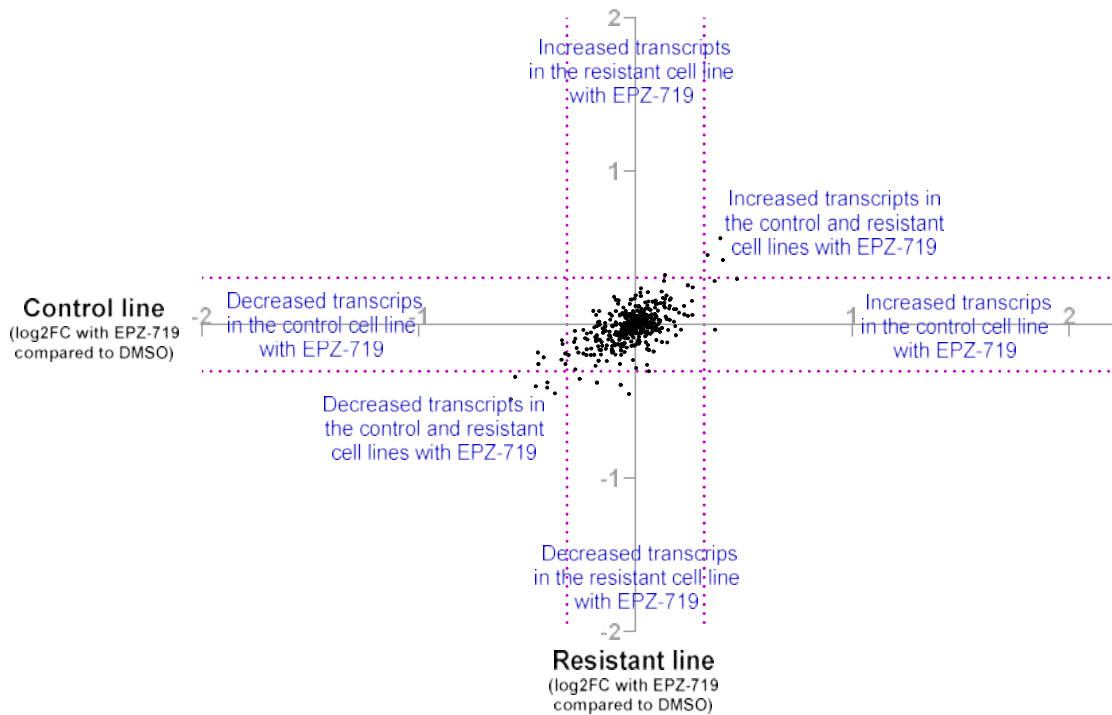


*Figure 6-13 Conceptual scatter plot of RNA-Seq results.*

Transcripts that demonstrated altered expression with EPZ-719 treatment (defined as  $\geq 3$  standard deviations from the mean log<sub>2</sub>FC for all transcripts) could be commonly changed in the IMiD-resistant and IMiD-sensitive setting, potentially indicating the mechanism of SETD2 activity in myeloma. Transcripts could also be changed in either the IMiD-resistant or the IMiD-sensitive setting, which might explain why the resistant cell lines were more sensitive to SETD2 inhibition.

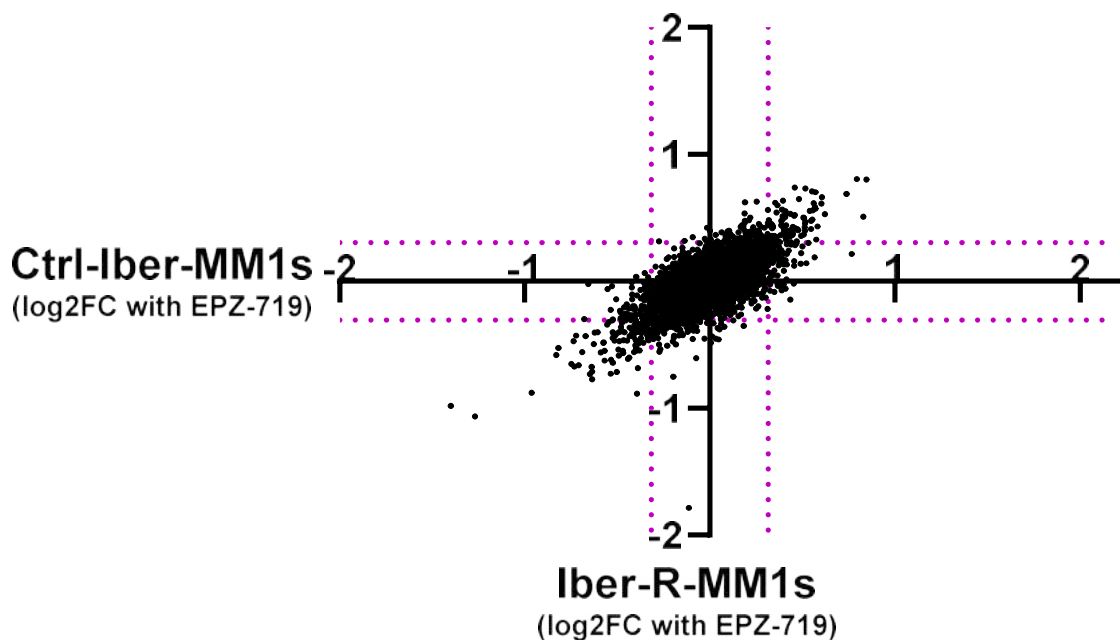


*Figure 6-14 Transcriptome changes with EPZ-719 treatment in Ctrl-Iber-MM1s and Iber-R-MM1s.*

The log<sub>2</sub>FCs in the abundance of each transcript with EPZ-719 treatment (compared to DMSO) in Ctrl-Iber-MM1s were plotted on the x-axis and in Iber-R-MM1s were plotted on the y-axis. Outliers were defined as values  $\geq 3$  standard deviations from the mean log<sub>2</sub>FC for each dataset.

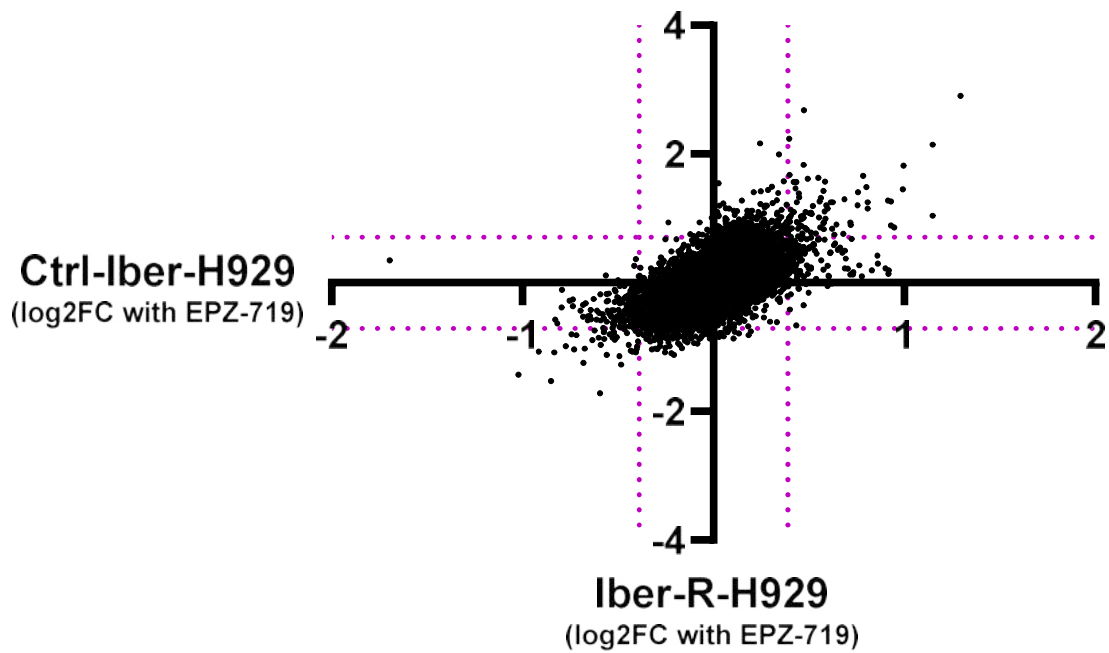


*Figure 6-15 Transcriptome changes with EPZ-719 treatment in Ctrl-Iber-H929 and Iber-R-H929.*

The log<sub>2</sub>FCs in the abundance each transcript with EPZ-719 treatment (compared to DMSO) in Ctrl-Iber-H929 were plotted on the x-axis and in Iber-R-H929 were plotted on the y-axis. Outliers were defined as values  $\geq 3$  standard deviations from the mean log<sub>2</sub>FC for each dataset.

In the MM1s lines (control and resistant) there were 93 commonly increased transcripts and in H929 lines there were 81 commonly increased transcripts. Between these two sets there were 9 common transcripts: *TLR7*, *GPR155*, *GCSAM*, *SCN3A*, *TRANK1*, *FRMD6*, *GIMAP8*, *SORL1* and *SATB1*. In the MM1s lines (control and resistant) there were 117 commonly decreased transcripts and in H929 lines there were 44 commonly decreased transcripts. Between these two sets there were 5 common transcripts: *CD68*, *GPC4*, *NECTIN3*, *ADD2* and *KCNS3*. The full names of these transcripts and a brief description of function can be found in **Supplementary Table 9-6**.

Differential response to EPZ-719 treatment in the IMiD/CELMoD sensitive and resistant settings was divided into 4 categories of transcript: 1) increased in the control lines but not in the resistant lines, 2) decreased in the control lines but not in the resistant lines, 3) increased in the resistant lines but not in the control lines and 4) decreased in the resistant lines but not in the control lines. Transcripts that fell into the same category for both the MM1s and H929 cell line pairs are shown in **Table 6-1**.

Category	Transcripts
Increased in the control lines only	<i>SOGA1, TASL</i>
Decreased in the control lines only	N/A
Increased in the resistant lines only	<i>CTSF, DDX60L, VWA5A, LOC645261, DNAH1, THBS3, SLC4A5, DDX60, ARHGAP6</i>
Decreased in the resistant lines only	<i>EMP2, NCAM1, TMSB15A</i>

**Table 6-1 Differentially altered transcripts with EPZ-719 treatment.**

Fourteen transcripts were differentially expressed after EPZ-719 treatment in the same manner in both the MM1s and H929 cell line pairs. Increased/decreased was defined as  $\geq 3$  standard deviations of the mean log<sub>2</sub>FC for each dataset. See **Supplementary Table 9-6** for full names and a brief description of function.

The changes in expression of transcripts that were commonly or differentially altered with EPZ-719 treatment in the same manner in both the MM1s and H929 cell line pairs are shown in the form of a heat map, **Figure 6-16**.

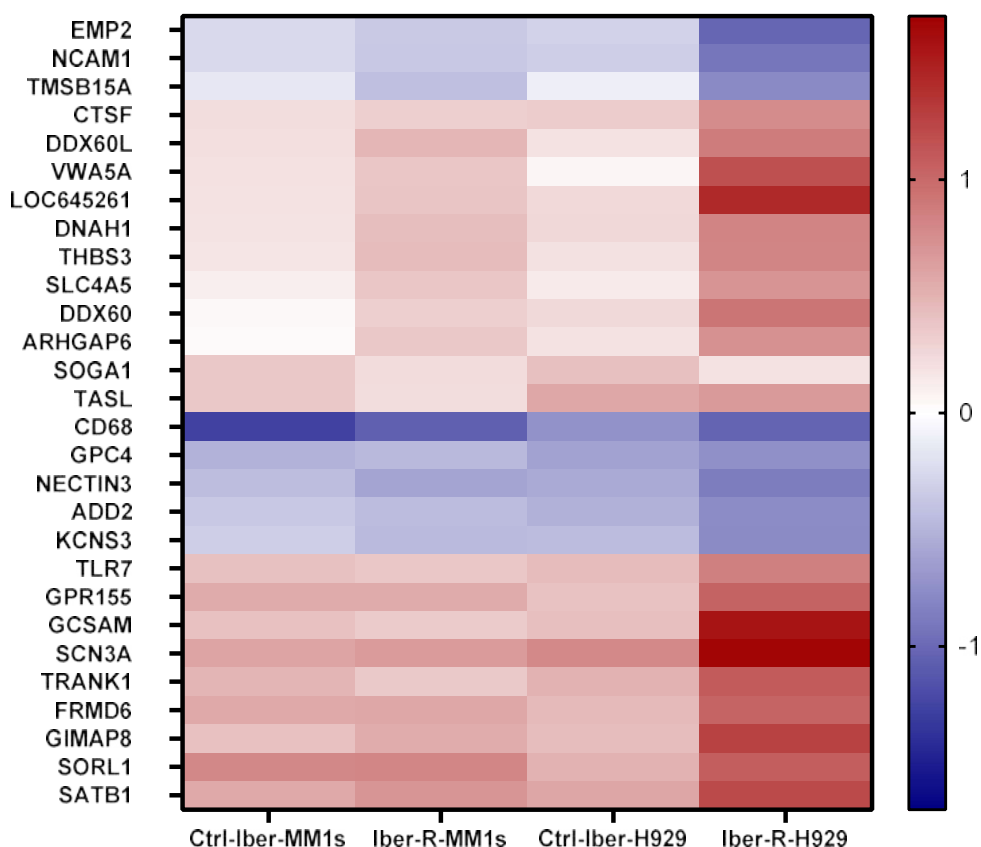


**Figure 6-16 Heat map showing transcripts altered with EPZ-719 treatment.**

Heat map showing transcripts altered with EPZ-719 treatment (with a log<sub>2</sub>FC  $\geq 3$  standard deviations from the mean for the dataset) in the same manner for both the MM1s and H929 cell line pairs (e.g. *EMP2* mRNA levels are decreased in the CELMoD-resistant line but not the CELMoD-sensitive control line for both the MM1s and H929 pairs). The log<sub>2</sub>FC after EPZ-719 treatment is plotted, with red indicating increased expression and blue indicating decreased expression.

As H3K36me3 is normally an activating mark, EPZ-719 treatment would be expected to decrease transcript levels. As the resistant cell lines are more

sensitive to the compound than the sensitive cell lines, transcripts that are decreased more in the resistant lines compared to the control lines could potentially indicate the mechanism of this novel dependency. This included Neural Cell Adhesion Molecule 1 (*NCAM1*)/*CD56*, Epithelial Membrane Protein 2 (*EMP2*) and Thymosin Beta 15A (*TMSB15A*). The expression change of these transcripts in each cell line was assessed individually (**Table 6-2, Figure 6-17**).

Cell line	Value	NCAM1/CD56	EMP2	TMSB15A
Ctrl-Iber-MM1s	Base mean	115	797	301
	Log2FC	-0.257	-0.259	-0.166
	adj p value	0.125	0.00397	0.257
Iber-R-MM1s	Base mean	105	1012	360
	Log2FC	-0.370	-0.365	-0.427
	adj p value	0.0615	0.00165	0.00119
Ctrl-Iber-H929	Base mean	3516	455	404
	Log2FC	-0.332	-0.304	-0.119
	adj p value	2.82E-07	0.0116	0.515
Iber-R-H929	Base mean	2149	260	171
	Log2FC	-0.914	-1.02	-0.782
	adj p value	1.74E-27	5.12E-13	3.46E-06

*Table 6-2 Transcript changes after EPZ-719 treatment in the individual cell lines.*

Transcript changes after EPZ-719 treatment (compared to DMSO control) in each of the 4 cell lines is shown with base mean, log2FC and adjusted p value.

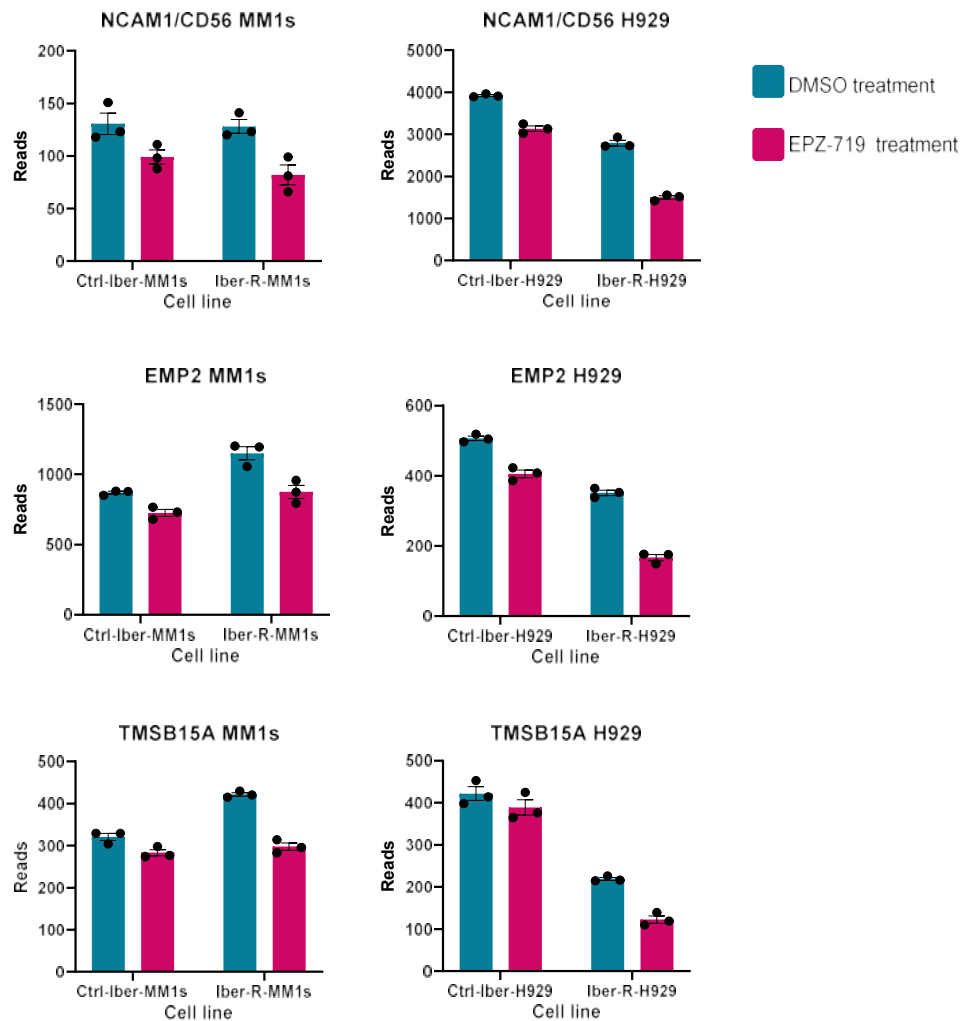


*Figure 6-17 Differentially decreased transcripts after EPZ-719 treatment in the resistant cell lines.*

Raw counts generated by ht-seq software (the number of reads aligned to each gene) were plotted. The individual points represent independent biological replicates, the bar represents the mean and error bars represent SEM.

NCAM1/CD56 is a cell adhesion molecule involved in cell-to-cell interactions as well as cell-matrix interactions. It is present at variable levels in about 70% of myeloma patients and a higher percentage of CD56-expressing cells correlates with inferior clinical outcomes (180). The functional role of NCAM1/CD56 is poorly understood but overexpression promotes myeloma cell line growth and viability, and silencing has the opposite effect, with reduced growth and apoptotic cell death (180). This suggests that the mechanism of reduced cell growth with SETD2 inhibition could be reduction of NCAM1/CD56, and this effect is more pronounced in the resistant lines. EMP2 regulates cell membrane composition and has been associated with several functions including endocytosis, cell signalling, cell proliferation, cell migration, cell adhesion, cell death, cholesterol homeostasis, urinary albumin excretion and embryo implantation (143). EMP2

has been proposed as a therapeutic target in a number of cancers including endometrial (173), breast (174) and glioblastoma (175). TMSB15A plays a role in organisation of the cytoskeleton (147) and very little is known about its role in the context of myeloma or other malignancies.

### ***ChIP-Seq results***

A complementary ChIP-Seq experiment was performed to evaluate the effect of EPZ-719 treatment at sites of H3K36me3 binding throughout the genome. The raw data was analysed with a ChIP-Seq pipeline built using Nextflow from the Institut Curie NGS/Bioinformatics core facility (<https://github.com/bioinfo-pf-curie/ChIP-seq>) (**see Methods Section 2.6.2**).

Initially density binding plots were used to provide an overview of the results. These plots compared the concentration of H3K36me3 binding at sites throughout the genome between pairs of conditions. The baseline pattern of H3K36me3 binding in Ctrl-Iber-MM1s and Iber-R-MM1s showed there were sites where decreased binding in the Iber-R-MM1s line (**Figure 6-18 A**). In contrast, the H3K36me3 binding pattern was similar between Ctrl-Iber-H929 and Iber-R-H929 (**Figure 6-18 B**). All four of the cell lines showed a broad reduction in H3K36me3 binding when treated with EPZ-719 but Iber-R-MM1s also showed a smaller group with increased binding (**Figure 6-18 C-F**). Overall, this data showed that EPZ-719 reduced H3K36me3 binding across several thousand sites rather than a few selected sites.

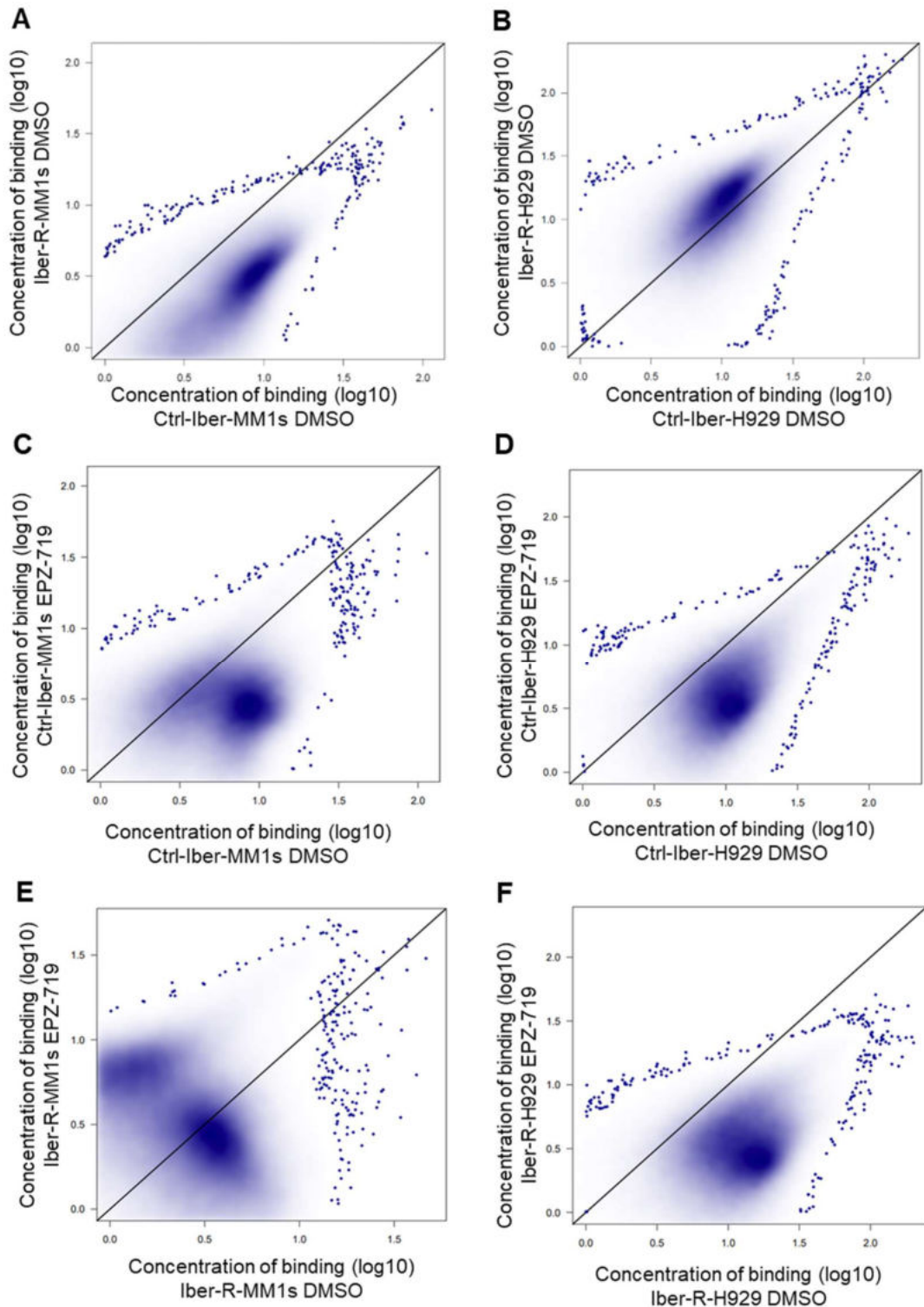


*Figure 6-18 Density binding plots showing concentration of H3K36me3 binding at each site in different pair wise comparisons.*

This is a smoothed plot, so instead of plotting each individual point (concentration of H3K36me3 binding at each site), darker blue is used to show that there are a lot of points in that area and lighter areas have few or no points. The axes show concentration of binding (the average number of reads for that binding site) for the two conditions. A) Comparison of the baseline pattern of H3K36me3 binding in Ctrl-Iber-MM1s and Iber-R-MM1s. B) Comparison of the baseline pattern of H3K36me3 binding in Ctrl-Iber-H929 and Iber-R-H929. C-F) All four of the cell lines showed a reduction in H3K36me3 binding when treated with EPZ-719.



The relative distribution of the H3K36me3 mark in distinct genic and intergenic regions was then examined in each condition. At baseline, the H3K36me3 mark was distributed very similarly in all four lines (**Figure 6-19**). After treatment with EPZ-719 the relative distributions were shifted in the same manner in all the lines, with a reduced proportion of binding in the promoter, 5' UTR, 3' UTR, 1<sup>st</sup> exon and other exons (**Figure 6-19**).

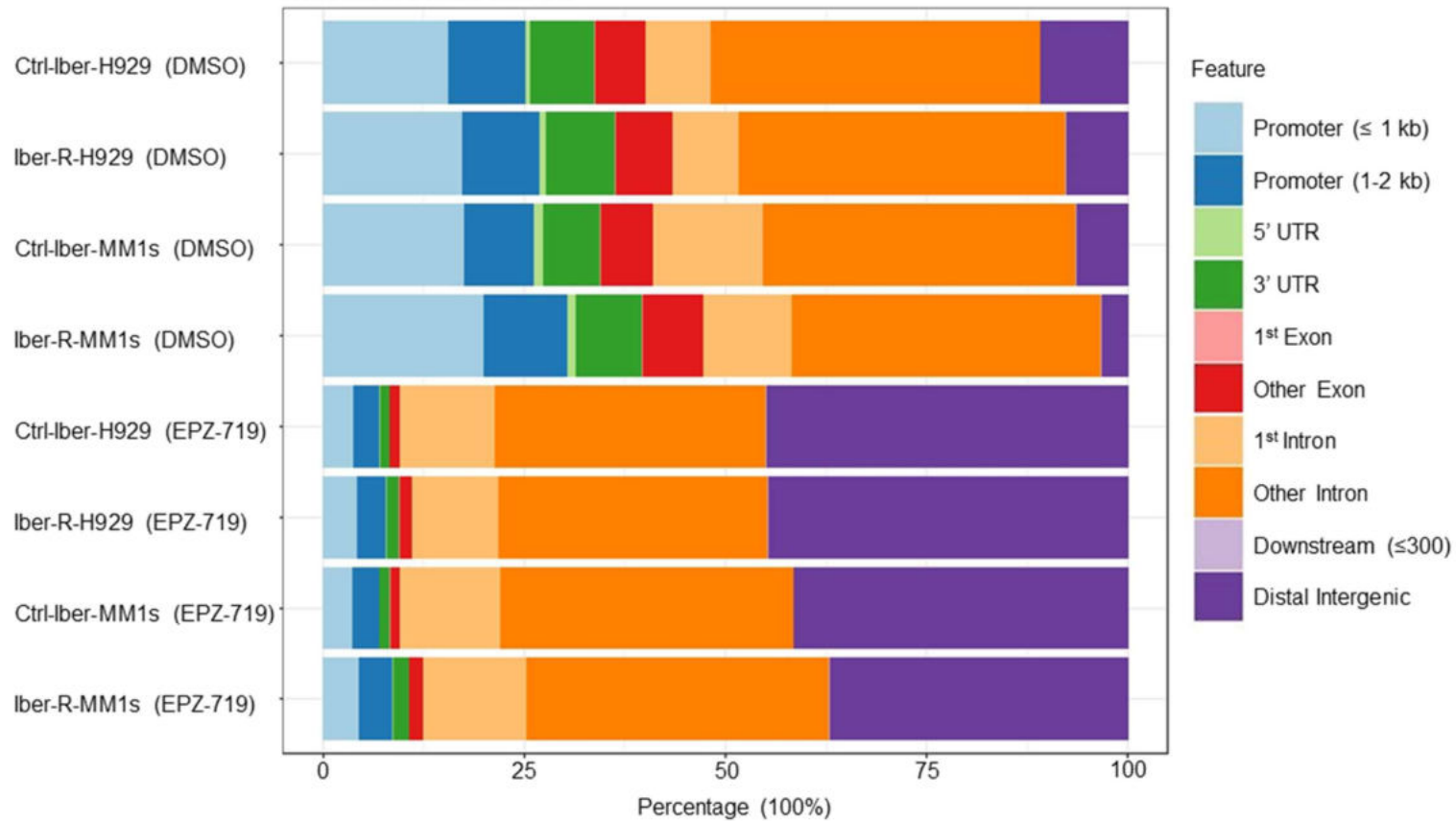
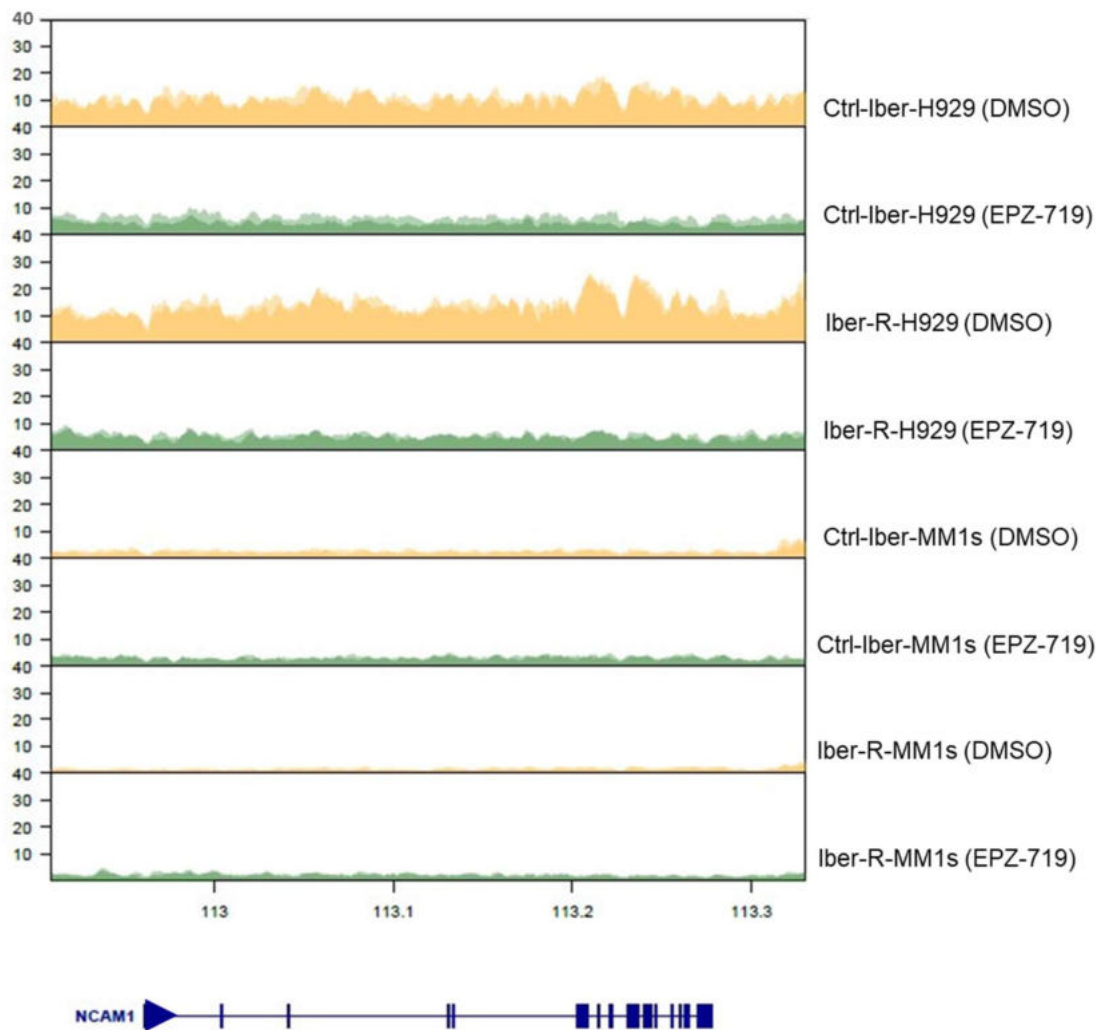


Figure 6-19 Bar chart showing the distribution of H3K36me3 binding across different genomic features in each condition.

Stacked bar chart showing the distribution of H3K36me3 binding in each cell line/treatment condition across different genomic features, coloured according to the key provided.

The RNA-Seq analysis had identified three transcripts that were reduced to a greater extent in the resistant lines compared to the control lines after EPZ-719 treatment: *NCAM1/CD56*, *EMP2* and *TMSB15A*. The H3K36me3 binding tracks for the genomic regions encoding *NCAM1/CD56*, *EMP2* and *TMSB15A* were therefore explored. In Ctrl-Iber-H929 and Iber-R-H929, *NCAM1/CD56* had H3K36me3 binding peaks throughout the gene that were reduced globally with EPZ-719 treatment (**Figure 6-20**). There was less H3K36me3 binding at baseline in the MM1s cell lines and no clear reduction in binding with EPZ-719 treatment (**Figure 6-20**).



**Figure 6-20** *NCAM1/CD56* H3K36me3 binding tracks.

Tracks show H3K36me3 ChIP-Seq read densities at genomic regions covering *NCAM/CD56* (chromosome 11). The x-axis denotes genomic position (megabases), and the y-axis shows coverage values (normalised to spike-in control and total input control). The Ctrl-Iber-H929 and Iber-R-H929 tracks show globally reduced H3K36me3 binding after EPZ-719 treatment. There was less H3K36me3 binding at baseline in the MM1s cell lines and no clear reduction in binding after EPZ-719 treatment. Tracks for the 2 technical replicates of each cell line/treatment condition are overlaid.

*EMP2* had H3K36me3 binding peaks throughout the gene in all four cell lines that were then globally reduced with EPZ-719 treatment (**Figure 6-21**).

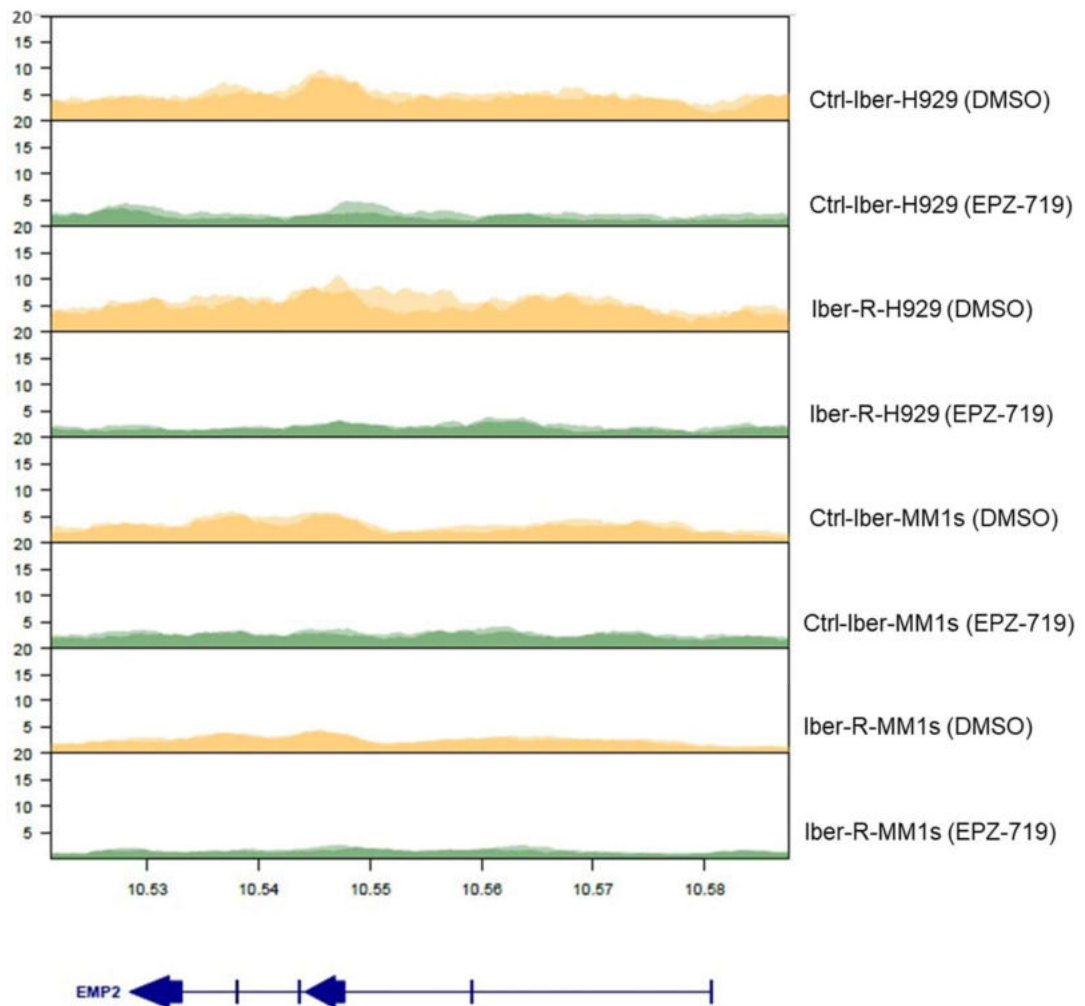


*Figure 6-21 EMP2 H3K36me3 binding tracks.*

Tracks show H3K36me3 ChIP-Seq read densities at genomic regions covering *EMP2* (chromosome 16). The x-axis denotes genomic position (megabases), and the y-axis shows coverage values (normalised to spike-in control and total input control). EPZ-719 treatment reduced H3K36me3 binding throughout *EMP2* in all four cell lines. Tracks for the 2 technical replicates of each cell line/treatment condition are overlaid.

*TMSB15A* had low levels of H3K36me3 binding in all of the cell lines that were reduced further with EPZ-719 treatment (**Figure 6-22**).

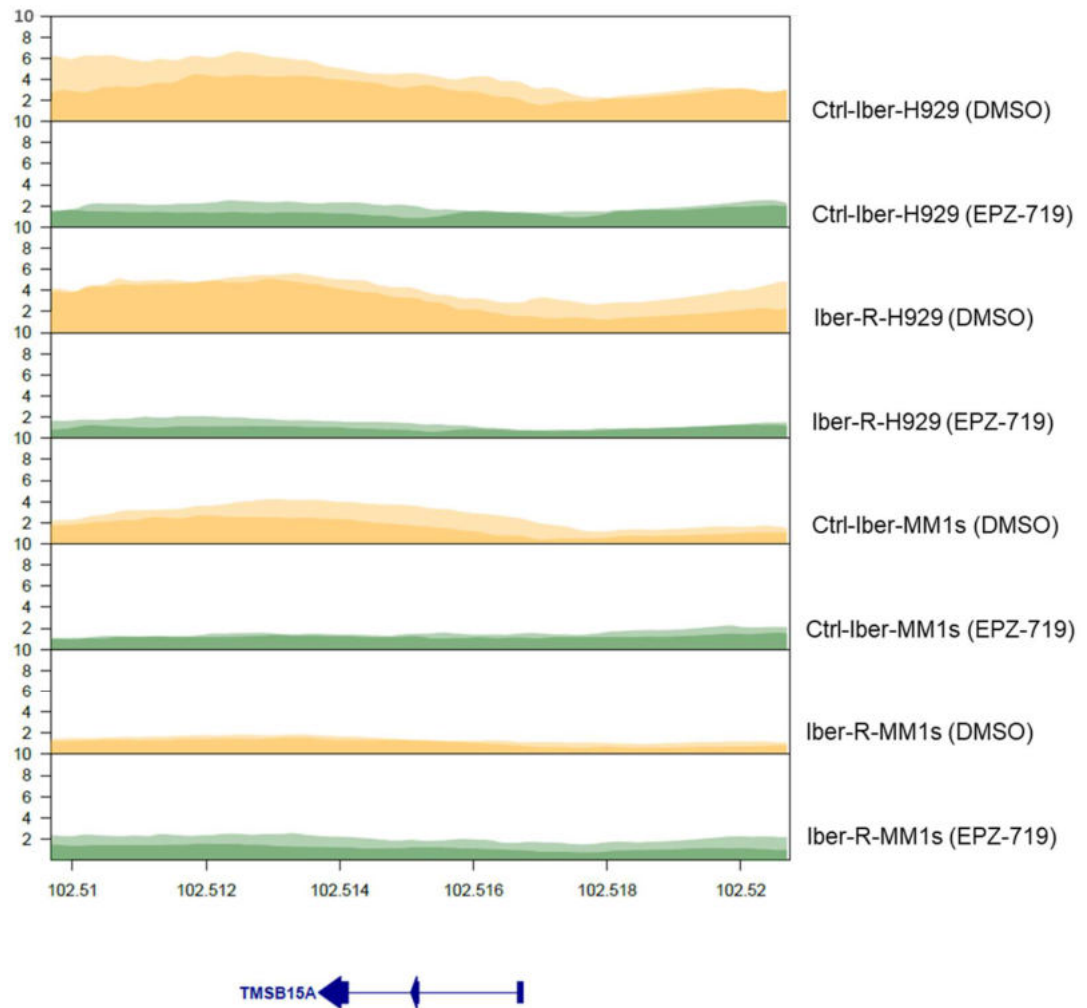


*Figure 6-22 TMSB15A H3K36me3 binding tracks.*

Tracks show H3K36me3 ChIP-Seq read densities at genomic regions covering *TMSB15A* (X chromosome). The x-axis denotes genomic position (megabases), and the y-axis shows coverage values (normalised to spike-in control and total input control). *TMSB15A* had low levels of H3K36me3 binding in all four cell lines that were reduced further by EPZ-719 treatment. Tracks for the 2 technical replicates of each cell line/treatment condition are overlaid.

### 6.3 Discussion

Inhibition of SETD2 with EPZ-719 and EZM0414 led to a greater reduction in cell proliferation in the acquired IMiD/CELMoD-resistant cell lines compared to their matched controls in 14-day growth assays. This effect was particularly striking in Pom-R-H929 and Iber-R-H929; in these two cell lines reduction in viability could be seen as early as day 5 with low concentrations of the inhibitors (~0.3 $\mu$ M). Synergy was seen between EPZ-719 and iberdomide in the control lines, in keeping with the literature (173). However, the IMiD/CELMoD-resistant cell lines instead demonstrated a novel vulnerability to single agent SETD2 inhibition.

To understand why SETD2 inhibition led to a greater reduction in cell growth in the resistant cell lines compared to sensitive counterparts, a paired RNA-Seq and ChIP-Seq experiment was performed. Of particular interest were transcripts that had reduced expression in both Iber-R-MM1s and Iber-R-H929 (compared to their respective control lines) as this could explain the differential response to SETD2 inhibition. Three transcripts, *NCAM1/CD56*, *EMP2* and *TMSB15A*, met these criteria. ChIP-Seq showed treatment with EPZ-719 led to a reduction in H3K36me3 at thousands of sites in each of the lines. H3K36me3 binding at the *NCAM1/CD56* gene was reduced with EPZ-719 treatment in Ctrl-Iber-H929 and Iber-R-H929 but this was less pronounced in Ctrl-Iber-MM1s and Iber-R-MM1s. *EMP2* and *TMSB15A* showed a reduction in H3K36me3 binding with EPZ-719 treatment in all 4 cell lines.

Knockout of *NCAM1/CD56* or *TMSB15A* was not found to be essential in Iber-R-MM1s (in the Chronos algorithm analysis), and *EMP2* was one of the few protein coding genes not targeted by the Brunello library used in the CRISPR screen. However, silencing of *NCAM1/CD56* has previously been shown to reduce proliferation in parental H929 (180). *NCAM1/CD56* is a glycoprotein normally expressed in neurons, NK and T cells but it is aberrantly expressed in >70% of myeloma patients (181). *NCAM1/CD56* expression is greater in malignant myeloma cells compared to normal plasma cells and the presence of >10% clonal *NCAM1/CD56*-expressing cells correlates with inferior survival outcomes (181). *NCAM1/CD56*+ve clone size and *NCAM1/CD56* mRNA expression has been shown to be greater in patients with t(4;14), a translocation which is observed in the H929 cell line and is associated with inferior outcomes in patients (181).

Furthermore, the t(4;14) subgroup has previously been suggested to be more sensitive to SETD2 inhibition (170).

Cottini *et al* showed overexpression of *NCAM1/CD56* in low *NCAM1/CD56* expressing cells lines (such as MM1s) promoted cell growth and adhesion to bone marrow stromal cells, whilst *NCAM1/CD56* silencing in highly expressing *NCAM1/CD56* cell lines (such as H929) led to the opposite effect (180). *NCAM1/CD56* may promote survival by activating a signalling cascade comprising of P90 Ribosomal S6 Kinase A3 (RSK2) and cAMP Responsive Element Binding Protein 1 (CREB1) which leads to activated transcription of anti-apoptotic genes, such as *BCL2* (B-cell Lymphoma 2) and *MCL1* (MCL1 Apoptosis Regulator, BCL2 Family Member) (180). Therefore, in the H929 cell lines reduced *NCAM1/CD56* expression caused by SETD2 inhibition may lead to cell death and this effect is greater in Iber-R-H929 because *NCAM1/CD56* is reduced more than in the control line. There was also a greater reduction in *NCAM1/CD56* mRNA expression in Iber-R-MM1s compared to Ctrl-Iber-MM1s after EPZ-719 treatment. MM1s cell lines have lower expression of *NCAM1/CD56* compared to H929 (as per the previous literature (182) and as seen by flow cytometry (**Supplementary Figure 9-16**)) and SETD2 was not a dependency in Iber-R-MM1s (in the CRISPR screen data). However, reduction of *NCAM1/CD56* could still affect cell growth in the MM1s lines and this may be why SET2 inhibition reduced cell growth to a greater extent the resistant H929 lines compared to the resistant MM1s lines.

It is then interesting to consider why there might be a greater reduction in *NCAM1/CD56* expression with SETD2 inhibition in the resistant lines. It has previously been shown that cells overexpressing *NCAM1/CD56* had reduced response to lenalidomide compared with control cells and conversely cells with reduced *NCAM1/CD56* expression were more sensitive to lenalidomide (180). Furthermore, combining lenalidomide treatment with RSK2 and/or CREB1 inhibition in highly expressing *NCAM1/CD56* cell lines (such as H929) showed synergistic effects (180). The mechanisms linking the *NCAM1/RSK2/CREB1* pathway to lenalidomide efficacy are unknown but interestingly overexpression of *NCAM1/CD56* led to reduced CRBN expression compared to control cells, whereas *NCAM1/CD56* silencing in cells with high *NCAM1/CD56* expression led

to increased CRBN levels (180). Therefore, NCAM1/CD56 expression can affect responses to lenalidomide, potentially through CRBN modulation. This may explain the synergy seen between SETD2 inhibitors and iberdomide in the control lines. Furthermore, as the IMiD/CELMoD-resistant cell lines have low levels of CRBN, this could play a role in the enhanced sensitivity of the resistant lines to SETD2 inhibition.

In summary, *SET2* knockout was identified as a novel vulnerability in IMiD/CELMoD-resistant cells in CRISPR screen data, and this was validated using two SETD2 inhibitors. A putative mechanism to explain this phenomenon is downregulation of NCAM1/CD56.



## Chapter 7 Changes in Lipid Synthesis Pathways in the IMiD/CELMoD-Resistant State

---

### 7.1 Introduction

Whole proteome analysis of the resistant cell lines (**Section 3.2.4**) and the analysis of vulnerabilities in the resistant state (**Section 5.2.3**) suggested that changes in lipid metabolism represented an interesting area for further exploration.

Altered cellular metabolism is a well-established “Hallmark of Cancer” (183). Common cancer-associated metabolic changes include: 1) deregulated uptake of glucose and amino acids, 2) opportunistic mechanisms of nutrient acquisition, 3) use of glycolysis/tricarboxylic acid (TCA) cycle intermediates for biosynthesis and NADPH (nicotinamide adenine dinucleotide phosphate) production, 4) increased demand for nitrogen, 5) changes in metabolite-driven gene regulation and 6) metabolic interactions with the microenvironment (184). Altered lipid metabolism is one of the most prominent metabolic changes in cancer. Lipids are used for energy, form components of biological membranes and act as signalling molecules (185).

Our understanding of the role of lipid metabolism in myeloma drug resistance is limited. It has been most explored in the context of proteasome inhibitor (PI) resistance (186). Fatty Acid Elongase 6 (ELOVL6) levels were found to be lower in myeloma cells from bortezomib non-responsive patients compared to responsive patients and also in cell line models with bortezomib resistance (187). Restoration of ELOVL6 re-sensitised the cells to bortezomib, largely via upregulation of ELOVL6-dependent ceramide species (187). Proteasome inhibition has been shown to lead to accumulation of lipids in myeloma cell lines due to elevated SREBP1/2 levels and combining PI and lovastatin (a lipid lowering drug) treatment has synergistic effects in myeloma cell lines (188). Synergism between PIs and the sphingosine-kinase 2 inhibitor K145 have also been observed and the combination can resensitise PI resistant cell lines (189).

Further exploration of changes in lipid pathways in the IMiD resistant state was therefore performed using compound assays, labelled-glucose experiments and proteomics in patient samples.

## 7.2 Results

### 7.2.1 Whole proteome analysis in the resistant cell lines

As discussed in Chapter 3, pathway analysis showed that lipid metabolism pathways were enriched in proteins that were downregulated in the resistant setting. At the individual protein level, Stearoyl-CoA Desaturase (SCD) was one of only 3 proteins with significantly altered expression in all 6 cell lines (with a log<sub>2</sub> fold change of +/- 0.2 and adj p value <0.05) (**Figure 7-1**). Several other lipid metabolism proteins were significantly altered in ≥4 resistant cell lines by quantitative proteomics (**Figure 7-2, Supplementary Table 9-3**).

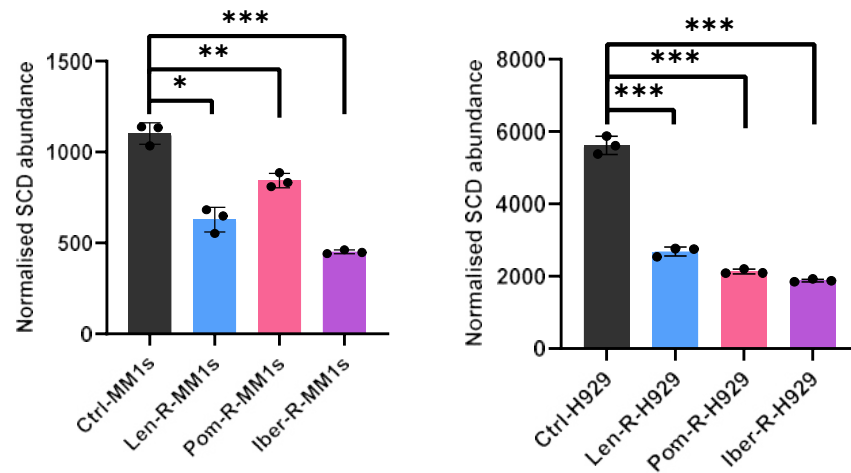


*Figure 7-1 SCD levels in the resistant cell lines.*

Normalised SCD abundance in a representative control line and the resistant lines. Quantitative proteomics data was analysed by a limma modified t-test in Phantasus (v1.19.3). \* adj p <0.05, \*\* adj p value <0.01, \*\*\* adj p value p value <0.001.

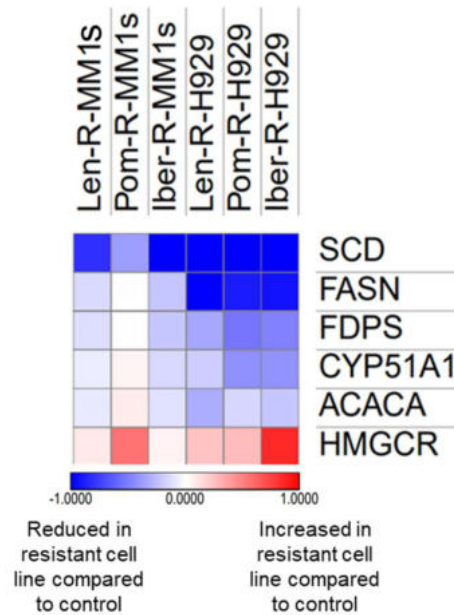
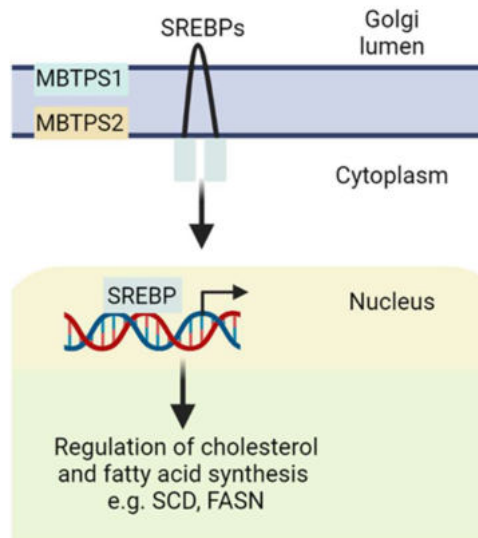


Figure 7-2 Heat map showing  $\log_2FCs$  of SREBP pathway proteins in the resistant cell lines.

This heatmap shows the  $\log_2FCs$  of SREBP pathway proteins (taken from the Reactome “Activation of gene expression of SREBF (SREBP)” gene set) in the resistant cell lines compared to control. Included proteins had a significant change ( $\text{adj } p < 0.05$ ) in at least 4 out of 6 lines. SCD (Stearoyl-CoA Desaturase), FASN (Fatty Acid Synthase), FDPS (Farnesyl Diphosphate Synthase), CYP51A1 (Cytochrome P450 Family 51 Subfamily A Member 1), ACACA (Acetyl-CoA Carboxylase Alpha), HMGCR (HMG-CoA Reductase).

### 7.2.2 The effect of compounds targeting lipid synthesis pathways in the resistant cell lines

The CRIPSR screen (Chapter 5) had suggested that knockout of *MBTPS1* and *SCD* were novel vulnerabilities in the resistant setting. Validation using selective inhibitors was therefore explored. As described previously *MBTPS1* activates *SREBP1* which in turn promotes the transcription of *SCD* (Figure 7-3).



*Figure 7-3 The SREBP pathway.*

SREBP (Sterol Regulatory Element Binding Protein) proteins need to be cleaved by MBTPS1 (Membrane Bound Transcription Factor Peptidase, Site 1) and MBTPS2 (Membrane Bound Transcription Factor Peptidase, Site 2) prior to translocation to the nucleus. They then function as transcription factors that regulate the transcription of critical cholesterol and fatty acid synthesis genes, for example SCD (Stearoyl-CoA Desaturase) and FASN (Fatty Acid Synthase).

### ***MBTPS1 inhibition***

In Chapter 5, the MBTPS1 inhibitor PF-429242 was found to reduce viability to a greater extent in Iber-R-H929 compared to its control. PF-429242 was therefore tested more extensively in each of the MM1s and H929 cell line pairs (**Figure 7-4**). In the MM1s cell lines PF-429242 only led to a reduction in viability at the highest concentration of 20 $\mu$ M and no differential response was observed. However, in the H929 lines PF-429242 treatment led to a greater reduction in viability in the resistant lines compared to their controls. This effect was minimal in Len-R-H929, but became more pronounced in Pom-R-H929 and Iber-R-H929.

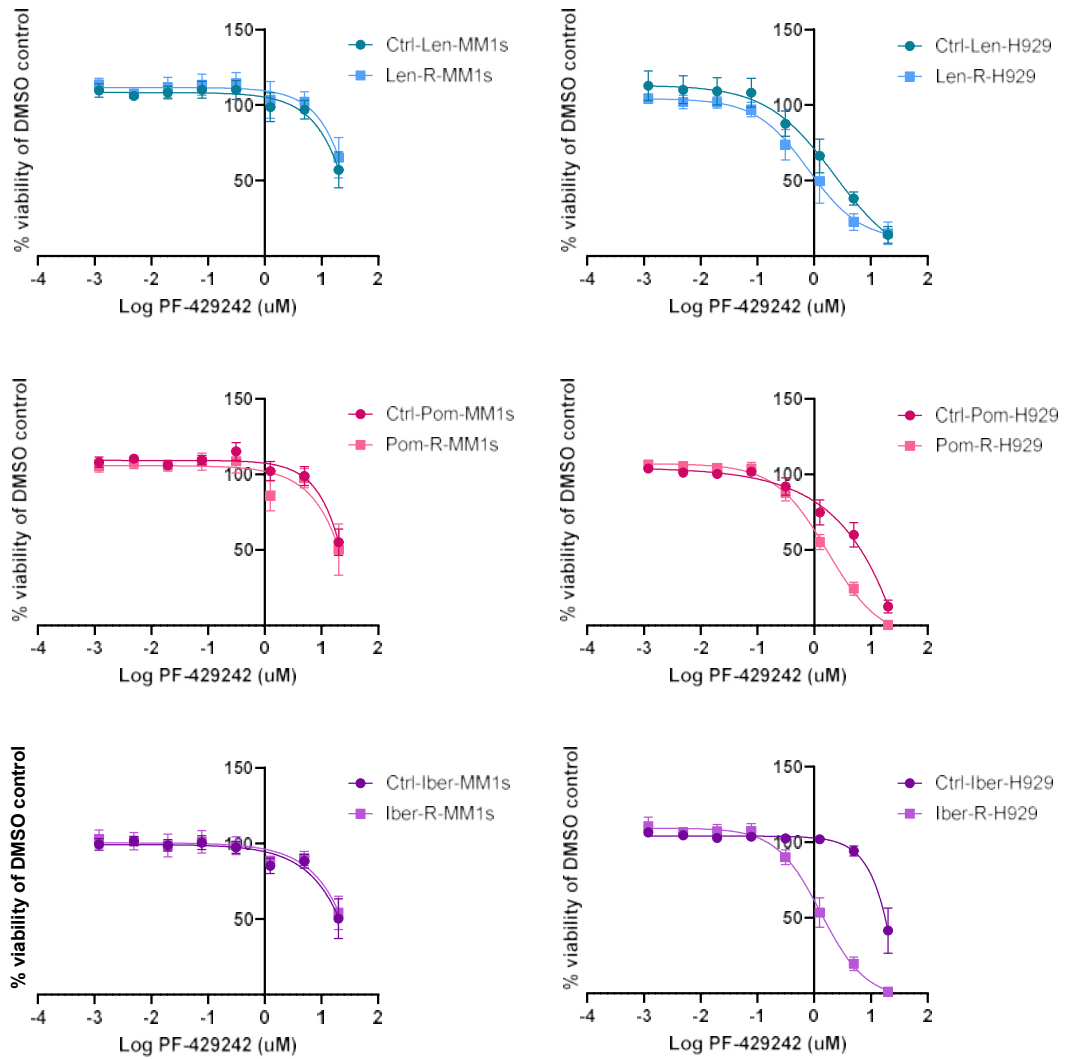


*Figure 7-4 Viability assays demonstrating response of the resistant cell lines to PF-429242 treatment.*

The effect of PF-429242 treatment on cell viability was assessed in 5-day CellTiter-Blue assays. The IMiD/CELMoD-resistant H929 cell lines showed a greater reduction in viability with PF-429242 treatment compared to their sensitive counterparts. N=4, graphs show mean and SEM.

A time course experiment was performed in Pom-R-H929 and Iber-R-H929 and the differential response was most clearly observed after 5 days of PF-429242 treatment (**Figure 7-5**).

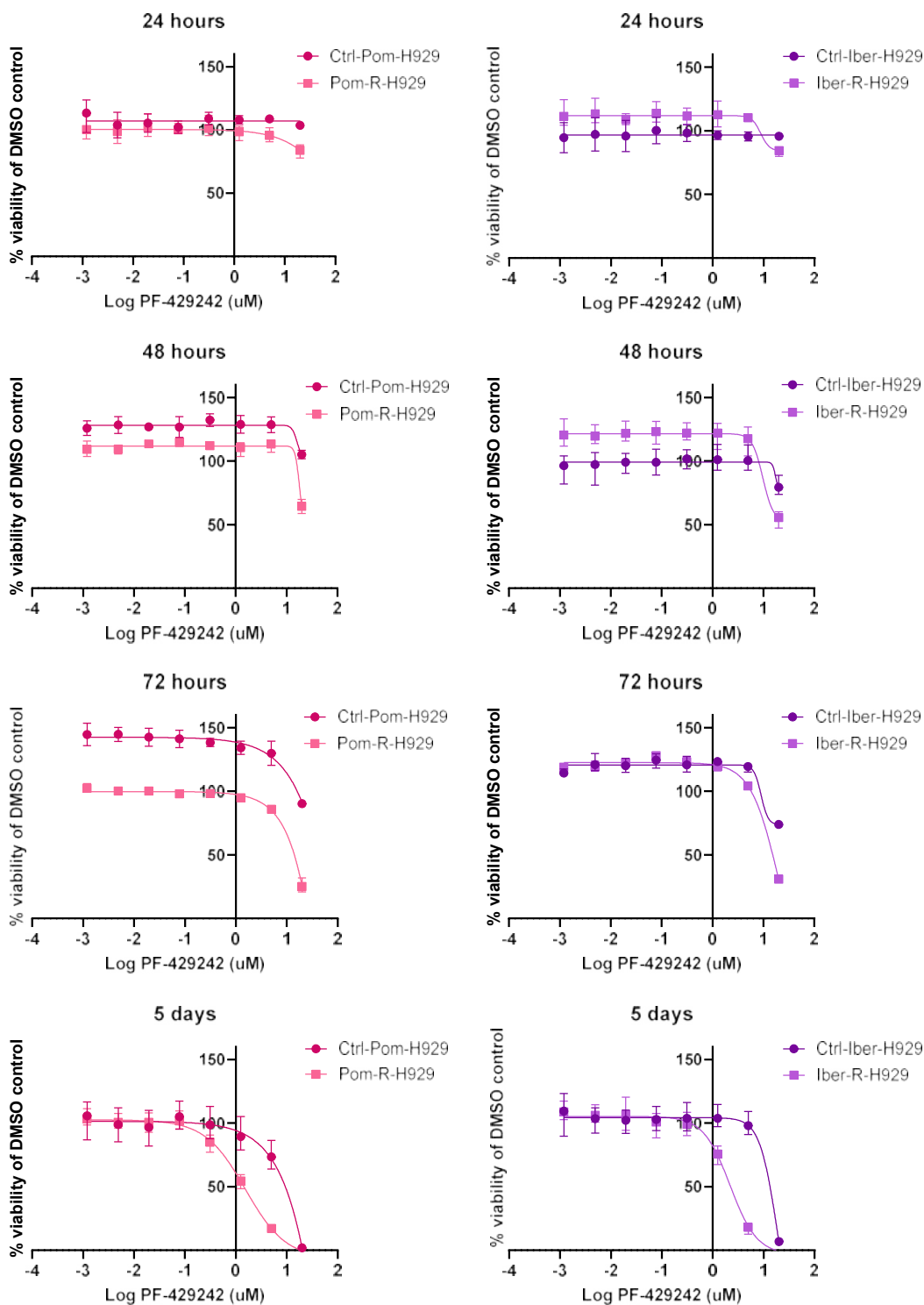


**Figure 7-5 Time course experiment with PF-429242 in the resistant cell lines.**

The effect of PF-429242 treatment on cell viability was assessed in CellTiter-Blue assays (highest concentration 20µM). The differential response was most clearly observed after 5 days of treatment. N=1 at each time point, graphs show mean and range of 3 technical triplicates.

### **SCD inhibition**

In Chapter 5 the SCD inhibitor A939572 was tested in the Iber-R-MM1s and Iber-R-H929 cell lines and was not active. Therefore, a second SCD inhibitor, GSK1940029, was tested in the cell lines. In a 5-day assay it had no effect on

viability in the MM1s lines and did not show a dose-dependent response in the H929 lines (**Supplementary Figure 9-17**).

### 7.2.3 Clonal competition assays to assess the impact of *SCD* and *MBTPS1* knockout on cell fitness

The MBTPS1 inhibitor PF-429242 had a differential effect on viability in the paired H929 cell lines but was not active in the MM1s cell lines. The SCD inhibitors A939572 and GSK1940029 also showed limited activity in both the MM1s and H929 lines. This lack of activity could suggest that MBTPS1 and SCD are not essential in the cell lines or that the tool compounds tested have low cellular uptake and/or low efficacy. Therefore, to explore the novel dependencies further, a genetic method was also utilised in the form of a clonal competition assay (190).

Cas9 expressing cells (Cas9-Ctrl-Iber-MM1s and Cas9-Iber-R-MM1s) were transduced with a vector containing a guide RNA (gRNA) targeting the gene of interest and a fluorescent (GFP) marker. An infection efficiency of ~50% was desirable at baseline so that half of the cells contained knockout of the gene of interest and half of the cells were wild-type (however the assay was flexible and transduction efficiencies ranging from 10-80% were suitable) (190). The relative abundance of the transduced population was then measured over time via flow cytometry for GFP expression (**Figure 7-6**) (190).

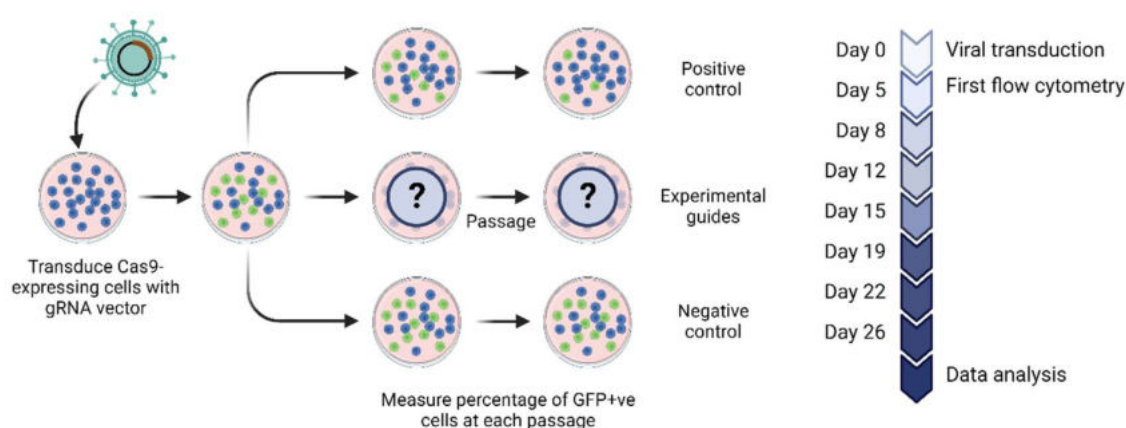


**Figure 7-6** Clonal competition assay workflow.

Cas9-expressing cells were transduced with a gRNA vector at a low multiplicity of infection. Transduced cells were GFP positive and had the gene of interest knocked out. The relative abundance of the transduced population was then measured over time using flow cytometry. Knockout of a gene essential for cell proliferation (e.g. positive control) leads to a decrease in the proportion of GFP positive cell over time. Conversely, if a non-essential gene is knocked out, the number of GFP positive cell remains stable. Adapted from Girish *et al* (190), image created using BioRender.

The clonal competition assay was performed in Cas9-Ctrl-Iber-MM1s and Cas9-Iber-R-MM1s. Different guides were cloned into the LRG2.1 vector which encodes a gRNA and GFP. This included 2 guides targeting MBTPS1, 2 guides targeting SCD, 1 guide against RPA3 (Replication Protein 3) as a positive control (this gene is known to be essential) and 2 guides against PKHD1L1 (PKHD1 Like 1) as negative controls (this gene is known to be non-essential). Empty LRG2.1 vector was also used as a non-targeting control. This assay would therefore show if *MBTPS1* and *SCD* are essential genes in Ctrl-Iber-MM1s and/or Iber-R-MM1s and potentially if there is a difference in dependency between the two lines. Despite several attempts it was not possible to transduce Ctrl-Iber-H929 and Iber-R-H929 with Cas9. This is because of the difficulty of transducing myeloma cell lines and the large size of the Cas9-containing plasmid pLX\_311-Cas9 (**Figure 2-4**).

#### Clonal competition assay for SCD knockout

SCD was confirmed to be a dependency in both Ctrl-Iber-MM1s and Iber-R-MM1s (**Figure 7-7**). Assessing whether Iber-R-MM1s cells were more dependent on SCD than parental MM1s was difficult due to variabilities such as viral transduction efficiency and Cas9 activity in the two cell lines. However, there was no large difference in dependency.

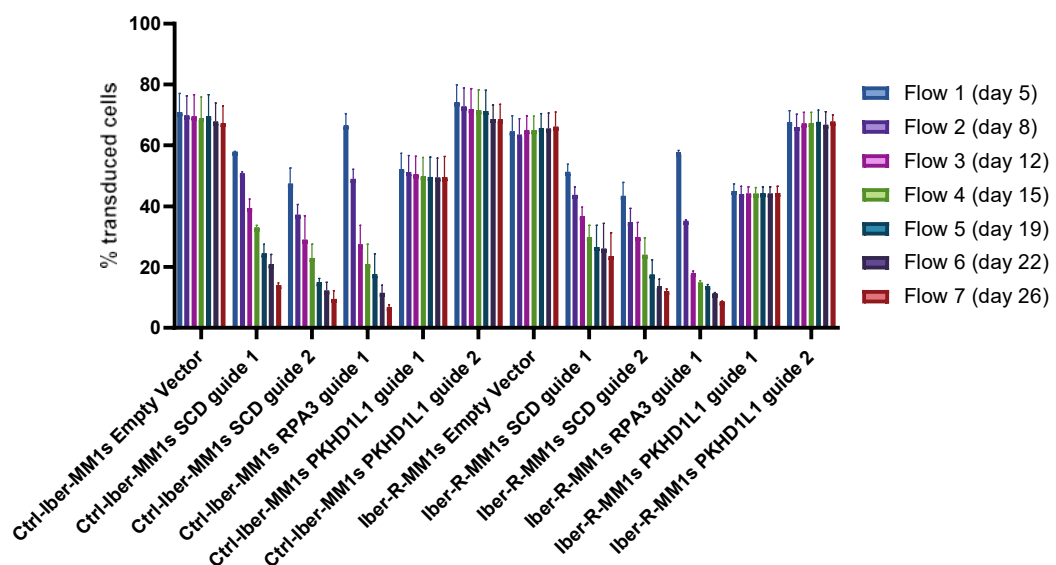


**Figure 7-7 SCD clonal competition assay results.**

SCD was confirmed as a dependency in both Ctrl-Iber-MM1s and Iber-R-MM1s. The percentage of transduced cells over time was assessed by flow cytometry (transduced cells were GFP +ve). N=2, bar represents the mean and error bars represent SEM.



### Clonal competition assay for MBTPS1 knockout

MBTPS1 was also confirmed to be a dependency in both Ctrl-Iber-MM1s and Iber-R-MM1s (**Figure 7-8**). Again assessing whether Iber-R-MM1s cells were more dependent on MBTPS1 than Ctrl-Iber-MM1s was difficult, but there was no large difference.

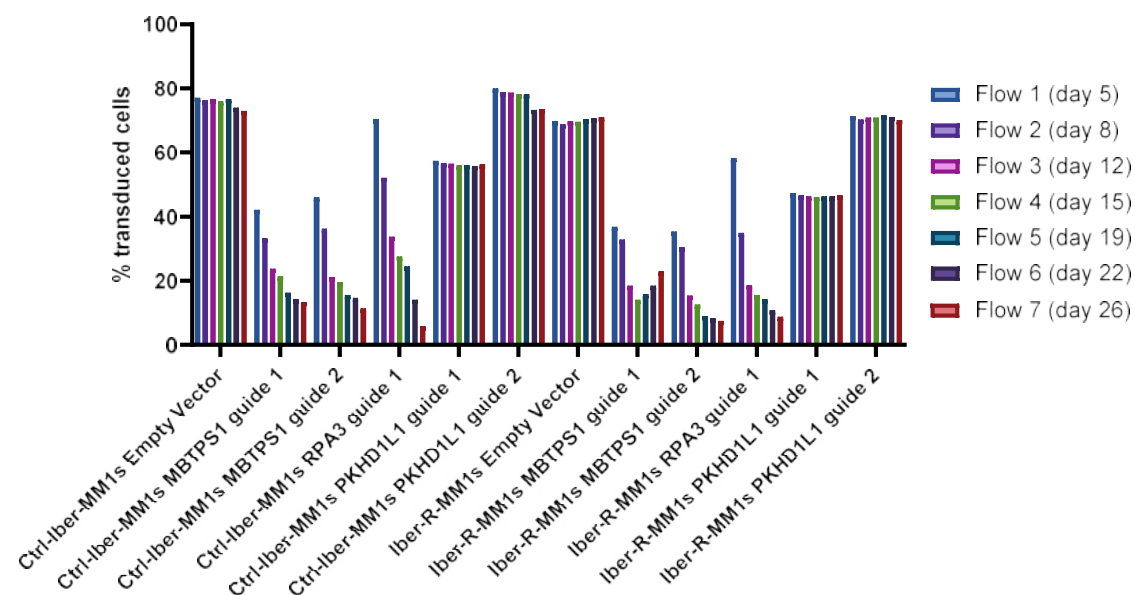


**Figure 7-8 MBTPS1 clonal competition assay results.**

MBTPS1 was confirmed as a dependency in both Ctrl-Iber-MM1s and Iber-R-MM1s. The percentage of transduced cells over time was assessed by flow cytometry (transduced cells were GFP +ve). N=1.

### 7.2.4 Lipidomics analysis in the resistant cell lines

The whole proteome analysis of the resistant lines (**Section 3.2.4**) identified altered abundance of proteins involved in lipid metabolism in the resistant state. However, it was important to see if this altered lipid levels and lipid flux through the cells. This was done by performing labelled glucose experiments in Iber-R-MM1s, Iber-R-H929 and their matched control lines. Cells were cultured in media containing  $^{13}\text{C}_6$ -glucose and the  $^{13}\text{C}$  atoms were transmitted to downstream metabolites, such as acetyl-CoA and newly synthesised fatty acids. Samples were analysed in collaboration with Professor Keun's team at Imperial College London; metabolites containing  $^{13}\text{C}$  were detected by mass spectrometry due to heavier mass. The process of *de novo* lipid synthesis in humans, in which palmitic acid is the major product, is shown in **Figure 7-9**.

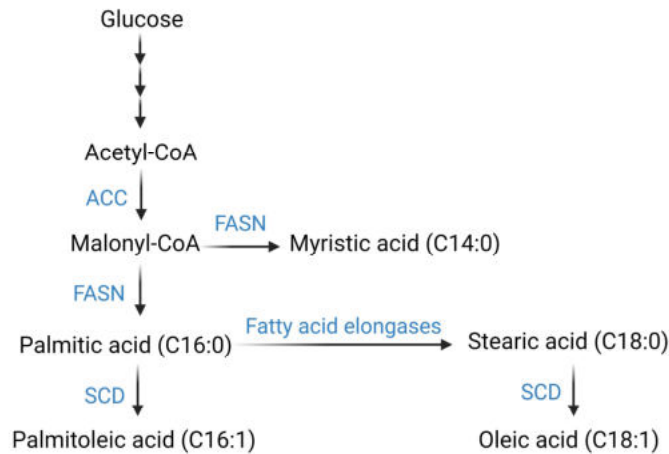


*Figure 7-9 A schematic of de novo lipogenesis.*

Acetyl-CoA, the substrate of fatty acid synthesis, is generated predominately from glucose via glycolysis and the tricarboxylic acid cycle (but also fatty acid and amino acid catabolism to a lesser extent). Acetyl-CoA is converted into malonyl-CoA by acetyl-CoA carboxylase (ACC), which is then used as a building block by the enzyme fatty acid synthase (FASN) to produce myristic acid (C14:0), which is in turn elongated to give palmitic acid (C16:0). Palmitic acid can be elongated (by fatty acid elongases) to generate stearic acid (C18:0). The desaturase stearoyl-CoA desaturase (SCD) catalyses desaturation of palmitic acid and stearic acid to generate palmitoleic acid (C16:1) and oleic acid (C18:1), respectively. C16:0 indicates the fatty acid has a 16 carbon backbone and no double bonds (i.e. saturated). Enzymes are shown in blue.

Initial analysis demonstrated that the H929 and MM1s cell lines had different fatty acid synthesis rates; after a 24 hour incubation with labelled glucose ~40% of the sampled fatty acids were newly synthesised in H929, compared to ~15% in MM1s (data not shown). Therefore, H929 cell lines were exposed to labelled glucose for 24 hours and MM1s lines were exposed for 48 hours. The proportion of de novo synthesised palmitate, stearate and myristate (the salts and esters of palmitic acid, stearic acid and myristic acid respectively) were reduced in Iber-R-H929. Likewise, the fraction of newly synthesised palmitate was decreased in Iber-R-MM1s. However, the proportions of stearate and myristate were not altered significantly. Given the relatively low abundance of newly synthesised fatty acids (due to reduced synthesis rate), the MM1s cells might be less sensitive to changes in fatty acid synthesis flux. Taken together these results suggest that fatty acid synthesis activity was downregulated in the IMiD/CELMoD-resistant state (**Figure 7-10**).

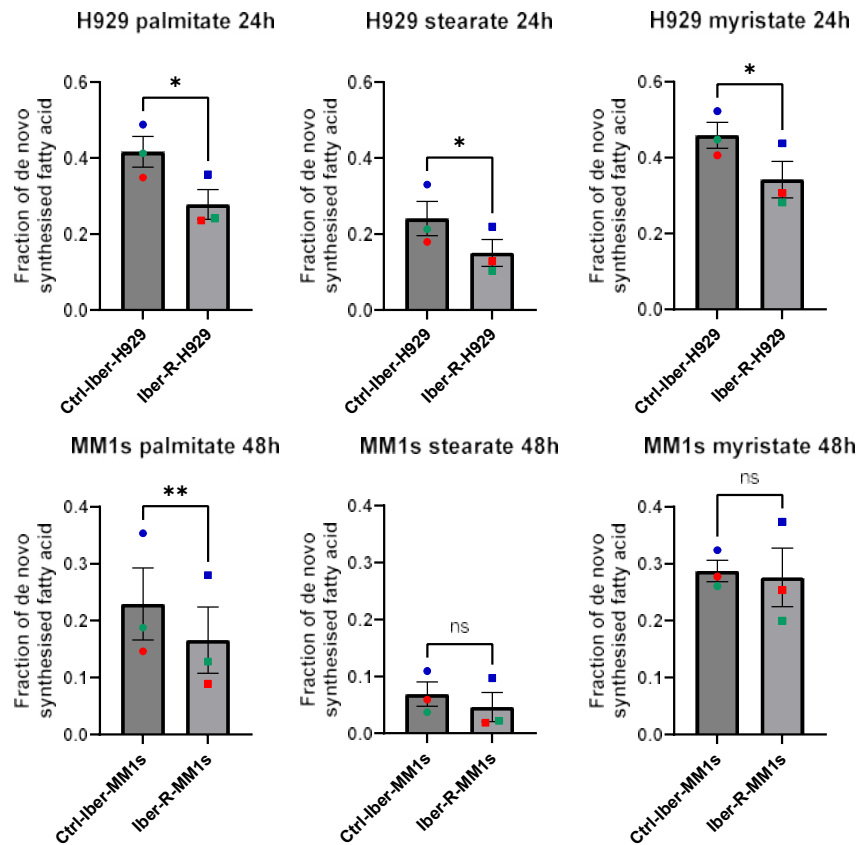


**Figure 7-10** Fraction of de novo synthesised fatty acids in the control and resistant cell lines.

The fraction of each fatty acid that was synthesised *de novo* during incubation with labelled glucose is shown. N=3, independent experiments shown, replicate 1 = red, replicate 2 = green, replicate 3 = blue. Differences between the cell lines were analysed using a paired t-test. \* = p<0.05, \*\* p<0.01.

The proportion of lipogenic acetyl-CoA (the substrate for fatty acid synthesis) derived from glucose was reduced in Iber-R-H929 compared to control (**Figure 7-11**). This suggested that the proportional contribution of glucose to fatty acid synthesis was decreased, and alternative carbon sources might compensate.

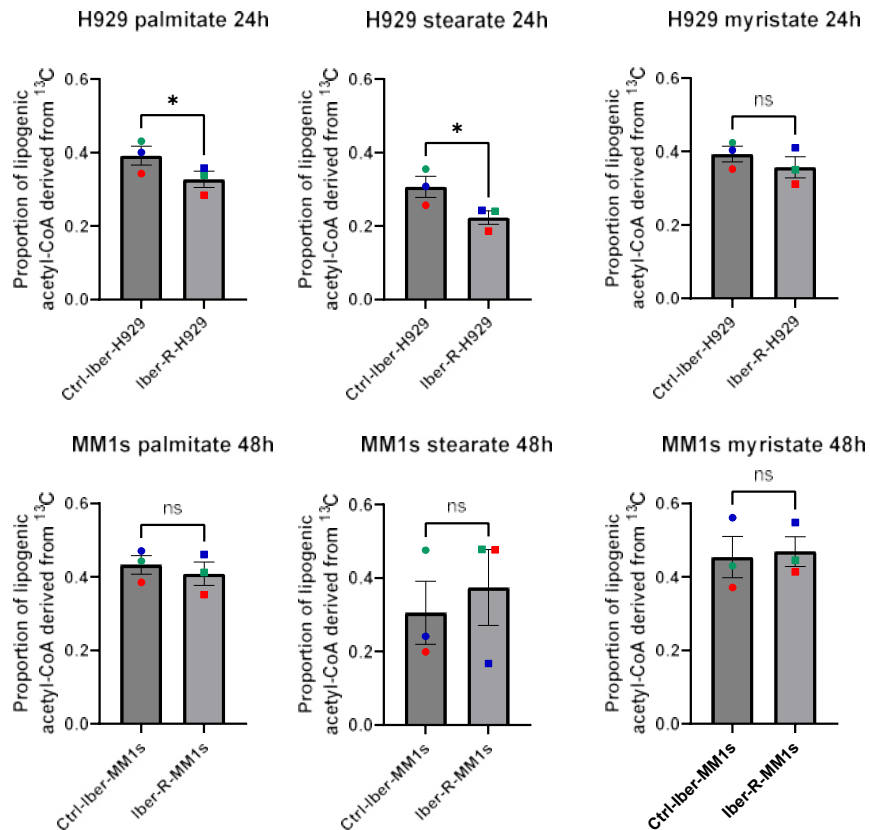


**Figure 7-11** Proportion of lipogenic acetyl-CoA derived from labelled carbon in the control and resistant cell lines.

The relative enrichment in precursor acetyl-CoA from the <sup>13</sup>C labelled glucose for each fatty acid is shown. N=3, independent experiments shown, replicate 1 = red, replicate 2 = green, replicate 3 = blue. Differences between the cell lines were analysed using a paired t-test. \* = p<0.05.

Furthermore, the ratios of oleate/stearate (18:1/18:0) and palmitoleate/palmitate (16:1/16:0) were decreased in Iber-R-H929, with a similar trend in Iber-R-MM1s, suggesting that the activity of fatty acid desaturation was reduced (**Figure 7-12**). SCD catalyses the conversion of saturated fatty acids into mono-unsaturated fatty acids, therefore this data is consistent with the reduction in SCD abundance seen at the protein level.

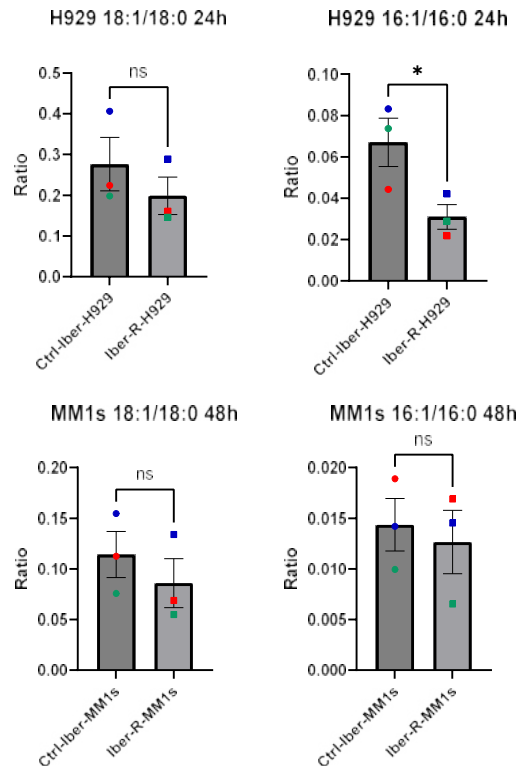


**Figure 7-12 Ratio of desaturated to saturated fatty acids in the control and resistant cell lines.**

The ratio of desaturated to saturated fatty acids for each cell line pair is shown. 18:1=oleate, 18:0=stearate, 16:1=palmitoleate, 16:0=palmitate. N=3, independent experiments shown, replicate 1 = red, replicate 2 = green, replicate 3 = blue. Differences between cell lines were analysed using a paired t-test. \* =  $p < 0.05$ .

## 7.2.5 Exploration of changes in lipid pathways in Myeloma patient samples

### **Exploration of the Celgene/BMS dataset**

It was important to explore if the lipid metabolism changes seen in the cell line models were reflected in patients. There were no available proteomics datasets of patient samples in which to explore this. However, Celgene/BMS had an available RNA-Seq dataset of 736 samples from newly diagnosed patients and 270 samples from lenalidomide refractory patients (RNA-Seq performed in myeloma cells isolated from patient bone marrow aspirates). In collaboration with Celgene/BMS, transcript levels for 15 lipid metabolism genes were assessed to see if there were changes between diagnosis and relapse. Thirteen of the genes had significantly altered expression between the two timepoints (**Figure 7-13**).

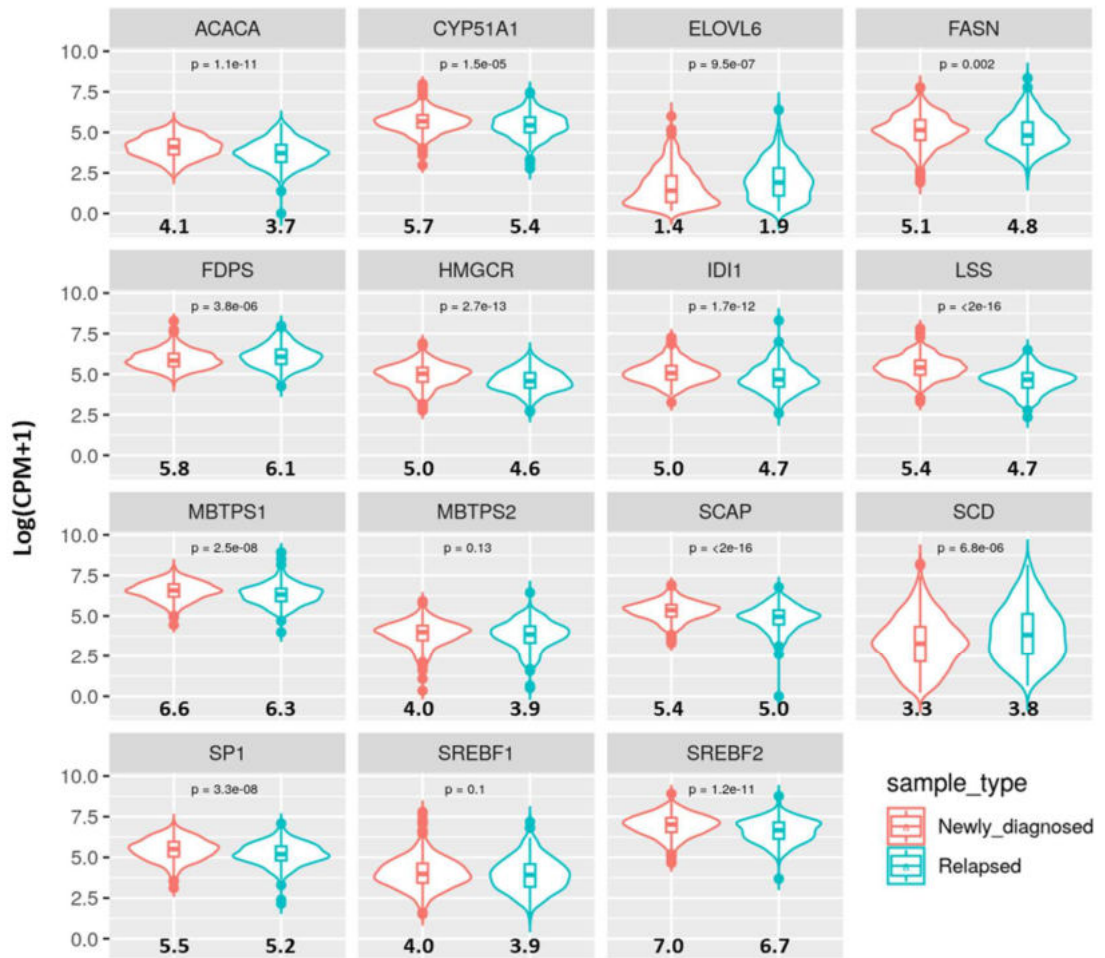


**Figure 7-13** mRNA expression of lipid genes in newly diagnosed and relapsed patient samples.

mRNA expression changes between samples from newly diagnosed and relapsed patients were investigated. Thirteen of the genes had significant expression changes. The median expression values are indicated within the plot and significance was tested using the Wilcoxon test. CMP = counts per million. *ACACA* (Acetyl-CoA Carboxylase Alpha), *CYP51A1* (Cytochrome P450 Family 51 Subfamily A Member 1), *ELOVL6* (ELOVL Fatty Acid Elongase 6), *FASN* (Fatty Acid Synthase), *FDPS* (Farnesyl Diphosphate Synthase), *HMGCR* (HMG-CoA Reductase), *IDI1* (Isopentenyl-Diphosphate Delta Isomerase 1), *LSS* (Lanosterol Synthase), *MBTPS1* (Membrane Bound Transcription Factor Peptidase, Site 1), *MBTPS2* (Membrane Bound Transcription Factor Peptidase, Site 2), *SCAP* (SREBF Chaperone), *SCD* (Stearoyl-CoA Desaturase), *SP1* (Specificity Protein 1), *SREBF1* (Sterol Regulatory Element Binding Transcription Factor 1) and *SREBF2* (Sterol Regulatory Element Binding Transcription Factor 2).

### Exploration of the MMRF dataset

It was also important to explore if there was any evidence that alterations in lipid gene expression might correlate with patient outcomes. In collaboration with Professor Brian Walker's team at Indiana University, the Multiple Myeloma Research Foundation (MMRF) CoMMpass dataset was used to see if there was a difference in PFS or OS based on expression of *MBTPS1* or *SCD* (in myeloma cells isolated from the bone marrow aspirates of newly diagnosed multiple

myeloma patients). High *MBTPS1* or *SCD* expression was associated with significantly shorter PFS and shorter OS than low expression (**Figure 7-14**).

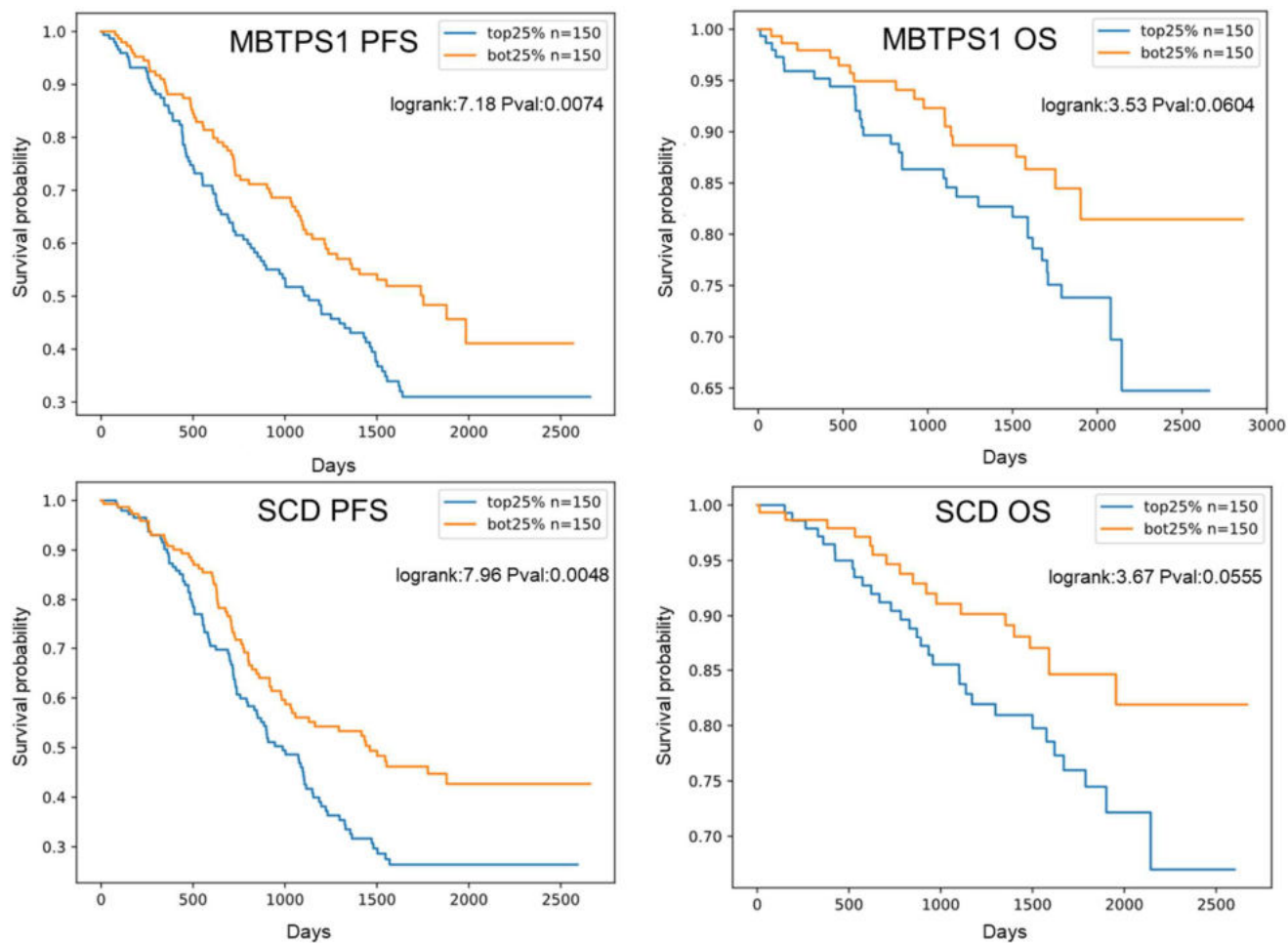


*Figure 7-14 Correlation of MBTPS1 and SCD mRNA expression at diagnosis with outcome.*

Kaplan-Meier curves show that high expression of MBTPS1 or SCD (blue) was associated with significantly shorter progression free survival (PFS) and shorter overall survival (OS), compared to low expression (orange). The logrank test was used to compare curves.



### ***Paired patient sample proteomics***

The analyses in Section 7.2.5 were performed using RNA data but the changes identified in the cell lines models were at the protein and lipid level. No large proteomic datasets were available, so whole proteome analysis using a TMT-multiplexing approach was performed on paired diagnosis and relapse (on lenalidomide) samples from 4 patients who had been enrolled in the Myeloma XI trial (**Figure 7-15**). Characteristics of the patients are shown in **Table 7-1**.



**Figure 7-15** Summary diagram of the Myeloma XI trial.

Patients received induction therapy with CTD (cyclophosphamide, thalidomide, dexamethasone), CRD (cyclophosphamide, lenalidomide, dexamethasone) or KCRD (carfilzomib, cyclophosphamide, lenalidomide, dexamethasone). Patients with a suboptimal response to induction (<very good partial response) were eligible for intensification. Patients with partial response/minimal response were randomised to CVD (cyclophosphamide, bortezomib and dexamethasone) or no further therapy. Patients with stable disease/progressive disease all received CVD. Transplant eligible patients then went on to receive autologous stem cell transplantation (ASCT). Patients were then randomised to receive lenalidomide maintenance or observation. Patients had a bone marrow examination performed at entry to the trial, and some also had a sample taken at relapse.

Patient ID	Sex	Age	Transplant eligible	Induction therapy	WHO performance status	ISS stage	Paraprotein class	Light chain type	Presence of adverse cytogenetic disease	Response before lenalidomide maintenance commenced
9102	Male	81	No	CRDa	0	2	IgG	Lambda	No	VGPR
12609	Female	57	Yes	CTD	2	Unknown	IgA	Kappa	Yes	VGPR
12986	Male	62	Yes	CRD	1	3	IgG	Lambda	No	VGPR
12408	Male	59	Yes	CRD	1	2	IgG	Kappa	No	PR

*Table 7-1 Patient characteristics of samples from the Myeloma XI trial.*

The characteristics of the four patients who had available bone marrow samples for analysis are described here. Adverse cytogenetic disease was defined as the presence of  $\geq 1$  of t(4;14), t(14;16), t(14;20), 1q+ and 17p-. CTD, cyclophosphamide, thalidomide, dexamethasone; CRD, cyclophosphamide, lenalidomide, dexamethasone; CRDa, attenuated CRD; WHO performance status, World Health Organisation performance status; ISS, international staging system; VGPR, very good partial response; PR, partial response. ISS is a prognostic staging system which defines 3 subgroups of patients with differing overall survival, with 1 being the best prognosis and 3 being the worst prognosis (191). The WHO performance score determines the fitness of patients, with 0 being asymptomatic and 5 being bedbound (192).

CRBN protein expression was decreased in the relapse sample compared to diagnosis sample in two patients (with log<sub>2</sub> fold changes of -0.72 and -0.15). Proteins that were commonly altered in the four patients were then explored. Using a log<sub>2</sub> fold change of >1 there was one commonly upregulated protein, Immunoglobulin Lambda Like Polypeptide 5 (IGLL5). Functional enrichment analysis of upregulated protein in ≥2 patients highlighted cell cycle pathways and signalling by Rho GTPases (**Figure 7-16**). Using a log<sub>2</sub> fold change of <-1 there were no commonly downregulated proteins in all patients. However, functional enrichment analysis of downregulated proteins in ≥ 2 patients highlighted cholesterol metabolism and folate metabolism (**Figure 7-17**). A relatively large fold change was employed because there was only one data set per sample, with no biological or technical repeats. Of note, SCD (which was commonly downregulated in all 6 of the resistant cell lines) was only downregulated at relapse (with a log<sub>2</sub> fold change of -0.28) in the patient with a large reduction in CRBN expression.

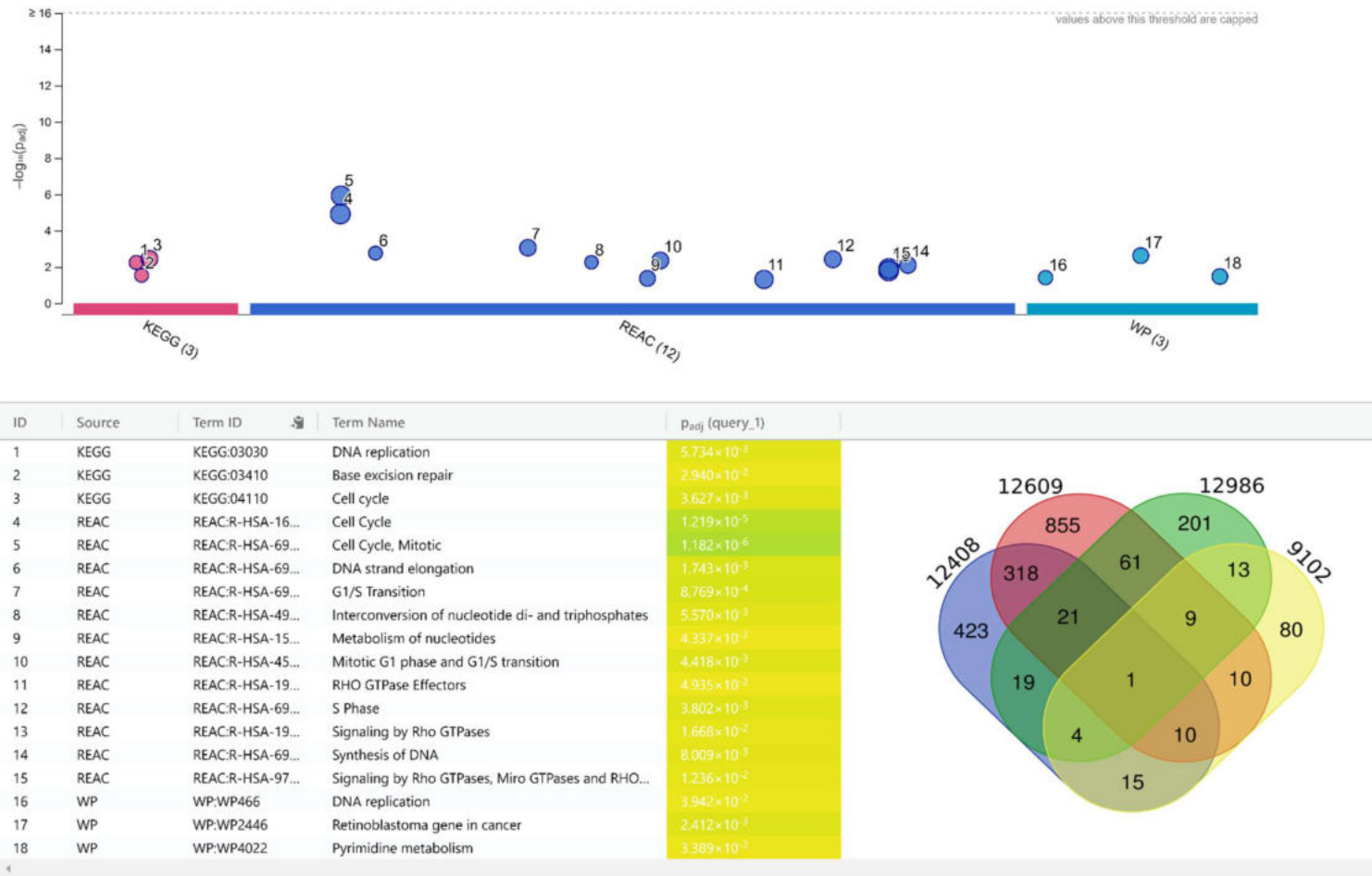
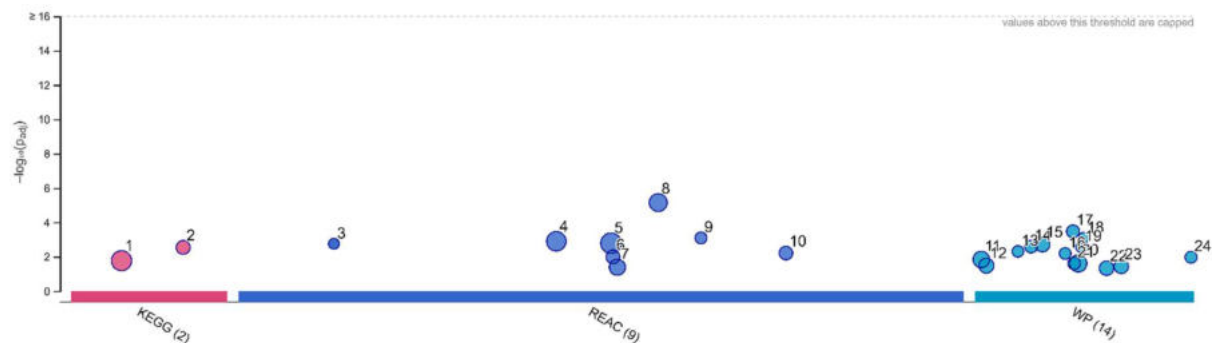


Figure 7-16 Functional enrichment analysis of commonly upregulated proteins at relapse on lenalidomide.

The Venn diagram shows the overlap between patients of proteins with a  $\log_2FC > 1$  (increased at relapse compared to diagnosis). Functional enrichment analysis was performed on upregulated proteins in  $\geq 2$  patients using g:Profiler (145). KEGG, Reactome and WikiPathways pathways are highlighted.



ID	Source	Term ID	Term Name	P <sub>adj</sub> (query_1)
1	KEGG	KEGG:01100	Metabolic pathways	$1.709 \times 10^{-3}$
2	KEGG	KEGG:04979	Cholesterol metabolism	$2.859 \times 10^{-3}$
3	REAC	REACR-HSA-89...	Chylomicron assembly	$1.761 \times 10^{-3}$
4	REAC	REACR-HSA-16...	Innate Immune System	$1.266 \times 10^{-3}$
5	REAC	REACR-HSA-14...	Metabolism	$1.637 \times 10^{-3}$
6	REAC	REACR-HSA-68...	Metabolism of fat-soluble vitamins	$1.024 \times 10^{-3}$
7	REAC	REACR-HSA-19...	Metabolism of vitamins and cofactors	$4.082 \times 10^{-4}$
8	REAC	REACR-HSA-67...	Neutrophil degranulation	$7.064 \times 10^{-5}$
9	REAC	REACR-HSA-89...	Plasma lipoprotein assembly	$8.057 \times 10^{-5}$
10	REAC	REACR-HSA-97...	Retinoid metabolism and transport	$6.138 \times 10^{-5}$
11	WP	WP:WP5115	Network map of SARS-CoV-2 signaling pathway	$1.445 \times 10^{-2}$
12	WP	WP:WP2806	Complement system	$3.327 \times 10^{-3}$
13	WP	WP:WP5112	Familial hyperlipidemia type 5	$4.909 \times 10^{-3}$
14	WP	WP:WP2878	PPAR-alpha pathway	$2.596 \times 10^{-3}$
15	WP	WP:WP15	Selenium micronutrient network	$1.949 \times 10^{-3}$
16	WP	WP:WP5109	Familial hyperlipidemia type 2	$6.482 \times 10^{-3}$
17	WP	WP:WP430	Statin inhibition of cholesterol production	$3.350 \times 10^{-4}$
18	WP	WP:WP3601	Lipid particles composition	$7.931 \times 10^{-4}$
19	WP	WP:WP5110	Familial hyperlipidemia type 3	$2.622 \times 10^{-3}$
20	WP	WP:WP2882	Nuclear receptors meta-pathway	$2.465 \times 10^{-4}$
21	WP	WP:WP5111	Familial hyperlipidemia type 4	$2.457 \times 10^{-3}$
22	WP	WP:WP5304	Cholesterol metabolism	$4.673 \times 10^{-4}$
23	WP	WP:WP176	Folate metabolism	$3.897 \times 10^{-4}$
24	WP	WP:WP5108	Familial hyperlipidemia type 1	$1.069 \times 10^{-2}$

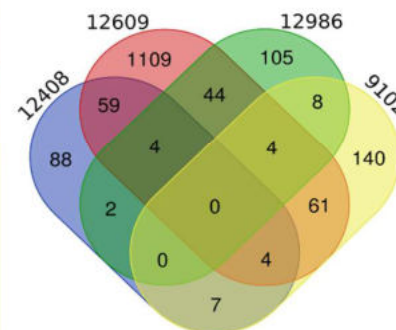
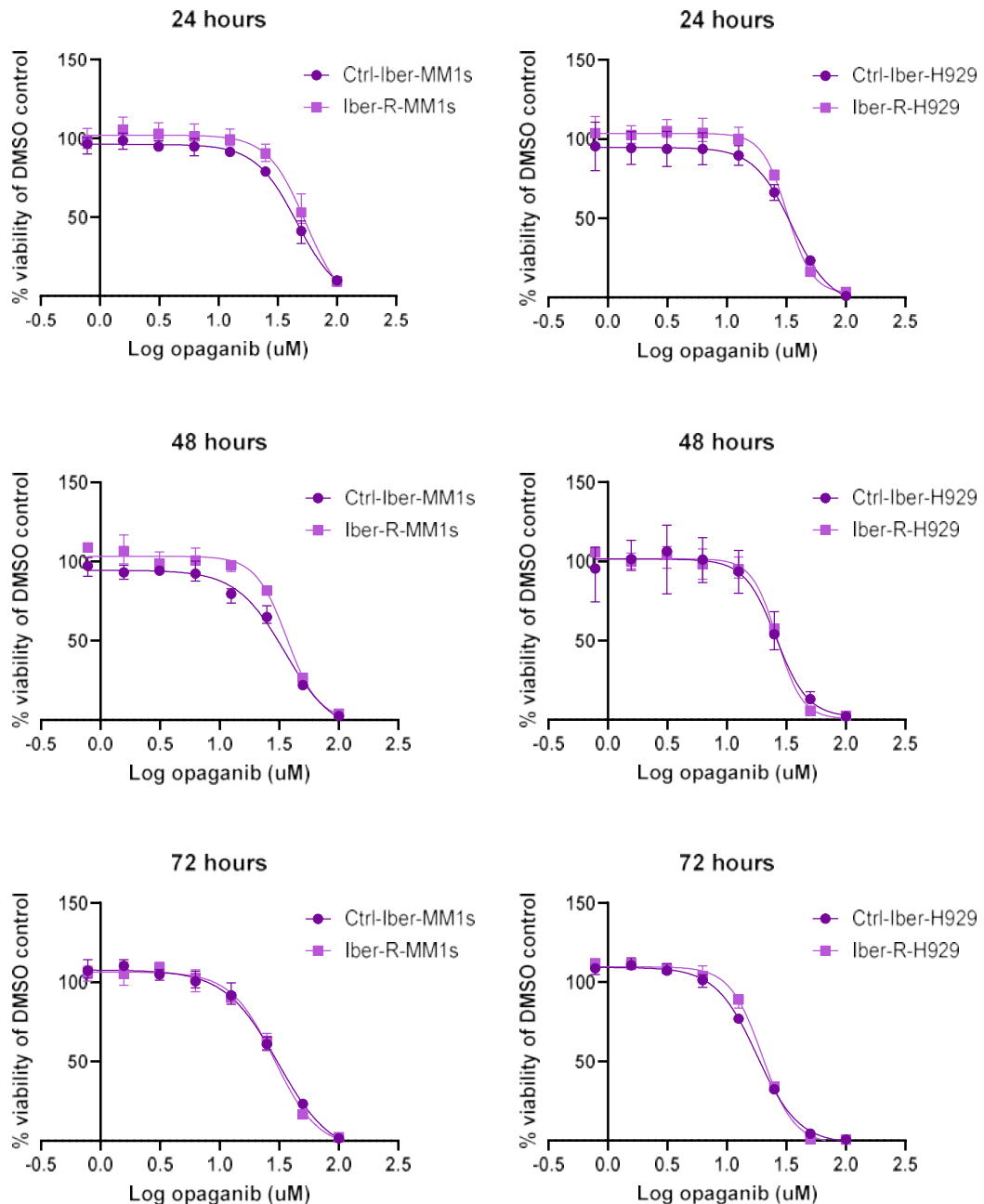


Figure 7-17 Functional enrichment analysis of commonly downregulated proteins at relapse on lenalidomide.

The Venn diagram shows the overlap between patients of proteins with a  $\log_2FC < -1$  (decreased at relapse compared to diagnosis). Functional enrichment analysis was performed on downregulated proteins in  $\geq 2$  patients using g:Profiler (145). KEGG, Reactome and WikiPathways pathways are highlighted.

### 7.2.6 Exploration of lipid targeting compounds in patient samples

Patient bone marrow aspirate samples were being collected in the laboratory as part of a research study (Royal Marsden Clinical Committee for Research approval number CCR5106, see **Methods Section 2.8** for details). Myeloma cells (CD138+ve plasma cells) were isolated from patient samples using magnetic bead isolation. I wanted to develop an in vitro method to test the effect of lipid targeting drugs on the viability of patient myeloma cells. Myeloma cells do not survive outside of the body for long; therefore any compounds used in viability assays must produce their effect within a short period. Unfortunately this meant that the SETD2 inhibitors (EPZ-719 and EZM0414) and the MBTPS1 inhibitor (PF-429242) could not be explored in this context. However, there were other lipid pathway targeting drugs that might act within this short window. Opaganib is a sphingosine kinase 2 inhibitor that has recently been evaluated in a phase 1 clinical trial for myeloma (193). It showed activity at the 24-, 48- and 72-hour time points, which suggested it might be applicable to testing in patient samples (**Figure 7-18, Supplementary Figure 9-18 and Supplementary Figure 9-19**). Although there was no differential response to opaganib treatment between the control and resistant cell lines, it was still important to make initial optimisation steps for compound testing in ex vivo patient cells.



**Figure 7-18** The effect of opaganib on viability in the iberdomide resistant cell lines.

The effect of opaganib on cell viability was assessed at 24, 48 and 72 hours in CellTiter-Blue assays (top concentration 100µM). N=1, graphs show mean and range.

In general small numbers of CD138+ve myeloma cells were isolated from each patient sample (< 1 million) and therefore assays using low cell numbers in a 96-well plate format were optimised. Initially timepoint and cell seeding density were explored. There was a decrease in cell viability in one sample (RMH022) between 24 and 48 hours in the DMSO treated conditions, suggesting that the assay timepoint should be 24 hours (**Figure 7-19 B**). Cell seeding density was trialled at 20,000 cells per well and 40,000 cells per well. Forty thousand cells provided

a bigger window between DMSO and opaganib and was therefore selected for ongoing experiments (**Figure 7-19 C**). In one sample (RMH038), 3 different concentrations of opaganib were tested and a dose dependent reduction in viability was observed (**Figure 7-19 D**).

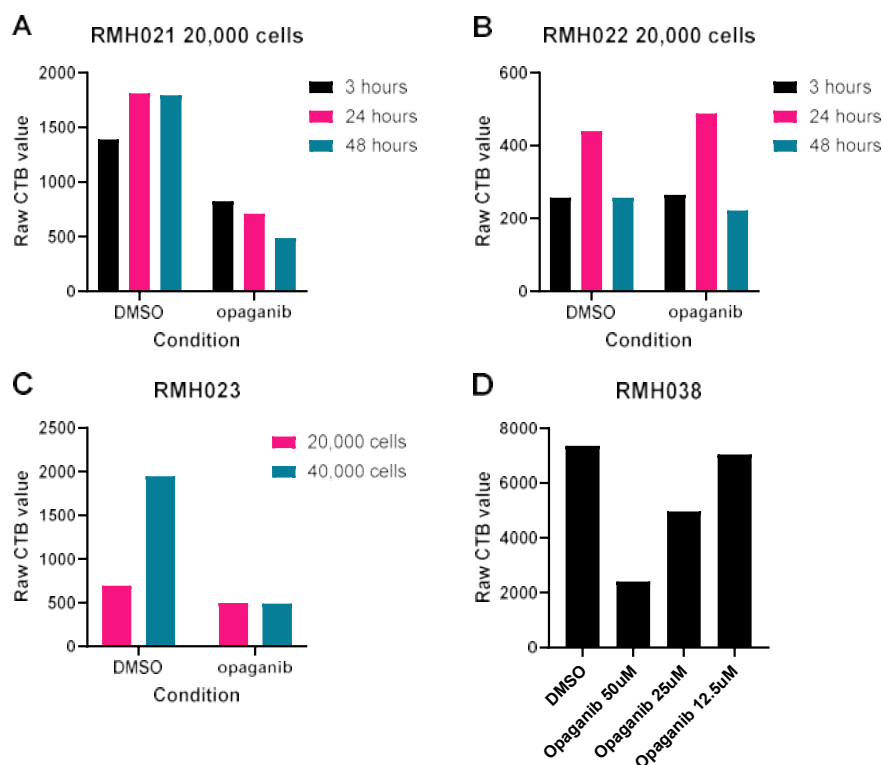


**Figure 7-19** Optimisation of viability assays with opaganib treatment in patient samples.

Cell viability was measured using CellTiter-Blue. A-B) RMH021 showed no change in viability between 24 and 48 hours in the DMSO treated conditions. However, there was a reduction in cell viability between 24 and 48 hours in the DMSO treated conditions in RMH022. This suggested that the assay timepoint should be 24 hours. Opaganib dose was 50µM in these assays. B) Cell seeding density was trialed at 20,000 cells per well and 40,000 cells per well. 40,000 cells provided a bigger window between DMSO and opaganib (at 50µM). C) There was a dose dependent reduction in viability with opaganib treatment at 24 hours with 40,000 cells seeded.

Data was then collated for samples assayed with the same parameters (40,000 cells exposed to opaganib 50µM for 24 hours). Five of the six patient samples showed a clear reduction in viability with opaganib (**Figure 7-20**). Patient characteristics are described in **Table 7-2**.



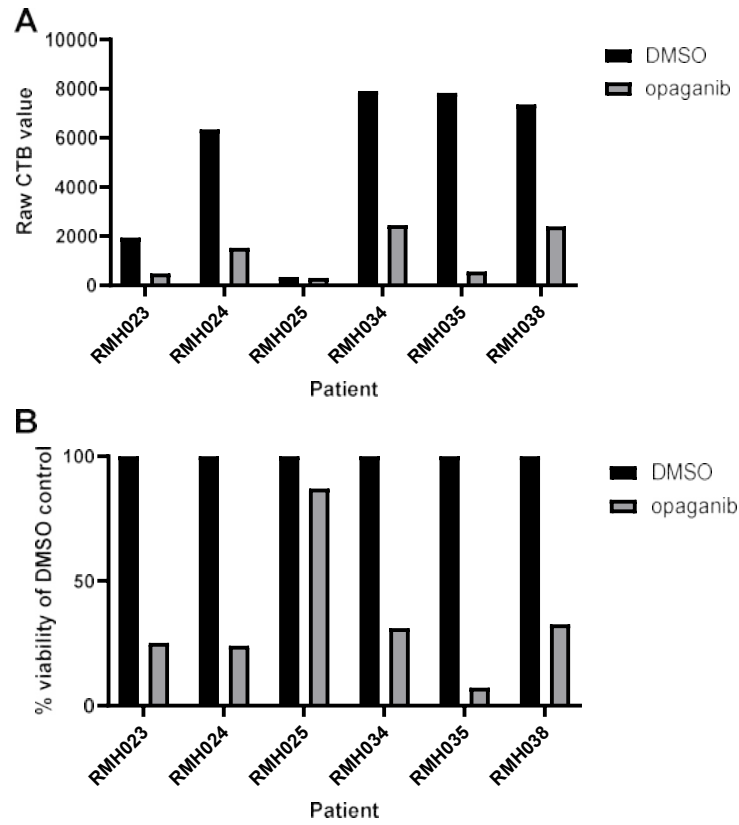


*Figure 7-20 The effect of opaganib treatment on the viability of ex vivo patient myeloma cells.*

24-hour cell viability assays (CellTiter-Blue) were performed with opaganib (50 $\mu$ M). A) shows raw CellTiter-Blue values and B) shows CellTiter-Blue readings normalised to the DMSO control for each patient sample.

Patient ID	Sex	Age	PP class	Light chain type	High risk disease	Line of therapy at time of marrow	Presence of progressive disease at time of marrow	IMiD refractory disease
RMH021	Male	80	IgA	Kappa	Yes	DVD (2 <sup>nd</sup> line)	Yes	No
RMH022	Female	65	IgA	Lambda	No	Isa/Pom/Dex (5 <sup>th</sup> line)	Yes	Yes
RMH023	Male	55	IgG	Kappa	Yes	Lenalidomide (2 <sup>nd</sup> line)	Yes	Yes
RMH024	Male	71	IgG	Kappa	No	No treatment (post ASCT 1 <sup>st</sup> line)	Yes	No
RMH025	Male	66	IgG	Kappa	No	IRD (3 <sup>rd</sup> line)	Yes	Yes
RMH034	Female	67	IgG	Kappa	Unknown	N/A	New diagnosis	Unknown
RMH035	Male	80	IgG	Lambda	Yes	Cyclo/pom/dex (4 <sup>th</sup> line)	Yes	Yes
RMH038	Female	75	IgA	Lambda	Yes	Lenalidomide (2 <sup>nd</sup> line)	Yes	Yes

*Table 7-2 Patient characteristics of samples exposed to opaganib.*

The characteristics of the eight patients who had available bone marrow samples for opaganib testing are presented. Adverse cytogenetic disease was defined as the presence of  $\geq 1$  of t(4;14), t(14;16), t(14;20), 1q+ and 17p-. DVD, daratumumab/bortezomib/dexamethasone; Isa/Pom/Dex, isatuximab, pomalidomide, dexamethasone; IRD, ixazomib, lenalidomide, dexamethasone. Progressive disease was defined by International Myeloma Working Group (IMWG) guidelines (194). IMiD refractory disease was also defined by IMWG criteria (presenting with non-responsive disease while on a IMiD-containing therapy or progressing within 60 days of the last dose of IMiD) (195).

### 7.3 Discussion

Changes in lipid synthesis pathway proteins were observed in the IMiD/CELMoD resistant cell lines on whole proteome analysis (**Section 3.2.4**). In addition, the genome wide CRISPR screen (**Section 5.2.3**) had highlighted knockout of *SCD* and *MBTPS1* as potential novel vulnerabilities in the IMiD/CELMoD-resistant state. Therefore, two independent datasets had both indicated that lipid metabolism could be important in IMiD/CELMoD resistance, and this chapter focused on exploring this avenue of research further.

Clonal competition assays confirmed that *SCD* and *MBTPS1* were dependencies in both the Ctrl-Iber-MM1s and Iber-R-MM1s cell lines (**Section 3.2.4**). However, the experimental design was not able to distinguish whether Iber-R-MM1s proliferation was more sensitive to the knockout of *SCD* and *MBTPS1* than the control line, because of variabilities such as viral transduction efficiency and Cas9 activity in the two cell lines. This would be better assessed in drug inhibitor assays, in which confounding factors can be more easily controlled. The clonal competition assay could not be performed in the Ctrl-Iber-H929 and Iber-R-H929 cells because, despite efforts, Cas9 could not be stably expressed in these lines.

The *MBTPS1* inhibitor PF-429242 reduced viability to a greater extent in the IMiD/CELMoD-resistant H929 cell lines compared to control. However, the inhibitor was only active in the MM1s lines at high concentrations and so no differential response could be detected. Unfortunately, neither of the two *SCD* inhibitors tested were active in control or resistant MM1s or H929 cell lines. Therefore, novel inhibitors of *MBTPS1* and *SCD* would be of great interest as research tools but also potentially as therapies for IMiD-resistant myeloma patients. For example, SSI-4 is a newly developed *SCD* inhibitor shown to have activity in hepatocellular carcinoma cell lines and patient-derived xenograft models (196).

Whole proteome analysis showed that all of the resistant cell lines had changes in lipid metabolism proteins (**Section 3.2.4**). *SCD* was one of only 3 proteins (*SCD*, *CRBN* and *FAM169A*) that were changed in all 6 of the resistant cell lines (log<sub>2</sub> fold change +/-0.2, adj p value <0.05) and 5 of the resistant cell lines showed enrichment of lipid metabolism pathways on functional enrichment

analysis of downregulated proteins. The next important question was whether these changes in proteins led to altered lipid flux through cells. Labelled glucose experiments suggested that the activity of fatty acid synthesis and the activity of fatty acid desaturation were both reduced in the IMiD/CELMoD-resistant cell lines. In addition, the percentage of lipogenic acetyl-CoA derived from glucose was reduced in Iber-R-H929, which suggests alternative carbon sources may be used to generate acetyl-CoA. In summary, these results provide early evidence that lipid flux through cells is altered in the IMiD/CELMoD-resistant setting, but it would be useful to validate these findings by expanding this work to include all of the resistant cell line pairs.

It was then important to confirm that changes in lipid metabolism pathways also occur in patients as they become resistant to IMiDs. Using a large pre-existing dataset, the mRNA expression of several lipid pathway genes was found to be altered between diagnosis and relapse on lenalidomide. However, one limitation of this dataset was that the samples were unpaired and heterogeneity between patients can lead to difficulty interpreting the results. Furthermore, the lipid pathway changes in the resistant cell lines were seen at the protein level, rather than the RNA level, and *SCD* and *MBTPS1* were not consistently altered in the resistant cell lines at the mRNA level. In the proteomics data *SCD* was decreased in all of the resistant cell lines, but in the BMS/Celgene mRNA dataset *SCD* expression was increased in lenalidomide resistant patients. This disconnect could be related to a feedback loop, in which cells are trying to compensate for the low level of *SCD* protein by upregulating mRNA transcription. However, this would imply a block on *SCD* protein expression or increased *SCD* turnover. In the BMS/Celgene dataset *MBTPS1* mRNA expression was decreased in lenalidomide resistant patients. *MBTPS1* was not detected in the MM1s proteomics but was upregulated in Pom-R-H929 (log<sub>2</sub> fold change 0.30, adj p <0.006) and was not significantly changed in Len-R-H929 or Iber-R-H929.

Interestingly, there was also a correlation between *MBTPS1* and *SCD* mRNA expression in bone marrow samples from newly diagnosed myeloma patients and outcomes such as PFS and OS. High *MBTPS1* or *SCD* expression was associated with significantly shorter PFS and shorter OS than low expression.

This provides supporting evidence that inhibition of MBTPS1 or SCD could be a feasible therapeutic strategy for patients.

Given the limitations with the BMS/Celgene mRNA dataset, paired myeloma cell samples (newly diagnosed and relapsed on lenalidomide) from 4 patients were examined by proteomics. Large scale proteomics has not previously been conducted in primary myeloma patient samples. Functional enrichment analysis of commonly downregulated proteins highlighted metabolic pathways and cholesterol metabolism, in keeping with cell line data. Furthermore, folate pathways were enriched, which were also highlighted in pathway analysis of novel dependencies identified by the Chronos analysis of the CRISPR screen data (**Figure 5-10**). Functional enrichment analysis of commonly upregulated proteins identified signalling by Rho GTPases pathway which was also enriched in the resistant setting in the cell line phosphoproteomics (**Figure 3-23, Figure 3-24**). Of note, there was only one commonly upregulated protein (with a log<sub>2</sub> fold change of  $\geq 1$ ) in all of the relapse samples (compared to their respective baseline samples), *IGLL5*. An analysis of the CoMMpass study (NCT01454297) found that the risk of early progressive disease after first line therapy was associated with *IGLL5* mutations (197). Point mutation and translocations in *IGLL5* have been identified in patient myeloma cells and are likely to contribute to myeloma pathogenesis, although their functional significance remains unknown (197). In summary, it appeared that the changes observed in the cell line models are broadly reflective of changes observed in IMiD-resistant patients.

I then wanted to develop an in vitro system in evaluate the effect of lipid targeting drugs on the viability of patient plasma cells. Patient myeloma cells remained viable in vitro for a period 24 hours. Unfortunately there was not an available MBTPS1 or SCD inhibitor that affected cell viability within this time frame. However, I was able to explore the effect of opaganib, a sphingosine kinase 2 inhibitor which has been assessed in a phase 1 study in relapsed and/or refractory myeloma patients (193). If time had allowed, I would have explored the use of inhibitors in models that support patient myeloma cell survival in vitro for prolonged periods, potentially using co-culture with bone marrow stroma cells (198). As new inhibitors of MBTPS1 and SCD become available it would be very

interesting to test them on patient myeloma cells or potentially in patient derived mouse xenograft models.

In summary, the data in this chapter confirms altered lipid metabolism in the IMiD/CELMoD-resistant setting and suggests these changes could represent novel targets for myeloma treatment.

## Chapter 8 Discussion

---

### 8.1 The importance of IMiD resistance in the treatment of myeloma patients

The treatment landscape of myeloma is rapidly evolving, particularly with the development of immunotherapies such as CAR-T cells and bispecific antibodies. Nevertheless, these novel treatments are not curative and combination therapy remains a core principle of myeloma treatment. IMiDs form a critical part of combination regimes and can also be used as a monotherapy in maintenance strategies. However, resistance inevitably develops in patients on continuing treatment. Therefore, understanding mechanisms of resistance and treating resistant disease is critical to improving patient outcomes.

The aim of the work presented in this thesis was to increase our understanding of the mechanisms driving the development of IMiD resistance and to find ways to reverse or treat the IMiD-resistant state. To do this I generated and characterised several cell line models of IMiD/CELMoD resistance. I used two different myeloma cells lines with different genetic backgrounds (MM1s and H929) and three different compounds (lenalidomide, pomalidomide and iberdomide). The IMiD/CELMoD-resistant cell lines were specifically resistant to IMiDs/CELMoDs and did not display cross resistance to a range of other drugs, as shown in a screen of nearly 500 compounds. Below is a table summarising some of the key features of the resistant lines (**Table 8-1**).

	Low CRBN expression	CRBN copy loss	CRBN mutation	Low SCD expression	Enrichment of lipid pathways	Increased sensitivity to SETD2 inhibition
Len-R-MM1s	✓	x	x	✓	✓	✓
Pom-R-MM1s	✓	x	✓	✓	x	✓
Iber-R-MM1s	✓	x	x	✓	✓	✓
Len-R-H929	✓	✓	x	✓	✓	✓
Pom-R-H929	✓	✓	✓	✓	✓	✓
Iber-R-H929	✓	x	✓	✓	✓	✓

*Table 8-1 Key features of the resistant cell lines.*

This table summarises some of the key features of the 6 resistant cell lines. Enrichment of lipid pathways was observed in functional enrichment analysis of downregulated proteins. There was a trend towards increased sensitivity to SETD2 inhibition in IMiD/CELMoD-resistant cell lines compared to IMiD/CELMoD-sensitive control lines.

Whilst cell line models do not always closely reflect the patient state, primary myeloma cells do not survive and proliferate in vitro and therefore to perform experiments requiring a large number of cells, such as the drug screen and the genome wide CRIPSR screen presented here, cell line models had to be used. However, where possible I then validated key findings using pre-existing patient datasets and patient samples in the laboratory.

Another issue with using cell line models, or isolated patient myeloma cells, is that the bone marrow microenvironment is not encapsulated. This niche is critically important in the initiation and progression of myeloma and must be considered when exploring new mechanisms of resistance. Myeloma evolution and drug resistance occurs secondary to intrinsic changes in the myeloma cell but also cellular interactions within the bone marrow niche. It is important to explore any potential therapeutic targets in the context of mixed cellular models or animal models to assess the complex influences of the microenvironment.

During the work presented in this thesis I initially undertook a multiomics approach to understanding IMiD/CELMoD resistance. This allowed me to take an



agnostic path to the identification of novel pathways and targets. However, with this approach many candidate genes and proteins are identified, and it can be difficult to narrow down targets for further exploration. I focused on genes/proteins that were highlighted in more than one analysis and those for which there was a plausible biological mechanism for importance in myeloma. These targets and pathways could then be explored in a more focused manner.

## **8.2 Mechanisms driving the development of IMiD/CELMoD resistance**

### **8.2.1 Reduction in CRBN expression as a key driver of resistance generation**

The IMiD sensitive MM1s and H929 cell lines were cultured with low doses of different IMiDs/CELMoDs over a period of several weeks until resistance developed. All of the resistant lines showed a significant reduction in CRBN levels by quantitative proteomics, although this was less pronounced in Len-R-H929. In the resistant lines there was a reduction in the degradation of Ikaros and Aiolos on treatment with IMiDs/CELMoDs (compared to their sensitive counterparts) indicating that the function of these compounds was abrogated in the resistant state.

The reduction in CRBN observed in the acquired resistant cell lines could be related to alterations that occur in the cells when exposed to IMiDs/CELMoDs. However, it is also possible that there are cells within the initial IMiD/CELMoD sensitive cell pool that already have low levels of CRBN expression, and these cells are selected for and proliferate. Natural selection of a pre-existing cell population better adapted to exist in a certain environment (in this case the presence of IMiD/CELMoD) is a fundamental biological principle. To explore this further would require detailed evaluation of the initial batch of MM1s and H929 cells used in the experiment, as well as cells at various time points along the course of resistance generation (potentially with single cell sequencing or proteomics). This difference in how drug resistance arises, de novo in the cells or from a population of pre-existing cells with a survival advantage, is also very important in patients. If pre-existing populations carrying potential resistance generating alterations could be identified, even at very low levels, prior to commencing treatment with a specific agent this may help to predict how quickly

resistance is likely to occur. Studies of serial samples from patients exposed to each agent would enable study of this concept and exploration of this hypothesis.

The reduction in CRBN abundance is likely the major cause of resistance in the resistant cell lines given the central role of CRBN in the function of IMiDs/CELMoDs. Indeed CRBN was one of only 3 proteins with altered expression in all of the resistant cell lines (with a log<sub>2</sub> fold change +/- 0.2, adj p <0.05). Re-expression of CRBN in the resistant lines led to a degree of partial re-sensitisation to IMiDs/CELMoDs. However, it was not possible to re-express CRBN in the resistant lines to the same level as their matched controls, potentially because CRBN was being inserted into lowly transcribed areas of the genome or the promoter driving CRBN expression was weak. It would therefore be interesting to see if the expression of more CRBN (to match the abundance observed in the control lines) would be able to further restore sensitivity in the resistant lines, or if complementary pathways were also influencing IMiD/CELMoD response. A further indication of the critical nature of CRBN levels came from the Len-R-H929 line. This cell line only had a small reduction in CRBN compared to its control line and resistance could be overcome by the more potent CRBN binders. However, Iber-R-H929 regained CRBN expression when it was cultured without iberdomide (i.e. the selection pressure was removed) but still remained resistant to IMiD/CELMoD treatment. Therefore, there are likely to be other mechanisms influencing resistance.

Immunohistochemical staining of paired diagnosis and lenalidomide refractory bone marrow biopsy samples has suggested that CRBN loss in patients is associated with IMiD resistance (74). However, one previous small proteomics study of 5 patients with paired diagnosis and relapse (on IMiD) samples did not show a reduction of CRBN expression in any of the patients at relapse (103). In the work presented in this thesis, whole proteome analysis using a TMT-multiplexing approach was performed on paired diagnosis and relapse (on lenalidomide) samples from 4 patients who had been enrolled in the Myeloma XI trial. One patient showed a large reduction in CRBN expression at relapse compared to diagnosis (log<sub>2</sub> fold change -0.72), with a second patient showing a smaller reduction (log<sub>2</sub> fold change -0.15). Therefore, reduction in CRBN levels may explain the cause of acquired IMiD resistance in some patients but does not

explain all cases. The models explored in this thesis are likely to be more representative of the subset of patients with reduced *CRBN* levels. Proteomics in a larger number of paired patient samples would enable us to further understand the frequency of reduced *CRBN* abundance in IMiD-refractory patients.

### **8.2.2 The multifactorial nature of *CRBN* reduction**

Three of the resistant lines (Pom-R-MM1s, Pom-R-H929 and Iber-R-H929) had *CRBN* mutations predicted to have a high impact on protein function and led to reduced protein abundance. However, the splice-site mutation found in Pom-R-MM1s had a variant allele frequency (VAF) of 26% and therefore this may not completely explain the large reduction in *CRBN* protein abundance (log<sub>2</sub> fold change -1.07, adj p <0.001) observed in the cell line.

Len-R-H929 and Pom-R-H929 both showed copy number loss at the *CRBN* locus, which has been identified as a potential resistance mechanism in patients (90). In Len-R-H929 this copy number loss may explain the small reduction in *CRBN* protein abundance. Pom-R-H929 showed the largest copy number loss at the *CRBN* locus of any of the resistant lines and also had an early stop codon mutation in *CRBN*. This cell line may therefore contain two distinct populations of cells with each of these features. Single cell analysis would help to distinguish whether these events occurred in the same or different cells.

The Len-R-MM1s and Iber-R-MM1s cell lines had very low *CRBN* levels without any detected mutations in *CRBN* or copy number loss at the *CRBN*, *COPS7B* or *COPS8* loci. Low levels of *CRBN* expression could be related to epigenetic changes. For example, it has previously been shown that DNA hypermethylation of an active intronic *CRBN* enhancer region downregulates *CRBN* expression (92). It would therefore be interesting to assess the methylation status of the promoter and enhancer regions in the *CRBN* gene, and also other epigenetic signatures, in the resistant cell lines. In addition, high exon-10 splicing of the *CRBN* transcript has been shown to lead to IMiD-resistance (91) but this could not be explored in the RNA-Seq data because of the library preparation used.

### **8.2.3 Implications for patients**

IMiD-resistant disease is associated with a reduction in *CRBN* abundance in a subset of patients. If designing trials to develop treatments specifically for the

IMiD/CELMoD-resistant group, it will be important to assess patients for CRBN expression levels. Patients with different CRBN levels may respond differently to CRBN binders. For example, resistant patients with ongoing CRBN expression may respond to more potent CRBN binders (just as Len-R-H929 was sensitive to mezigdomide and CC-885). Finding more potent CRBN binders could be achieved by screening cell lines with acquired resistance to IMiDs that have low CRBN levels, for example an H929 cell line with acquired resistance to lenalidomide was used to identify mezigdomide (119). A cell line with acquired iberdomide or mezigdomide resistance could potentially be used to find even more potent CRBN binders. It would be interesting to explore if there was a threshold level of CRBN below which even the most potent CRBN binders cannot function.

It would also be important to assess patient myeloma cells for *CRBN* mutations. Some mutations might not affect protein levels of CRBN but could still cause the expression of totally non-functional CRBN. These patients might not respond to even the most potent CRBN binders. However, other mutations might lead to the expression of partially functional CRBN or not affect CRBN function at all. It would be possible to model different *CRBN* mutations in the laboratory, either in silico or in cell line models, to predict response to IMiDs/CELMoDs.

Another way to assess whether patient myeloma cells have functional CRBN would be to explore the degradation of Ikaros and Aiolos in response to treatment with CRBN binders ex vivo, detecting the reduced levels of these neosubstrates by western blot or quantitative proteomics. It would then be possible to see if the ability to degrade Ikaros and Aiolos correlated with response to treatment and could be used as a predictive biomarker.

### **8.3 Treating the IMiD/CELMoD resistant state**

Conceptually, targeting drug resistant disease could be achieved by either reversing the IMiD/CELMoD-resistant state (allowing effective IMiD/CELMoD treatment to be continued) or by exploiting novel vulnerabilities that might develop during the course of resistance generation.

### 8.3.1 Reversing the IMiD/CELMoD resistant state

Low CRBN is a uniting feature of the generated resistant cell line models and is also observed in a subset of patients with IMiD-refractory disease. Therefore, finding ways to increase functional CRBN expression might lead to the reversal of resistance. This could potentially be achieved through the use of epigenetic drugs that might alter CRBN expression.

To find ways to reverse IMiD/CELMoD-resistance, either by restoring CRBN levels or through alternative pathways, I carried out a genome wide knockout CRISPR screen in Iber-R-MM1s. This screen would identify genes that when knocked out could restore IMiD/CELMoD sensitivity. Any validated genes could then be assessed further to see if their knockout affected CRBN levels. In the screen the knockout of any single gene in Iber-R-MM1s did not restore sensitivity to iberdomide. This may reflect the complexity of resistance and its multifactorial nature.

### 8.3.2 Targeting novel vulnerabilities that develop during the acquisition of IMiD/CELMoD resistance

I also wanted to explore whether the development of IMiD/CELMoD resistance might induce pathway alterations in myeloma cells that could lead to novel vulnerabilities. These pathway alterations could be the cause of low CRBN, the consequence of low CRBN, or unrelated to CRBN changes; however, in any case, they could still be exploited to treat resistant disease.

A screen of nearly 500 compounds was performed in Iber-R-MM1s and no compounds led to a greater reduction in viability in the resistant line compared to the control line. I then used the data generated by the genome wide CRISPR screen, also performed in Iber-R-MM1s, to evaluate the effect of knocking out each gene on cell fitness in the resistant state. This generated gene effect scores for each gene in Iber-R-MM1s that could be compared to publicly available data from DepMap for parental MM1s. The knockout of several individual genes, including *SETD2*, *SCD* and *MBTPS1*, was suggested to reduce proliferation more in Iber-R-MM1s compared to parental MM1s. Therefore, these genes might represent novel dependencies in the resistant state.

### ***SETD2 inhibition in the IMiD/CELMoD resistant state***

Targeting SETD2 as a strategy to treat IMiD/CELMoD-resistant disease was of particular interest because the SETD2 inhibitor EZM0414 is currently being evaluated in a phase 1 trial including patients with myeloma and diffuse large B cell lymphoma (DLBCL) (NCT05121103). SETD2 inhibition was being explored in these B cell malignancies because histone modifications play a key role in both diseases, with histone H1 mutations frequently driving DLBCL development and H3K36 methylation changes playing a critical pathogenic role in the t(4;14) subgroup of myeloma patients (176). In the work presented in this thesis, SETD2 inhibition was found to reduce viability to a greater extent in the IMiD/CELMoD-resistant lines compared to sensitive control lines, which is a novel finding.

To explore this phenomenon paired RNA-Seq and ChIP-Seq experiments were performed. Treatment with the SETD2 inhibitor EPZ-719 led to reduced expression of 3 transcripts (*NCAM1/CD56*, *EMP2* and *TMSB15A*) to a greater extent in Iber-R-MM1s and Iber-R-H929 compared to their respective controls. *NCAM1/CD56* is present at variable levels in about 70% of myeloma patients, and its presence is associated with inferior clinical outcomes (180). *NCAM1/CD56* is highly expressed in the H929 cell line and has lower expression in the MM1s cell line. *NCAM1/CD56* silencing in cell line models (H929, OPM-2 and RPMI-8226) has been shown to lead to reduced myeloma cell growth and apoptotic cell death (180). Therefore, a possible mechanism of action of SETD2 inhibition in the H929 lines could be reduction of *NCAM1/CD56* leading to cell death (which was enhanced in the IMiD/CELMoD resistant cell lines). Supporting this, ChIP-Seq showed a reduction in H3K36me3 binding over the genomic region of *NCAM1/CD56* with EPZ-719 treatment in both the resistant and sensitive H929 cell lines.

*NCAM1/CD56* reduction could also explain the increased sensitivity of IMiD/CELMoD-resistant MM1s cell lines to SETD2 inhibition. The reduction in proliferation in the IMiD/CELMoD-resistant setting was less pronounced in the MM1s cell line pairs compared to the H929 cell line pairs. *NCAM1/CD56* was not identified as an essential gene in the Iber-R-MM1s CRISPR screen but this could be due to technical reasons, such as the efficiency of the genetic knockout. Furthermore, if *NCAM1/CD56* knockout only leads to a small reduction in 'fitness'

of MM1s cell lines this might not be detectable (depending on the resolution of the screen).

To explore this further, it would initially be important to see if SETD2 inhibition reduces NCAM1/CD56 levels, which could be done by flow cytometry. NCAM1/CD56 could then be genetically manipulated in control and resistant H929 and MM1s cell lines. However, it is also possible that reduction in cell proliferation in response to SETD2 inhibition might be related to reduced expression of a combination of genes. It is also necessary to consider why SETD2 inhibition is more active in the IMiD/CELMoD-resistant state. The resistant cell lines all have reduced CRBN and a relationship between NCAM1/CD56 and CRBN has previously been suggested (182).

The mechanism behind SETD2 reduction as a novel vulnerability in the acquired IMiD/CELMoD-resistant cells lines is yet to be fully explained but the RNA-Seq data presented in this thesis provides some interesting avenues for further research. The cell line data suggests that IMiD/CELMoD-resistant patients may benefit from treatment with SETD2 inhibition, and it will be important to see how the IMiD-refractory subgroup of patients responds in the clinical trial setting. Given EZM0414 is currently in a clinical trial, rapid translation to treat IMiD-resistant patients would be possible. Performing a subanalysis of IMiD-resistant versus IMiD-sensitive patients would be interesting if numbers allow a properly powered comparison. If NCAM1/CD56 reduction was indeed found to be important in the mechanism of action of SETD2 inhibition, it would then be interesting to explore NCAM1/CD56's role in myeloma further and also consider if NCAM1/CD56 could be used a response biomarker to SETD2 inhibition.

### ***Changes in lipid metabolism in the IMiD/CELMoD resistant state***

The second major finding of this thesis was that the acquisition of IMiD/CELMoD resistance is associated with alterations in lipid metabolism which may represent targetable vulnerabilities. A number of lipid metabolism proteins had reduced abundance in the resistant cell lines, including SCD which was one of only 3 proteins with commonly altered expression in all 6 resistant cell lines compared to control (log<sub>2</sub> fold change +/- 0.2, adj p <0.05). Lipid pathways, including SREBP, fatty acid metabolism and cholesterol biosynthesis, were commonly enriched in 5 out of the 6 resistant lines when functional enrichment analysis was

performed on downregulated proteins. Furthermore, labelled glucose experiments confirmed reduced lipid flux through the resistant cell lines compared to their control lines. I then wanted to confirm that the lipid pathway changes seen in the cell line models were reflective of IMiD-resistant patients. Four paired (diagnosis and relapse on lenalidomide) patient samples were evaluated by proteomics and functional enrichment analysis of downregulated proteins (in  $\geq 2$  patients) highlighted metabolic pathways and cholesterol metabolism pathways, in keeping with the cell line data.

Changes in lipid metabolism in IMiD/CELMoD-resistant myeloma cells might also be detectable in the blood. Testing patients' myeloma cells for protein or lipid changes requires patients to undergo a painful bone marrow biopsy. However, it has previously been shown in a small study of myeloma patients that metabolite changes during the disease course can be detected in serial serum blood samples (199). If the lipid changes associated with IMiD/CELMoD resistance could be detected in the blood this might allow us to identify early markers of IMiD resistant disease and biomarkers of disease outcome.

It is also important to consider why IMiD/CELMoD resistance leads to changes in lipid metabolism proteins. A cell line with acute knockout of *CRBN* did not show enrichment of lipid metabolism pathways on functional enrichment analysis of down-regulated proteins. However, acute knockout of *CRBN* and a slow reduction in *CRBN* over time are very different processes. Interestingly only one patient showed a large reduction in *CRBN* (log<sub>2</sub> fold change -0.72) at relapse and this patient was the only patient to have reduced *SCD* (log<sub>2</sub> fold change -0.28) at relapse. Alternatively, altered lipid metabolism in the resistant state may be independent of *CRBN* and related to changes in other pathways.

An analysis of the CRISPR screen data suggested that the individual knockout of two lipid metabolism genes, *MBTPS1* and *SCD*, led to a greater reduction in proliferation in Iber-R-MM1s cells compared to parental MM1s. *MBTPS1* and *SCD* were confirmed to be essential genes by clonal competition assay and treatment with the *MBTPS1* inhibitor PF-429242 led to a greater reduction in viability in the IMiD/CELMoD-resistant H929 lines compared to their sensitive counterparts. PF-429232 reduced viability in the H929 lines after 5 days of



exposure and therefore unfortunately this compound could not be explored in ex vivo patient samples (which survived for only 24-48 hours).

MBTPS1 and SCD represent exciting targets for the treatment of IMiD/CELMoD resistant myeloma and based on the data presented here novel compounds should be developed. I hypothesise that the decreased levels of lipid metabolism proteins in the resistant state leads to a condition similar to that of haploinsufficiency, allowing an inhibitor to act preferentially in the resistant state.

Future work includes more extensive compound testing of newly available SCD inhibitors, using models incorporating primary myeloma cells with bone marrow stroma support. It would also be important to work with chemistry teams to develop MBTPS1 and SCD inhibitors with optimised ADMET (absorption, distribution, metabolism, excretion and toxicity) properties which could be tested in vivo (initially in patient derived mouse xenograft models).

## **8.4 Wider implications**

### **8.4.1 Implications for other malignancies**

Whilst IMiDs/CELMoDs are predominately used for the treatment of myeloma, lenalidomide has single agent activity in a range of B cell malignancies, and in combination therapy leads to durable responses in chronic lymphocytic leukaemia (CLL) and several non-Hodgkin lymphomas (NHLs) including follicular lymphoma (FL), diffuse large B cell lymphoma (DLBCL) and mantle cell lymphoma (MCL) (77). Indeed lenalidomide in combination with rituximab has been approved for the treatment to relapsed/refractory follicular lymphoma (77). Furthermore, the CELMoD avadomide has shown promising early clinical efficacy in DLBCL (77). Therefore, understanding mechanisms of resistance has implications for other B cell malignancies.

As we learn more about the mechanisms of resistance to IMiDs/CELMoDs this will also aid our understanding of possible resistance mechanisms to novel molecular glues and PROTACs (small molecules that induce the ubiquitination and subsequent degradation of target proteins). To date, the only FDA approved molecular glues are thalidomide, lenalidomide and pomalidomide but novel glues are being studied in clinical trials. For example, MRT-2359 is a GSPT1 (G1 to S Phase Transition 1)-directed molecular glue, currently being tested in patients

with a wide range of cancers including non-small cell lung cancer, small cell lung cancer, high-grade neuroendocrine cancers, DLBCL and solid tumours with L-MYC or N-MYC amplification (NCT05546268). A molecular glue brings together the substrate of interest, in this case GSPT1, with the substrate receptor of a ubiquitin ligase, in this case CRBN. Therefore, it can be hypothesised that downregulation of CRBN could potentially occur if this drug is given for a prolonged period and this could lead to therapy resistance.

SETD2 inhibition is currently being evaluated for the treatment of myeloma and DLBCL (NCT05121103) and the RNA-Seq and ChIP-Seq data presented in this thesis may also provide insights into the mechanism of action of SETD2 inhibition in DLBCL. However, the mechanism of action may differ between the two B cell malignancies, as NCAM1/CD56 expression in DLBCL is rare and its clinical relevance is currently unknown (200). The work presented in this thesis has also highlighted the importance of lipid pathway changes in IMiD/CELMoD resistance. Metabolic changes are emerging as a hallmark of cancer and could provide a wealth of novel therapeutic targets in myeloma and also other haematological malignancies and solid cancers.

#### **8.4.2 The future of IMiD/CELMoD resistance research**

Studying resistance to IMiDs remains complex due to the heterogenous nature of resistance generation in patients. Focussing on common features of resistance where possible is important because targeting these changes may provide therapeutic benefit to the greatest number of patients. As we move forwards, exploring resistance in patient samples will be critical. Performing paired proteomics on patient samples at diagnosis and at relapse on IMiDs/CELMoDs could provide a wealth of information. Our small sample of four patients suggested patient myeloma cells have changes in lipid synthesis pathways at relapse and it would be important to confirm this in a larger cohort. However, paired sample proteomics could also uncover other novel pathway changes and potential therapeutic targets that develop alongside the acquisition of IMiD resistance and enable the development of prognostic signatures. Paired patient sample proteomics could also be coupled with paired metabolomic analysis to assess the metabolite changes that occur in resistance. There is very little paired proteomics in the literature at the moment (103) and expanding this, using well

annotated samples from previous trials or collecting samples prospectively, would be of great interest. Patient myeloma cell samples are a limited and critical resource, so it is also important to optimise the processing of samples for proteomics and metabolomics to limit wastage.

In conclusion, acquired resistance to IMiDs remains a major barrier to improving outcomes for myeloma patients. IMiD/CELMoD resistance can be tackled by exploring ways to restore CRBN levels or by developing compounds that better utilise low levels of CRBN. Alternatively IMiD/CELMoD-resistant disease can be treated by targeting vulnerabilities that develop alongside the generation of resistance. Inhibition of SETD2 may reduce proliferation of IMiD/CELMoD-resistant myeloma cells to a greater extent than their sensitive counterparts, potentially due to reduction of NCAM1/CD56. In addition, changes in lipid metabolism pathways occur in the IMiD/CELMoD-resistant state and MBTPS1 and SCD represent potentially exciting novel drug targets in myeloma.

## Chapter 9 Supplementary Results

### 9.1 Generation and Characterisation of Models to Explore Acquired IMiD/CELMOd Resistance

#### 9.1.1 Proliferation in the resistant and control cell line pairs

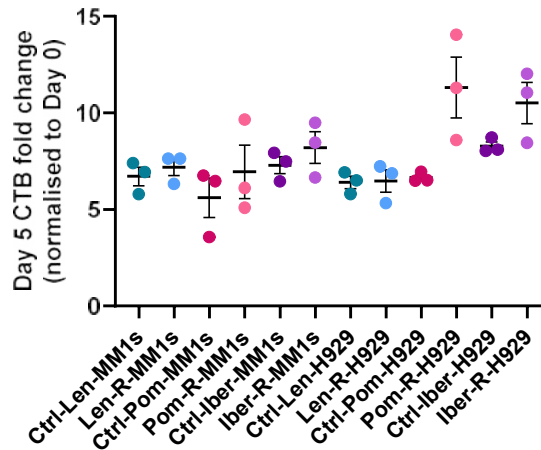


Figure 9-1 Proliferation of the control and resistant cell lines.

10,000 cells were seeded, and CellTiter-Blue (CTB) readings taken at Day 0 and Day 5. Individual points represent independent experiments, n=3. The horizontal bar shows the mean and error bars represent SEM. Paired t-tests showed no significant difference in proliferation in each control and resistant pair.

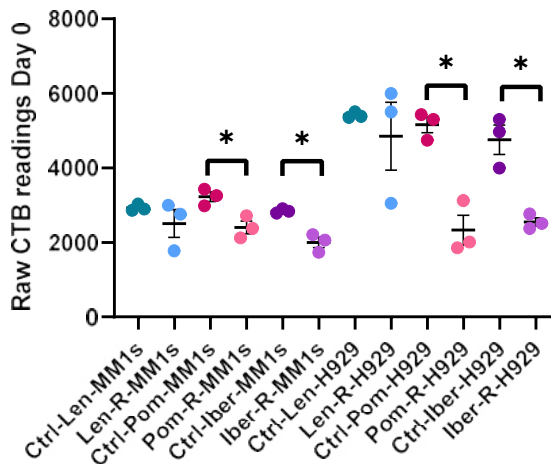


Figure 9-2 Raw CellTiter-Blue readings in the control and resistant cell lines.

The resistant cell lines appear to process CellTiter-Blue (CTB) differently compared to their matched controls. Individual points represent independent experiments, n=3. The horizontal bar shows the mean and error bars represent SEM. Paired t-tests were performed for each pair of control and resistant lines, \* p<0.05.

## 9.1.2 Mutations in the resistant cell lines

Cell line	Mutated genes (with predicted high impact on the resultant protein)
Len-R-MM1s	AC004997.1, Cytosolic Arginine Sensor for MTORC1 Subunit 1 ( <i>CASTOR1</i> ), DS Cell Adhesion Molecule ( <i>DSCAM</i> ), Fibronectin Type III Domain Containing 7 ( <i>FNDC7</i> ), Katanin Regulatory Subunit B1 Like 1 ( <i>KATNBL1</i> ), Marker of Proliferation Ki-67 ( <i>MKI67</i> ), Peptidyl Arginine Deiminase 3 ( <i>PADI3</i> ), Plexin A3 ( <i>PLXNA3</i> ), Solute Carrier Family 38 Member 8 ( <i>SLC38A8</i> ), Syncoilin Intermediate Filament Protein ( <i>SYNC</i> ), WASP Like Actin Nucleation Promoting Factor ( <i>WASL</i> ), Zinc Finger Protein 746 ( <i>ZNF746</i> )
Pom-R-MM1s	ATP Binding Cassette Subfamily A Member 2 ( <i>ABCA2</i> ), AL109761.1, Amyloid Beta Precursor Protein Binding Family A Member 1 ( <i>APBA1</i> ), ATPase H+ Transporting V1 Subunit F ( <i>ATP6V1F</i> ), CD22 Molecule ( <i>CD22</i> ), Cereblon ( <i>CRBN</i> ), Diacylglycerol Kinase Kappa ( <i>DGKK</i> ), Fibronectin Type III Domain Containing 7 ( <i>FNDC7</i> ), Katanin Regulatory Subunit B1 Like 1 ( <i>KATNBL1</i> ), Kinesin Family Member 13B ( <i>KIF13B</i> ), Laminin Subunit Alpha 3 ( <i>LAMA3</i> ), Marker of Proliferation Ki-67 ( <i>MKI67</i> ), Matrix Metalloproteinase 28 ( <i>MMP28</i> ), Polycystin 1 Like 1, Transient Receptor Potential Channel Interacting ( <i>PKD1L1</i> ), Receptor Interacting Serine/Threonine Kinase 4 ( <i>RIPK4</i> ), Ryanodine Receptor 2 ( <i>RYR2</i> ), Solute Carrier Family 4 Member 10 ( <i>SLC4A10</i> ), Signal Peptide Peptidase Like 2B ( <i>SPPL2B</i> ), Spectrin Alpha Erythrocytic 1 ( <i>SPTA1</i> ), Tigger Transposable Element Derived 4 ( <i>TIGD4</i> ), Thrombospondin 3 ( <i>THBS3</i> ), Thioredoxin Like 1 ( <i>TXNL1</i> ), Ubiquitin Protein Ligase E3 Component N-Recognin 2 ( <i>UBR2</i> )
Iber-R-MM1s	ATP Binding Cassette Subfamily A Member 2 ( <i>ABCA2</i> ), Amyloid Beta Precursor Protein Binding Family A Member 1 ( <i>APBA1</i> ), CD22 Molecule ( <i>CD22</i> ), DS Cell Adhesion Molecule ( <i>DSCAM</i> ), Elongation Factor For RNA Polymerase II 2 ( <i>ELL2</i> ), Fibronectin Type III Domain Containing 7 ( <i>FNDC7</i> ), Marker of Proliferation Ki-67 ( <i>MKI67</i> ), Myosin IH ( <i>MYO1H</i> ), Polycystin 1 Like 1, Transient Receptor Potential Channel Interacting ( <i>PKD1L1</i> ), Spectrin Alpha Erythrocytic 1 ( <i>SPTA1</i> ), Syncoilin Intermediate Filament Protein ( <i>SYNC</i> ), Thrombospondin 3 ( <i>THBS3</i> ), Thioredoxin Like 1 ( <i>TXNL1</i> )
Len-R-H929	Acyl-CoA Dehydrogenase Very Long Chain ( <i>ACADVL</i> ), Titin ( <i>TTN</i> ), Thioredoxin Reductase 3 ( <i>TXNRD3</i> )
Pom-R-H929	ATP Binding Cassette Subfamily B Member 11 ( <i>ABCB11</i> ), Ankyrin Repeat Domain 36 ( <i>ANKRD36</i> ), Complement C5 ( <i>C5</i> ), Cyclin T1 ( <i>CCNT1</i> ), Cereblon ( <i>CRBN</i> ), Disco Interacting Protein 2 Homolog B ( <i>DIP2B</i> ), Interferon Gamma Inducible Protein 16 ( <i>IFI16</i> ), Laminin Subunit Gamma 3 ( <i>LAMC3</i> ), Myelin Associated Glycoprotein ( <i>MAG</i> ), MAGUK P55 Scaffold Protein 1 ( <i>MPP1</i> ), Mitochondrial Transcription Rescue Factor 1 ( <i>MTRES1</i> ), Myosin Heavy Chain 1 ( <i>MYH1</i> ), Neurobeachin ( <i>NBEA</i> ), Solute Carrier Family 4 Member 1 Adaptor

	Protein ( <i>SLC4A1AP</i> ), Transforming Acidic Coiled-Coil Containing Protein 2 ( <i>TACC2</i> ), Yes1 Associated Transcriptional Regulator ( <i>YAP1</i> ), Zinc Finger And BTB Domain Containing 41 ( <i>ZBTB41</i> )
Iber-R-H929	Cyclin T1 ( <i>CCNT1</i> ), Cereblon ( <i>CRBN</i> ), Mitochondrial Transcription Rescue Factor 1 ( <i>MTRES1</i> )

*Table 9-1 Mutations present in the resistant cell lines.*

### 9.1.3 Common transcriptome changes in the resistant cell lines

Gene symbol	Full name	Details of protein function
<b>Upregulated</b>		
<i>BIRC3</i>	Baculoviral IAP Repeat Containing 3	Member of the IAP (Inhibitor of Apoptosis) family of proteins that inhibit apoptosis.
<i>CA8</i>	Carbonic Anhydrase 8	Function unclear, does not have carbonic anhydrase catalytic function.
<i>CBLN2</i>	Cerebellin 2 Precursor	Predicted to be involved in the maintenance of synapse structure and spontaneous synaptic transmission.
<i>DOCK4</i>	Dedicator Of Cytokinesis 4	Functions as a guanine nucleotide exchange factor and is involved in regulation of adherens junctions between cells.
<i>FAM169A</i>	Family With Sequence Similarity 169 Member A	Function unknown.
<i>FNBP1</i>	Formin Binding Protein 1	Member of the formin-binding protein family.
<i>KAT6B</i>	Lysine Acetyltransferase 6B	Histone acetyltransferase which may be involved in both positive and negative regulation of transcription.
<i>KCNC4</i>	Potassium Voltage-Gated Channel Subfamily C Member 4	Mediates the voltage-dependent potassium ion permeability of excitable membranes.
<i>KLF10</i>	KLF Transcription Factor 10	Member of a family of proteins that have C2H2-type zinc finger domains. Involved in the regulation of transforming growth factor beta (TGF $\beta$ ) signalling.
<i>MEST</i>	Mesoderm Specific Transcript	Encodes a member of the alpha/beta hydrolase superfamily. May play a role in development.
<i>METTL7A</i>	Methyltransferase Like 7A	Predicted to enable methyltransferase activity.

<i>NEGR1</i>	Neuronal Growth Regulator 1	Function unclear, may be involved in cell adhesion.
<i>NFIX</i>	Nuclear Factor I X	Transcription factor that binds to the palindromic sequence 5'-TTGGCNNNNNGCCAA-3' in viral and cellular promoters.
<i>PLK2</i>	Polo Like Kinase 2	Member of the polo family of serine/threonine protein kinases that have a role in cell division.
<i>ST8SIA2</i>	ST8 Alpha-N-Acetyl-Neuraminide Alpha-2,8-Sialyltransferase 2	Type II membrane protein that catalyses the transfer of sialic acid from CMP-sialic acid to N-linked oligosaccharides and glycoproteins.
<i>SULT1A3</i>	Sulfotransferase Family 1A Member 3	Catalyses the sulfate conjugation of many hormones, neurotransmitters, drugs, and xenobiotic compounds.
<i>TNFAIP3</i>	TNF Alpha Induced Protein 3	Inhibits NFκB activation and TNF mediated apoptosis and has ubiquitin ligase and deubiquitinase activities.
<b>Downregulated</b>		
<i>ANXA9</i>	Annexin A9	Member of a family of calcium-dependent phospholipid-binding proteins.
<i>BBS7</i>	Bardet-Biedl Syndrome 7	Thought to be required for the sorting of specific membrane proteins to primary cilia.
<i>C2</i>	Complement C2	Serum glycoprotein that functions as part of the classical pathway of the complement system.
<i>CMTM7</i>	CKLF Like MARVEL Transmembrane Domain Containing 7	Tumour suppressor that regulates G1/S transition in the cell cycle and influences epidermal growth factor receptor/protein kinase B signalling during tumour pathogenesis.
<i>CRBN</i>	Cereblon	Substrate receptor of the CRL4 <sup>CRBN</sup> E3 ubiquitin ligase.
<i>LINC00665</i>	Long Intergenic Non-Protein Coding RNA 665	RNA Gene, affiliated with the long non-coding RNA class.
<i>MED8</i>	Mediator Complex Subunit 8	Component of the Mediator complex, which is involved in the regulated transcription of nearly all RNA polymerase II-dependent genes.
<i>POGLUT3</i>	Protein O-Glucosyltransferase 3	Protein glucosyltransferase that may be involved in regulation of the NOTCH signalling pathway.

<i>RPS6KA2</i>	Ribosomal Protein S6 Kinase A2	Serine/threonine-protein kinase that acts downstream of ERK (Extracellular Signal Regulated Kinases) signalling.
<i>TBC1D9</i>	TBC1 Domain Family Member 9	Predicted to be involved in activation of GTPase activity and intracellular protein transport.

*Table 9-2 Common differentially expressed genes in the resistant cell lines.*

This table contains the details of 27 transcripts that were commonly changed in  $\geq 5$  of the 6 resistant cell lines compared to their respective controls (log<sub>2</sub> fold change  $\pm$  0.2, adjusted p value of  $<0.05$ ). Details regarding the function of the resultant proteins were taken from GeneCards (147).

#### 9.1.4 Common proteome changes in the resistant cell lines

Protein	Full name	Details of protein function
<b>Upregulated</b>		
AMPD1	Adenosine Monophosphate Deaminase 1	Plays a critical role in energy metabolism.
CA8	Carbonic Anhydrase 8	Function unclear, does not have carbonic anhydrase catalytic function.
CORO1B	Coronin 1B	Regulates cell motility.
FAM169A	Family With Sequence Similarity Member A 169	Function unknown.
GPC4	Glypican 4	Cell surface proteoglycan that may play a role in the control of cell division and growth regulation.
HMGCR	HMG-CoA Reductase	Catalyses the rate limiting step in cholesterol biosynthesis.
MBD3	Methyl-CpG Binding Domain Protein 3	Component of the histone deacetylase NuRD (Nucleosome Remodeling Deacetylase) complex which participates in the remodeling of chromatin.
METTL7A	Methyltransferase Like 7A	Predicted to enable methyltransferase activity.
MX1	MX Dynamin Like GTPase 1	Encodes a guanosine triphosphate (GTP)-metabolising protein that participates in the cellular antiviral response.
ODC1	Ornithine Decarboxylase 1	Catalyses the first (and rate-limiting) step of polyamine biosynthesis.
SP100	SP100 Nuclear Antigen	Tumour suppressor that is a major component of PML (promyelocytic leukaemia) bodies which are involved in cell growth, differentiation and apoptosis.



SP110	SP110 Nuclear Body Protein	Component of the nuclear body, a multiprotein complex that may have a role in the regulation of gene transcription.
SULT1A1	Sulfotransferase Family 1A Member 1	Catalyses the sulfate conjugation of many hormones, neurotransmitters, drugs, and xenobiotic compounds.
SULT1A3/ SULT1A4	Sulfotransferase Family 1A Member 3/4	Catalyses the sulfate conjugation of many hormones, neurotransmitters, drugs, and xenobiotic compounds.
<b>Downregulated</b>		
ACSL4	Acyl-CoA Synthetase Long Chain Family Member 4	Catalyses the conversion of long-chain fatty acids to their active form acyl-CoA, thereby playing a key role in lipid biosynthesis and fatty acid degradation.
ADM	Adrenomedullin	Encodes a preprohormone which is cleaved to form two biologically active peptides, adrenomedullin and proadrenomedullin N-terminal 20 peptide.
CAV1	Caveolin 1	Main component of caveolae plasma membranes.
CKMT1B/C KMT1A	Creatine Kinase, Mitochondrial 1B/A	Responsible for the transfer of high energy phosphate from mitochondria to the cytosolic carrier, creatine.
CRBN	Cereblon	Substrate receptor of the CRL4 <sup>CRBN</sup> E3 ubiquitin ligase.
CRIP1	Cysteine Rich Protein 1	Appears to have a role in zinc absorption and may function as an intracellular zinc transport protein.
FASN	Fatty Acid Synthase	Catalyses the synthesis of palmitate from acetyl-CoA and malonyl-CoA.
FDPS	Farnesyl Diphosphate Synthase	Key enzyme in isoprenoid biosynthesis which catalyses the formation of farnesyl diphosphate (FPP), a precursor for several classes of essential metabolites including sterols, dolichols, carotenoids, and ubiquinones.
HSPB1	Heat Shock Protein Family B (Small) Member 1	Member of the small heat shock protein family of proteins.
MAGED1	MAGE Family Member D1	Involved in the apoptotic response after nerve growth factor (NGF) binding in neuronal cells.
OAT	Ornithine Aminotransferase	Key enzyme in the pathway that converts arginine and ornithine into the major excitatory and inhibitory neurotransmitters glutamate and GABA.
P4HA1	Prolyl 4-Hydroxylase Subunit Alpha 1	Component of prolyl 4-hydroxylase, a key enzyme in collagen synthesis.

PAPSS2	3'-Phosphoadenosine 5'-Phosphosulfate Synthase 2	Bifunctional enzyme which mediates two steps in the sulfate activation pathway.
PCK2	Phosphoenolpyruvate Carboxykinase 2, Mitochondrial	Mitochondrial enzyme that catalyses the conversion of oxaloacetate to phosphoenolpyruvate.
PGRMC1	Progesterone Receptor Membrane Component 1	Putative membrane-associated progesterone steroid receptor.
PLOD2	Procollagen-Lysine, 2-Oxoglutarate 5-Dioxygenase 2	Catalyses the hydroxylation of lysyl residues in collagen-like peptides. The resultant hydroxylysyl groups are attachment sites for carbohydrates in collagen and thus are critical for the stability of intermolecular crosslinks.
PSPH	Phosphoserine Phosphatase	Catalyses the last irreversible step in the biosynthesis of L-serine from carbohydrates.
SCD	Stearoyl-CoA Desaturase	Enzyme involved in fatty acid biosynthesis, primarily the synthesis of oleic acid.
SLC2A1	Solute Carrier Family 2 Member 1	Major glucose transporter in the mammalian blood-brain barrier.
SUOX	Sulfite Oxidase	Catalyses the oxidation of sulfite to sulfate, the final reaction in the oxidative degradation of the sulfur amino acids cysteine and methionine.

*Table 9-3 Common proteins with altered expression in the resistant cell lines.*

Table contains the details of 34 proteins that were commonly changed in  $\geq 4$  of the 6 resistant cell lines compared to their respective controls (log<sub>2</sub> fold change  $\pm$  0.2, adjusted p value of  $< 0.05$ ). Details regarding protein function were taken from GeneCards (147).

### 9.1.5 Common sites of altered phosphorylation in the resistant cell lines

Phosphosite	Protein
<b>Increased phosphorylation</b>	
Q13576 [S16]	Ras GTPase-activating-like protein IQGAP2
Q96T58 [S847]	Msx2-interacting protein
O95236 [S315]	Apolipoprotein L3
P42566 [S796]	Epidermal growth factor receptor substrate 15
P10636 [S519]	Microtubule-associated protein tau
Q13153 [T212]	Serine/threonine-protein kinase PAK 1

P25098 [S670]	Beta-adrenergic receptor kinase 1
Q03164 [3500-3524]	Histone-lysine N-methyltransferase 2A
Q6Y7W6 [S1100]	GRB10-interacting GYF protein 2
Q86VM9 [S868]	Zinc finger CCCH domain-containing protein 18
O14681 [S46]	Etoposide-induced protein 2.4 homolog
Q96T23 [T408]	Remodeling and spacing factor 1
Q15027 [T739]	Arf-GAP with coiled-coil, ANK repeat and PH domain-containing protein 1
Q12802 [T2411]	A-kinase anchor protein 13
O95758 [S56]	Polypyrimidine tract-binding protein 3
A6NC98 [S1379]	Coiled-coil domain-containing protein 88B
Q03164 [S532]	Histone-lysine N-methyltransferase 2A
P35659 [S288]	Protein DEK
P50552 [S305]	Vasodilator-stimulated phosphoprotein
Q7Z2K8 [S615]	G protein-regulated inducer of neurite outgrowth 1
Q92608 [S587]	Dedicator of cytokinesis protein 2
Q96T58 [S623]	Msx2-interacting protein
P16150 [S368]	Leukosialin
Q8N3D4 [S1017]	EH domain-binding protein 1-like protein 1
Q9NYF8 [S397]	Bcl-2-associated transcription factor 1
Q9UEY8 [S681]	Gamma-adducin
Q96T58 [S2120]	Msx2-interacting protein
Q96T37 [S97]	RNA-binding protein 15
P16150 [S351; S355]	Leukosialin
P16150 [S355]	Leukosialin
Q9ULW0 [S252]	Targeting protein for Xklp2
P80723 [S164]	Brain acid soluble protein 1
Q9UN36 [S338]	Protein NDRG2
P42331 [S533]	Rho GTPase-activating protein 25
Q8N3D4 [S1218]	EH domain-binding protein 1-like protein 1
Q96CJ1 [S144]	ELL-associated factor 2
Q9NUL3 [T488; S492]	Double-stranded RNA-binding protein Staufen homolog 2
Q92925 [196-226]	SWI/SNF-related matrix-associated actin-dependent regulator of chromatin subfamily D member 2
O94868 [S675]	F-BAR and double SH3 domains protein 2
P16150 [S336]	Leukosialin
P50579 [S45]	Methionine aminopeptidase 2
P07900 [S231]	Heat shock protein HSP 90-alpha
P21580 [S645]	Tumor necrosis factor alpha-induced protein 3

Q9P0L2 [S414]	Serine/threonine-protein kinase MARK1
<b>Decreased phosphorylation</b>	
P04792 [S15]	Heat shock protein beta-1
P04792 [S82]	Heat shock protein beta-1
P46013 [S2828]	Proliferation marker protein Ki-67
Q13501 [S24]	Sequestosome-1
P46013 [T1923]	Proliferation marker protein Ki-67
P46013 [S584]	Proliferation marker protein Ki-67
P46013 [S1861]	Proliferation marker protein Ki-67
P46013 [S605]	Proliferation marker protein Ki-67
P46013 [T2085]	Proliferation marker protein Ki-67
P46013 [S859]	Proliferation marker protein Ki-67
P46013 [S2505]	Proliferation marker protein Ki-67
P46013 [S3005]	Proliferation marker protein Ki-67
P46013 [T844]	Proliferation marker protein Ki-67
P46013 [1371-1388]	Proliferation marker protein Ki-67
P46013 [S128]	Proliferation marker protein Ki-67
P08670 [S9]	Vimentin
Q14195 [S522]	Dihydropyrimidinase-related protein 3
P53999 [T42]	Activated RNA polymerase II transcriptional coactivator p15
P02545 [S392]	Prelamin-A/C
P02545 [S22]	Prelamin-A/C
Q99490 [S648]	Arf-GAP with GTPase, ANK repeat and PH domain-containing protein 2
P08670 [S51]	Vimentin
P08670 [S29]	Vimentin
P82094 [T401]	TATA element modulatory factor
P16455 [S201]	Methylated-DNA--protein-cysteine methyltransferase
Q9BPX5 [S64]	Actin-related protein 2/3 complex subunit 5-like protein
Q9BY11 [T184]	Protein kinase C and casein kinase substrate in neurons protein 1
Q05655 [S645]	Protein kinase C delta type
Q09666 [S5731]	Neuroblast differentiation-associated protein AHNAK
P47712 [S729]	Cytosolic phospholipase A2
Q9H8Y5 [T607]	tRNA endonuclease ANKZF1
Q92522 [S31]	Histone H1.10
Q9NR19 [S30]	Acetyl-coenzyme A synthetase, cytoplasmic
O43847 [S94]	Nardilysin
Q92934 [S134]	Bcl2-associated agonist of cell death
P49327 [S207]	Fatty acid synthase
Q9BXF6 [S395]	Rab11 family-interacting protein 5

Q9P2M7 [S252]	Cingulin
Q8N3Y1 [S85]	F-box/WD repeat-containing protein 8
Q8IVB4 [S612]	Sodium/hydrogen exchanger 9
Q12873 [S713]	Chromodomain-helicase-DNA-binding protein 3
P51617 [367-380]	Interleukin-1 receptor-associated kinase 1
O75683 [S138]	Surfeit locus protein 6
Q53EU6 [S68]	Glycerol-3-phosphate acyltransferase 3
P48960 [S831]	Adhesion G protein-coupled receptor E5
Q9NNX9 [S27]	Variable charge X-linked protein 3
Q9Y4E6 [S935]	WD repeat-containing protein 7
O95831 [S266]	Apoptosis-inducing factor 1, mitochondrial
Q6ZSZ5 [S155]	Rho guanine nucleotide exchange factor 18
Q3KQU3 [S446]	MAP7 domain-containing protein 1
Q9ULS5 [S216]	Transmembrane and coiled-coil domain protein 3
Q9BXF6 [S482]	Rab11 family-interacting protein 5
Q9C0C4 [S717]	Semaphorin-4C
Q3KQU3 [T97]	MAP7 domain-containing protein 1
Q6GYQ0 [S734]	Ral GTPase-activating protein subunit alpha-1
Q9Y6M7 [75-93]	Sodium bicarbonate cotransporter 3
Q8NEY1 [S1000]	Neuron navigator 1
P49327 [T2204]	Fatty acid synthase
Q9P2M7 [S149]	Rab11 family-interacting protein 1
Q6WKZ4 [S529]	Rab11 family-interacting protein 1
Q8N5J2 [S441]	Ubiquitin carboxyl-terminal hydrolase MINDY-1
Q9P2M7 [S131]	Cingulin
Q9UGP4 [S316]	LIM domain-containing protein 1
Q9H1B7 [S659]	Probable E3 ubiquitin-protein ligase IRF2BPL
O95049 [S164]	Tight junction protein ZO-3
Q9Y6M7 [S233]	Sodium bicarbonate cotransporter 3
Q9BXF6 [S357]	Rab11 family-interacting protein 5

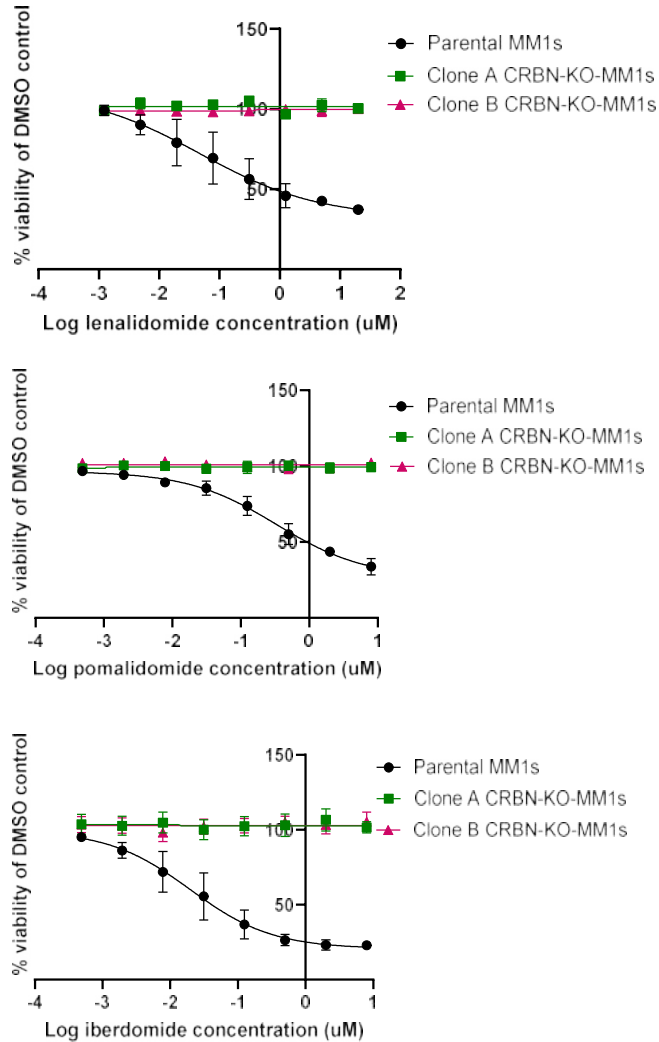
*Table 9-4 Common sites with altered phosphorylation in the resistant cell lines.*

Table contains the details of 111 sites with altered phosphorylation in  $\geq 3$  of the 6 resistant cell lines compared to their respective controls (log<sub>2</sub> fold change  $\pm$  0.2, adjusted p value of  $<0.05$ ).

### 9.1.6 Validation of the *CRBN* knockout MM1s cell lines

Two different *CRBN* knockout models were used during this work, Clone A and Clone B. The clones were generated by Dr Laura Chan using CRISPR-Cas9 and the validation work included below was performed by Dr Yakinthi Chrisochidou. Successful knockout of *CRBN* was confirmed using NGS; Clone A had a homozygous deletion chr3:3172863-3179679 and Clone B had a homozygous

deletion chr3:3179660-3183271. The models were resistant to IMiDs and CELMoDs (**Figure 9-3**), had no CRBN on western blotting (**Figure 9-4**) and did not show degradation of Ikaros and Aiolos (or reduction in *IRF4* mRNA levels) (**Figure 9-5**) with IMiD/CELMoD treatment.



**Figure 9-3** The effect of IMiDs/CELMoDs on the viability of the CRBN knockout MM1s cell lines.

Clone A CRBN-KO-MM1s and Clone B CRBN-KO-MM1s were resistant to lenalidomide, pomalidomide and iberdomide at the highest concentrations tested (20 $\mu$ M, 8 $\mu$ M and 8 $\mu$ M respectively). Cell viability was measured in a CellTiter-Blue assay after 5 days of incubation with each IMiD/CELMoD. N=3, mean and SEM shown.

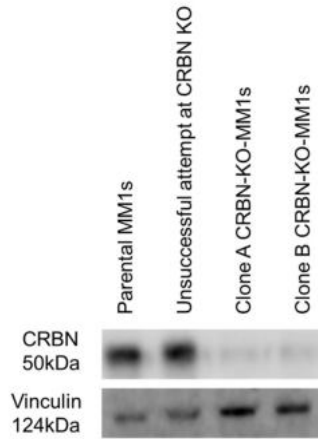


Figure 9-4 CRBN protein levels in the CRBN knockout cell lines.

Clones A and B showed reduced CRBN protein on western blotting compared to parental MM1s (representative blot shown, n=2). An unsuccessful attempt at knockout is also shown on the blot for comparison.

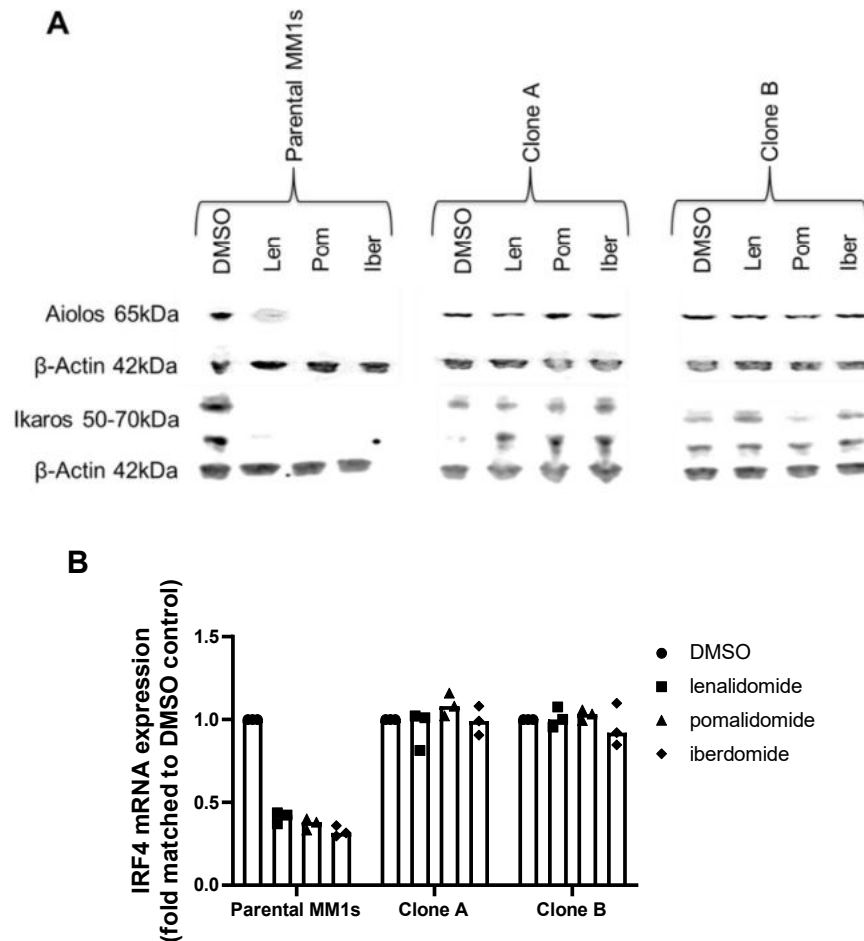


Figure 9-5 The effect of IMiD/CELMOd treatment on Aiolos, Ikaros and IRF4 levels in the CRBN knockout MM1s cell lines.

A) Aiolos and Ikaros were degraded in parental MM1s after 24 hours of IMiD/CELMOd treatment, but this effect was abrogated in the CRBN knockout cell lines (representative western blot, n=2). B) IRF4 mRNA expression (assessed by quantitative RT-PCR) was reduced in parental MM1s after 24 hours of exposure to IMiD/CELMOd but this was not observed in the CRBN knockout lines. Individual points represent independent experiments (n=3) and the bar represents the median. Clone A, Clone A CRBN-KO MM1s; Clone B, Clone B CRBN-KO MM1s.

## 9.2 Identification of Pharmacological Sensitivities in IMiD/CELMoD Resistance

### 9.2.1 Hit compounds from the screen

Proliferation reduced to a greater extent in the resistant cell line (at 800, 200 or 80 nM)	
Name of compound	Description
Bexarotene	A retinoid specifically selective for retinoid X receptors. Used as an oral antineoplastic agent in the treatment of cutaneous T-cell lymphoma.
Gemcitabine HCl (Gemzar)	DNA synthesis inhibitor.
Ganetespib (STA-9090)	HSP90 (heat shock protein 90) inhibitor.
Alisertib (MLN8237)	Selective Aurora A inhibitor with a >200-fold higher selectivity for Aurora A than Aurora B.
Bendamustine HCl	DNA-damaging agent.
Floxuridine	Prodrug that is rapidly catabolised to 5-fluorouracil in vivo. Floxuridine is used to treat various cancers, particularly metastases to the liver. Floxuridine inhibits Poly(ADP-Ribose) polymerase and induces DNA damage and apoptosis.
Flavopiridol HCl	Competes with ATP to inhibit cyclin dependent kinases (CDKs) including CDK1, CDK2, CDK4 and CDK6.
MK-0752	Moderately potent $\gamma$ -secretase inhibitor which reduces amyloid- $\beta$ 40 (A $\beta$ 40) production.
17-DMAG (Alvespimycin) HCl	Potent HSP90 inhibitor.
ML 141	Potent, selective, and reversible non-competitive inhibitor of Cdc42 GTPase (a member of the Rho family). ML141 is associated with an increase in the activation of p38 (a subgroup of MAP kinases) and may induce p38-dependent apoptosis/senescence.
17-AAG (Tanespimycin)	Potent HSP90 inhibitor which induces apoptosis, necrosis, autophagy and mitophagy.
MG 149	Potent histone acetyltransferase inhibitor.
Maraviroc	CCR5 receptor antagonist used in the treatment of HIV infection.
BAY 61-3606	Potent and selective inhibitor of Syk kinase which induces cell cycle arrest and apoptosis.
BMS-345541	Highly selective inhibitor of the catalytic subunits of IKK-2 and IKK-1 (members of the NF $\kappa$ B pathway).



<b>Proliferation reduced to a greater extent in the sensitive cell line (at 800, 200 or 80 nM)</b>	
Mitoxantrone HCl	Inhibitor of type II topoisomerase and protein kinase C (PKC). Inhibits cell proliferation also induces apoptosis.
Methotrexate	Analogue of folic acid that is a nonspecific inhibitor of dihydrofolate reductase (DHFR). Induces apoptosis.
MLN9708	MLN9708 is immediately hydrolyzed to ixazomib, the biologically active form, on exposure to aqueous solutions or plasma. Ixazomib inhibits the 20S proteasome.
GANT 61	Selective inhibitor of GLI1 (GLI Family Zinc Finger 1) and GLI2 (GLI Family Zinc Finger 2) transcription factors, which participate in the hedgehog signalling pathway.
Fenretinide	Synthetic derivative of retinoic acid that has a broad-spectrum of cytotoxic activity against cancer cells.
Fingolimod (FTY720) HCl	Sphingosine-1-phosphate (S1P) antagonist.
Volasertib (BI 6727)	Highly potent PLK1 (a serine/threonine protein kinase) inhibitor which induces cell cycle arrest and apoptosis in various cancer cells.
BI 2536	Potent PLK1 inhibitor which induces apoptosis and attenuates autophagy.
IWR-1-endo	Wnt pathway inhibitor which induces Axin2 protein levels and promotes $\beta$ -catenin phosphorylation.
Lenalidomide (CC-5013)	Binds to the CRBN component of the CRL4 E3 ubiquitin ligase and causes selective ubiquitination and degradation of two lymphoid transcription factors, Ikaros and Aiolos.
FT-207 (NSC 148958)	5-Fluorouracil prodrug.
Apicidin	Histone deacetylase inhibitor.
MK-1775	Potent and selective Wee1 (a checkpoint kinase) inhibitor.
LY2157299	Potent TGF $\beta$ receptor I (T $\beta$ RI) inhibitor.
17-AAG (Tanespimycin)	Potent HSP90 inhibitor which induces apoptosis, necrosis, autophagy and mitophagy.
JNJ-7706621	Potent inhibitor of several cyclin-dependent kinases and Aurora kinases.
Pomalidomide	Binds to the CRBN component of the CRL4 E3 ubiquitin ligase and causes selective ubiquitination and degradation of two lymphoid transcription factors, Ikaros and Aiolos.
Geldanamycin	A naturally existing HSP90 inhibitor.
AZD7762	Potent checkpoint kinase 1 (Chk1) and checkpoint kinase 2 (Chk2) inhibitor.
<b><math>\geq</math>80% reduction in cell viability in both cell lines at 80 nM</b>	
AUY922 (NVP-AUY922)	Highly potent HSP90 inhibitor. AUY-922 effectively downregulates and destabilizes the IGF-1R $\beta$ (Insulin Like Growth Factor 1 Receptor Beta) protein, resulting in growth inhibition, autophagy, and apoptosis.

Gemcitabine	Nucleic acid synthesis inhibitor which is a very potent and specific deoxycytidine analogue. Gemcitabine induces potent p53-dependent apoptosis.
QNZ (EVP4593)	Potent inhibitory activity toward both NFκB activation and TNF-α production.
Panobinostat (LBH589)	Broad-spectrum histone deacetylase (HDAC) inhibitor which induces autophagy and apoptosis.
Elesclomol (STA-4783)	Novel potent oxidative stress inducer that elicits pro-apoptotic events in tumor cells.
Quisinostat (JNJ- 26481585)	HDAC inhibitor with highest potency for HDAC1.
YM155 (Sepantronium Bromide)	Potent Survivin (member of the inhibitor of apoptosis family of proteins) suppressant.
Docetaxel	Analogue of paclitaxel which inhibits depolymerisation of microtubules.
Paclitaxel	Microtubule polymer stabiliser which can cause both mitotic arrest and apoptotic cell death.
Plinabulin (NPI-2358)	Vascular disrupting agent that inhibits tubulin polymerisation.
Raltitrexed	Thymidylate synthase inhibitor.
Doxorubicin (Adriamycin)	Cytotoxic anthracycline antibiotic that inhibits topoisomerase II, thus stopping DNA replication.
Epirubicin HCl	Semi-synthetic derivative of doxorubicin that inhibits topoisomerase II.
Idarubicin HCl	Anthracycline antibiotic and DNA topoisomerase II inhibitor.
Epothilone A	Paclitaxel-like microtubule-stabilising agent.
Epothilone B (EPO906, Patupilone)	Paclitaxel-like microtubule-stabilising agent.
Ispinesib (SB- 715992)	Potent, specific, and reversible inhibitor of kinesin spindle protein. Induces mitotic arrest and apoptotic cell death.
Vinorelbine	Semi-synthetic vinca alkaloid which inhibits mitosis through interaction with tubulin.
Teniposide	Inhibits topoisomerase II.
SB743921	Kinesin spindle protein inhibitor.
GSK461364	Inhibits PLK1.
GSK2126458 (GSK458)	Selective and potent PI3K (phosphoinositide 3-kinase)/mTOR (mammalian target of rapamycin) inhibitor.
KX2-391	The first clinical Src inhibitor.

APO866 (FK866)	Inhibits nicotinamide phosphoribosyltransferase.
INK 128 (MLN0128)	Potent and selective mTOR inhibitor.
Daunorubicin HCl	Topoisomerase II inhibitor.
Triptolide (PG490)	Functions as a NFκB inhibitor by disruption of p65/CBP (CREB Binding Protein) interaction and by reduction of p65 protein. Triptolide (PG490) also abrogates the transactivation function of HSTF (Heat Shock Transcription Factor 1) and inhibits MDM2 (Mouse Double Minute 2 Homolog).
KPT-330	Selective CRM1 (Exportin 1) inhibitor.
Combretastatin A4	Microtubule-targeting agent.

*Table 9-5 Hit compounds identified in the screen.*

Hit compounds from the screen are listed with descriptions taken from the Selleck website (<https://www.selleckchem.com>).

### 9.3 Reversing IMiD/CELMoD Resistance and Identifying Genetic Vulnerabilities in the IMiD/CELMoD-Resistant State

A genome wide loss-of-function CRISPR screen was performed in Iber-R-MM1s. This section provides more information about the preliminary experiments performed and the running of the screen.

#### 9.3.1 Validation of the Brunello library

Brunello plasmid pool was kindly provided by Dr Paul Clarke, ICR. Dr Marco Licciardello had expanded the Brunello library using the GeCKO library protocol and then confirmed library representation (**Figure 9-6**). Reads were aligned to an gRNA index and then the number of uniquely aligned reads for each library sequence calculated. The numbers of reads of each unique gRNA per sample were then normalised as follows: normalised reads per gRNA = (reads per gRNA/total reads of all gRNAs in the sample) $\times 10^6 + 1$ .

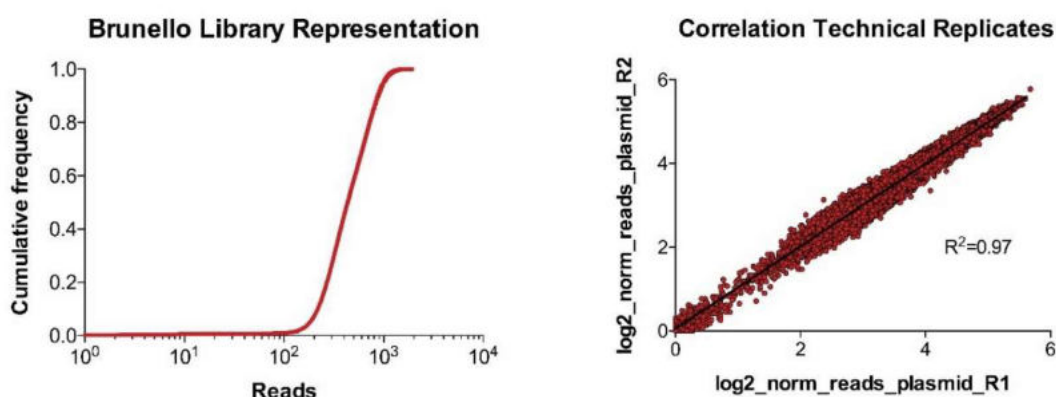


*Figure 9-6 Brunello library representation.*

The plasmid pool used in the CRISPR screen was confirmed to have correct representation. Data kindly provided by Dr Marco Licciardello.

#### 9.3.2 Optimisation of polybrene concentration

Viral transduction of MM1s required optimisation of the dose of polybrene (hexadimethrine bromide) used to transduce cells. Polybrene is a cationic polymer that improves transduction efficiency by neutralising the negative electrostatic charge between virus particles and the cell surface (201). However, it can slow cell proliferation and recovery time after transduction (201). The percentage of cells infected with Brunello plasmid pool when different concentrations of polybrene were used was calculated. 2 $\mu$ g/ml of polybrene provided a similar infection efficiency to 4-8 $\mu$ g/ml and was therefore used in

ongoing experiments (**Figure 9-7**). The percentage of infected cells was calculated by splitting cells transduced with Brunello library into two distinct wells of a 6-well plate 24 hours after transduction and treating one well with puromycin (the selection marker for the library). At day 5, the cells in both wells were counted, and the percentage of infected cells calculated (number of cells in the well with puromycin/number of cells in the well without puromycin x 100).

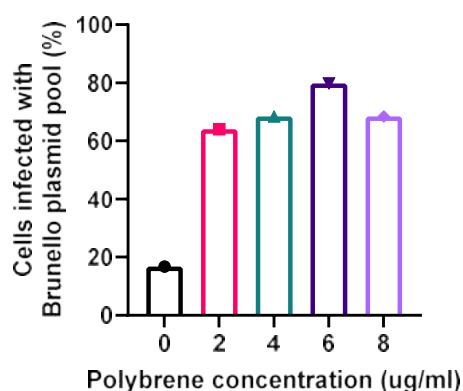


*Figure 9-7 Polybrene optimisation.*

2µg/ml of polybrene produced a similar infection efficiency to 4-8µg/ml. Individual data points shown (n=1).

### 9.3.3 Assessment of Cas9 activity with the EGFP reporter assay

Ctrl-Iber-MM1s and Iber-R-MM1s expressing Cas9 were generated by transducing cells with the pLEX\_311-Cas9v2 vector (forming Cas9-Ctrl-Iber-MM1s and Cas9-Iber-R-MM1s respectively). I was unable to blot for Cas9 in the cells (despite using 2 different antibodies), but presence was detected at the mRNA level (**Figure 9-8**).

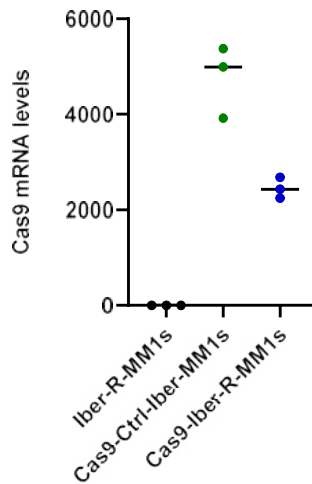


*Figure 9-8 Cas9 mRNA levels.*

Cas9 was expressed in the transduced Cas9-Ctrl-Iber-MM1s and Cas9-Iber-R-MM1s cells. N=1, graph shows individual technical repeats with a line representing the median.

However, it is critical that cells being used in the screen have enough Cas9 **activity** to knockout a given gene when transduced with the Brunello library. This was assessed using a second lentiviral vector system. In the absence of Cas9, Iber-R-MM1s and Ctrl-Iber-MM1s transduced with pXPR\_011 sgEGFP express EGFP. However, in Cas9-Iber-R-MM1s and Cas9-Ctrl-Iber-MM1s cells transduced with pXPR\_011 sgEGFP, the gRNA expressed from the vector targets EGFP and the cells no longer express EGFP. The fraction of EGFP-positive and negative cells can then be quantitated by flow cytometry. Cas9-Iber-R-MM1s cells transduced with the pXPR\_011 sgEGFP plasmid had a GFP positive fraction of 17.4% on flow cytometry compared to 84.5% of control cells. This suggested excellent Cas9 activity (**Figure 9-9**).

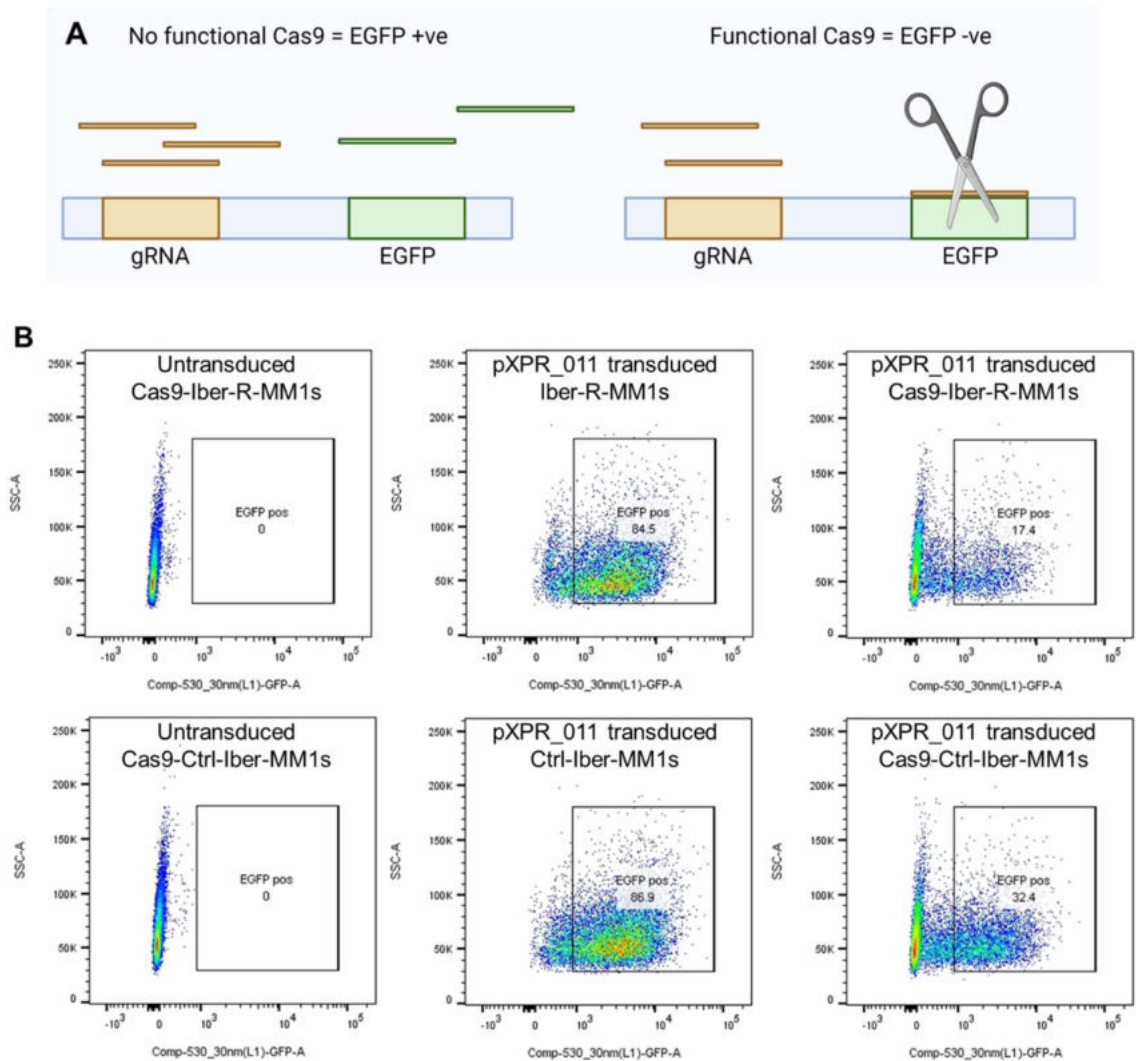


**Figure 9-9 Assessing the activity of Cas9.**

A) In the absence of Cas9, cells transduced with pXPR\_011 sgEGFP express EGFP. However, if Cas9-expressing cells are transduced with pXPR\_011 sgEGFP, the gRNA expressed from the vector targets EGFP and the cells no longer express EGFP. B) Cas9-Iber-R-MM1s cells transduced with the pXPR\_011 sgEGFP plasmid had a GFP positive fraction of 17.4% on flow cytometry compared to 84.5% of control cells. Cas9-Ctrl-Iber-MM1s cells transduced with the pXPR\_011 sgEGFP plasmid had a GFP positive fraction of 32.4% on flow cytometry compared to 86.9% of control cells. Two independent flow cytometry experiments were performed and representative data from one biological replicate is shown.

### 9.3.4 Calculation of multiplicity of infection

A critical factor in the screen is calculating the amount of virus needed to achieve the appropriate multiplicity of infection (MOI) of 0.3-0.5. It is crucial that a maximum of one viral particle enters a given cell so that a maximum of one gene will be knocked out. For the batch of Brunello plasmid pool virus generated for the CRISPR screen, the quantity of virus needed to infect ~39% of cells was used, which corresponds to an MOI of 0.49 (**Figure 9-10**).

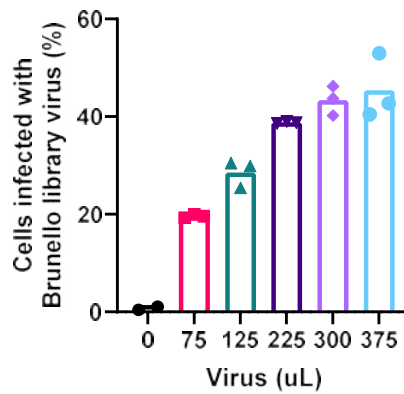


*Figure 9-10 Calculation of the MOI for Brunello library virus.*

With this batch of Brunello library virus, 225 $\mu$ L of virus with  $3 \times 10^6$  cells in a total volume of 4ml of media led to 39% of cells being infected. This corresponded to an MOI of 0.49.

### 9.3.5 CRISPR screen flow

Prior to commencing the screen, Cas9-Iber-R-MM1s cells were fully resistant to iberdomide. A batch of cells was cultured in media without iberdomide for the duration of the screen and was confirmed to remain resistant until completion of the screen. This provided assurance that cells cultured in the DMSO branch of the screen did not regain sensitivity to IMiDs/CELMoDs due to removal of the selection pressure (which would confound the results) (**Figure 9-11**). Cas9-Iber-R-MM1s cells were exposed to blasticidin for 72 hours prior to commencing the screen to ensure selection of Cas9-expressing cells and 5 independent biological replicates of the screen were performed.

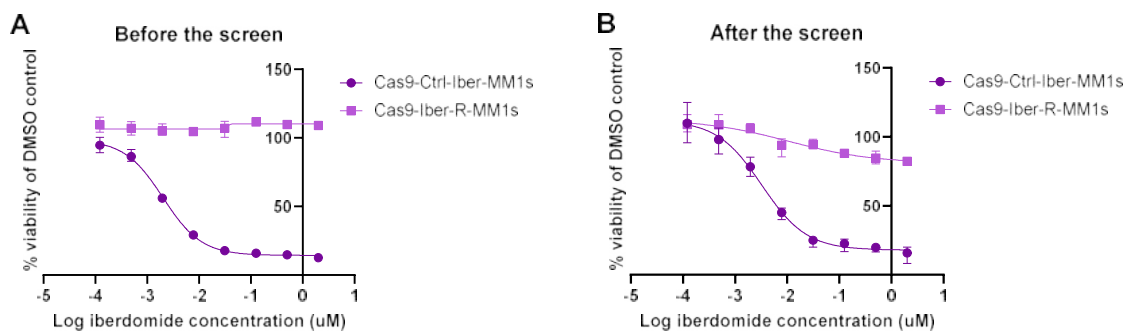


*Figure 9-11 Cells did not regain sensitivity to iberdomide due to removal of selection pressure during the duration of the screen.*

A) Cas9-Iber-R-MM1s were fully resistant to iberdomide prior to the screen commencing and B) retained resistance when cultured without iberdomide for the duration of the screen. N=1, graphs show mean and range of 3 technical triplicates.



### 9.3.6 Processing CRISPR screen samples and quality control

An initial time zero sample (T<sub>0</sub>), final sample from the DMSO arm (T<sub>finalDMSO</sub>) and final sample from the iberdomide arm (T<sub>finaliberdomide</sub>) were processed for each of the 5 biological replicates, creating a total of 15 samples. Genomic DNA (gDNA) was extracted from the cell pellets and the gRNA cassettes were amplified using 2 sequential PCR reactions, the second of which barcoded the cassettes for each sample to allow downstream deconvolution after next generation sequencing (NGS). The number of PCR#2 cycles was optimised (**Figure 9-12**).

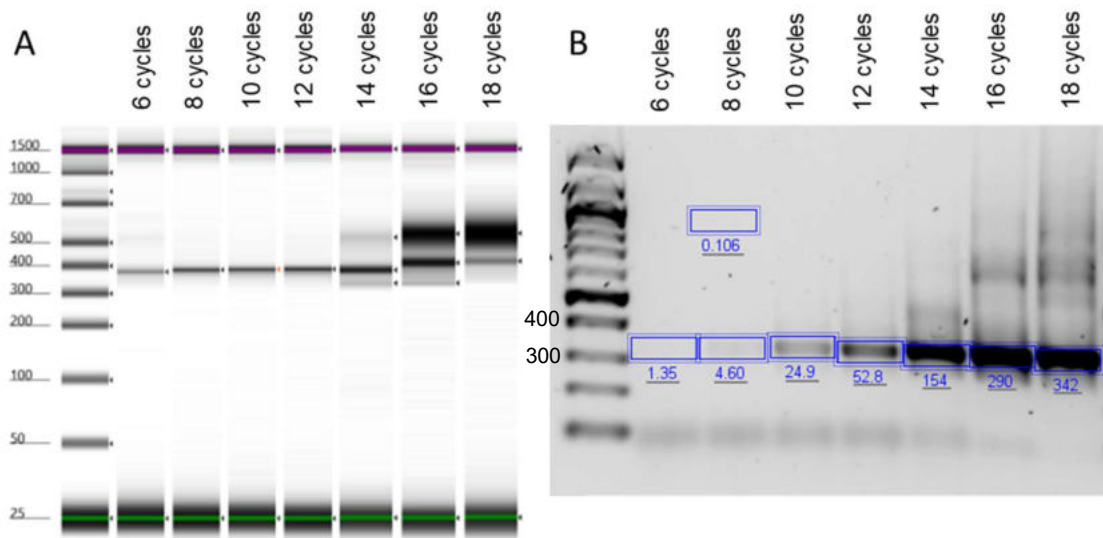


**Figure 9-12** Optimisation of gRNA cassette PCR.

The Agilent D1000 Screen Tape System was used to assess the quality of samples run with different numbers of PCR#2 cycles. (A) Running too many PCR cycles results in a product with two bands. A good quality sample has one band at ~370bp. Each individual sample must be quantified on DNA gel (B) so that it can be pooled in equimolar amounts prior to the pool being run on a gel and extracted. Therefore, enough PCR#2 cycles must be run to allow visualisation on a standard DNA gel. Twelve cycles of PCR#2 was chosen because it forms one band at 370bp on tape station analysis and it can be visualised clearly on a DNA gel.

The samples were quantified on a DNA gel and then combined in equimolar amounts into 2 pools, a pool of 6 samples and a pool of 9 samples (**Figure 9-13**). The pooled samples were then run on a gel, extracted, quantified on a Qubit fluorometer, and analysed on the Agilent D1000 ScreenTape System (**Figure 9-14**). Two SP flow cells were used to run the samples with a 20% PhiX spike (Source Bioscience). This method ensured enough reads for each of the 15 samples.

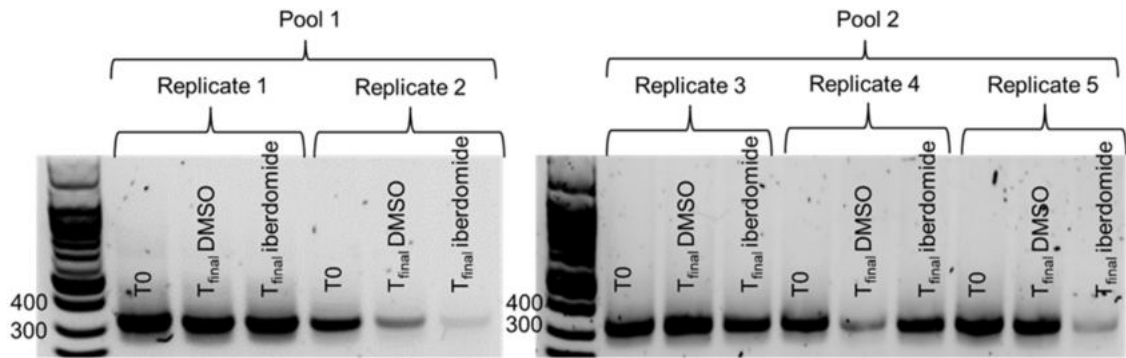


**Figure 9-13** Pooling of the CRISPR screen samples.

Each sample was run on a DNA gel and imaged using the LI-COR Odyssey Fc imaging system. The bands were quantified to allow equimolar amounts of each sample to be pooled.

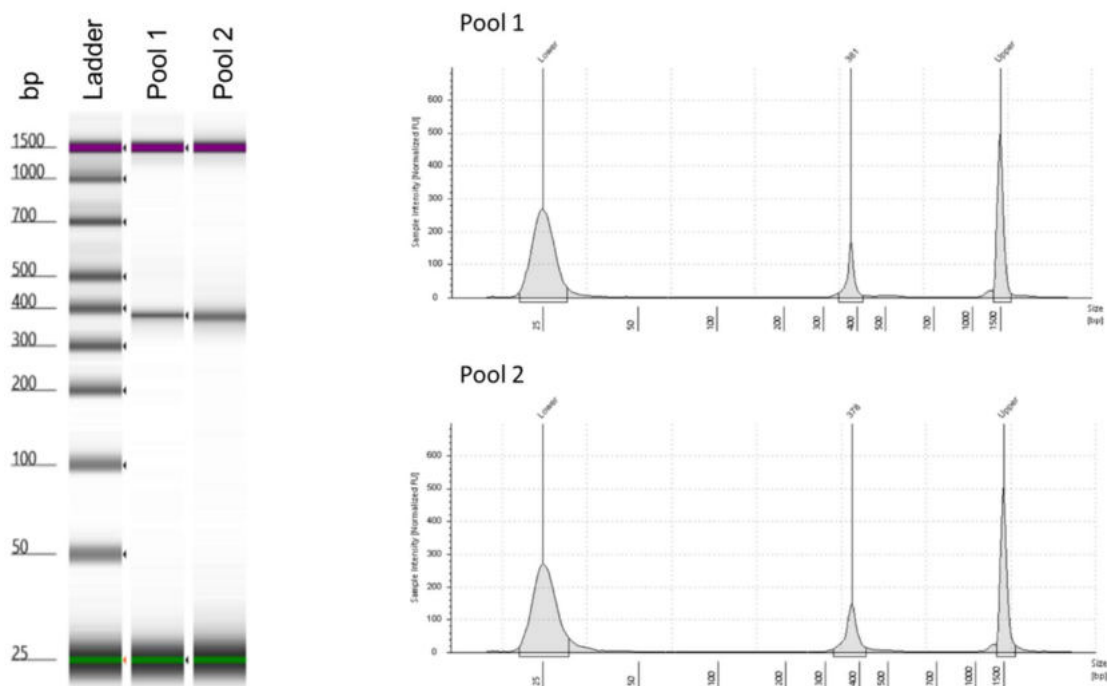


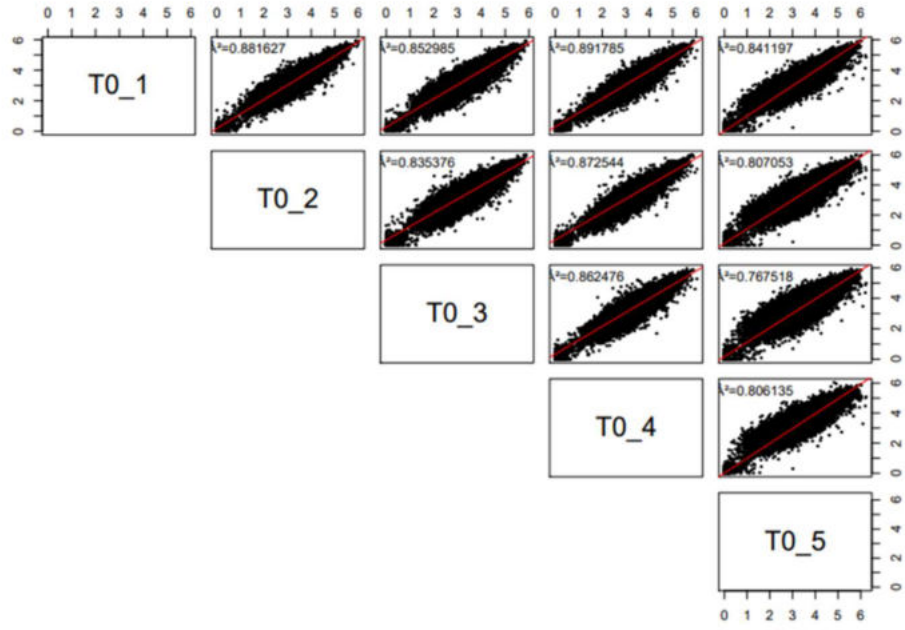
**Figure 9-14** Quality check of the pooled CRISPR screen samples.

The Agilent D1000 Screen Tape System was used to assess the quality of the pooled samples prior to sending for NGS. Each pool showed a single peak at ~370 base pairs.

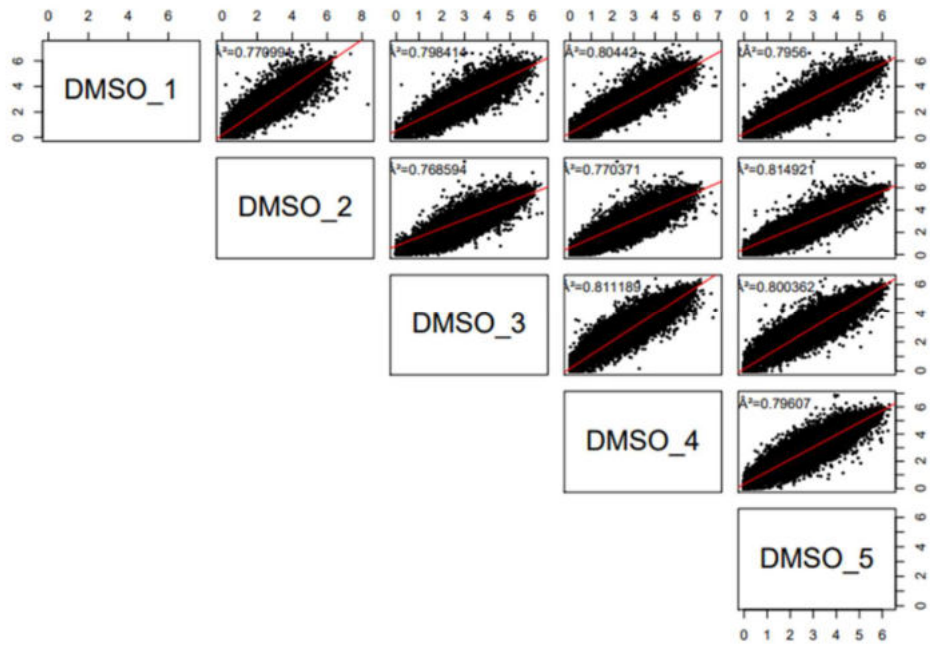
### 9.3.7 Assessment of data quality

Data was returned as a FastQ file for each of the pools. PoolQ (v3.3.1) was used to deconvolute each sample and count the number of reads of each gRNA per sample. PoolQ also provided information regarding data quality and demonstrated a low frequency of uncounted reads and good barcode tracking. Replicates showed good correlation (**Figure 9-15**) and the 1000 non-targeting controls present in the Brunello library were not altered between the Tfinal and T0 conditions.

### Biological Replicates T0



### Biological Replicates DMSO



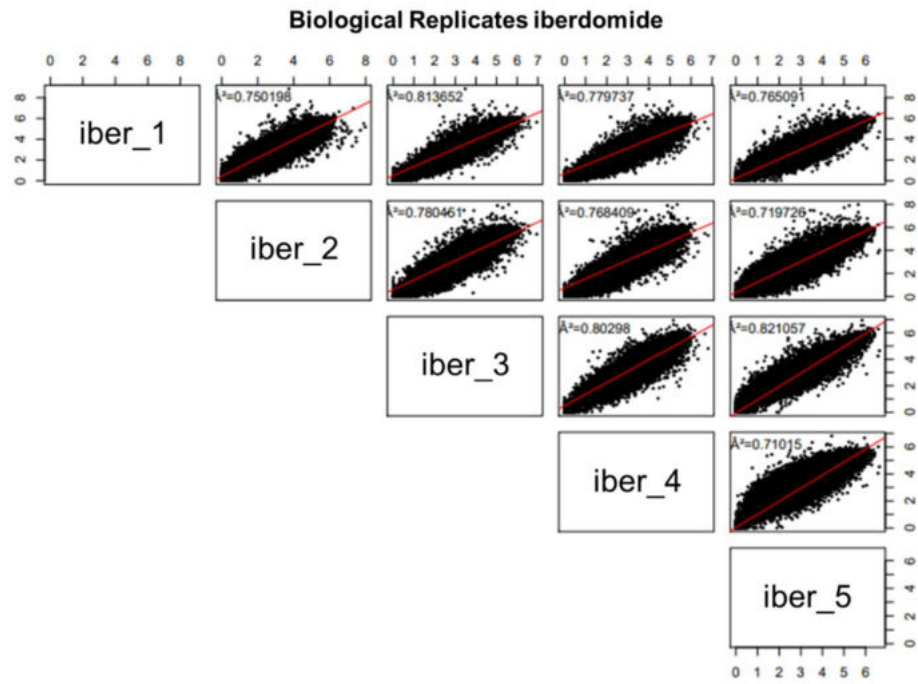


*Figure 9-15 Correlation of biological replicates.*

Good correlation between biological replicates of the CRISPR screen was observed.

## 9.4 SETD2 Inhibition in IMiD/CELMoD Resistance

### 9.4.1 Transcripts altered with EPZ-719 treatment

Symbol	Full name	Description
EMP2	Epithelial Membrane Protein 2	Regulates cell membrane composition. It has been associated with various functions including endocytosis, cell signalling, cell proliferation, cell migration, cell adhesion, cell death, cholesterol homeostasis, urinary albumin excretion, and embryo implantation.
NCAM1/CD56	Neural Cell Adhesion Molecule 1	Cell adhesion protein which is a member of the immunoglobulin superfamily.
TMSB15A	Thymosin Beta 15A	Plays an important role in the organisation of the cytoskeleton.
CTSF	Cathepsin F	A papain family cysteine proteinase that is thought to participate in intracellular degradation and turnover of proteins.
DDX60L	DExD/H-Box 60 Like	Member of the DExD/H-box helicase family of proteins, a subset of the super family 2 helicases.
VWA5A	Von Willebrand Factor A Domain Containing 5A	May act as a tumor suppressor.
LOC645261	LOC645261	RNA Gene, affiliated with the non-coding RNA class.
DNAH1	Dynein Axonemal Heavy Chain 1	Encodes an inner dynein arm heavy chain that provides structural support between the radial spokes and the outer doublet of the sperm tail.
THBS3	Thrombospondin 3	Adhesive glycoprotein that mediates cell-to-cell and cell-to-matrix interactions.
SLC4A5	Solute Carrier Family 4 Member 5	Member of the sodium bicarbonate cotransporter (NBC) family, part of the bicarbonate transporter superfamily.
DDX60	DExD/H-Box Helicase 60	Encodes an RNA helicase which may be involved in several cellular processes.
ARHGAP6	Rho GTPase Activating Protein 6	Member of the rhoGAP family of proteins which play a role in the regulation of actin polymerisation at the plasma membrane during several cellular processes.

SOGA1	Suppressor Of Glucose, Autophagy Associated 1	Predicted to be involved in the insulin receptor signalling pathway.
TASL	TLR Adaptor Interacting With Endolysosomal SLC15A4	Involved in positive regulation of the innate immune response, positive regulation of toll-like receptor signalling pathways, and regulation of lysosomal lumen pH.
CD68	CD68 Molecule	May play a role in phagocytic activities of tissue macrophages.
GPC4	Glypican 4	Cell surface proteoglycan that bears heparan sulfate.
NECTIN3	Nectin Cell Adhesion Molecule 3	Encodes a member of the nectin family of proteins, which function as adhesion molecules at adherens junctions.
ADD2	Adducin 2	Membrane-cytoskeleton-associated protein that promotes the assembly of the spectrin-actin network.
KCNS3	Potassium Voltage-Gated Channel Modifier Subfamily S Member 3	Potassium channel subunit.
TLR7	Toll Like Receptor 7	Member of the Toll-like receptor (TLR) family which plays a fundamental role in pathogen recognition and activation of innate immunity.
GPR155	G Protein-Coupled Receptor 155	Involved in cognition.
GCSAM	Germinal Center Associated Signaling And Motility	Encodes a protein which may function in signal transduction pathways. Involved in the negative regulation of lymphocyte motility.
SCN3A	Sodium Voltage-Gated Channel Alpha Subunit 3	Mediates the voltage-dependent sodium ion permeability of excitable membranes.
TRANK1	Tetratricopeptide Repeat And Ankyrin Repeat Containing 1	Predicted to enable ATP binding activity.
FRMD6	FERM Domain Containing 6	Predicted to be involved in actomyosin structure organisation.
GIMAP8	GTPase, IMAP Family Member 8	Has an anti-apoptotic effect on the immune system and participates in responses to infections.
SORL1	Sortilin Related Receptor 1	May function as a sorting receptor that directs several proteins to their correct location within the cell.

SATB1	SATB Homeobox 1	Encodes a matrix protein which is involved in the regulation of chromatin structure.
-------	-----------------	--

*Table 9-6 Details of transcripts altered with EPZ-719 treatment in both the MM1s and H929 cell lines.*

Symbol, full name and a brief description are provided for transcripts altered with EPZ-719 in both the MM1s and H929 cell lines. Descriptions taken from GeneCards (147).

## 9.4.2 NCAM1/CD56 expression in the resistant cell lines

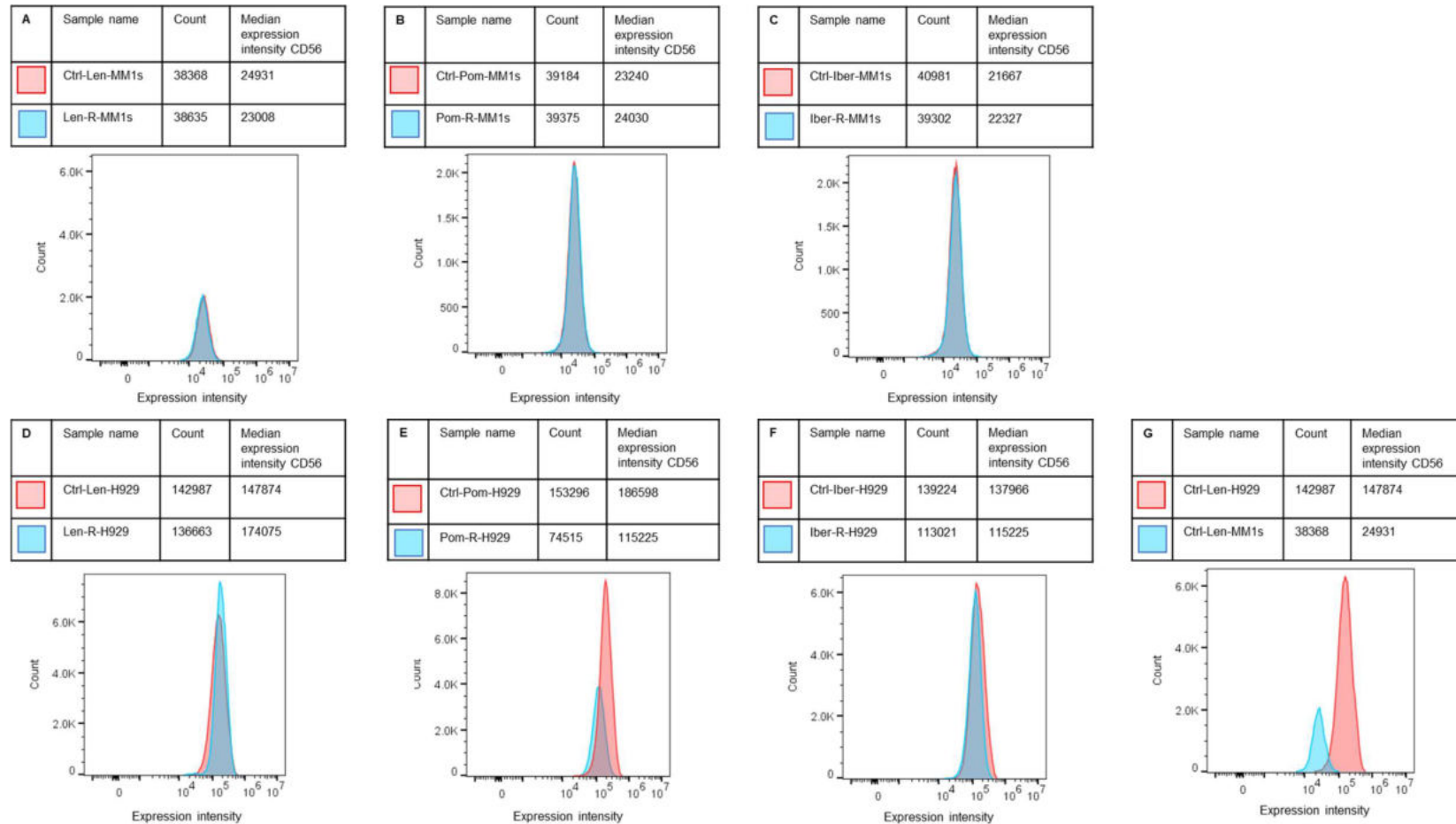


Figure 9-16 NCAM1/CD56 expression in the resistant cell line pairs.

A-F) The expression of NCAM1/CD56 (as assessed by flow cytometry) was the same in each control and resistant cell line pair. G) H929 had more surface expression of NCAM1/CD56 compared to MM1s.



## 9.5 Changes in Lipid Synthesis Pathways in the IMiD/CELMoD-resistant State

### 9.5.1 SCD inhibition with GSK1940029 in the resistant cell lines

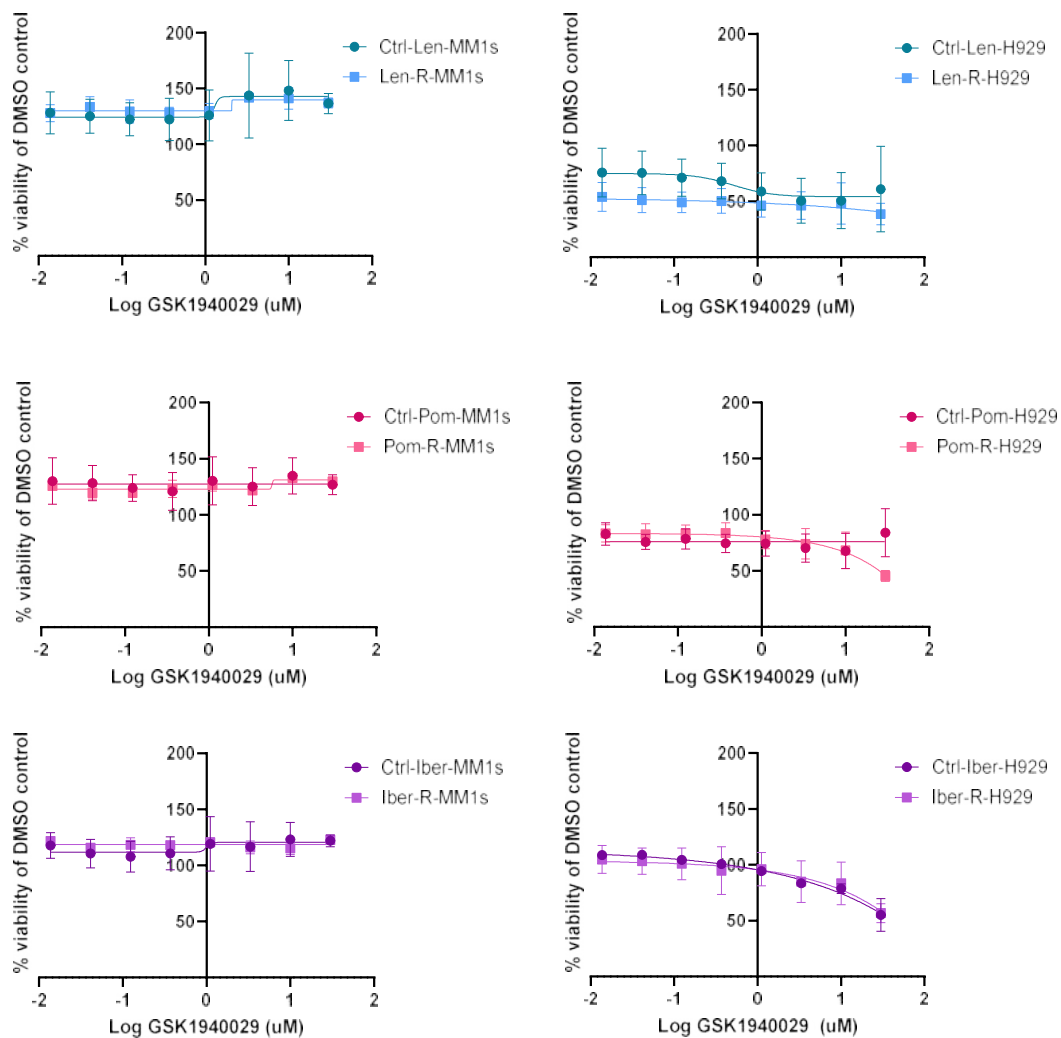


*Figure 9-17 Viability assays showing the effect of GSK1940029 in the resistant cell lines.*

The effect of GSK1940029 on cell viability was assessed in 5-day CellTiter-Blue assays (top concentration 30 $\mu$ M). N=2, graphs show mean and SEM.

## 9.5.2 The effect of opaganib on viability in the resistant cell lines

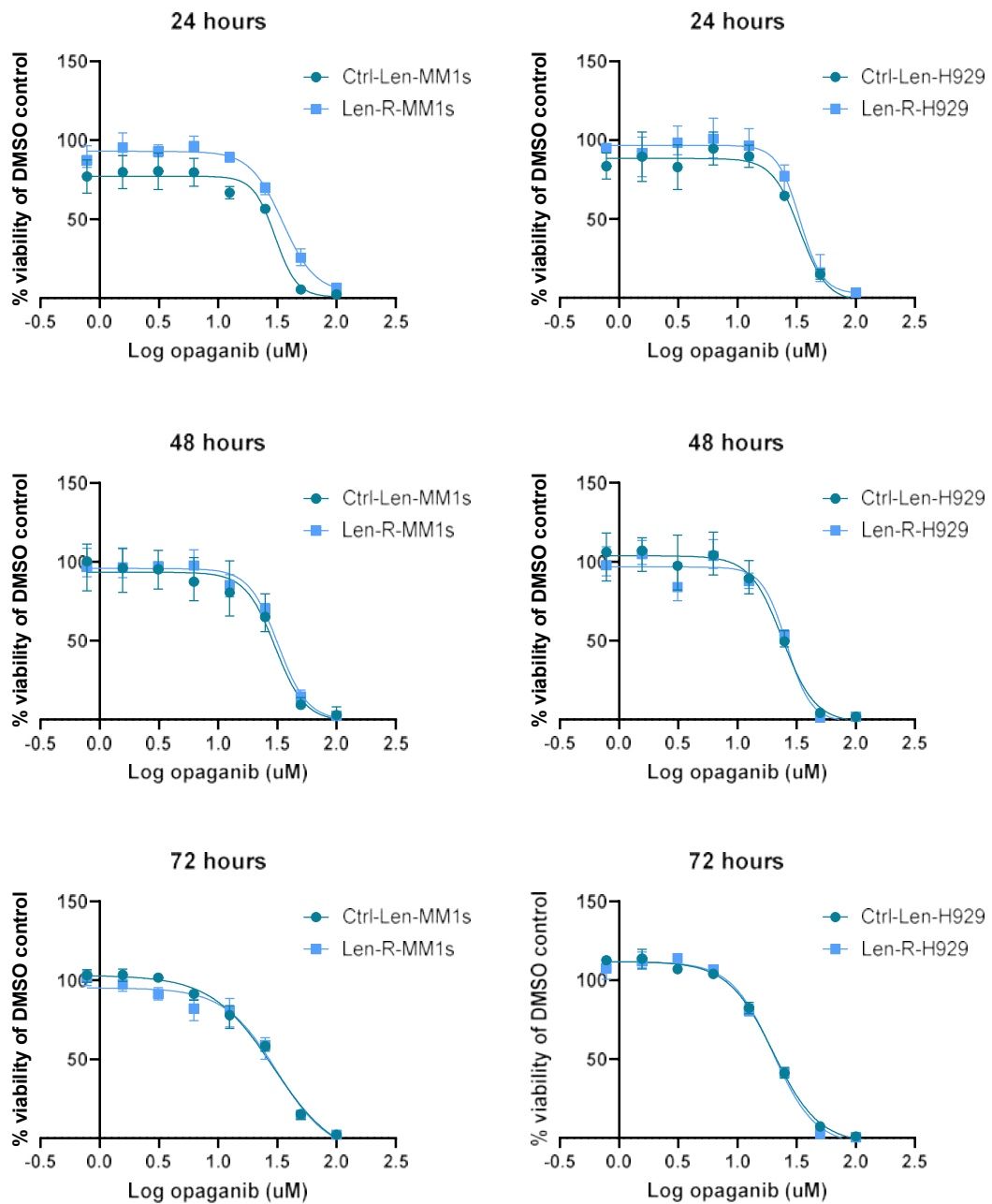


*Figure 9-18 Viability assays showing the effect of opaganib in the lenalidomide resistant cell lines.*

The effect of opaganib on cell viability was assessed at 24, 48 and 72 hours in CellTiter-Blue assays (top concentration  $100\mu\text{M}$ ). N=1, graphs show mean and range of 3 technical replicates.

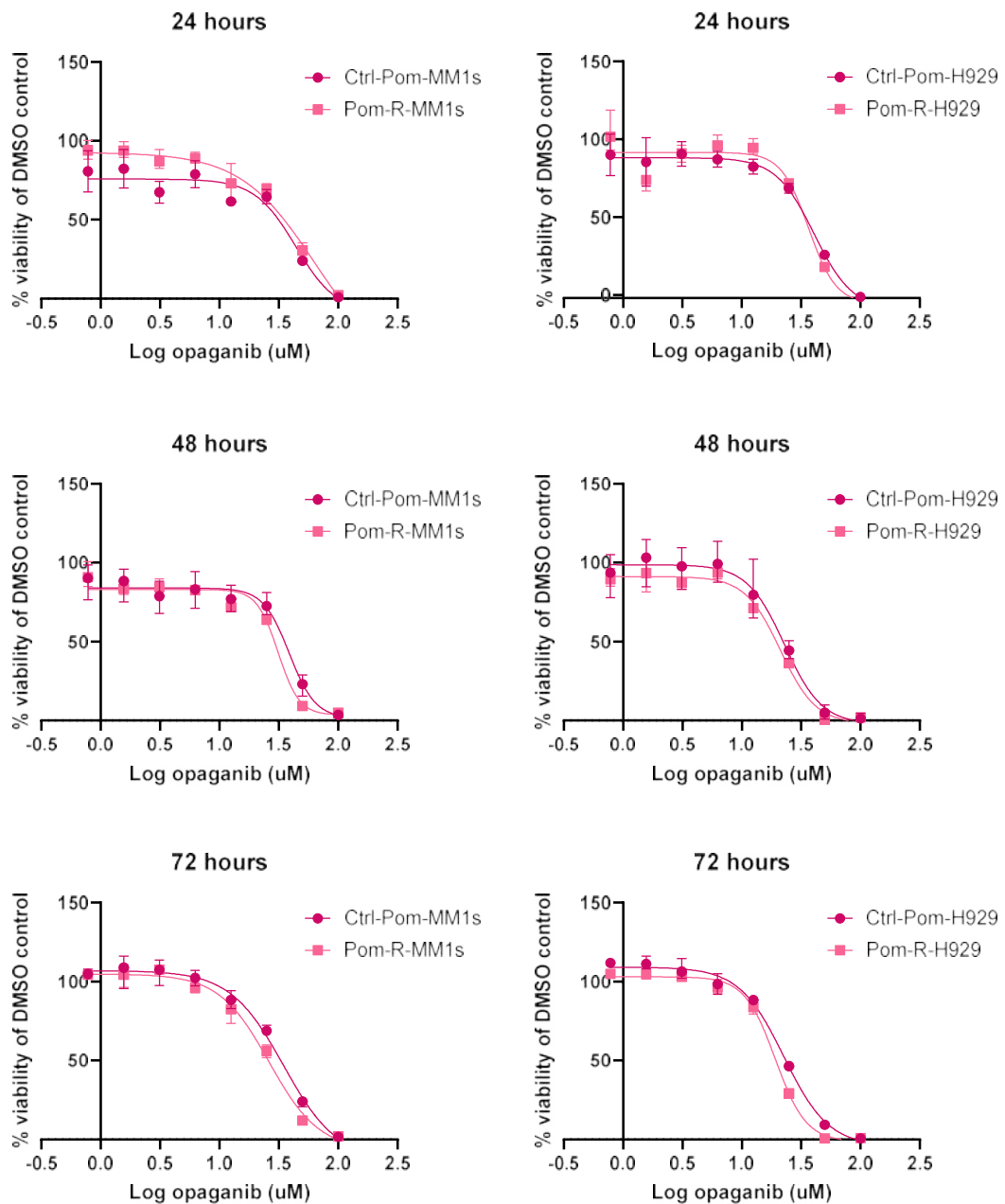


*Figure 9-19 Viability assays showing the effect of opaganib in the pomalidomide resistant cell lines.*

The effect of opaganib on cell viability was assessed at 24, 48 and 72 hours in CellTiter-Blue assays (top concentration 100µM). N=1, graphs show mean and range of 3 technical triplicates.

## Chapter 10    Supplementary Methods

---

### 10.1 Whole proteome analysis

#### ***Sample preparation***

Samples for quantitative proteomics and phosphoproteomics were prepared using the SimPLIT workflow (131). Briefly, the cell pellets were lysed in a buffer containing 150 $\mu$ L 0.1M triethylammonium bicarbonate (TEAB), 1% sodium deoxycholate (SDC), 10% isopropanol, 50mM NaCl, 5mM tris-2-carboxyethyl phosphine (TCEP), 10mM iodoacetamide (IAA) and universal nuclease, supplemented with protease and phosphatase inhibitors. Samples were bath sonicated for 5 minutes, incubated at room temperature for 45 minutes and protein concentration was measured with the Bradford Protein Assay (Bio-Rad) according to the manufacturer's instructions. Aliquots containing 15 $\mu$ g or 60 $\mu$ g of total protein were used for proteomics or phosphoproteomics experiments respectively. Proteins were then digested with the addition of 3 $\mu$ L of trypsin stock solution (500ng/ $\mu$ L in 0.1% formic acid, Pierce, 90059). The resultant peptides were labelled with a tandem mass tag (TMTpro) multiplex reagent vial (Thermo Fisher Scientific) according to the manufacturer's instructions. All of the TMT-labelled samples were combined in equal amounts to a single tube. The TMT-peptide mixture was acidified with 1% formic acid and the precipitated sodium deoxycholate (SDC) was removed by centrifugation. The sample was then dried with a centrifugal vacuum concentrator.

#### ***High-pH reversed-phase peptide fractionation***

Offline peptide fractionation was based on high pH Reverse Phase (RP) chromatography using the Waters XBridge C18 column (2.1  $\times$  150 mm, 3.5  $\mu$ m) on a Dionex Ultimate 3000 HPLC system at a 0.85% gradient with flow rate 0.2 mL/min. Mobile phase A was 0.1% ammonium hydroxide, and mobile phase B was 100% acetonitrile, 0.1% ammonium hydroxide. Retention time-based fractions were collected and pooled into thirty samples for LC-MS analysis.

#### ***Phosphopeptide enrichment***

After peptide fractionation, the phosphopeptides were enriched using Fe-NTA Phosphopeptide Enrichment Kit (Pierce, #88300) according to manufacturer's instructions. The eluted peptides (phosphoproteome) and the flow-through

(proteome) were dried with a centrifugal vacuum concentrator and resuspended in 5% formic acid.

### ***Liquid chromatography-mass spectrometry (LC-MS) analysis***

LC-MS analysis was performed on the Dionex UltiMate 3000 UHPLC system coupled with the Orbitrap Ascend Tribrid mass spectrometer (Thermo Fisher Scientific). Samples were analysed with the PepMap C18 capillary column (75µm × 50cm, 2µm) at 50°C.

Mobile phase A was 0.1% formic acid and mobile phase B was 80% acetonitrile, 0.1% formic acid. The gradient separation method was as follows: 150 minutes gradient up to 38% B, for 10 minutes up to 95% B, for 5 minutes isocratic at 95% B, re-equilibration to 5% B in 10 minutes, for 10 minutes isocratic at 5% B. Precursors between 375 and 1500 m/z were selected with a mass resolution of 120,000, automatic gain control (AGC) of  $4 \times 10^5$ , and IT (injection time) of 50 milliseconds, with the top speed mode in 3 seconds for high collision dissociation (HCD) fragmentation with a quadrupole isolation width of 0.7 Th (Thomson unit). The collision energy was set at 35%, with AGC at  $1 \times 10^5$  and IT at 86 milliseconds. The HCD MS2 spectra were acquired with a fixed first mass at 100 m/z and a resolution of 45,000. Targeted precursors were dynamically excluded for further isolation and activation for 45 seconds with 7 ppm mass tolerance.

### ***Database search and protein quantification***

The SEQUEST-HT search engine was used to analyse the acquired mass spectra in Proteome Discoverer 2.4 (Thermo Fisher Scientific) for protein identification and quantification. The precursor mass tolerance was set at 20 ppm, and the fragment ion mass tolerance was set at 0.5 Da. Spectra were searched for fully tryptic peptides with maximum 2 mis-cleavages. TMTpro on lysine residues and peptide N termini (304.2071 Da) and carbamidomethylation of cysteine residues (+57.0215 Da) were set as static modifications while oxidation of methionine residues (+15.9949 Da) and deamidation of asparagine and glutamine (+0.9848 Da) was set as a variable modification. Peptide confidence was estimated with the Percolator. The peptide FDR was set at 0.01, and validation was based on the q value and a decoy database search. All spectra were searched against UniProt-SwissProt proteomes of *Homo sapiens* protein entries appended with contaminants. The reporter ion quantifier node included a

TMTpro quantification method with an integration window tolerance of 15 ppm and integration method based on the most confident centroid peak at the MS3 level. Only unique peptides were used for quantification, with protein groups considered for peptide uniqueness. Peptides with an average reporter signal-to-noise ratio of >3 were used for protein quantification. Correction for isotopic impurity of reporter quantification values was applied. Only spectra with at least 50% of the SPS masses matching to the identified peptides were used for quantification.

Normalised protein abundance values for resistant versus control comparisons were performed using a moderated t-test in limma (implemented in Phantasus) (132).

## 10.2 Genome wide knockout CRISPR screen

### 10.2.1 Genomic DNA extraction

The Blood and Cell Culture DNA Maxi Kit (Qiagen 13362) was used to extract genomic DNA. The following protocol was adapted from the manufacturer's instructions as follows. Frozen cell pellets were allowed to thaw at room temperature and were then re-suspended in PBS (Phosphate Buffered Saline) at  $1 \times 10^7$  cells/ml (i.e. 8ml for 80 million cells). One volume of ice-cold buffer C1 and 3 volumes of ice-cold DNase/RNase free water were added and the mixture incubated on ice for 10 minutes. The sample was then centrifuged for 15 minutes at 10,000 RPM at 4°C and the supernatant discarded. 2ml of ice-cold buffer C1 and 6ml of ice-cold DNase/RNase free water were added and the pellet re-suspended by vortexing. The sample was then centrifuged for 15 minutes at 10,000 RPM at 4°C and the supernatant discarded. 10ml of buffer G2 was added and the pellet re-suspended by vortexing for 30 seconds at maximum speed. 200µl of reconstituted Qiagen protease and 20µl of RNase A 100mg/ml (final concentration 200 µg/ml) were added. The sample was then mixed and incubated at 50°C for 1 hour (with the sample mixed again after the first 30 minutes). A Qiagen genomic-tip 500/G was equilibrated with 5ml buffer QBT. 5ml of the same buffer added to the sample, which was then vortexed for 10 seconds at maximum speed. The sample was then added to the equilibrated tip and allowed to enter the resin by gravity flow. The flow through was discarded and the tip washed with 2x 15ml buffer QC. The flow through was discarded and the genomic tip placed in a clean tube. The gDNA was eluted with 15ml of buffer QF (pre-warmed to 50°C). The gDNA was precipitated by adding 10.5ml of isopropanol and mixing. The sample was centrifuged for 30 minutes at 12,857 RCF at 4°C and the supernatant discarded. The pellet was washed with 4ml of cold 70% EtOH and vortexed briefly. The sample was then centrifuged for 30 minutes at 12,857 RCF at 4°C and the supernatant discarded. The pellet was air dried and resuspended in 200µl of TE buffer at 50°C for 30 minutes to 1 hour.

### 10.2.2 PCR of Brunello gRNAs for NGS

In order to maintain library representation a minimum amount of gDNA must be amplified. Given 500x coverage for the 77,441 gRNAs of the Brunello library is required, and assuming a single diploid cell provides 6.6pg of gDNA, ~260µg of

gDNA was needed for each sample. Herculase II Fusion DNA Polymerase (Agilent 600679) works with 10µg of gDNA in 100µl (202); therefore the total amount of gDNA to be amplified has to be split among  $n$  identical PCR#1 reactions each with 10 µg of gDNA in 100 µl. Therefore, 28 PCR#1 reactions were performed for each sample. PCR#1 used standard desalted primers and PCR#2 used ultramers (both from Integrated DNA technologies). The primer sequences were taken from the protocol by Shalem *et al* (202).

#### **PCR#1 (total reaction volume 100µl)**

- x µl water (up to 100µl)
- 20µl 5x Herculase II reaction buffer
- 1µl dNTPs 100mM stock
- x µl DNA template (up to 10µg)
- 2.5µl F1+R1 primer 10µM stock
- 1µl Herculase II Fusion DNA Polymerase

Cycling parameters:

- 95°C for 2 minutes
- 20x cycles of:
  - 95°C for 20 seconds
  - 60°C for 20 seconds
  - 72°C for 30 seconds
- 72°C for 3 minutes

All PCR#1 reactions for the same sample were combined and PCR#2 commenced.

#### **PCR#2 (total reaction volume 100µl)**

In order to ensure sufficient template complexity during NGS it is advisable to use a mixture of  $\geq 6$  different staggers in the same sequencing lane/flow cell. This was achieved by pooling at least 6 samples that had been amplified with 6 different primers (different F2 barcoding primers were used for each sample run on the same flow cell to allow later deconvolution of samples). For each sample, a PCR#2 reaction must be performed every 10,000 gRNA constructs; therefore 8



PCR#2 reactions were performed for each sample. The number of cycles of PCR#2 was optimised in advance and 12 cycles was used (**Figure 9-12**).

- 68µl water (up to 100µl)
- 20µl 5x Herculase II reaction buffer
- 1µl dNTPs 100mM stock
- 5µl DNA template from PCR#1
- 2.5µl F2 primer(s) 10µM stock
- 2.5µl R2 primer 10µM stock
- 1µl Herculase II Fusion DNA Polymerase

Cycling parameters:

- 95°C for 2 minutes
- 12x cycles:
  - 95°C for 20 seconds
  - 60°C for 20 seconds
  - 72°C for 30 seconds
- 72°C for 3 minutes

All PCR#2 reactions for the same sample were pooled together and the amplicon checked on an agarose gel (expected band size 370 bp). Then PCR#2 products from each sample were quantified on the LI-COR using GelGreen nucleic acid stain. Equimolar amounts of samples were pooled together, run on a gel, cut out using a scalpel and Blue Light Transilluminator (Accuris), and extracted using the QIAquick Gel Extraction Kit (Qiagen 28104) as per the manufacturer's instructions (except a temperature of 30°C was used to melt the gel slices). Pooled and ready-to-be-sequenced samples were stored in low-DNA binding tubes (Eppendorf). Concentration of the dsDNA in the pooled sample was assessed using a Qubit and quality was assessed using the Agilent D1000 ScreenTape System.

## 10.3 ChIP-Seq

### 10.3.1 High-throughput ChIP-Seq

Fixed cell pellets were processed following the method below, with the buffers described in **Table 10-1**.

#### *Sonication and immunoprecipitation*

The cell pellet was thawed on ice and rotated for 15 minutes at 4<sup>0</sup>C with 15ml of cytoplasmic buffer. This was then centrifuged at 1,200 RCF for 15 minutes at 4<sup>0</sup>C and the supernatant discarded. Another 15ml of cytoplasmic buffer was added to the sample, followed by a second rotation at 4<sup>0</sup>C for 15 minutes. This was then centrifuged at 1,200 RCF for 15 minutes at 4<sup>0</sup>C. The supernatant was discarded and 15ml of nucleic buffer added, followed by a further 15 minute rotation at 4<sup>0</sup>C and then centrifugation at 1,200 RCF for 15 minutes at 4<sup>0</sup>C. 850µL of sonication buffer was added to the pellet and the solution transferred to an AFA tube which was then sonicated for 15 minutes using the Covaris E220. Dynabead Protein G beads (Invitrogen 10003D) were washed with dilution buffer and added to the lysate (50µl/ml of lysate) which had been transferred to a 1.5ml microcentrifuge tube. This was rotated for 1 hour at 4<sup>0</sup>C. The beads were then magnetised, and the lysate collected. 100µL of sample, 900µL of dilution buffer, 5µg of H3K36me3 antibody (Diagenode C15410192), 50ng of spike-in chromatin (Active Motif 53083) and 2µg of spike-in antibody (Active Motif 61686) were combined and rotated overnight at 4<sup>0</sup>C. For the input control 20µL of sample was combined with 180µL of buffer and stored at -20<sup>0</sup>C. The next day, new Dynabead beads were washed with dilution buffer x2 and 30µl was added to the sample, followed by a further 2 hours of rotation at 4<sup>0</sup>C. Wash steps were then carried out as follows:

- WBI x1: 150µl
- WBII x1:150µl
- WBIII x1:150µl
- TE x2: 150µl
- Tris-HCl (pH 8) x2: 150µl

The supernatant was discarded and 29µl of tagmentation buffer (14.5µL of x2 Tagmentation buffer (Diagenode C01019043) and 14.5µL of H<sub>2</sub>O) was added. This was incubated at 37<sup>0</sup>C for 5 minutes and then 1µl tagmentase enzyme (Tn5

transposase, Diagenode C01070012) was added. This was incubated at 37°C for a further 10 minutes (with shaking at 1,400 RPM). The sample was then cooled on ice, washed with 150µL WBI x2 and resuspended in 20µL of nuclease free H<sub>2</sub>O.

### ***PCR amplification***

Kappa HiFi master mix (Roche) was heated at 98°C for 90 seconds and then cooled to 4°C. The sample was mixed with 25µL of the Kappa HiFi master mix and 3.5µL of diagenode index (UDI for tagmented libraries set I and II, Diagenode C01011034, C01011036) in a PCR tube. Cycling conditions were as follows:

- 72°C for 5 minutes
- 98°C for 30 seconds
- 11 cycles of:
  - 98°C for 10 seconds
  - 63°C for 30 seconds
  - 72°C for 30 seconds
- 72°C for 1 minute
- 4°C ∞

### ***Library purification***

Kappa Pure beads (Roche KK8000) and elution buffer were warmed to 32°C for 10 minutes. The PCR sample was magnetised, and the clear liquid put into a fresh microcentrifuge tube. Kappa beads (x1.8 volume of the sample) were added to the sample and mixed. After a 10 minute incubation at room temperature the beads were magnetised, and the supernatant discarded. Beads were washed with 500µl 80% ethanol x2 and then air dried. 50µl of elution buffer (Qiagen 19086) was added and incubated for 5 minutes. Beads were magnetised and the solution transferred to a new microcentrifuge tube.

### ***Size selection***

x0.6 kappa beads (compared to the sample volume) were added to the sample and incubated at room temperature for 10 minutes. Beads were then magnetised, and the supernatant moved to a new microcentrifuge tube. x0.85 kappa beads were added to the sample and incubated at room temperature for 10 minutes. The beads were then magnetised, and the supernatant discarded. The beads were then washed with 500µl 80% ethanol x2 and left to air dry. 28µl of elution

buffer (Qiagen 19086) was added to the beads and incubated for 5 minutes. The sample was then magnetised, and supernatant transferred to a new microcentrifuge tube. The sample was then assessed for quality using the Agilent 2100 Bioanalyser System.

<b>Cell lysis buffer</b>	<b>Final concentration</b>
Hepes-KOH pH 7.5	50mM
NaCl	150mM
EDTA	1mM
Triton X-100	1%
Na-deoxycholate	0.1%
SDS	0.1%
H <sub>2</sub> O	
<b>Nuclear lysis buffer</b>	<b>Final concentration</b>
Hepes-KOH pH 7.5	50mM
NaCl	150mM
EDTA	1mM
Triton X-100	1%
Na-deoxycholate	0.1%
SDS	1%
H <sub>2</sub> O	
<b>Sonication buffer</b>	<b>Final concentration</b>
Tris/HCl pH 8.0	10mM
SDS	0.1%
EDTA	1mM
H <sub>2</sub> O	
<b>Dilution buffer</b>	<b>Final concentration</b>
Tris/HCl pH 8.0	50mM
NaCl	225mM
NaDOC	0.15%
Triton X-100	1.5%
H <sub>2</sub> O	
<b>Wash buffer I</b>	<b>Final concentration</b>
Tris/HCl pH 8.0	50mM
NaCl	150mM
SDS	0.1%
NaDOC	0.1%
Triton X-100	1%
EDTA	1mM
H <sub>2</sub> O	

<b>Wash buffer II</b>	<b>Final concentration</b>
Tris/HCl pH 8.0	50mM
NaCl	500mM
SDS	0.1%
NaDOC	0.1%
Triton X-100	1%
EDTA	1mM
H <sub>2</sub> O	
<b>Wash buffer III</b>	<b>Final concentration</b>
Tris/HCl pH 8.0	10mM
LiCl	250mM
NP-40	0.5%
NaDOC	0.5%
EDTA	1mM
H <sub>2</sub> O	
<b>TE buffer</b>	<b>Final concentration</b>
Tris/HCl pH 8.0	10mM
EDTA	1mM
H <sub>2</sub> O	

*Table 10-1 Buffers used in the ChIP protocol.*

Components of the buffers used in the ChIP protocol.

### 10.3.2 ChIP protocol for input controls

The following protocol was used to process the total input controls. Each input control sample was defrosted and 25µl SDS 20% (Thermo Fisher Scientific) and 25µl Proteinase K (Qiagen) were added. The mixture was incubated overnight at 65°C, shaking at 1,100 RPM. The next day the sample was cooled to 23°C, 300µl Phenol:Chloroform:Isoamylalcohol (Thermo Fisher Scientific) was added and the solution was vortexed well. The sample was then centrifuged at 21,000 RCF for 5 minutes at room temperature. The upper phase was transferred to a clean microcentrifuge tube (~250 µl) and 1000µl 100% ethanol, 150µl sodium acetate 3M (Thermo Fisher Scientific) and 1.5µl GlycoBlue (Thermo Fisher Scientific) were added. The solution was vortexed well and put at -80°C for 30-40 minutes. It was then centrifuged at 21,000 RCF for 20 minutes at 4°C. The supernatant was discarded, and the pellet washed with 500µl 80% ethanol. This was then centrifuged at 21,000 RCF for 3 minutes at 4°C. The supernatant was discarded and the pellet air dried for ~2 minutes. The next steps used buffers from the Zymo Clean and Concentrate kit (D4033). 50µl of elution buffer was added, and the

pellet dissolved at 37°C whilst shaking. 250µl of DNA binding buffer was added and the sample centrifuged at maximum speed for 1 minute. The sample was then washed with 200µl wash buffer x2 and eluted into a clean tube with 25µl elution buffer. The sample was then stored at -20°C. From this point the tagmentation, PCR amplification, library purification and size selection steps were the same as the protocol above.

## 10.4 Labelled glucose experiments

### 10.4.1 Sample preparation

After methanol quenching and extraction, dual-phase extraction was performed to separate and enrich non-polar metabolites (e.g. fatty acids) for further analysis. 300µl of chloroform (Honeywell)/methanol (Thermo Fisher Scientific) mix (2:1 v/v) and 300µl of water (Thermo Fisher Scientific) was added to each sample. After vortexing, the samples were centrifuged at 16,000 RCF for 10 min at 4°C to achieve separation of polar and non-polar phases. The polar phase was collected, and the extraction was repeated to improve extraction efficiency. The polar phase was combined and 10µl of myristic acid-d27 (Sigma-Aldrich) was added as an internal standard. The samples were then dried under N<sub>2</sub> flow and kept at -80°C.

Next, the samples were derivatized for GC-MS analysis. Specifically, 300µl of methanol/toluene (Sigma-Aldrich) mix (1:1 v/v) and 200µl of 0.5M sodium methoxide (Sigma-Aldrich) solution (in methanol) were added to the samples for lipid transmethylation. The samples were vortexed thoroughly and kept on a Thermomixer (Eppendorf) at 800 RPM for 1 hour at room temperature. To stop the reaction, 500µl of 1M sodium chloride (Sigma-Aldrich) solution (in water) and 20µl of 37% hydrochloric acid (Sigma-Aldrich) (w/w) were added and the samples were vortexed thoroughly. Because water reacts with the derivatization reagent, a further extraction step was performed to eliminate water. 500µl of hexane (Honeywell) was added and the samples were vortexed thoroughly. After brief centrifugation to separate polar and non-polar phases, the non-polar phase was collected into a clean vial with magnesium sulfate to achieve better water elimination. The extraction was repeated, and the non-polar phase was pooled and transferred to a clean vial for drying under N<sub>2</sub> flow. The samples were then derivatized by adding 40µl acetonitrile (Thermo Fisher Scientific) and 40µl MSTFA (N-Methyl-N-trimethylsilyl-trifluoroacetamide) derivatizing reagent (Thermo Fisher Scientific). After thorough vortexing, the samples were placed on the Thermomixer at 800 RPM for 30 minutes at 37°C. The quality control sample was made by pooling 5µl from each sample.

#### 10.4.2 GC-MS and data analysis

The order of the samples was randomised before GC-MS analysis. GC-MS analysis was performed on an Agilent 7890 GC coupled to an Agilent 5975 MSD (Agilent Technologies). An Agilent 7693 autosampler was used to inject the samples in splitless mode. Metabolites were then separated on a 30m DB-5MS capillary column using helium as a carrier gas and ionized by electron impact ionization. An in-house created compound library and the deconvolution software AMDIS were used for metabolite identification (203). The MATLAB based algorithm GAVIN was employed to integrate isotopomer peaks and correct for natural abundance of elemental isotopes (204).

Next, Isotopomer Spectral Analysis (ISA) modelling was performed based on the mass isotopomer distribution of fatty acids using a MATLAB based algorithm as described by Tredwell & Keun (135). Briefly, two parameters to describe fatty acid synthesis were estimated: 1) the proportion of lipogenic acetyl-CoA that is derived from a  $^{13}\text{C}$  tracer (parameter D) and 2) the fraction of fatty acids that are *de novo* synthesised during the incubation ( $g(t)$ ). To verify parameter errors, a Monte Carlo approach based parameter sensitivity analysis was performed.



## References

---

1. CRUK. Myeloma statistics 2023 [Available from: <https://www.cancerresearchuk.org/health-professional/cancer-statistics/statistics-by-cancer-type/myeloma>.
2. Bird SA, Boyd K. Multiple myeloma: an overview of management. *Palliat Care Soc Pract*. 2019;13:1178224219868235.
3. Davis LN, Sherbenou DW. Emerging Therapeutic Strategies to Overcome Drug Resistance in Multiple Myeloma. *Cancers*. 2021;13(7):1686.
4. Bianchi G, Munshi NC. Pathogenesis beyond the cancer clone(s) in multiple myeloma. *Blood*. 2015;125(20):3049-58.
5. Ria R, Vacca A. Bone Marrow Stromal Cells-Induced Drug Resistance in Multiple Myeloma. *Int J Mol Sci*. 2020;21(2).
6. Pawlyn C, Davies FE, Kaiser MF, Cairns DA, Striha A, Collett C, et al. Primary IMiD Refractory Myeloma; Results from 3894 Patients Treated in the Phase III Myeloma XI Study. *Blood*. 2016;128(22):1144.
7. Lecat CSY, Taube JB, Wilson W, Carmichael J, Parrish C, Wallis G, et al. Defining Unmet Need Following Lenalidomide Refractoriness: Real-World Evidence of Outcomes in Patients With Multiple Myeloma. *Front Oncol*. 2021;11:703233.
8. Rajkumar SV, Kumar S. Multiple Myeloma: Diagnosis and Treatment. *Mayo Clin Proc*. 2016;91(1):101-19.
9. Morgan GJ, Walker BA, Davies FE. The genetic architecture of multiple myeloma. *Nat Rev Cancer*. 2012;12(5):335-48.
10. Kumar S, Fonseca R, Ketterling RP, Dispenzieri A, Lacy MQ, Gertz MA, et al. Trisomies in multiple myeloma: impact on survival in patients with high-risk cytogenetics. *Blood*. 2012;119(9):2100-5.
11. Bergsagel PL, Kuehl WM, Zhan F, Sawyer J, Barlogie B, Shaughnessy J. Cyclin D dysregulation: an early and unifying pathogenic event in multiple myeloma. *Blood*. 2005;106(1):296-303.
12. Wiedmeier-Nutor JE, Bergsagel PL. Review of Multiple Myeloma Genetics including Effects on Prognosis, Response to Treatment, and Diagnostic Workup. *Life (Basel)*. 2022;12(6).
13. Schmidt TM, Fonseca R, Usmani SZ. Chromosome 1q21 abnormalities in multiple myeloma. *Blood Cancer J*. 2021;11(4):83.
14. Hu Y, Chen W, Wang J. Progress in the identification of gene mutations involved in multiple myeloma. *Onco Targets Ther*. 2019;12:4075-80.
15. van Beers EH, van Vliet MH, Kuiper R, de Best L, Anderson KC, Chari A, et al. Prognostic Validation of SKY92 and Its Combination With ISS in an Independent Cohort of Patients With Multiple Myeloma. *Clin Lymphoma Myeloma Leuk*. 2017;17(9):555-62.
16. Keats JJ, Chesi M, Egan JB, Garbitt VM, Palmer SE, Braggio E, et al. Clonal competition with alternating dominance in multiple myeloma. *Blood*. 2012;120(5):1067-76.
17. Jones JR, Weinhold N, Ashby C, Walker BA, Wardell C, Pawlyn C, et al. Clonal evolution in myeloma: the impact of maintenance lenalidomide and depth of response on the genetics and sub-clonal structure of relapsed disease in uniformly treated newly diagnosed patients. *Haematologica*. 2019;104(7):1440-50.
18. Alzrigat M, Párraga AA, Jernberg-Wiklund H. Epigenetics in multiple myeloma: From mechanisms to therapy. *Semin Cancer Biol*. 2018;51:101-15.

19. Dupont C, Armant DR, Brenner CA. Epigenetics: definition, mechanisms and clinical perspective. *Semin Reprod Med.* 2009;27(5):351-7.
20. Bollati V, Fabris S, Pegoraro V, Ronchetti D, Mosca L, Deliliers GL, et al. Differential repetitive DNA methylation in multiple myeloma molecular subgroups. *Carcinogenesis.* 2009;30(8):1330-5.
21. Sive JI, Feber A, Smith D, Quinn J, Beck S, Yong K. Global hypomethylation in myeloma is associated with poor prognosis. *Br J Haematol.* 2016;172(3):473-5.
22. Pawlyn C, Bright MD, Buros AF, Stein CK, Walters Z, Aronson LI, et al. Overexpression of EZH2 in multiple myeloma is associated with poor prognosis and dysregulation of cell cycle control. *Blood Cancer J.* 2017;7(3):e549.
23. Dimopoulos K, Gimsing P, Grønbaek K. The role of epigenetics in the biology of multiple myeloma. *Blood Cancer J.* 2014;4(5):e207.
24. Leone E, Morelli E, Di Martino MT, Amodio N, Foresta U, Gullà A, et al. Targeting miR-21 inhibits in vitro and in vivo multiple myeloma cell growth. *Clin Cancer Res.* 2013;19(8):2096-106.
25. García-Ortiz A, Rodríguez-García Y, Encinas J, Maroto-Martín E, Castellano E, Teixidó J, et al. The Role of Tumor Microenvironment in Multiple Myeloma Development and Progression. *Cancers (Basel).* 2021;13(2).
26. Manier S, Sacco A, Leleu X, Ghobrial IM, Roccaro AM. Bone marrow microenvironment in multiple myeloma progression. *J Biomed Biotechnol.* 2012;2012:157496.
27. Silbermann R, Roodman GD. Myeloma bone disease: Pathophysiology and management. *J Bone Oncol.* 2013;2(2):59-69.
28. Dimopoulos MA, Kastiris E, Rosinol L, Bladé J, Ludwig H. Pathogenesis and treatment of renal failure in multiple myeloma. *Leukemia.* 2008;22(8):1485-93.
29. Lakshman A, Kumar SK. Chimeric antigen receptor T-cells, bispecific antibodies, and antibody-drug conjugates for multiple myeloma: An update. *Am J Hematol.* 2022;97(1):99-118.
30. Burwick N, Sharma S. Glucocorticoids in multiple myeloma: past, present, and future. *Ann Hematol.* 2019;98(1):19-28.
31. Poczta A, Rogalska A, Marczak A. Treatment of Multiple Myeloma and the Role of Melphalan in the Era of Modern Therapies-Current Research and Clinical Approaches. *J Clin Med.* 2021;10(9).
32. van der Zanden SY, Qiao X, Neefjes J. New insights into the activities and toxicities of the old anticancer drug doxorubicin. *FEBS J.* 2021;288(21):6095-111.
33. Ito S. Proteasome Inhibitors for the Treatment of Multiple Myeloma. *Cancers (Basel).* 2020;12(2).
34. Collins I, Wang H, Caldwell JJ, Chopra R. Chemical approaches to targeted protein degradation through modulation of the ubiquitin-proteasome pathway. *The Biochemical journal.* 2017;474(7):1127-47.
35. Deleu S ME, Valckenborgh EV, Van Camp B, Fraczek J, Vande Broek I, Rogiers V, Vanderkerken K. Histone deacetylase inhibitors in multiple myeloma. *Hematol Rev.* 2009;1(1):e9.
36. Chari A, Vogl DT, Gavriatopoulou M, Nooka AK, Yee AJ, Huff CA, et al. Oral Selinexor-Dexamethasone for Triple-Class Refractory Multiple Myeloma. *N Engl J Med.* 2019;381(8):727-38.
37. Romano A, Storti P, Marchica V, Scandura G, Notarfranchi L, Craviotto L, et al. Mechanisms of Action of the New Antibodies in Use in Multiple Myeloma. *Front Oncol.* 2021;11:684561.

38. NICE. Lenalidomide maintenance treatment after an autologous stem cell transplant for newly diagnosed multiple myeloma. NICE guidelines 2021.
39. Anderson K, Ismaila N, Kyle RA. Role of Bone-Modifying Agents in Multiple Myeloma: American Society of Clinical Oncology Clinical Practice Guideline Update Summary. *J Oncol Pract*. 2018;14(4):266-9.
40. Yong K, Delforge M, Driessen C, Fink L, Flinois A, Gonzalez-McQuire S, et al. Multiple myeloma: patient outcomes in real-world practice. 2016;175(2):252-64.
41. Kronke J, Hurst SN, Ebert BL. Lenalidomide induces degradation of IKZF1 and IKZF3. *Oncoimmunology*. 2014;3(7):e941742.
42. Richardson PG, Xie W, Jagannath S, Jakubowiak A, Lonial S, Raje NS, et al. A phase 2 trial of lenalidomide, bortezomib, and dexamethasone in patients with relapsed and relapsed/refractory myeloma. *Blood*. 2014;123(10):1461-9.
43. Garderet L, Iacobelli S, Moreau P, Dib M, Lafon I, Niederwieser D, et al. Superiority of the triple combination of bortezomib-thalidomide-dexamethasone over the dual combination of thalidomide-dexamethasone in patients with multiple myeloma progressing or relapsing after autologous transplantation: the MMVAR/IFM 2005-04 Randomized Phase III Trial from the Chronic Leukemia Working Party of the European Group for Blood and Marrow Transplantation. *J Clin Oncol*. 2012;30(20):2475-82.
44. Cavo M, Tacchetti P, Patriarca F, Petrucci MT, Pantani L, Galli M, et al. Bortezomib with thalidomide plus dexamethasone compared with thalidomide plus dexamethasone as induction therapy before, and consolidation therapy after, double autologous stem-cell transplantation in newly diagnosed multiple myeloma: a randomised phase 3 study. *Lancet*. 2010;376(9758):2075-85.
45. Durie BGM, Hoering A, Sexton R, Abidi MH, Epstein J, Rajkumar SV, et al. Longer term follow-up of the randomized phase III trial SWOG S0777: bortezomib, lenalidomide and dexamethasone vs. lenalidomide and dexamethasone in patients (Pts) with previously untreated multiple myeloma without an intent for immediate autologous stem cell transplant (ASCT). *Blood Cancer J*. 2020;10(5):53.
46. Verma R, Mai Z, Xu M, Zhang L, Dhodapkar K, Dhodapkar MV. Identification of a Cereblon-Independent Protein Degradation Pathway in Residual Myeloma Cells Treated with Immunomodulatory Drugs. *Blood*. 2015;126(23):913.
47. Dimopoulos MA, Oriol A, Nahi H, San-Miguel J, Bahlis NJ, Usmani SZ, et al. Daratumumab, Lenalidomide, and Dexamethasone for Multiple Myeloma. *N Engl J Med*. 2016;375(14):1319-31.
48. Bahlis NJ, Dimopoulos MA, White DJ, Benboubker L, Cook G, Leiba M, et al. Daratumumab plus lenalidomide and dexamethasone in relapsed/refractory multiple myeloma: extended follow-up of POLLUX, a randomized, open-label, phase 3 study. *Leukemia*. 2020;34(7):1875-84.
49. Gavriatopoulou M, Kastiris E, Ntanasis-Stathopoulos I, Fotiou D, Roussou M, Migkou M, et al. The addition of IMiDs for patients with daratumumab-refractory multiple myeloma can overcome refractoriness to both agents. *Blood*. 2018;131(4):464-7.
50. Bansal R, Reshef R. Revving the CAR - Combination strategies to enhance CAR T cell effectiveness. *Blood Rev*. 2021;45:100695.
51. Housman G, Byler S, Heerboth S, Lapinska K, Longacre M, Snyder N, et al. Drug resistance in cancer: an overview. *Cancers (Basel)*. 2014;6(3):1769-92.

52. Holstein SA. The evolving tale of immunomodulatory drugs and cereblon. *Clin Pharmacol Ther.* 2014;96(5):538-41.
53. Holstein SA, McCarthy PL. Immunomodulatory Drugs in Multiple Myeloma: Mechanisms of Action and Clinical Experience. *Drugs.* 2017;77(5):505-20.
54. Ito T, Ando H, Suzuki T, Ogura T, Hotta K, Imamura Y, et al. Identification of a Primary Target of Thalidomide Teratogenicity. *Science (New York, NY).* 2010;327(5971):1345-50.
55. Lu G, Middleton RE, Sun H, Naniong M, Ott CJ, Mitsiades CS, et al. The myeloma drug lenalidomide promotes the cereblon-dependent destruction of Ikaros proteins. *Science (New York, NY).* 2014;343(6168):305-9.
56. Shaffer AL, Emre NC, Lamy L, Ngo VN, Wright G, Xiao W, et al. IRF4 addiction in multiple myeloma. *Nature.* 2008;454(7201):226-31.
57. Sievers QL, Petzold G, Bunker RD, Renneville A, Słabicki M, Liddicoat BJ, et al. Defining the human C2H2 zinc finger degrome targeted by thalidomide analogs through CRBN. *Science (New York, NY).* 2018;362(6414):eaat0572.
58. An J, Ponthier CM, Sack R, Seebacher J, Stadler MB, Donovan KA, et al. pSILAC mass spectrometry reveals ZFP91 as IMiD-dependent substrate of the CRL4(CRBN) ubiquitin ligase. *Nat Commun.* 2017;8:15398.
59. Chung D, Dellaire G. The Role of the COP9 Signalosome and Neddylation in DNA Damage Signaling and Repair. *Biomolecules.* 2015;5(4):2388-416.
60. Eichner R, Heider M, Fernandez-Saiz V, van Bebber F, Garz AK, Lemeer S, et al. Immunomodulatory drugs disrupt the cereblon-CD147-MCT1 axis to exert antitumor activity and teratogenicity. *Nat Med.* 2016;22(7):735-43.
61. Heider M, Eichner R, Stroh J, Morath V, Kuisl A, Zecha J, et al. The IMiD target CRBN determines HSP90 activity toward transmembrane proteins essential in multiple myeloma. *Mol Cell.* 2021;81(6):1170-86 e10.
62. Bird S, Pawlyn C. IMiD resistance in multiple myeloma: current understanding of the underpinning biology and clinical impact. *Blood.* 2023;142(2):131-40.
63. Jones JR, Barber A, Le Bihan YV, Weinhold N, Ashby C, Walker BA, et al. Mutations in CRBN and other cereblon pathway genes are infrequently associated with acquired resistance to immunomodulatory drugs. *Leukemia.* 2021;35(10):3017-20.
64. Kortum KM, Zhu YX, Shi CX, Jedlowski P, Stewart AK. Cereblon binding molecules in multiple myeloma. *Blood reviews.* 2015;29(5):329-34.
65. D'Souza C, Prince HM, Neeson PJ. Understanding the Role of T-Cells in the Antimyeloma Effect of Immunomodulatory Drugs. *Frontiers in immunology.* 2021;12:632399.
66. Thakurta A, Pierceall WE, Amatangelo MD, Flynt E, Agarwal A. Developing next generation immunomodulatory drugs and their combinations in multiple myeloma. *Oncotarget.* 2021;12(15):1555-63.
67. Dimopoulos MA, Palumbo A, Corradini P, Cavo M, Delforge M, Di Raimondo F, et al. Safety and efficacy of pomalidomide plus low-dose dexamethasone in STRATUS (MM-010): a phase 3b study in refractory multiple myeloma. *Blood.* 2016;128(4):497-503.
68. Richardson PG, Schjesvold F, Weisel K, Moreau P, Anderson LD, Jr., White D, et al. Pomalidomide, bortezomib, and dexamethasone at first relapse in lenalidomide-pretreated myeloma: A subanalysis of OPTIMISMM by clinical characteristics. *European journal of haematology.* 2022;108(1):73-83.

69. van de Donk NWCJ, Popat R, Larsen J, Minnema MC, Jagannath S, Oriol A, et al. First Results of IBERDOMIDE (IBER; CC-220) in Combination with Dexamethasone (DEX) and Daratumumab (DARA) or Bortezomib (BORT) in Patients with Relapsed/Refractory Multiple Myeloma (RRMM). *Blood*. 2020;136(Supplement 1):16-7.
70. Lonial S, Donk NWCJvd, Popat R, Zonder JA, Minnema MC, Larsen J, et al. First clinical (phase 1b/2a) study of iberdomide (CC-220; IBER), a CELMoD, in combination with dexamethasone (DEX) in patients (pts) with relapsed/refractory multiple myeloma (RRMM). *Journal of Clinical Oncology*. 2019;37(15\_suppl):8006.
71. Richardson PG, Trudel S, Quach H, Popat R, Lonial S, Orlowski RZ, et al. Mezigdomide (CC-92480), a Potent, Novel Cereblon E3 Ligase Modulator (CELMoD), Combined with Dexamethasone (DEX) in Patients (pts) with Relapsed/Refractory Multiple Myeloma (RRMM): Preliminary Results from the Dose-Expansion Phase of the CC-92480-MM-001 Trial. *Blood*. 2022;140(Supplement 1):1366-8.
72. Lonial S, Popat R, Hulin C, Jagannath S, Oriol A, Richardson PG, et al. IBERDOMIDE plus dexamethasone in heavily pretreated late-line relapsed or refractory multiple myeloma (CC-220-MM-001): a multicentre, multicohort, open-label, phase 1/2 trial. *The Lancet Haematology*. 2022;9(11):e822-e32.
73. Zhu YX, Braggio E, Shi CX, Bruins LA, Schmidt JE, Van Wier S, et al. Cereblon expression is required for the antimyeloma activity of lenalidomide and pomalidomide. *Blood*. 2011;118(18):4771-9.
74. Franssen LE, Nijhof IS, Couto S, Levin MD, Bos GMJ, Broijl A, et al. Cereblon loss and up-regulation of c-Myc are associated with lenalidomide resistance in multiple myeloma patients. *Haematologica*. 2018;103(8):e368-e71.
75. Sperling AS, Burgess M, Keshishian H, Gasser JA, Bhatt S, Jan M, et al. Patterns of substrate affinity, competition, and degradation kinetics underlie biological activity of thalidomide analogs. *Blood*. 2019;134(2):160-70.
76. Asatsuma-Okumura T, Ito T, Handa H. Molecular mechanisms of cereblon-based drugs. *Pharmacol Ther*. 2019;202:132-9.
77. Ioannou N, Jain K, Ramsay AG. Immunomodulatory Drugs for the Treatment of B Cell Malignancies. *Int J Mol Sci*. 2021;22(16).
78. Carpio C, Bouabdallah R, Ysebaert L, Sancho JM, Salles G, Cordoba R, et al. Avadomide monotherapy in relapsed/refractory DLBCL: safety, efficacy, and a predictive gene classifier. *Blood*. 2020;135(13):996-1007.
79. Churcher I. PROTAC-Induced Protein Degradation in Drug Discovery: Breaking the Rules or Just Making New Ones? *J Med Chem*. 2018;61(2):444-52.
80. Giavridis T, van der Stegen SJC, Eyquem J, Hamieh M, Piersigilli A, Sadelain M. CAR T cell-induced cytokine release syndrome is mediated by macrophages and abated by IL-1 blockade. *Nat Med*. 2018;24(6):731-8.
81. Jan M, Scarfò I, Larson RC, Walker A, Schmidts A, Guirguis AA, et al. Reversible ON- and OFF-switch chimeric antigen receptors controlled by lenalidomide. *Sci Transl Med*. 2021;13(575).
82. Lopez-Girona A, Mendy D, Ito T, Miller K, Gandhi AK, Kang J, et al. Cereblon is a direct protein target for immunomodulatory and antiproliferative activities of lenalidomide and pomalidomide. *Leukemia*. 2012;26(11):2326-35.
83. Ocio EM, Fernandez-Lazaro D, San-Segundo L, Lopez-Corral L, Corchete LA, Gutierrez NC, et al. In vivo murine model of acquired resistance in myeloma reveals differential mechanisms for lenalidomide and pomalidomide in combination with dexamethasone. *Leukemia*. 2015;29(3):705-14.

84. Liu J, Song T, Zhou W, Xing L, Wang S, Ho M, et al. A genome-scale CRISPR-Cas9 screening in myeloma cells identifies regulators of immunomodulatory drug sensitivity. *Leukemia*. 2019;33(1):171-80.
85. Sievers QL, Gasser JA, Cowley GS, Fischer ES, Ebert BL. Genome-wide screen identifies cullin-RING ligase machinery required for lenalidomide-dependent CRL4(CRBN) activity. *Blood*. 2018;132(12):1293-303.
86. Shirasaki R, Matthews GM, Gandolfi S, de Matos Simoes R, Buckley DL, Raja Vora J, et al. Functional Genomics Identify Distinct and Overlapping Genes Mediating Resistance to Different Classes of Heterobifunctional Degraders of Oncoproteins. *Cell Reports*. 2021;34(1):108532.
87. Skerget S, Benard B, Christofferson A, Legendre C, Aldrich J, Nasser S, et al. A Molecular Analysis of Cereblon-Related Immunomodulatory Drug Resistance in Commpass Multiple Myeloma Patients. *Blood*. 2017;130(Supplement 1):1754.
88. Kortum KM, Mai EK, Hanafiah NH, Shi CX, Zhu YX, Bruins L, et al. Targeted sequencing of refractory myeloma reveals a high incidence of mutations in CRBN and Ras pathway genes. *Blood*. 2016;128(9):1226-33.
89. Barrio S, Munawar U, Zhu YX, Giesen N, Shi CX, Via MD, et al. IKZF1/3 and CRL4(CRBN) E3 ubiquitin ligase mutations and resistance to immunomodulatory drugs in multiple myeloma. *Haematologica*. 2020;105(5):e237-e41.
90. Gooding S, Ansari-Pour N, Towfic F, Ortiz Estevez M, Chamberlain PP, Tsai KT, et al. Multiple cereblon genetic changes are associated with acquired resistance to lenalidomide or pomalidomide in multiple myeloma. *Blood*. 2021;137(2):232-7.
91. Neri P, Maity R, Keats JJ, Tagoug I, Simms J, Auclair D, et al. Cereblon Splicing of Exon 10 Mediates IMiDs Resistance in Multiple Myeloma: Clinical Validation in the CoMMpass Trial. *Blood*. 2016;128(22):120.
92. Haertle L, Barrio S, Munawar U, Han S, Zhou X, Vogt C, et al. Cereblon enhancer methylation and IMiD resistance in multiple myeloma. *Blood*. 2021;138(18):1721-6.
93. Dimopoulos K, Sogaard Helbo A, Fibiger Munch-Petersen H, Sjo L, Christensen J, Sommer Kristensen L, et al. Dual inhibition of DNMTs and EZH2 can overcome both intrinsic and acquired resistance of myeloma cells to IMiDs in a cereblon-independent manner. *Mol Oncol*. 2018;12(2):180-95.
94. Drew AE, Motwani V, Eichinger L, Smith J, Raimondi A. Abstract 807: Mechanism of action of synergistic activity of EZH2 inhibition and IMiDs in preclinical multiple myeloma models. *Cancer Research*. 2018;78(13\_Supplement):807.
95. Gooding S, Ansari-Pour N, Kazeroun MH, Karagoz K, Polonskaia A, Angulo Salazar M, et al. Loss Of COP9-Signalosome Genes At 2q37 Is Associated With IMiD Agent Resistance In Multiple Myeloma. *Blood*. 2022.
96. Tilmont R, Maity R, Leblay N, Lee H, Barakat E, Neri P, et al. CRBN Structural Changes, Copy Number Changes and COP9 Signalosome Subunits Gene Expression Mediate Sensitivity to New Celmod Compound CC-92480 in Multiple Myeloma Patients. *ASH; New Orleans 2022*.
97. Zhou N, Gutierrez-Uzquiza A, Zheng XY, Chang R, Vogl DT, Garfall AL, et al. RUNX proteins desensitize multiple myeloma to lenalidomide via protecting IKZFs from degradation. *Leukemia*. 2019;33(8):2006-21.

98. Barwick BG, Neri P, Bahlis NJ, Nooka AK, Dhodapkar MV, Jaye DL, et al. Multiple myeloma immunoglobulin lambda translocations portend poor prognosis. *Nat Commun.* 2019;10(1):1911.
99. Davis LN, Sherbenou DW. Emerging Therapeutic Strategies to Overcome Drug Resistance in Multiple Myeloma. *Cancers.* 2021;13(7).
100. Liu J, Hideshima T, Xing L, Wang S, Zhou W, Samur MK, et al. ERK signaling mediates resistance to immunomodulatory drugs in the bone marrow microenvironment. *Sci Adv.* 2021;7(23).
101. Zhu YX, Shi CX, Bruins LA, Wang X, Riggs DL, Porter B, et al. Identification of lenalidomide resistance pathways in myeloma and targeted resensitization using cereblon replacement, inhibition of STAT3 or targeting of IRF4. *Blood cancer journal.* 2019;9(2):19.
102. Neri P, Tagoug I, Maity R, Stein CK, Kong M, Keats J, et al. Transcriptional Plasticity Compensates for Ikaros and Aiolos Proteasomal Degradation and Mediates Resistance to IMiDs in Multiple Myeloma (MM). *Blood.* 2017;130(Supplement 1):63.
103. Ng YLD, Ramberger E, Bohl SR, Dolnik A, Steinebach C, Conrad T, et al. Proteomic profiling reveals CDK6 upregulation as a targetable resistance mechanism for lenalidomide in multiple myeloma. *Nat Commun.* 2022;13(1):1009.
104. Neri PE, Tagoug I, Ren L, Maity R, Simms J, Duggan P, et al. Transcriptome Profiling of Lenalidomide Treated Myeloma Patients Identifies an Interferon Signature Gene Response and a Novel IRF4/MYC Independent Mechanism of Resistance. *Blood.* 2014;124(21):170.
105. Van Oekelen O, Amatangelo M, Guo M, Upadhyaya B, Kelly G, Patel M, et al. Large-Scale Mass Cytometry Reveals Significant Activation of Innate and Adaptive Immunity in Bone Marrow Tumor Microenvironment of Ibrandomide-Treated Myeloma Patients. *Blood.* 2021;138(Supplement 1):730.
106. Chung DJ, Pronschinske KB, Shyer JA, Sharma S, Leung S, Curran SA, et al. T-cell Exhaustion in Multiple Myeloma Relapse after Autotransplant: Optimal Timing of Immunotherapy. *Cancer Immunol Res.* 2016;4(1):61-71.
107. Batorov EV, Aristova TA, Sergeevicheva VV, Sizikova SA, Ushakova GY, Pronkina NV, et al. Quantitative and functional characteristics of circulating and bone marrow PD-1- and TIM-3-positive T cells in treated multiple myeloma patients. *Sci Rep.* 2020;10(1):20846.
108. van der Veer MS, de Weers M, van Kessel B, Bakker JM, Wittebol S, Parren PW, et al. Towards effective immunotherapy of myeloma: enhanced elimination of myeloma cells by combination of lenalidomide with the human CD38 monoclonal antibody daratumumab. *Haematologica.* 2011;96(2):284-90.
109. van der Veer MS, de Weers M, van Kessel B, Bakker JM, Wittebol S, Parren PW, et al. The therapeutic human CD38 antibody daratumumab improves the anti-myeloma effect of newly emerging multi-drug therapies. *Blood Cancer J.* 2011;1(10):e41.
110. Casneuf T, Adams HC, van de Donk NWCJ, Abraham Y, Bald J, Vanhoof G, et al. Deep immune profiling of patients treated with lenalidomide and dexamethasone with or without daratumumab. *Leukemia.* 2021;35(2):573-84.
111. Pierceall WE, Amatangelo MD, Bahlis NJ, Siegel DS, Rahman A, Van Oekelen O, et al. Immunomodulation in Pomalidomide, Dexamethasone, and Daratumumab-Treated Patients with Relapsed/Refractory Multiple Myeloma. *Clinical Cancer Research.* 2020;26(22):5895-902.

112. Tamura H, Ishibashi M, Sunakawa-Kii M, Inokuchi K. PD-L1-PD-1 Pathway in the Pathophysiology of Multiple Myeloma. *Cancers (Basel)*. 2020;12(4).
113. Mateos MV, Orlowski RZ, Ocio EM, Rodríguez-Otero P, Reece D, Moreau P, et al. Pembrolizumab combined with lenalidomide and low-dose dexamethasone for relapsed or refractory multiple myeloma: phase I KEYNOTE-023 study. *Br J Haematol*. 2019;186(5):e117-e21.
114. Mateos MV, Blacklock H, Schjesvold F, Oriol A, Simpson D, George A, et al. Pembrolizumab plus pomalidomide and dexamethasone for patients with relapsed or refractory multiple myeloma (KEYNOTE-183): a randomised, open-label, phase 3 trial. *Lancet Haematol*. 2019;6(9):e459-e69.
115. Usmani SZ, Schjesvold F, Oriol A, Karlin L, Cavo M, Rifkin RM, et al. Pembrolizumab plus lenalidomide and dexamethasone for patients with treatment-naive multiple myeloma (KEYNOTE-185): a randomised, open-label, phase 3 trial. *Lancet Haematol*. 2019;6(9):e448-e58.
116. Gandhi AK, Mendy D, Waldman M, Chen G, Rychak E, Miller K, et al. Measuring cereblon as a biomarker of response or resistance to lenalidomide and pomalidomide requires use of standardized reagents and understanding of gene complexity. *British journal of haematology*. 2014;164(2):233-44.
117. Costacurta M, Vervoort SJ, Hogg SJ, Martin BP, Johnstone RW, Shortt J. Whole genome CRISPR screening identifies TOP2B as a potential target for IMiD sensitization in multiple myeloma. *Haematologica*. 2021;106(7):2013-7.
118. Lopez-Girona A, Havens CG, Lu G, Rychak E, Mendy D, Gaffney B, et al. CC-92480 Is a Novel Cereblon E3 Ligase Modulator with Enhanced Tumoricidal and Immunomodulatory Activity Against Sensitive and Resistant Multiple Myeloma Cells. *Blood*. 2019;134(Supplement\_1):1812.
119. Hansen JD, Correa M, Nagy MA, Alexander M, Plantevin V, Grant V, et al. Discovery of CRBN E3 Ligase Modulator CC-92480 for the Treatment of Relapsed and Refractory Multiple Myeloma. *Journal of medicinal chemistry*. 2020;63(13):6648-76.
120. Walker ZJ, VanWyngarden MJ, Stevens BM, Abbott D, Hammes A, Langouet-Astrie C, et al. Measurement of ex vivo resistance to proteasome inhibitors, IMiDs, and daratumumab during multiple myeloma progression. *Blood advances*. 2020;4(8):1628-39.
121. Broyl A, Kuiper R, van Duin M, van der Holt B, el Jarari L, Bertsch U, et al. High cereblon expression is associated with better survival in patients with newly diagnosed multiple myeloma treated with thalidomide maintenance. *Blood*. 2013;121(4):624-7.
122. Misiewicz-Krzeminska I, Corchete LA, Rojas EA, Martinez-Lopez J, Garcia-Sanz R, Oriol A, et al. A novel nano-immunoassay method for quantification of proteins from CD138-purified myeloma cells: biological and clinical utility. *Haematologica*. 2018;103(5):880-9.
123. Misiewicz-Krzeminska I, de Ramón C, Corchete LA, Krzeminski P, Rojas EA, Isidro I, et al. Quantitative expression of Ikaros, IRF4, and PSMD10 proteins predicts survival in VRD-treated patients with multiple myeloma. *Blood advances*. 2020;4(23):6023-33.
124. Agnarelli A, Chevassut T, Mancini EJ. IRF4 in multiple myeloma-Biology, disease and therapeutic target. *Leuk Res*. 2018;72:52-8.
125. Walker BA, Boyle EM, Wardell CP, Murison A, Begum DB, Dahir NM, et al. Mutational Spectrum, Copy Number Changes, and Outcome: Results of a Sequencing Study of Patients With Newly Diagnosed Myeloma. *Journal of clinical*



oncology : official journal of the American Society of Clinical Oncology. 2015;33(33):3911-20.

126. Ferguson ID, Patiño-Escobar B, Tuomivaara ST, Lin YT, Nix MA, Leung KK, et al. The surfaceome of multiple myeloma cells suggests potential immunotherapeutic strategies and protein markers of drug resistance. *Nat Commun.* 2022;13(1):4121.

127. Bjorklund CC, Kang J, Amatangelo M, Polonskaia A, Katz M, Chiu H, et al. Iberdomide (CC-220) is a potent cereblon E3 ligase modulator with antitumor and immunostimulatory activities in lenalidomide- and pomalidomide-resistant multiple myeloma cells with dysregulated CRBN. *Leukemia.* 2020;34(4):1197-201.

128. Lonial S, Shambavi R, Matous J, , Yee AM, Shah U, et al., editors. Pharmacokinetic (PK) Profile of a Novel IKZF1/3 Degradable, CFT7455, Enables Significant Potency Advantage over Other IKZF1/3 Degradable in Models of Multiple Myeloma (MM) and the Results of the Initial Treatment Cohort from a First-in-Human (FIH) Phase 1/2 Study of CFT7455 in MM. AACR; 2022; New Orleans.

129. McLaren W, Gil L, Hunt SE, Riat HS, Ritchie GR, Thormann A, et al. The Ensembl Variant Effect Predictor. *Genome Biol.* 2016;17(1):122.

130. Ewels PA, Peltzer A, Fillinger S, Patel H, Alneberg J, Wilm A, et al. The nf-core framework for community-curated bioinformatics pipelines. *Nature biotechnology.* 2020;38(3):276-8.

131. Sialana FJ, Roumeliotis TI, Bouguenina H, Chan Wah Hak L, Wang H, Caldwell J, et al. SimPLIT: Simplified Sample Preparation for Large-Scale Isobaric Tagging Proteomics. *J Proteome Res.* 2022;21(8):1842-56.

132. Zenkova D, Kamenev V, Sablina R, Artyomov M, Sergushichev A. Phantasm: visual and interactive gene expression analysis. 2018.

133. Zhang JH, Chung TD, Oldenburg KR. A Simple Statistical Parameter for Use in Evaluation and Validation of High Throughput Screening Assays. *J Biomol Screen.* 1999;4(2):67-73.

134. Egan B, Yuan CC, Craske ML, Labhart P, Guler GD, Arnott D, et al. An Alternative Approach to ChIP-Seq Normalization Enables Detection of Genome-Wide Changes in Histone H3 Lysine 27 Trimethylation upon EZH2 Inhibition. *PLoS One.* 2016;11(11):e0166438.

135. Tredwell GD, Keun HC. convISA: A simple, convoluted method for isotopomer spectral analysis of fatty acids and cholesterol. *Metab Eng.* 2015;32:125-32.

136. Sarin V, Yu K, Ferguson ID, Gugliemini O, Nix MA, Hann B, et al. Evaluating the efficacy of multiple myeloma cell lines as models for patient tumors via transcriptomic correlation analysis. *Leukemia.* 2020;34(10):2754-65.

137. Bam R, Khan S, Ling W, Randal SS, Li X, Barlogie B, et al. Primary myeloma interaction and growth in coculture with healthy donor hematopoietic bone marrow. *BMC Cancer.* 2015;15:864.

138. Yue Y, Cao Y, Mao X, Wang F, Fan P, Qian L, et al. Novel myeloma patient-derived xenograft models unveil the potency of anlotinib to overcome bortezomib resistance. *Front Oncol.* 2022;12:894279.

139. Lab K. Keats Lab Myeloma Cell Lines 2023.

140. McDermott M, Eustace AJ, Busschots S, Breen L, Crown J, Clynes M, et al. In vitro Development of Chemotherapy and Targeted Therapy Drug-Resistant Cancer Cell Lines: A Practical Guide with Case Studies. *Front Oncol.* 2014;4:40.

141. Gu L, Zhang G, Zhang Y. A novel method to establish glucocorticoid resistant acute lymphoblastic leukemia cell lines. *J Exp Clin Cancer Res.* 2019;38(1):269.
142. Ben-David U, Siranosian B, Ha G, Tang H, Oren Y, Hinohara K, et al. Genetic and transcriptional evolution alters cancer cell line drug response. *Nature.* 2018;560(7718):325-30.
143. Gooding S, Ansari-Pour N, Towfic F, Ortiz Estévez M, Chamberlain PP, Tsai KT, et al. Multiple cereblon genetic changes are associated with acquired resistance to lenalidomide or pomalidomide in multiple myeloma. *Blood.* 2021;137(2):232-7.
144. Talevich E, Shain AH, Botton T, Bastian BC. CNVkit: Genome-Wide Copy Number Detection and Visualization from Targeted DNA Sequencing. *PLoS Comput Biol.* 2016;12(4):e1004873.
145. Raudvere U, Kolberg L, Kuzmin I, Arak T, Adler P, Peterson H, et al. g:Profiler: a web server for functional enrichment analysis and conversions of gene lists (2019 update). *Nucleic Acids Res.* 2019;47(W1):W191-W8.
146. Roy P, Sarkar UA, Basak S. The NF- $\kappa$ B Activating Pathways in Multiple Myeloma. *Biomedicines.* 2018;6(2).
147. Stelzer G, Rosen N, Plaschkes I, Zimmerman S, Twik M, Fishilevich S, et al. The GeneCards Suite: From Gene Data Mining to Disease Genome Sequence Analyses. *Curr Protoc Bioinformatics.* 2016;54:1.30.1-1.30.33.
148. Egan JB, Kortuem KM, Kurdoglu A, Izatt T, Aldrich J, Reiman R, et al. Extramedullary myeloma whole genome sequencing reveals novel mutations in Cereblon, proteasome subunit G2 and the glucocorticoid receptor in multi drug resistant disease. *Br J Haematol.* 2013;161(5):748-51.
149. Atrash S, Robinson M, Taneja A, Paul B, Cassetta K, Ndiaye A, et al. Bone marrow Ki-67 index is of prognostic value in newly diagnosed multiple myeloma. *Eur J Haematol.* 2023;111(3):373-381.
150. Demchenko YN, Kuehl WM. A critical role for the NF $\kappa$ B pathway in multiple myeloma. *Oncotarget.* 2010;1(1):59-68.
151. Wertz IE, O'Rourke KM, Zhou H, Eby M, Aravind L, Seshagiri S, et al. De-ubiquitination and ubiquitin ligase domains of A20 downregulate NF- $\kappa$ B signalling. *Nature.* 2004;430(7000):694-9.
152. Frazzi R. BIRC3 and BIRC5: multi-faceted inhibitors in cancer. *Cell Biosci.* 2021;11(1):8.
153. Haga RB, Ridley AJ. Rho GTPases: Regulation and roles in cancer cell biology. *Small GTPases.* 2016;7(4):207-21.
154. Wang L, Leite de Oliveira R, Huijberts S, Bosdriesz E, Pencheva N, Brunen D, et al. An Acquired Vulnerability of Drug-Resistant Melanoma with Therapeutic Potential. *Cell.* 2018;173(6):1413-25.e14.
155. Chen J, Wang X, Yuan Y, Chen H, Zhang L, Xiao H, et al. Exploiting the acquired vulnerability of cisplatin-resistant tumors with a hypoxia-amplifying DNA repair-inhibiting (HYDRI) nanomedicine. *Sci Adv.* 2021;7(13).
156. Wexler P. *Encyclopedia of Toxicology*: Elsevier; 2014.
157. Kort E, Jovinge S. Drug Repurposing: Claiming the Full Benefit from Drug Development. *Curr Cardiol Rep.* 2021;23(6):62.
158. Zhang L, Fok JH, Davies FE. Heat shock proteins in multiple myeloma. *Oncotarget.* 2014;5(5):1132-48.
159. Singh AV, Bandi M, Raje N, Richardson P, Palladino MA, Chauhan D, et al. A novel vascular disrupting agent plinabulin triggers JNK-mediated apoptosis

- and inhibits angiogenesis in multiple myeloma cells. *Blood*. 2011;117(21):5692-700.
160. Hernández-García S, San-Segundo L, González-Méndez L, Corchete LA, Misiewicz-Krzeminska I, Martín-Sánchez M, et al. The kinesin spindle protein inhibitor filanesib enhances the activity of pomalidomide and dexamethasone in multiple myeloma. *Haematologica*. 2017;102(12):2113-24.
161. Li J, Zhu J, Cao B, Mao X. The mTOR signaling pathway is an emerging therapeutic target in multiple myeloma. *Curr Pharm Des*. 2014;20(1):125-35.
162. Hau M, Zenk F, Ganesan A, Iovino N, Jung M. Cellular analysis of the action of epigenetic drugs and probes. *Epigenetics*. 2017;12(5):308-22.
163. Boutros M, Ahringer J. The art and design of genetic screens: RNA interference. *Nat Rev Genet*. 2008;9(7):554-66.
164. Redman M, King A, Watson C, King D. What is CRISPR/Cas9? *Arch Dis Child Educ Pract Ed*. 2016;101(4):213-5.
165. McLean B, Istadi A, Clack T, Vankan M, Schramek D, Neely GG, et al. A CRISPR Path to Finding Vulnerabilities and Solving Drug Resistance: Targeting the Diverse Cancer Landscape and Its Ecosystem. *Adv Genet (Hoboken)*. 2022;3(4):2200014.
166. Guo C, Ma X, Gao F, Guo Y. Off-target effects in CRISPR/Cas9 gene editing. *Front Bioeng Biotechnol*. 2023;11:1143157.
167. Smith I, Greenside PG, Natoli T, Lahr DL, Wadden D, Tirosh I, et al. Evaluation of RNAi and CRISPR technologies by large-scale gene expression profiling in the Connectivity Map. *PLoS Biol*. 2017;15(11):e2003213.
168. Wang B, Wang M, Zhang W, Xiao T, Chen CH, Wu A, et al. Integrative analysis of pooled CRISPR genetic screens using MAGeCKFlute. *Nat Protoc*. 2019;14(3):756-80.
169. Dempster JM, Boyle I, Vazquez F, Root DE, Boehm JS, Hahn WC, et al. Chronos: a cell population dynamics model of CRISPR experiments that improves inference of gene fitness effects. *Genome Biol*. 2021;22(1):343.
170. Thomenius MJ, Totman J, Cosmopoulos K, Brach D, Ci L, Farrow N, et al. Identification of a First-in-Class SETD2 Inhibitor That Shows Potent and Selective Anti-Proliferative Activity in t(4;14) Multiple Myeloma: T(4;14) Multiple Myeloma Cells Are Dependent on Both H3K36 Di and Tri-Methylation. *Blood*. 2018;132(Supplement 1):3207.
171. Butler K, Banday AR. APOBEC3-mediated mutagenesis in cancer: causes, clinical significance and therapeutic potential. *J Hematol Oncol*. 2023;16(1):31.
172. Li Y, Wu S, Zhao X, Hao S, Li F, Wang Y, et al. Key events in cancer: Dysregulation of SREBPs. *Front Pharmacol*. 2023;14:1130747.
173. Totman J, Brach D, Motwani V, Howe S, Deutschman E, Lampe J, et al. Pharmacologic Inhibition of the Histone Methyltransferase SETD2 with EZM0414 As a Novel Therapeutic Strategy in Relapsed or Refractory Multiple Myeloma and Diffuse Large B-Cell Lymphoma. *Blood*. 2021;138(Supplement 1):1142.
174. Molenaar TM, van Leeuwen F. SETD2: from chromatin modifier to multipronged regulator of the genome and beyond. *Cell Mol Life Sci*. 2022;79(6):346.
175. Kalff A, Spencer A. The t(4;14) translocation and FGFR3 overexpression in multiple myeloma: prognostic implications and current clinical strategies. *Blood Cancer J*. 2012;2(9):e89.
176. Alford JS, Lampe JW, Brach D, Chesworth R, Cosmopoulos K, Duncan KW, et al. Conformational-Design-Driven Discovery of EZM0414: A Selective,

- Potent SETD2 Inhibitor for Clinical Studies. *ACS Med Chem Lett.* 2022;13(7):1137-43.
177. Ianevski A, Giri AK, Aittokallio T. SynergyFinder 3.0: an interactive analysis and consensus interpretation of multi-drug synergies across multiple samples. *Nucleic Acids Res.* 2022;50(W1):W739-W43.
178. Yadav B, Wennerberg K, Aittokallio T, Tang J. Searching for Drug Synergy in Complex Dose-Response Landscapes Using an Interaction Potency Model. *Comput Struct Biotechnol J.* 2015;13:504-13.
179. Roell KR, Reif DM, Motsinger-Reif AA. An Introduction to Terminology and Methodology of Chemical Synergy-Perspectives from Across Disciplines. *Front Pharmacol.* 2017;8:158.
180. Cottini F, Rodriguez J, Hughes T, Sharma N, Guo L, Lozanski G, et al. Redefining CD56 as a Biomarker and Therapeutic Target in Multiple Myeloma. *Mol Cancer Res.* 2022;20(7):1083-95.
181. Cottini F, Benson D. To be or not to be: the role of CD56 in multiple myeloma. *Oncotarget.* 2023;14:47-9.
182. Cottini F, Rodriguez J, Birmingham M, Hughes T, Sharma N, Lozanski G, et al. CD56 Has a Critical Role in Regulating Multiple Myeloma Cell Growth and Response to Therapies. *Blood.* 2021;138(Supplement 1):889-.
183. Hanahan D. Hallmarks of Cancer: New Dimensions. *Cancer Discov.* 2022;12(1):31-46.
184. Pavlova NN, Thompson CB. The Emerging Hallmarks of Cancer Metabolism. *Cell Metab.* 2016;23(1):27-47.
185. Snaebjornsson MT, Janaki-Raman S, Schulze A. Greasing the Wheels of the Cancer Machine: The Role of Lipid Metabolism in Cancer. *Cell Metab.* 2020;31(1):62-76.
186. Weir P, Donaldson D, McMullin MF, Crawford L. Metabolic Alterations in Multiple Myeloma: From Oncogenesis to Proteasome Inhibitor Resistance. *Cancers (Basel).* 2023;15(6).
187. Lipchick BC, Utley A, Han Z, Moparthy S, Yun DH, Bianchi-Smiraglia A, et al. The fatty acid elongase ELOVL6 regulates bortezomib resistance in multiple myeloma. *Blood Adv.* 2021;5(7):1933-46.
188. Xu G, Huang S, Peng J, Gao X, Li M, Yu S, et al. Targeting lipid metabolism in multiple myeloma cells: Rational development of a synergistic strategy with proteasome inhibitors. *Br J Pharmacol.* 2021;178(23):4741-57.
189. Bennett MK, Li M, Tea MN, Pitman MR, Toubia J, Wang PP, et al. Resensitising proteasome inhibitor-resistant myeloma with sphingosine kinase 2 inhibition. *Neoplasia.* 2022;24(1):1-11.
190. Girish V, Sheltzer JM. A CRISPR Competition Assay to Identify Cancer Genetic Dependencies. *Bio Protoc.* 2020;10(14):e3682.
191. Greipp PR, San Miguel J, Durie BG, Crowley JJ, Barlogie B, Bladé J, et al. International staging system for multiple myeloma. *J Clin Oncol.* 2005;23(15):3412-20.
192. Oken MM, Creech RH, Tormey DC, Horton J, Davis TE, McFadden ET, et al. Toxicity and response criteria of the Eastern Cooperative Oncology Group. *Am J Clin Oncol.* 1982;5(6):649-55.
193. Kang Y, Sundaramoorthy P, Gasparetto C, Feinberg D, Fan S, Long G, et al. Phase I study of opaganib, an oral sphingosine kinase 2-specific inhibitor, in relapsed and/or refractory multiple myeloma. *Ann Hematol.* 2023;102(2):369-83.
194. Kumar S, Paiva B, Anderson KC, Durie B, Landgren O, Moreau P, et al. International Myeloma Working Group consensus criteria for response and

- minimal residual disease assessment in multiple myeloma. *Lancet Oncol.* 2016;17(8):e328-e46.
195. Rajkumar SV. Updated Diagnostic Criteria and Staging System for Multiple Myeloma. *Am Soc Clin Oncol Educ Book.* 2016;35:e418-23.
196. Gleba JJ, Alasonyalilar-Demirer A, Pawlush ML, Bilgili A, Hickman PG, Mody K, et al. Abstract 5489: Synergistic activity of SCD1 blockade in combination with tyrosine kinase inhibitors lenvatinib and cabozantinib in hepatocellular carcinoma (HCC). *Cancer Research.* 2023;83(7\_Supplement):5489.
197. D'Agostino M, Zaccaria GM, Ziccheddu B, Rustad EH, Genuardi E, Capra A, et al. Early Relapse Risk in Patients with Newly Diagnosed Multiple Myeloma Characterized by Next-generation Sequencing. *Clin Cancer Res.* 2020;26(18):4832-41.
198. Zlei M, Egert S, Wider D, Ihorst G, Wäsch R, Engelhardt M. Characterization of in vitro growth of multiple myeloma cells. *Exp Hematol.* 2007;35(10):1550-61.
199. Lodi A, Tiziani S, Khanim FL, Günther UL, Viant MR, Morgan GJ, et al. Proton NMR-based metabolite analyses of archived serial paired serum and urine samples from myeloma patients at different stages of disease activity identifies acetylcarnitine as a novel marker of active disease. *PLoS One.* 2013;8(2):e56422.
200. Liu Y, Shen J, Awal Issah M, Liu T, Zhou H, Fu H. CD56-positive diffuse large B-cell lymphoma/leukemia with. *J Int Med Res.* 2020;48(5):300060520918087.
201. Lin P, Correa D, Lin Y, Caplan AI. Polybrene inhibits human mesenchymal stem cell proliferation during lentiviral transduction. *PLoS One.* 2011;6(8):e23891.
202. Shalem O, Sanjana NE, Hartenian E, Shi X, Scott DA, Mikkelsen T, et al. Genome-scale CRISPR-Cas9 knockout screening in human cells. *Science (New York, NY).* 2014;343(6166):84-7.
203. Stein, S. An integrated method for spectrum extraction and compound identification from gas chromatography/mass spectrometry data. *J Am Soc Mass Spectrom;* 1999. p. 770-81.
204. Behrends V, Tredwell GD, Bundy JG. A software complement to AMDIS for processing GC-MS metabolomic data. *Anal Biochem.* 2011;415(2):206-8.